INVESTIGATING THE ROLE OF TETRASPANIN TSPAN15 AND ADAM10 IN CELL INVASION AND CANCER

by

RHIANNON JANE MOSS

A thesis submitted to the University of Birmingham for the degree of
DOCTOR OF PHILOSOPHY

School of Biosciences
College of Life and Environmental Sciences
University of Birmingham
February 2024

UNIVERSITY OF
BIRMINGHAM

University of Birmingham Research Archive

e-theses repository

This unpublished thesis/dissertation is copyright of the author and/or third parties. The intellectual property rights of the author or third parties in respect of this work are as defined by The Copyright Designs and Patents Act 1988 or as modified by any successor legislation.

Any use made of information contained in this thesis/dissertation must be in accordance with that legislation and must be properly acknowledged. Further distribution or reproduction in any format is prohibited without the permission of the copyright holder.

ABSTRACT

ADAM10 is a ubiquitously expressed transmembrane sheddase involved in the ectodomain shedding of over 100 substrates. The tetraspanin superfamily is an evolutionarily conserved group of transmembrane proteins, which interact with specific partner proteins to regulate their trafficking, lateral mobility, clustering, and signalling. The TspanC8 subgroup of tetraspanins (Tspan5, Tspan10, Tspan14, Tspan15, Tspan17, and Tspan33) are important regulators of ADAM10, including its substrate specificity, and as such ADAM10 exists as six different 'molecular scissors'. Further to this, Tspan15 has been reported to promote NF-κB signalling via its interaction with β-TrCP.

ADAM10 and Tspan15 have been shown to mediate the invasion of various tumours, and in some malignancies, their role extends to promoting proliferation. However, Tspan15's role in cancer is not as well characterised as ADAM10's and very few studies consider the two proteins as a complex. As such, the overarching aim of this thesis was to investigate the role of Tspan15 in cancer and determine whether its mechanism of action is ADAM10-dependent and/or -independent. This thesis provided evidence from the analysis of patient data that ADAM10 and Tspan15 are individually or co-upregulated in a number of cancers, which in some cases is unfavourable for patient survival. However, despite being co-upregulated in pancreatic adenocarcinoma, follow-up *in vitro* experiments suggested that ADAM10 and Tspan15 do not regulate the invasion or proliferation of this malignancy. In contrast, Tspan15 was shown to promote the invasion of human embryonic kidney HEK-293T cells in an ADAM10-dependent manner, likely through N-cadherin shedding and FGF receptor signalling. Finally, this thesis also provided no evidence to support Tspan15's involvement in mediating NF-κB signalling, warranting additional follow-up studies. In summary, this work furthers our understanding of the potential role of the Tspan15/ADAM10 'molecular scissor' in tumour progression, and as such could inform the design of future anti-cancer therapeutics.

ACKNOWLEDGMENTS

Firstly, a massive thank you to my two supervisors, Mike Tomlinson and Farhat Khanim, your continued support and guidance throughout this entire process has been invaluable. To the rest of the eighth floor (and seventh floor), thank you for making my time in the lab so much more enjoyable. Connie, I've thoroughly enjoyed our, at times, highly speculative science discussions. Rachel, thank you for adopting me as one of the seventh floor, and teaching me how to use ChimeraX (Friday night party). Chris, I'm going to miss you bobbling my bobble hats and the office flowers.

Rachel, Amalia, and Shabana, I'm not sure what I'm going to do without our weekly cheesy chips and science discussions. Some of my best ideas came from those discussions.

Thank you to my favourite Harborne Hornets for not letting me live in the lab or write 24/7! El, Emma, Lucy, and Maddie, I'm beyond grateful for your words of encouragement (but most importantly constant supply of sweets).

A special thank you to my parents and incredible partner, David, without whom none of this would have been possible. David, thank you for providing me with all of the mac and cheese, mango, and sweets needed to finish writing this thesis, and for always reminding me that I could do this.

Finally, I'm very grateful for the project funding provided by the Medical Research Council, as well as the School of Biosciences that allowed me to present my work at the 10th European Conference on Tetraspanins.

TABLE OF CONTENTS

CHAPTER 1 GENERAL INTRODUCTION 1

1.1 An overview of tumourigenesis and the hallmarks of cancer 1

1.1.1 Activating invasion in malignant progression 2

1.2 The a disintegrin and metalloprotease family 4

1.2.1 An overview of the a disintegrin and metalloprotease family 4

1.3 The molecular scissor a disintegrin and metalloprotease 10 (ADAM10) 5

1.3.1 ADAM10 has a characteristic modular structure 5

1.3.2 ADAM10 is a sheddase with important roles in health and disease 7

1.4 The tetraspanin family 10

1.4.1 An overview of the tetraspanin family 10

1.4.2 Tetraspanins have a characteristic four-transmembrane structure and can exist in different conformations 11

1.4.3 Tetraspanins interact with and regulate specific partner proteins 15

1.4.3.1 Tetraspanins form nanodomains with their associated partner proteins 15

1.4.3.2 Tetraspanins modulate the function of their partner proteins 16

1.5 The TspanC8 tetraspanins 17

1.5.1 An overview of the TspanC8 tetraspanins 17

1.5.2 ADAM10-dependent functions of the TspanC8 tetraspanins 18

1.5.2.1 The TspanC8 tetraspanins are required for the maturation and expression of ADAM10 18

1.5.2.2 ADAM10 substrate shedding is differentially controlled by the TspanC8s – the 'six scissor' hypothesis 20

1.5.2.2.1 Potential mechanisms underlying TspanC8/ADAM10 substrate specificity 22

1.5.2.2.1.1 The TspanC8s regulate the subcellular localisation and dynamics of ADAM10 22

1.5.2.2.1.2 ADAM10 exists in different conformations depending on the TspanC8 it's in complex with 23

1.5.3 Other functions of the TspanC8 tetraspanins 25

1.5.3.1 Tspan15 promotes the nuclear translocation of NF-κB 25

1.5.4 Tspan15 26

1.5.4.1 Tspan15 dysregulation in disease 26

1.6 The cell adhesion protein N-cadherin 28

1.6.1 N-cadherin regulates various pro-metastatic signalling pathways 28

1.6.1.1 N-cadherin drives the augmentation of FGFR signalling 29
1.6.1.2 Canonical Wnt signalling is modulated by N-cadherin 31
1.7 Project aims and objectives 34
CHAPTER 2 MATERIALS AND METHODS 36
2.1 Antibodies 36
2.2 Cell biology techniques 37
2.2.1 2D cell culture 37
2.2.2 3D cell culture 38
2.2.3 Generation of knockout cell lines by CRISPR/Cas9 38
2.2.3.1 Transfection of cells with Lipofectamine 2000 39
2.2.3.2 Selection of CRISPR-targeted cells 39
2.2.3.3 Negative cell sorting with Dynabeads 40
2.2.3.3.1 Direct negative cell sorting with Dynabeads 40
2.2.3.3.2 Indirect negative cell sorting with Dynabeads 40
2.2.3.4 Negative cell sorting by fluorescence-activated cell sorting (FACS) 41
2.2.4 Generation of Tspan15 overexpressing cell lines by Lentiviral transduction 41
2.2.4.1 Transfection with PEI 42
2.2.4.2 Lentiviral transduction and selection of targeted cells 42
2.2.5 Transient transfection of cells with PEI 43
2.3 Protein biochemistry techniques 43
2.3.1 Flow cytometry 43
2.3.2 Protein extraction 44
2.3.2.1 Whole-cell 44
2.3.2.2 Co-immunoprecipitation 44
2.3.3 Western blotting 45
2.3.4 HiSPECS proteomics 46
2.4 Cell-based assays 47
2.4.1 Proliferation assay 47
2.4.1.1 2D proliferation assay 47
2.4.1.2 3D proliferation assay 47
2.4.2 Transwell invasion assay 47
2.4.3 Cell viability assay 48
2.5 FGFR signalling assay 49

2.6 NF-kB luciferase reporter assay 49
2.7 Microscopy 50
2.7.1 Light microscopy 50
2.7.2 Live cell imaging 50
2.7.3 Fluorescence microscopy 51
2.7.3.1 Immunostaining 51
2.7.3.2 Airyscan confocal microscopy 51
2.8 Analysis of cancer samples using GEPIA2 52
2.8.1 Gene expression analysis 52
2.8.2 Patient survival analysis 52
2.9 Statistical analysis 52
CHAPTER 3 THE EXPRESSION OF ADAM10 AND TSPAN15 HAS THE POTENTIAL TO BE CLINICALLY SIGNIFICANT IN MULTIPLE DIFFERENT CANCERS 53
3.1 Introduction 53
3.2 Results 53
3.2.1 Pancreatic adenocarcinoma tumours exhibit increased expression of ADAM10 in addition to Tspan15; high tumour expression of both proteins is associated with a reduced survival rate 53
3.2.2 ADAM10 and Tspan15 are co-upregulated in oesophageal carcinoma, but high tumour expression of neither protein affects patient prognosis. 56
3.2.3 The gene expression of both ADAM10 and Tspan15 is increased in cholangiocarcinoma .. 57
3.2.4 Tspan15 is upregulated in liver hepatocellular carcinoma and high tumour expression is associated with unfavourable patient survival 59
3.2.5 Tspan15, unlike ADAM10, is upregulated in ovarian serous cystadenocarcinoma, but high Tspan15 tumour expression does not affect patient survival, whereas high ADAM10 expression is a potential prognostic biomarker 61
3.2.6 The gene expression of ADAM10 but not Tspan15 is upregulated in prostate adenocarcinoma tumours 63
3.2.7 Colon adenocarcinoma patients exhibit an upregulation of ADAM10 expression that is Tspan15-independent 65
3.2.8 ADAM10 is differentially expressed in glioblastoma multiforme tumours but does not affect patient survival 66
3.2.9 Skin cutaneous melanoma tumours exhibit increased ADAM10 gene expression, but this is not a prognostic biomarker 68
3.2.10 ADAM10 gene expression is increased in stomach adenocarcinoma 70

3.2.11 ADAM10 and Tspan15 gene expression is subtly upregulated in breast cancer tumours compared to corresponding non-tumour tissues and high ADAM10 tumour expression is unfavourable for patient survival 71

3.2.12 Lung squamous cell carcinoma tumours do not exhibit significantly altered expression of either ADAM10 or Tspan15, but the overall survival rate is reduced when ADAM10 tumour expression is high 73

3.2.13 Neither ADAM10 nor Tspan15 gene expression is upregulated in lung adenocarcinoma tumours and tumour expression is not associated with patient survival 75

3.2.14 Other members of the ADAM and TspanC8 families are upregulated in pancreatic adenocarcinoma tumours 77

3.2.15 High expression of multiple ADAM and TspanC8 family members has an effect on pancreatic adenocarcinoma patient prognosis 79

3.3 Discussion 82

CHAPTER 4 ADAM10 AND TSPAN15 DO NOT REGULATE THE IN VITRO PROLIFERATION OR INVASION OF PANCREATIC CANCER CELL LINES 88

4.1 Introduction 88

4.2 Results 89

4.2.1 The generation and validation of ADAM10 and Tspan15 KO pancreatic cancer cell lines .. 89

4.2.2 ADAM10 and Tspan15 KO pools can be purified using magnetic Dynabeads 92

4.2.3 The generation and validation of pancreatic cancer cell lines overexpressing Tspan15 95

4.2.4 ADAM10 and Tspan15 do not regulate the 2D proliferation of PANC-1 and AsPC-1 cells .. 98

4.2.5 Loss of neither ADAM10 nor Tspan15 affects the invasive capabilities of pancreatic cancer cell lines 100

4.2.6 The invasion of pancreatic cancer cell lines is unaffected by Tspan15 overexpression 104

4.3 Discussion 105

CHAPTER 5 TSPAN15 PROMOTES THE INVASION OF HEK-293T CELLS IN AN ADAM10-DEPENDENT MANNER VIA N-CADHERIN SHEDDING AND FGF RECEPTOR SIGNALLING 109

5.1 Introduction 109

5.2 Results 110

5.2.1 The generation and validation of ADAM10 and Tspan15 KO HEK-293T cells 110

5.2.2 The morphology of HEK-293T cells is unaffected by the loss of ADAM10 or Tspan15 112

5.2.3 The loss of ADAM10 and Tspan15 does not affect the motility of HEK-293T cells 113

5.2.4 The generation and validation of HEK-293T cells overexpressing Tspan15 114

5.2.5 The morphology of HEK-293T cells is unaffected by the overexpression of Tspan15 118

5.2.6 A striking clumping phenotype is observed in HEK-293T cells overexpressing Tspan15 50-fold, irrespective of ADAM10 expression 120
5.2.7 The overexpression of Tspan15 regulates the path confinement of HEK-293T cells in an ADAM10-dependent manner 121
5.2.8 Tspan15 does not activate NF-κB signalling in HEK-293T cells 123
5.2.9 The expression levels of ADAM10 and Tspan15 do not affect the proliferation of HEK-293T cells 125
5.2.10 ADAM10 and Tspan15 do not mediate the proliferation of HEK-293T spheroids 128
5.2.11 Loss of ADAM10 or Tspan15 impairs the invasive capabilities of HEK-293T cells 130
5.2.12 Increasing levels of Tspan15 surface expression promotes HEK-293T cell invasion 132
5.2.13 Tspan15 promotes the invasion of HEK-293T cells in an ADAM10-dependent manner . 133
5.2.14 N-cadherin is a substrate of the Tspan15/ADAM10 'molecular scissor' 136
5.2.15 The N-terminal fragment of N-cadherin promotes the invasion of HEK-293T cells 138
5.2.16 The N-cadherin ectodomain promotes invasion via FGF receptors 140
5.2.17 Inhibition of FGF receptors impairs proliferation but not cell viability 142
5.2.18 Recombinant N-cadherin ectodomain does not sustain FGF-induced MAPK/ERK activation in HEK-293T cells 144
5.2.19 The upregulation of Tspan15 expression increases MAPK/ERK signalling 145
5.2.20 Treatment with Tspan15 antibodies does not impair the invasion of HEK-293T cells 147
5.3 Discussion 149
CHAPTER 6 INVESTIGATING THE ROLE OF TSPAN15 AND ADAM10 IN ACTIVATING NF-KB IN AN OESOPHAGEAL CARCINOMA CELL LINE 154
6.1 Introduction 154
6.2 Results 154
6.2.1 KYSE-30 cells express Tspan15 and ADAM10 154
6.2.2 Tspan15 does not appear to interact with β-TrCP in KYSE-30 cells 155
6.2.3 Tspan15 does not promote the nuclear translocation of NF-κB 159
6.2.4 The generation and validation of Tspan15 and ADAM10 KO oesophageal carcinoma cell lines 160
6.2.5 Purification using magnetic Dynabeads is insufficient to generate pure KYSE-30 Tspan15 and ADAM10 KO pools 161
6.2.6 Purification using fluorescence-activated cell sorting was sufficient to purify KYSE-30 Tspan15 and ADAM10 KO pools 162
6.3 Discussion 163
CHAPTER 7 GENERAL DISCUSSION 167

7.1 Overview 167

7.2 Tspan15 promotes invasion in an ADAM10-dependent manner and the underlying mechanism likely involves the interplay between different signalling pathways 167

7.3 Tspan15 and ADAM10 are implicated in cancer and their role may extend beyond promoting invasion 171

7.4 Tspan15 may exhibit ADAM10-independent activity 173

7.5 The binding partners of Tspan15 may extend beyond ADAM10 174

7.6 Tspan15 may exist outside of a 1:1 heterodimer with ADAM10 176

7.7 Therapeutic potential of inhibiting Tspan15 to inhibit invasion 178

7.8 Concluding remarks 180

APPENDIX 181

REFERENCES 185

LIST OF FIGURES

CHAPTER 1 GENERAL INTRODUCTION

Figure 1: The hallmarks of cancer 2
Figure 2: ADAM10 has a characteristic modular structure with a globular ectodomain 7
Figure 3: The tetraspanin family is an evolutionarily conserved group of transmembrane proteins, with 33 being expressed in humans 11
Figure 4: Tetraspanins have a cone-like structure that can exist in 'closed', 'open', and 'extended' conformations 15
Figure 5: ADAM10's maturation, expression, and subcellular localisation are regulated by the TspanC8s 19
Figure 6: The 'six scissor' hypothesis 22
Figure 7: Tspan15 plays a role in the NF-κB signalling pathway. 26
Figure 8: N-cadherin directly interacts with FGFRs to potentiate downstream signalling 31
Figure 9: The interaction between N-cadherin and β-catenin regulates Wnt signalling. 34

CHAPTER 3 THE EXPRESSION OF ADAM10 AND TSPAN15 HAS THE POTENTIAL TO BE CLINICALLY SIGNIFICANT IN MULTIPLE DIFFERENT CANCERS

Figure 10: ADAM10 and Tspan15 are co-upregulated in pancreatic adenocarcinoma and patient survival is impaired by high tumour expression 55
Figure 11: The gene expression of both ADAM10 and Tspan15 is increased in oesophageal carcinoma, but high tumour expression is not associated with unfavourable patient survival 57
Figure 12: ADAM10 and Tspan15 gene expression is co-upregulated in cholangiocarcinoma tumours 58
Figure 13: The gene expression of Tspan15 is elevated in liver hepatocellular and high tumour expression is a potential prognostic biomarker 60
Figure 14: The gene expression of Tspan15 is increased independently of ADAM10 in ovarian serous cystadenocarcinoma tumours, but high Tspan15 tumour expression is not unfavourable for patient survival, whereas high ADAM10 expression is 62
Figure 15: ADAM10 is upregulated independently of Tspan15 in prostate adenocarcinoma tumours 64
Figure 16: ADAM10, unlike Tspan15, is overexpressed in colon adenocarcinoma; neither protein though is a potential prognostic biomarker 66
Figure 17: ADAM10 is overexpressed in glioblastoma multiforme tumours, but expression levels are not associated with an altered patient prognosis 67
Figure 18: Skin cutaneous melanoma patients exhibit increased ADAM10 gene expression, but high tumour expression is not associated with an adverse prognosis 69
Figure 19: Stomach adenocarcinoma patients exhibit an upregulation in ADAM10 gene expression, but high tumour expression does not affect overall survival 71
Figure 20: A slight differential expression of ADAM10 and Tspan15 is observed in breast cancer tumours and the probability of patient survival is negatively correlated with high ADAM10 tumour expression 72

Figure 21: Neither ADAM10 nor Tspan15 gene expression is significantly changed in lung squamous cell carcinoma tumours compared to control samples, but high ADAM10 tumour expression is associated with a worse prognosis. 74
Figure 22: Lung adenocarcinoma patients do not exhibit a differential expression of either ADAM10 or Tspan15 and patient prognosis is not affected by tumour expression 76
Figure 23: Multiple members of the ADAM and TspanC8 families are upregulated in pancreatic adenocarcinoma tumours 79
Figure 24: Pancreatic adenocarcinoma patient survival is affected by the high expression of multiple members of the ADAM and TspanC8 families 82

CHAPTER 4 ADAM10 AND TSPAN15 DO NOT REGULATE THE IN VITRO PROLIFERATION OR INVASION OF PANCREATIC CANCER CELL LINES

Figure 25: Generation and validation of PANC-1 and AsPC-1 ADAM10 and Tspan15 KO pools..... 91
Figure 26: Validation of PANC-1 and AsPC-1 ADAM10 and Tspan15 KO pools following purification with magnetic Dynabeads 94
Figure 27: Validation of PANC-1 and AsPC-1 cells overexpressing Tspan15. 97
Figure 28: The proliferation of PANC-1 and AsPC-1 cells is unaffected by ADAM10 or Tspan15 knockout, and Tspan15 overexpression..... 100
Figure 29: The invasive capabilities of PANC-1 and AsPC-1 cells are unaffected by the loss of ADAM10 or Tspan15..... 103
Figure 30: Tspan15 overexpression does not alter PANC-1 or AsPC-1 invasion through a Matrigel matrix 105

CHAPTER 5 TSPAN15 PROMOTES THE INVASION OF HEK-293T CELLS IN AN ADAM10-DEPENDENT MANNER VIA N-CADHERIN SHEDDING AND FGF RECEPTOR SIGNALLING

Figure 31: Validation of HEK-293T ADAM10 and Tspan15 KO pools 112
Figure 32: Morphological characterisation of ADAM10 and Tspan15 KO HEK-293T cells. 113
Figure 33: Loss of ADAM10 and Tspan15 does not affect the motility of HEK-293T cells..... 114
Figure 34: Validation of HEK-293T WT and ADAM10 KO cells overexpressing Tspan15 117
Figure 35: Morphological characterisation of HEK-293T cells overexpressing Tspan15 in the presence and absence of ADAM10 expression. 119
Figure 36: The overexpression of Tspan15 50-fold is associated with a striking clumping phenotype that is independent of ADAM10 expression 120
Figure 37: Elevated levels of Tspan15 expression affect how directly HEK-293T cells move but not their velocity..... 122
Figure 38: NF-κB signalling is not mediated by Tspan15 in HEK-293T cells 124
Figure 39: ADAM10 and Tspan15 do not regulate the 2D proliferation of HEK-293T cells 127
Figure 40: The proliferation of HEK-293T spheroids is not regulated by ADAM10 or Tspan15 129
Figure 41: ADAM10- and Tspan15-knockout HEK-293T cells exhibit impaired invasive capabilities... 131
Figure 42: Overexpression of Tspan15 in HEK-293T WT cells increases invasion..... 133

Figure 43: Overexpression of Tspan15 in the absence of ADAM10 surface expression does not alter the invasive capabilities of HEK-293T cells 135
Figure 44: N-cadherin (CDH2) shedding is significantly reduced in both ADAM10 and Tspan15 KO HEK-293T cells 137
Figure 45: The N-cadherin ectodomain increases the invasive capabilities of HEK-293T control and Tspan15 KO cells 139
Figure 46: The pro-invasive effect of the N-cadherin ectodomain requires FGFR activity 141
Figure 47: PD173074 reduces proliferation but not cell viability 143
Figure 48: FGF-mediated activation of MAPK/ERK signalling is not sustained by recombinant N-terminal N-cadherin 145
Figure 49: MAPK/ERK signalling is increased in HEK-293T cells overexpressing Tspan15 146
Figure 50: The invasive capabilities of HEK-293T cells are not impaired by treatment with Tspan15 mAbs 148
Figure 51: Tspan15 promotes the invasion of HEK-293T cells in an ADAM10-dependent manner ... 151

CHAPTER 6 INVESTIGATING THE ROLE OF TSPAN15 AND ADAM10 IN ACTIVATING NF-KB IN AN OESOPHAGEAL CARCINOMA CELL LINE

Figure 52: Tspan15 and ADAM10 are expressed on the surface of KYSE-30 cells. 155
Figure 53: ADAM10 but not βTrCP co-immunoprecipitates with Tspan15 in KYSE-30 cells. 158
Figure 54: NF-κB is predominantly localised within the cytoplasm of KYSE-30 cells 160
Figure 55: Generation and validation of KYSE-30 Tspan15 and ADAM10 KO pools 161
Figure 56: Validation of KYSE-30 Tspan15 and ADAM10 KO pools following purification with magnetic Dynabeads. 162
Figure 57: Validation of KYSE-30 Tspan15 and ADAM10 KO pools following purification by FACS 163

CHAPTER 7 GENERAL DISCUSSION

Figure 58: Proposed model of the mechanisms by which the Tspan15/ADAM10 complex promotes invasion. 171

APPENDIX

Figure A 1: pSpCas9(BB)-2A-Puro (PX459) V2.0 plasmid map 181
Figure A 2: pLVX-EF1α-IRES-Puro lentiviral transfer plasmid map 182

LIST OF TABLES

CHAPTER 2 MATERIALS AND METHODS

Table 1: Summary of antibodies 36
Table 2: List of CRISPR/Cas9 ADAM10 and Tspan15 guide oligos. 38
Table 3: Optimal puromycin concentration used for each cell line 39

APPENDIX

Table A 1: Summary of genes encoding identified proteins from hiSPECS analysis. 183

LIST OF ABBREVIATIONS

Aβ	Amyloid β
ADAM	A Disintegrin and Metalloprotease
ANOVA	Analysis of variance
APC	Adenomatous polyposis coli
APP	Amyloid precursor protein
ATP	Adenosine triphosphate
BSA	Bovine serum albumin
β-TrCP	Beta transducin repeat containing E3 ubiquitin protein ligase
B4GALT5	β-1,4-galactosyltransferase 5
CACHD1	Cache domain containing 1
CK1	Casein kinase 1
Cryo-EM	Cryo-electron microscopy
CTGF	Connective tissue growth factor
DMEM	Dulbecco's Modified Eagle medium
DNA	Deoxyribonucleic acid
DTT	Dithiothreitol
EDTA	Ethylenediaminetetraacetic acid
EGF	Epidermal growth factor
EGFR	Epidermal growth factor receptor
EMT	Epithelial-to-mesenchymal
ER	Endoplasmic reticulum
ERK	Extracellular signal-regulated kinases
EVs	Extracellular vesicles
FACS	Fluorescence-activated cell sorting
FBS	Fetal bovine serum
FGF	Fibroblast growth factor
FGFR	Fibroblast growth factor receptor
FITC	Fluorescein isothiocyanate
FZD4	Frizzled-4
GEPIA	Gene Expression Profiling Interactive Analysis
GSK-3β	Glycogen synthase kinase-3 beta
GTEx	Genotype-Tissue Expression
GPVI	Glycoprotein VI
HEK-293T	Human embryonic kidney cells expressing the simian virus 40 large T-antigen
hiSPECS	High-performance secretome protein enrichment with click sugars
HR	Hazards ratio
Ig	Immunoglobulin
KO	Knockout
LEF	Lymphoid enhancer factor
LEL	Large extracellular loop
mAb	Monoclonal antibody
MAPK	Mitogen-activaed protein kinase
MMP-9	Matrix metalloproteinase-9

NaCl	Sodium chloride
NaN_3	Sodium azide
NF-κB	Nuclear factor kappa B
NrCAM	Neuronal cell adhesion molecule
NSCLC	Non-small cell lung cancer
PAGE	Polyacrylamide gel electrophoresis
PBS	phosphate-buffered saline
PDB	Protein Data Bank
PEI	Polyethylenimine
PET	Polyester
PI3K	Phosphoinositide 3-kinasae
PMA	Phorbol myristate acetate
PRP^C	Cellular prion protein
PVDF	Polyvinylidene difluoride
RNA	Ribonucleic acid
RNA-seq	Ribonucleic acid sequencing
RPMI	Rowell Park Memorial Institute
SDS	Sodium dodecyl sulfate
SEL	Small extracellular loop
SH3	Src homology domain 3
SMALPs	Styrene-maleic acid lipid particles
SPECS	Secretome protein enrichment with click sugars
STED	Stimulated emission depletion
T-ALL	T-cell acute lymphoblastic leukaemia
TBS	Tris-buffered saline
TCF	T-cell factor
TCGA	The Cancer Genome Atlas
TEMs	Tetraspanin-enriched microdomains
TME	Tumour microenvironment
TPM	Transcripts per million
WT	Wild-type

CHAPTER 1 GENERAL INTRODUCTION

1.1 An overview of tumourigenesis and the hallmarks of cancer

Cancer is one of the leading causes of death worldwide (Sung et al., 2021). The transition of non-cancerous cells to a malignant state is a multi-step process involving the development of functional characteristics, commonly referred to as the hallmarks of cancer. These acquired capabilities include sustaining proliferation, avoiding growth suppression, evading immune destruction, attaining replicative immortality, activating the invasion-metastasis cascade, inducing angiogenesis, resisting apoptosis, deregulating cellular metabolism, and developing phenotypic plasticity (Figure 1) (Hanahan and Weinberg, 2000; Hanahan and Weinberg, 2011; Hanahan, 2022). While these core hallmarks are functionally distinct, a single oncogene can modulate the development of multiple malignant traits (Hanahan, 2022). For example, Notch has been shown to promote angiogenesis (Funahashi et al., 2008), proliferation (Palomero et al., 2006; Zhang et al., 2010), resistance to apoptosis (Zhang et al., 2010; Fassl et al., 2012), and changes in cellular energetics (Herranz et al., 2015). Fundamental to the development of these functional traits, and consequently tumourigenesis, are several other hallmarks; epigenetic reprogramming, tumour-promoting inflammation, polymorphic microbiomes, and genome instability are regarded as the enabling characteristics (Figure 1) (Hanahan and Weinberg, 2011; Hanahan, 2022). Additionally, the tumour microenvironment (TME), which is composed of stromal cells and extracellular matrix components, contributes to malignant progression via its interaction with cancer cells (Hanahan and Weinberg, 2011; Hanahan, 2022).

As the hallmarks of cancer are regarded as essential traits for tumour development and malignant progression, therapeutic targeting could have significant benefits for patient survival (Hanahan and Weinberg, 2011). However, although individual targeting of most of these pathways has improved patient survival, at least to some extent, resistance to therapy is a major issue; the suppression of certain hallmarks, such as angiogenesis, can ultimately result in the upregulation of other hallmarks

(Al-Bedeary et al., 2020). As such, an updated therapeutic strategy of co-targeting multiple hallmarks has been proposed (Hanahan and Weinberg, 2011).

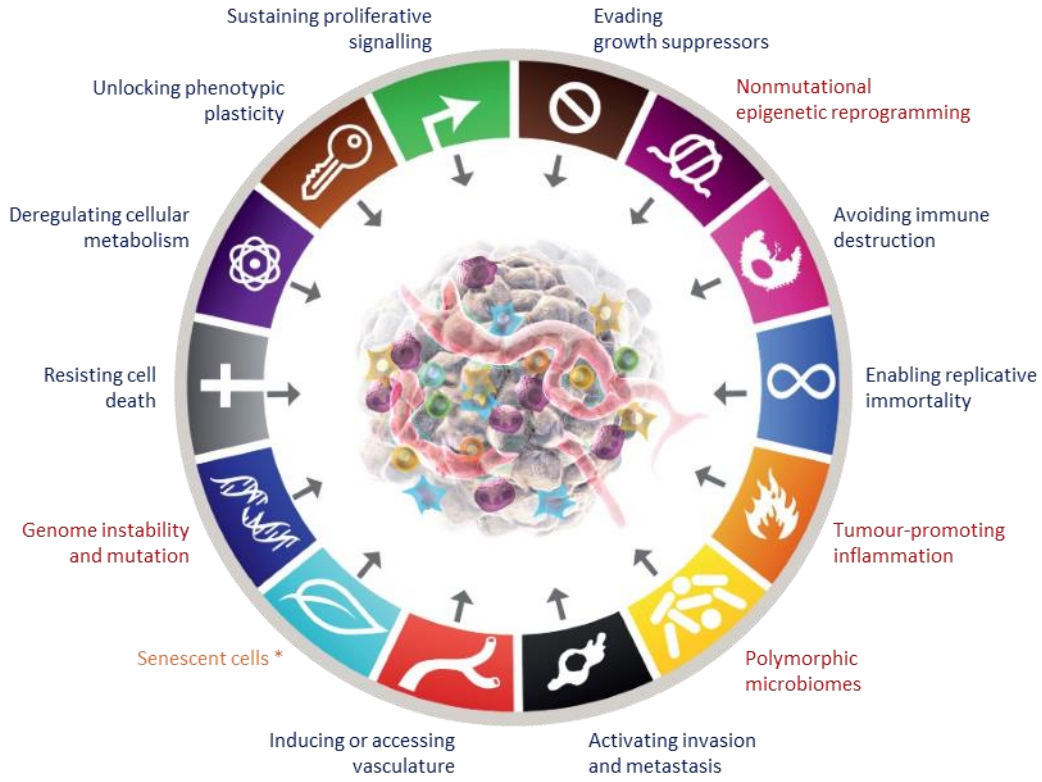


Figure 1: The hallmarks of cancer. The multistep process of tumourigenesis involves the development of functional (indicated in blue) and enabling (indicated in green) characteristics, often referred to as the hallmarks of cancer. Additionally, the tumour microenvironment, including stromal cells and their senescent derivatives (denoted in orange), plays a role in the acquisition of the core hallmarks. (Figure adapted from Hanahan, 2022).

1.1.1 Activating invasion in malignant progression

Invasion is an early step of the metastatic process (Talmadge and Fidler, 2010). Although a source of controversy over the years, it is now widely accepted that metastasis is predominantly facilitated by the epithelial-to-mesenchymal (EMT) transition, in which epithelial cells acquire an invasive, mesenchymal-like phenotype (Polyak and Weinberg, 2009; Thiery et al., 2009). A characteristic feature of EMT is the downregulation of epithelial (E)-cadherin expression and the associated increase in mesenchymal cadherins, often N-cadherin, in a process referred to as cadherin switching

(Cavallaro and Christofori, 2004; Wheelock et al., 2008; Mrozik et al., 2018). Indeed, the downregulation of E-cadherin mediates the transition to a mesenchymal morphology and promotes invasion (Vleminckx et al., 1991; Perl et al., 1998). Furthermore, the transfection of E-cadherin into highly invasive epithelial tumour cell lines has been shown to impair invasion (Vleminckx et al., 1991).

Regulation of the epithelial-to-mesenchymal transition is complex, with four interconnected networks playing a role; cadherin expression is modulated by transcriptional control, alternative splicing, non-coding RNAs, and post-translational modifications (De Craene and Berx, 2013). Several EMT-promoting transcription factors are thought to have a central role, including the SNAIL, ZEB, and TWIST families. Whilst some factors directly inhibit expression by binding to the promoter region of the E-cadherin gene, others act indirectly (Wheelock et al., 2008; Polyak and Weinberg, 2009; De Craene and Berx, 2013). Regardless, expression of these transcription factors is regulated by various signalling cascades, including TGFβ, Wnt, Notch, and NF-κB (Polyak and Weinberg, 2009; Loh et al., 2019). It has also been proposed that crosstalk between these signalling pathways results in positive feedback loops, which are responsible for stabilising the established mesenchymal phenotype (Polyak and Weinberg, 2009; Loh et al., 2019). Moreover, the ectodomain cleavage of cadherins by metalloproteases is an example of a post-translational modification that affects their expression (Lichtenthaler et al., 2018).

The downregulation of E-cadherin expression disrupts cell-cell junctions and thus facilitates local invasion (Wheelock et al., 2008). By comparison, N-cadherin upregulation is thought to promote metastasis via the modulation of various signalling pathways (Mrozik et al., 2018), which is covered in more detail in Section 1.6. Consequently, this switch between E-cadherin and N-cadherin expression has been associated with an adverse prognosis in multiple tumours (Gravdal et al., 2007; Araki et al., 2011; Lade-Keller et al., 2013; Aleskandarany et al., 2014; van der Heijden et al., 2020).

1.2 The a disintegrin and metalloprotease family

1.2.1 An overview of the a disintegrin and metalloprotease family

Ectodomain shedding, which involves the proteolytic cleavage of membrane protein extracellular domains proximal to the transmembrane region, is a regulatory post-translational modification that can have a major impact on cell function. In addition to downregulating protein expression, the release of a protein's soluble ectodomain can affect its functionality (Lichtenthaler et al., 2018). Examples include the existing functions of full-length adhesion proteins or receptors being terminated (Maretzky et al., 2005; Reiss et al., 2005; Lichtenthaler et al., 2018); the generation of soluble signalling factors, including ligands for the epidermal growth factor receptor (EGFR) (Sahin et al., 2004; Lichtenthaler et al., 2018); or the initiation of an intracellular signalling pathway, for instance, Notch signalling (van Tetering et al., 2009; Lichtenthaler et al., 2018).

This cleavage process is mediated by sheddases and of particular note is the a disintegrin and metalloprotease (ADAM) family, a conserved group of Zn^{2+}-dependent proteases (Weber and Saftig, 2012; Lichtenthaler et al., 2018). In humans, 12 catalytically active members (ADAM8, 9, 10, 12, 15, 17, 19, 20, 21, 28, 30, and 33) have been identified, in addition to 10 that are catalytically inactive and poorly characterised (Weber and Saftig, 2012; Lichtenthaler et al., 2018). Of these active sheddases, ADAM10 and ADAM17, which are ubiquitously expressed, are the best-characterised, with over 100 substrates each (Weber and Saftig, 2012; Lichtenthaler et al., 2018). ADAM10 is critical for embryonic development as the activator of Notch signalling (Hartmann et al., 2002; Jorissen et al., 2010; Chaimowitz et al., 2011; Weber et al., 2011b; Tsai et al., 2014; Mizuno et al., 2015; Zhuang et al., 2015). By comparison, ADAM17 has a major role in response to injury and infection via the cleavage of tumour necrosis factor α (TNFα) and EGFR ligands (Zunke and Rose-John, 2017). Although ADAM17 has also been proposed to cleave Notch (Brou et al., 2000; Mumm et al., 2000), ADAM17-knockout mice (Peschon et al., 1998), unlike mice depleted of ADAM10 (Hartmann et al., 2002), do

not exhibit phenotypes associated with a deficiency in Notch signalling (Huppert et al., 2000; Krebs et al., 2000).

ADAM family members play a critical role in health and disease, and as such their catalytic activity is tightly regulated, for example by partner proteins (Matthews et al., 2017a). ADAM10 is regulated by the six TspanC8 tetraspanins, which will be discussed further in Section 1.5.2 (Matthews et al., 2017a), whereas ADAM17 activity is mediated, in part, by two proteolytically inactive rhomboids, iRhom1 and iRhom2 (Matthews et al., 2017a; Düsterhöft et al., 2019).

1.3 The molecular scissor a disintegrin and metalloprotease 10 (ADAM10)

1.3.1 ADAM10 has a characteristic modular structure

ADAM10 is a single-pass transmembrane protein with a modular structure. The ectodomain consists of an N-terminal signal sequence, inhibitory prodomain, catalytic metalloprotease domain, disintegrin domain, cysteine-rich region, and membrane-proximal stalk. This is then followed by a transmembrane domain and cytoplasmic tail (Figure 2) (Edwards et al., 2008; Seegar et al., 2017; Harrison et al., 2021). Full-length ADAM10 (~100 kDa) is catalytically inactive, as the prodomain, which is important for the correct folding of the active site, has an autoinhibitory role (Anders et al., 2001; Wong et al., 2015). Indeed, a recombinant version selectively inhibits ADAM10 catalytic activity (Moss et al., 2007). Removal of the prodomain occurs in the Golgi and requires cleavage by proprotein convertases at two sites, one within the prodomain itself, and a second between the prodomain and catalytic domain. This generates the functional, mature form of ADAM10 (~70 kDa) by uncovering the catalytic site within the metalloprotease domain (Figure 2) (Anders et al., 2001; Wong et al., 2015).

In isolation, the ADAM10 ectodomain is visualised in a ‘closed’ conformation, with the cysteine-rich region partially occluding the active site of the metalloprotease domain (Seegar et al., 2017). This configuration results in further autoinhibition by restricting substrate access and thus prevents

uncontrolled sheddase activity. As such, in order for substrate shedding to occur, ADAM10 must undergo a conformational change (Seegar et al., 2017). In fact, the recent cryo-EM structure of ADAM10 in complex with Tspan15 reveals ADAM10 in an 'open' conformation, with the autoinhibition having been relieved (Lipper et al., 2023). It also shows the ADAM10 metalloprotease domain positioned close to the membrane for efficient substrate cleavage (Lipper et al., 2023). Interestingly though, substrates do not have a shared cut site, and instead, ADAM10 selectively cleaves transmembrane proteins upstream of a hydrophobic or aromatic residue (Caescu et al., 2009; Tucher et al., 2014; Seegar et al., 2017; Scharfenberg et al., 2020).

Functionally important motifs have also been identified within the cytoplasmic region of ADAM10 (Marcello et al., 2010; Ebsen et al., 2014), including two proline-rich regions, which act as binding sites for Src homology 3 (SH3) domain-containing proteins (Ebsen et al., 2014). As such, non-receptor tyrosine kinases and adaptor proteins can bind to the cytoplasmic tail of ADAM10 to regulate its trafficking to the membrane and/or interaction with the cytoskeleton (Ebsen et al., 2014). Additionally, an endoplasmic reticulum (ER)-retention motif, which is arginine-rich, is located at R722-724 and has an inhibitory role on ADAM10's exit from the ER. Truncation of the cytoplasmic tail resulting in the deletion of this sequence, as well as its mutation to AAA, results in strong surface expression. An RAR mutant is also sufficient for surface expression, unlike ARR and RRA mutants, suggesting that ^{723}R has the greatest inhibitory role on exit from the ER (Marcello et al., 2010).

ADAM10 has been visualised in a 1:1 heterodimer with Tspan15 (Lipper et al., 2023). However, there is evidence to suggest that ADAM10 monomers can dimerize via their cytoplasmic tails (Xu et al., 2012), with the structural support of an adjacent transmembrane domain (Deng et al., 2014).

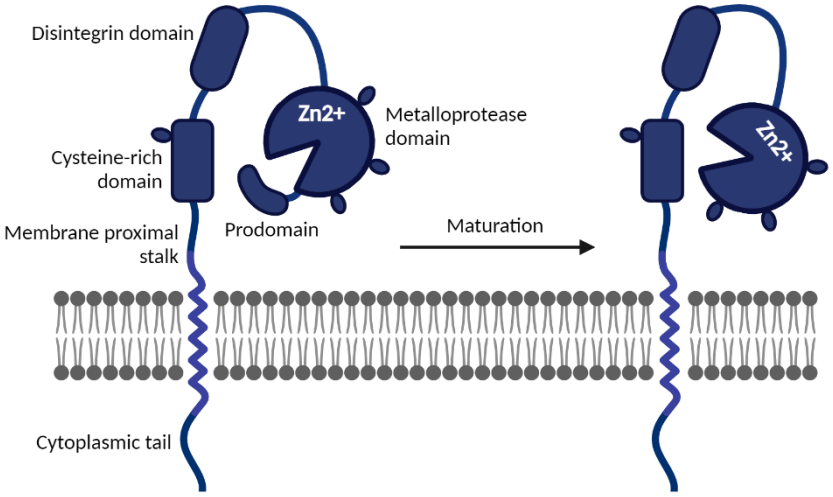


Figure 2: ADAM10 has a characteristic modular structure with a globular ectodomain. It is synthesised as a proenzyme with a prodomain occluding the Zn^{2+}-containing active site. Removal of this prodomain by furin and PC7 results in a mature, catalytically active protease. Sites of N-glycosylation are indicated by shaded ovals. (Figure created with Biorender.com).

1.3.2 ADAM10 is a sheddase with important roles in health and disease

ADAM10-deficient mice demonstrate the importance of ADAM10 in development. For example, ADAM10-knockout mice die at embryonic day 9.5 as a result of developmental defects in the central nervous and cardiovascular systems (Hartmann et al., 2002). As these phenotypes are similar to those observed in Notch1 and Notch4 double-knockout mice (Huppert et al., 2000; Krebs et al., 2000), ADAM10-mediated shedding of Notch is likely critical for development (Hartmann et al., 2002). Furthermore, tissue-specific conditional ADAM10-knockout mice have highlighted the importance of ADAM10 in the development of specific organ systems (Jorissen et al., 2010; Chaimowitz et al., 2011; Weber et al., 2011; Tsai et al., 2014; Mizuno et al., 2015; Zhuang et al., 2015). This role is predominantly associated with ADAM10-mediated activation of Notch signalling (Jorissen et al., 2010; Weber et al., 2011; Tsai et al., 2014; Mizuno et al., 2015; Zhuang et al., 2015), but the cleavage of other substrates has also been implicated (Jorissen et al., 2010).

ADAM10 is a major sheddase with other substrates including the amyloid precursor protein (APP) (Kuhn et al., 2010), the platelet glycoprotein VI (GPVI) (Gardiner et al., 2007), cadherins (Maretzky et al., 2005; Reiss et al., 2005; Schulz et al., 2008), the EGFR ligands epidermal growth factor (EGF) and betacellulin (Sahin et al., 2004), CD44 (Nagano et al., 2004), and the receptor for advanced glycation end products (RAGE) (Raucci et al., 2008). In some cases, ADAM10-mediated shedding has the potential to prevent disease progression (Harrison et al., 2021). The most notable example is APP shedding, which is thought to protect against the development of Alzheimer's disease (Postina et al., 2004; Kuhn et al., 2010; Manzine et al., 2019). ADAM10 cleaves APP within the amyloid β (Aβ) sequence releasing the ectodomain. This prevents the β- and γ-secretase-mediated generation of Aβ peptides, which are associated with the formation of pathogenic plaques (Postina et al., 2004; Manzine et al., 2019). Furthermore, late-onset Alzheimer's disease is associated with two missense mutations, Q170H and R181G, located within the ADAM10 prodomain. Due to folding defects associated with impaired chaperone functioning of the prodomain, these mutations decrease ADAM10-mediated shedding of APP and increase amyloid β levels, resulting in Alzheimer's disease-related pathology (Kim et al., 2009; Suh et al., 2013). ADAM10-directed cleavage of GPVI, which rapidly downregulates GPVI expression, may also suppress the onset of disease. Indeed, GPVI-depleted mice show reduced arterial thrombosis (Bender et al., 2011) and antibody targeting promotes the disaggregation of human thrombi (Ahmed et al., 2020). Furthermore, five deleterious ADAM10 mutations (three truncating, a splice site, and a missense) have been shown to underlie reticulate acropigmentation of Kitamura, a rare pigmentary disorder of the skin (Kono et al., 2013). However, it is worth noting that for this disease, the affected substrate shedding is yet to be determined. Nevertheless, therapeutic activation of ADAM10 activity has the potential to inhibit the progression of several diseases.

By comparison, ADAM10-mediated shedding can also promote disease and has been shown to have extensive pro-tumorigenic functions (Harrison et al., 2021). For example, the ectodomain cleavage of

cadherins mediates the progression of various tumours (Kohutek et al., 2009; Ma et al., 2016; Sépult et al., 2019; Yuan et al., 2020). In malignant pleural mesothelioma, a cancer primarily caused by asbestos exposure, ADAM10 expression is upregulated and promotes *in vivo* tumour progression, as well as *in vitro* migration and invasion (Sépult et al., 2019). ADAM10's pro-migratory role was linked to the shedding of N-cadherin, which was proposed to drive migration via the activation of fibroblast growth factor receptor (FGFR) signalling. Indeed, FGFR inhibition blocked the pro-migratory effects of the soluble N-terminal N-cadherin fragment (Sépult et al., 2019). Another example is non-small cell lung cancer (NSCLC) (Guo et al., 2012), which is the leading cause of cancer mortality worldwide (Sung et al., 2021); ADAM10 expression levels are increased in NSCLC patient tissues and associated with metastasis (Guo et al., 2012). Downregulation of ADAM10 *in vitro* also decreases the migration and invasion of a highly metastatic NSCLC cell line, likely due to impaired Notch1 activation (Guo et al., 2012). Finally, in contrast to its neuroprotective role in Alzheimer's disease, the proteolytic cleavage of APP by ADAM10 has also been shown to promote proliferation and invasion in breast cancer (Tsang et al., 2018), as well as the growth and survival of pancreatic cancer cell lines (Woods and Padmanabhan, 2013). As such, the consequences of ADAM10-mediated shedding are likely context-dependent.

Given the extensive role of ADAM10 in disease, it is regarded as an attractive therapeutic target. However, inhibition or activation without off-target effects is difficult due to its broad expression profile and extensive range of substrates (Wetzel et al., 2017; Smith et al., 2020). As such, future therapies will need to target ADAM10 in a cell type-, tissue-, or substrate-specific manner (Wetzel et al., 2017).

1.4 The tetraspanin family

1.4.1 An overview of the tetraspanin family

Tetraspanins are an evolutionarily conserved group of transmembrane proteins, with 33 being expressed in humans (Figure 3) (Charrin et al., 2014; Termini and Gillette, 2017). They have a characteristic structure composed of two extracellular loops, one small (SEL) and one large (LEL); four transmembrane domains; a small intracellular loop between the second and third transmembrane helices; and two short cytoplasmic tails at the N- and C- terminals (Charrin et al., 2014; Termini and Gillette, 2017) (Figure 4A). Within their large extracellular domain, the majority of tetraspanins have between four and eight paired cysteine residues, including two within a conserved Cys-Cys-Gly (CCG) motif. These residues form disulfide bridges, which are important for structure stabilisation (Stipp et al., 2003; Kovalenko et al., 2005; Charrin et al., 2014; Termini and Gillette, 2017). However, unlike most tetraspanins, peripherin 2 and ROM-1 have seven cysteine residues, three paired and a singular one. This unpaired cysteine residue facilitates the formation of homo- and hetero-oligomers between the two tetraspanins (Charrin et al., 2014).

The expression profiles of tetraspanins are distinct and related to function; whilst some tetraspanins are broadly expressed, others are expressed in a cell-type or tissue-specific manner (Termini and Gillette, 2017). Functionally, tetraspanins are key regulators of membrane organisation through the assembly of tetraspanin nanodomains, which typically contain a single member of the tetraspanin family and are non-randomly distributed; clusters of different tetraspanins tend not to overlap but are often positioned in close proximity to each other and to their partner proteins in the plasma membrane (Zuidscherwoude et al., 2015). The resulting compartmentalisation creates an environment in which tetraspanins can modulate the trafficking, lateral mobility, clustering, and signalling of their partner proteins (Charrin et al., 2014; Termini and Gillette, 2017; van Deventer et al., 2017). The functions of tetraspanins will be discussed in more detail in Section 1.4.3.

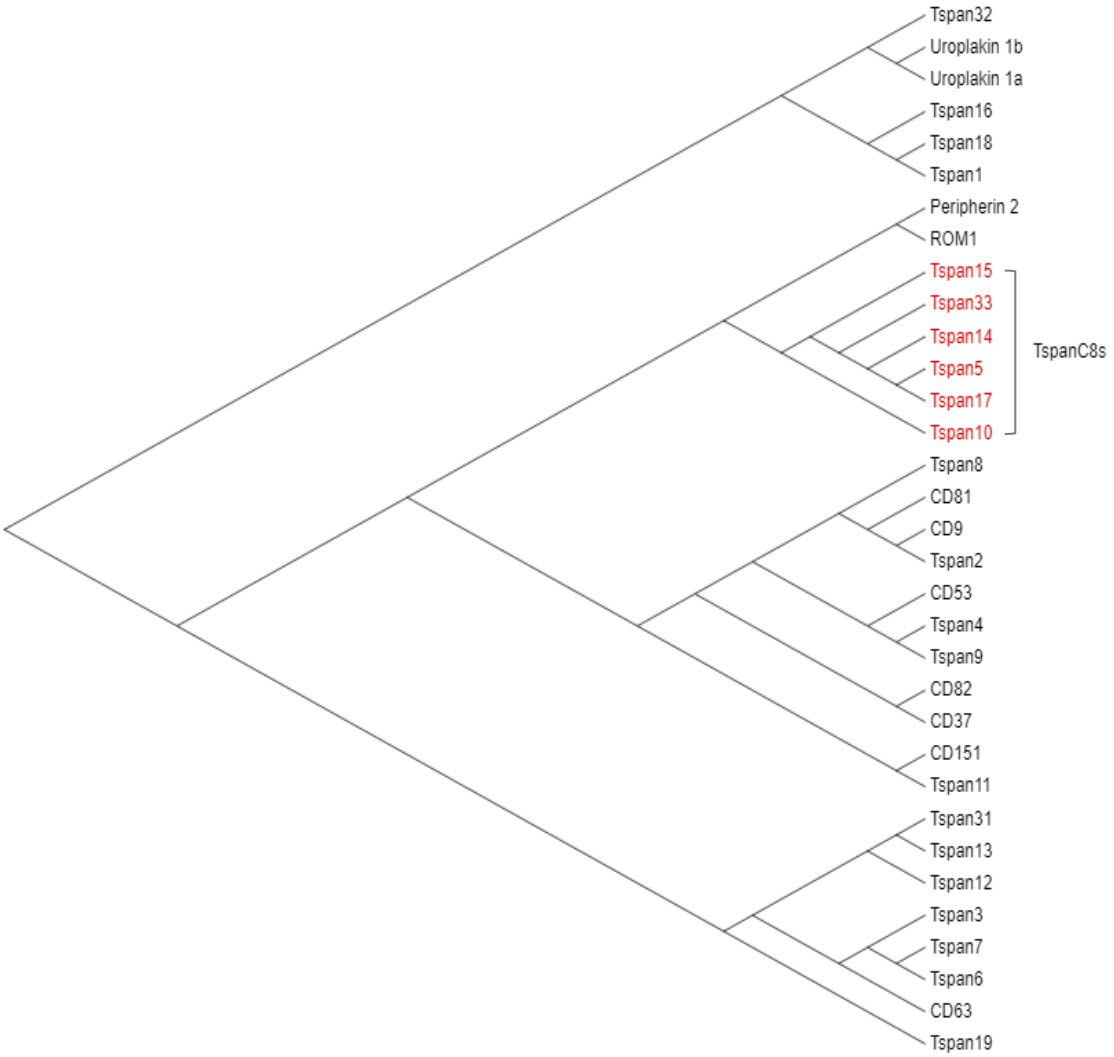


Figure 3: The tetraspanin family is an evolutionarily conserved group of transmembrane proteins, with 33 being expressed in humans. The relationships between the human tetraspanins are shown on this phylogenetic tree. Protein sequences were obtained from UniProt (Consortium, 2022) and aligned using Clustal Omega (Madeira et al., 2022). The phylogenetic tree was then created from these alignments on the same platform (Madeira et al., 2022) and visualised using the Interactive Tree of Life web-based tool (Letunic and Bork, 2021).

1.4.2 Tetraspanins have a characteristic four-transmembrane structure and can exist in different conformations

The large extracellular loop of tetraspanins, which often exhibits N-linked glycosylation (Figure 4A), has been the focus of many structural studies (Stipp et al., 2003); an X-ray crystal structure of the human CD81 large extracellular loop was the first of any tetraspanin domain characterised (Kitadokoro et al., 2001). It is subdivided into two regions: a conserved one, which is formed from

three helices (A, B, and E), and a variable one that connects the B and E helices (Kitadokoro et al., 2001; Stipp et al., 2003; Termini and Gillette, 2017; Susa et al., 2024). Structurally, the variable region differs substantially between tetraspanins, with four representative tetraspanins (CD9, CD81, CD151, and Tspan7) having an average sequence identity of 6.7% (Stipp et al., 2003). Indeed, in CD81 this region consists of two helices (C and D) (Kitadokoro et al., 2001; Zimmerman et al., 2016), whereas C and D adopt a more loop-like configuration in CD9 (Oosterheert et al., 2020). Furthermore, Tspan15 by comparison has a larger variable region, which is composed of loops as well as some helical regions (Lipper et al., 2022).

The first crystal structure of a full-length tetraspanin, human CD81, was reported in 2016. It revealed a cone-like configuration in which two pairs of helices, TM1/TM2 and TM3/TM4, converge at the inner membrane to create an intramembrane cavity, which is capped by the large extracellular loop (Figure 4B) (Zimmerman et al., 2016). Cholesterol was found bound within this pocket and was required for CD81 to adopt a 'closed' conformation. Indeed, molecular dynamics simulations revealed an 'open' conformation in the absence of cholesterol; the LEL separated from TM1/TM2 and extended upwards (Zimmerman et al., 2016). This extended, cholesterol-free conformation is also visualised in the cryo-electron microscopy (cryo-EM) structure of CD81 in complex with CD19 (Figure 4B), indicating that interaction with this binding partner causes a conformational change (Susa et al., 2021).

The crystal structures of two additional full-length tetraspanins, CD9 and CD53, have since been resolved (Umeda et al., 2020; Yang et al., 2020). Similar to CD81 (Zimmerman et al., 2016), the transmembrane domains adopt a cone-like configuration (Figure 4B) (Umeda et al., 2020; Yang et al., 2020), suggesting that this structure is likely conserved between tetraspanins. Interestingly, the small extracellular loop was visualised for the first time, showing that it is not a structurally disordered domain (Umeda et al., 2020; Yang et al., 2020) as was proposed by Zimmerman et al. (2016). In CD9, the SEL interacted with the LEL to cap the intramembrane space, resulting in a 'closed' conformation

similar to CD81 (Figure 4B). However, MD simulations predicted that the two extracellular loops exhibited conformational flexibility, with CD9 shown to spontaneously transition between a 'closed', 'open' and 'semi-open' shape (Umeda et al., 2020). By comparison, CD53 was captured in an 'open' conformation; the LEL rotates upwards, away from the membrane, and is structurally supported by the SEL (Figure 4B) (Yang et al., 2020).

The intramembrane cavity of the CD9 and CD53 structures contained monoolein, a lipid used in the crystallisation process, which supports the hypothesis of lipid binding (Umeda et al., 2020; Yang et al., 2020). However, molecular simulations suggest that cholesterol is unlikely to mediate transitions between the 'closed' and 'open' conformations (Umeda et al., 2020; Yang et al., 2020). Instead, it was proposed that lipids may stabilise the structure of the transmembrane domain (Yang et al., 2020). Given that cholesterol has been shown to modulate tetraspanin function (Charrin et al., 2003; Silvie et al., 2006; Zimmerman et al., 2016; Huang et al., 2020; Palor et al., 2020), the role of the lipid-binding cavity in different tetraspanins requires further characterisation.

In addition to the CD81/CD19 complex, three further cryo-EM tetraspanin/partner protein structures have been reported, including CD9 with EWI-F (Oosterheert et al., 2020) or EWI-2 (Umeda et al., 2020), and Tspan15 with ADAM10 (Lipper et al., 2023). CD9 exhibits a hetero-tetrameric arrangement with EWI; a central EWI dimer is bound on either side by a CD9 molecule (Oosterheert et al., 2020; Umeda et al., 2020). In both complexes, CD9 adopts an 'open' conformation with the LEL rotated upwards (Oosterheert et al., 2020; Umeda et al., 2020), similar to the structure of CD81 in complex with CD19 (Zimmerman et al., 2016). In contrast, Tspan15 adopts a 'closed' configuration in complex with ADAM10 (Lipper et al., 2023), suggesting that tetraspanin family members bind to their partners in different ways. It is worth noting that although the Tspan15/ADAM10 complex was resolved at 3.3 Å (Lipper et al., 2023), the structures of CD9 in complex with EWI-F or EWI-2 were relatively low resolution (Oosterheert et al., 2020; Umeda et al., 2020).

The cytoplasmic domain of tetraspanins is highly divergent; the average shared sequence identity is between 21 and 38%, with the exact similarity varying between the two intracellular tails and the cytoplasmic loop (Stipp et al., 2003). The N- and C-terminal tails can interact directly or indirectly with intracellular proteins; different tetraspanins have been shown to exhibit specific interactions (Stipp et al., 2003). For example, the adaptor protein syntenin-1 interacts with CD63 (Latysheva et al., 2006); phosphatidylinositol-4-kinase with CD9, CD63, CD81, and CD151 (Yauch et al., 1998; Yauch and Hemler, 2000); and the cytoskeletal protein α-actinin-1 with CD81 (Gordón-Alonso et al., 2012). Furthermore, palmitoylation of intracellular cysteine residues, which was visualised in the CD9 crystal structure (Yang et al., 2020), contributes to interactions with other proteins (Berditchevski et al., 2002; Charrin et al., 2002; Yang et al., 2002). Indeed, mutation of the CD151 palmitoylation sites has been shown to impair its association with α3β1 integrin (Berditchevski et al., 2002), as well as CD9 and CD63 (Yang et al., 2002). However, it is important to note that cells in the latter study were lysed in 1% Brij-96, a relatively low-stringency lysis buffer (Yang et al., 2002), and as such the identified proteins likely interact with CD151 indirectly. Indeed, there is no evidence to suggest that CD151 binds to CD9 or CD63 directly.

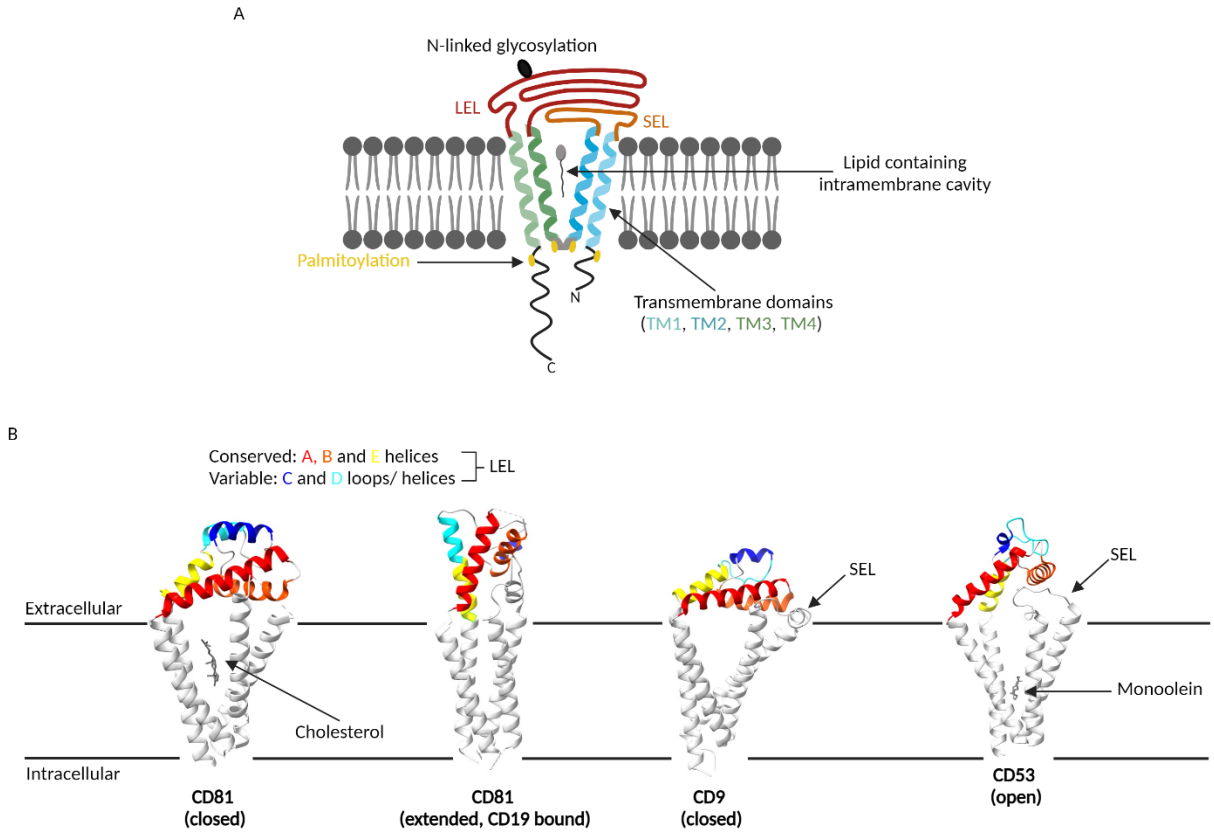


Figure 4: Tetraspanins have a cone-like structure that can exist in 'closed', 'open', and 'extended' conformations. (A) Schematic representation of a tetraspanin showing the main structural domains and post-translational modifications. (B) The crystal structures of three distinct full-length tetraspanins: CD81 (Protein Data Bank (PDB) ID: 5TCX) (Zimmerman et al., 2016), the CD81/CD19 complex (PDB ID: 7JIC) (Susa et al., 2021), CD9 (PDB ID: 6K4J) (Umeda et al., 2020), and CD53 (PDB ID: 6WVG) (Yang et al., 2020). (Figure adapted from Koo, 2021 and created with Biorender.com)

1.4.3 Tetraspanins interact with and regulate specific partner proteins

1.4.3.1 Tetraspanins form nanodomains with their associated partner proteins

Tetraspanins were thought to mediate membrane protein organisation through the formation of tetraspanin-enriched microdomains (TEMs), as determined from biochemical experiments (Berditchevski et al., 1996; Le Naour et al., 2006; Charrin et al., 2009; van Deventer et al., 2021). However, single-molecule imaging of four tetraspanins (CD37, CD53, CD81, and CD82) characterised the spatiotemporal organisation of tetraspanin domains, revealing organisation on a nanoscale (Zuidscherwoude et al., 2015). As such, the concept of TEMs has been updated to tetraspanin

nanodomains to reflect these findings (van Deventer et al., 2021). Tetraspanins have now been shown to form distinct nanoclusters, which are ~120 nm in diameter and are predicted to contain less than ten molecules of the same tetraspanin (Zuidscherwoude et al., 2015). Although tetraspanin nanodomains are predominantly formed of tetraspanin homo-oligomers and their associated partner proteins, with minimal overlap between different tetraspanins, their positioning relative to clusters of different tetraspanins is non-random. As such, it was proposed that weak heterotypic interactions between tetraspanins in adjacent nanodomains may result in a dynamic 'tetraspanin web' (Zuidscherwoude et al., 2015). The precise arrangement of tetraspanins and their partner proteins within nanodomains can also differ. CD81 nanoclusters, for example, have an enrichment of CD19 at the edges (Zuidscherwoude et al., 2015; van Deventer et al., 2021), whereas neuroligin-1, a postsynaptic adhesion molecule, is incorporated into the middle of Tspan5-specific nanodomains (Moretto et al., 2019; van Deventer et al., 2021). By contrast, CD9 and EWI-F have a linear arrangement in which tetraspanin-partner protein dimers are arranged into tetramers, with two central EWI-F molecules (Oosterheert et al., 2020). It is tempting to speculate that these different organisational models may have functional relevance associated with the distinct clustering patterns.

1.4.3.2 Tetraspanins modulate the function of their partner proteins

Tetraspanins are key regulators of vital cellular processes due to their modulation of partner protein function (Charrin et al., 2014). This regulatory role is well-characterised, with tetraspanin deficiency impairing the functionality of their associated partner proteins. There are several notable disease-related examples in humans, including CD81 with the B-cell co-receptor CD19, CD151 with the laminin-binding integrins, and Tspan12 with the Wnt/Norrin receptor Frizzled-4 (FZD4).

Tetraspanin CD81 and Ig superfamily member CD19 are two subunits of the B cell co-receptor, of which CD21 and CD225 are also components (Susa et al., 2020). The transport of CD19 to the surface of B cells is mediated by its interaction with the CD81 LEL. This interaction is dynamic with CD19

dissociating following B cell activation, which is thought to mediate signalling (Mattila et al., 2013; Susa et al., 2020). A patient with a homozygous splice mutation in CD81 presented with a complete loss of CD19 on the surface of B cells and a resultant antibody deficiency disorder (van Zelm et al., 2010), highlighting the significance of the interaction between CD81 and CD19.

CD151 forms complexes with the laminin-binding integrins and mediates their functionality with regard to adhesion, migration, and signalling (Berditchevski et al., 2002; Kazarov et al., 2002; Sterk et al., 2002; Lammerding et al., 2003; Yamada et al., 2008). The importance of this interaction is demonstrated in three patients with a CD151 deficiency resulting from a frameshift mutation associated with protein truncation. Although the related symptoms were broad, including end-stage kidney disease, skin lesions, and deafness, they were linked to the requirement of laminin-binding integrins to assemble and maintain kidney and skin basement membranes (Karamatic Crew et al., 2004). It has also been shown that CD151-deficient mice similarly exhibit kidney failure, as do those with a deficiency in the α3 integrin (Sachs et al., 2006).

Tspan12 interacts with Frizzled-4 (FZD4) to promote its multimerization and initiate downstream signalling within the Norrin-β-catenin pathway, which is important in retinal vascularisation (Junge et al., 2009). Consequently, various mutations in Tspan12 and FZD4 have been implicated in familial exudative vitreoretinopathy, a disease characterised by abnormal vascularisation of the retina (Nikopoulos et al., 2010; Poulter et al., 2010; Poulter et al., 2012). Interestingly, an agonist for FZD4-LRP5, which promotes downstream signalling, restores retinal angiogenesis in Tspan12 KO mice during development (Zhang et al., 2023).

1.5 The TspanC8 tetraspanins

1.5.1 An overview of the TspanC8 tetraspanins

Six tetraspanins (Tspan5, Tspan10, Tspan14, Tspan15, Tspan17, and Tspan33), referred to as the TspanC8 subgroup, directly interact with ADAM10 via their extracellular region (Dornier et al., 2012;

Haining et al., 2012; Noy et al., 2016; Lipper et al., 2023). These tetraspanins have eight conserved cysteine residues within their large extracellular loop and are relatively highly conserved at the amino acid level (Figure 3) (Dornier et al., 2012; Haining et al., 2012; Matthews et al., 2017b). The most closely related TspanC8s, Tspan5 and Tspan17, share 78% sequence identity, while Tspan10 and Tspan15 are the most divergent with a shared sequence identity of 26%. Interestingly, despite high variability within the extracellular region between tetraspanin family members in general, this region is well conserved between the TspanC8s (Matthews et al., 2017b), consistent with the finding that the extracellular region is important for their interaction with ADAM10 (Noy et al., 2016; Lipper et al., 2023). However, the TspanC8 cytoplasmic tails are comparatively divergent; the average sequence identity across the subgroup is 25% for the N-terminal tail and 27% for the C-terminal tail. This is also likely an underrepresentation of variability, as it doesn't account for the considerable differences in length (Matthews et al., 2017b). Given the role of tetraspanin tails in interacting with intracellular proteins (Stipp et al., 2003; Berditchevski and Odintsova, 2007), it is tempting to speculate that this sequence variability enables the TspanC8s to interact with a range of different proteins.

Although the expression of each TspanC8 varies between different tissues and cell types (Matthews et al., 2017b; Matthews et al., 2018; Harrison et al., 2021), all six TspanC8s play an important role in regulating ADAM10, which will be detailed in Section 1.5.2.

1.5.2 ADAM10-dependent functions of the TspanC8 tetraspanins

1.5.2.1 The TspanC8 tetraspanins are required for the maturation and expression of ADAM10

The TspanC8 tetraspanins promote ADAM10 exit from the endoplasmic reticulum and its subsequent trafficking to the Golgi apparatus where it undergoes maturation (Figure 5) (Dornier et al., 2012; Haining et al., 2012; Prox et al., 2012). Catalytically active ADAM10 is then targeted for the plasma membrane or late endosomes, depending on the TspanC8 it is in complex with (Figure 5) (Dornier et

al., 2012). The importance of the TspanC8s for ADAM10 expression has also been shown *in vivo* (Haining et al., 2012; Seipold et al., 2018), with a reduction in ADAM10 expression observed in mice deficient in Tspan15 (Seipold et al., 2018) or Tspan33 (Haining et al., 2012). ADAM10 has similarly been shown to play a role in the expression of Tspan5 (Saint-Pol et al., 2017a) and Tspan15 (Koo et al., 2020), demonstrating a reciprocal relationship. It is likely that this relationship extends to other members of the TspanC8 family, but confirmation is limited by the lack of available antibodies.

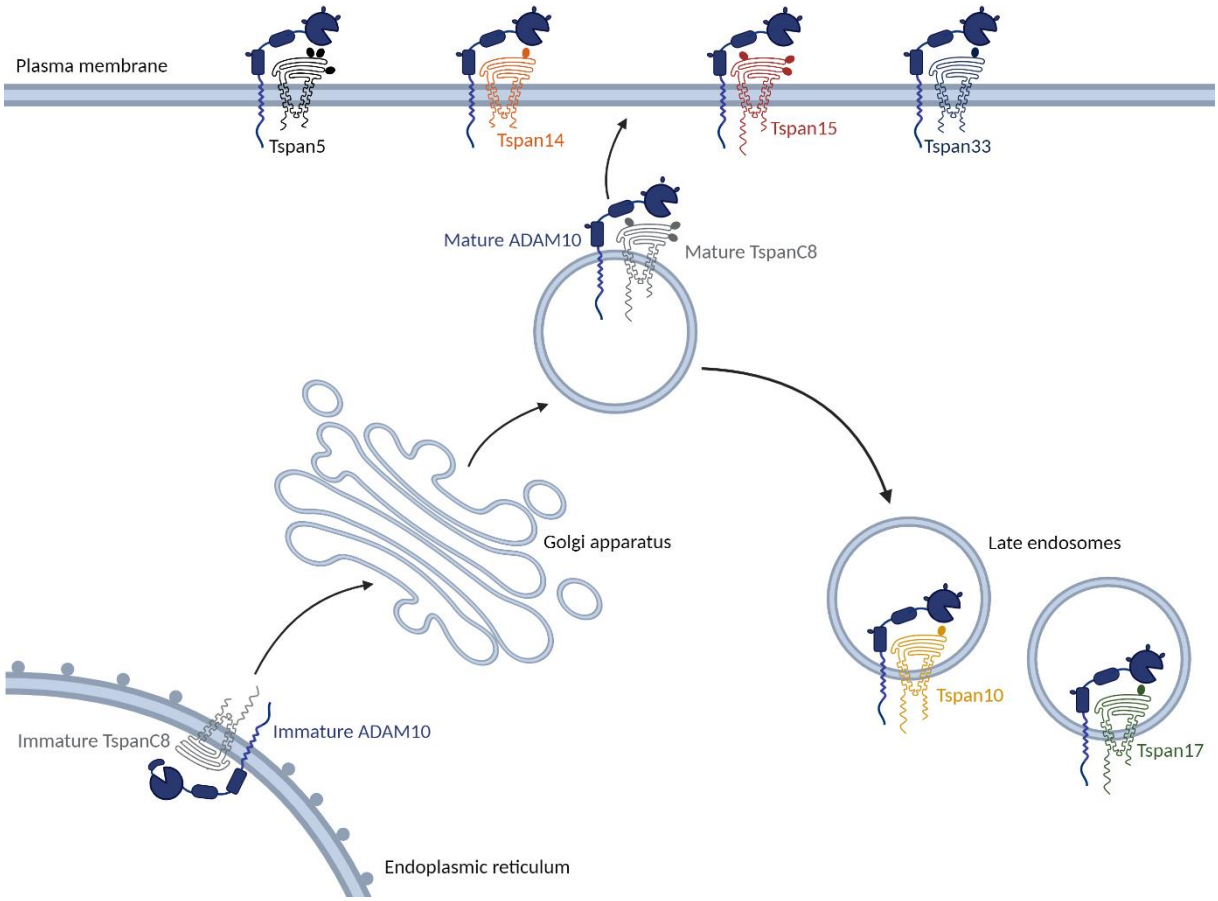


Figure 5: ADAM10's maturation, expression, and subcellular localisation are regulated by the TspanC8s. The TspanC8 tetraspanins promote ADAM10 exit from the endoplasmic reticulum, its maturation in the Golgi apparatus, and subsequent trafficking. Whilst four TspanC8s (Tspan5, Tspan14, Tspan15, and Tspan33) promote ADAM10 expression at the cell surface, Tspan10 and Tspan17 preferentially traffic ADAM10 to late endosomes. (Figure adapted from Harrison et al. 2021 and created with BioRender.com).

1.5.2.2 ADAM10 substrate shedding is differentially controlled by the TspanC8s – the 'six scissor' hypothesis

The TspanC8s have also been shown to differentially control ADAM10 substrate specificity, ultimately resulting in six different 'molecular scissors' with distinct substrate profiles (Jouannet et al., 2016; Noy et al., 2016; Matthews et al., 2018). For example, Tspan15 has been shown to regulate ADAM10-mediated cleavage of N-cadherin both *in vitro* and *in vivo* (Figure 6) (Prox et al., 2012; Jouannet et al., 2016; Noy et al., 2016; Seipold et al., 2018; Hiroshima et al., 2019; Szyroka, 2019; Lipper et al., 2022; Lipper et al., 2023). Indeed, Tspan15-knockout mice exhibit significantly reduced N-cadherin shedding in the brain (Seipold et al., 2018). The Tspan15/ADAM10 complex has also been shown to cleave platelet glycoprotein (GP) VI (Noy et al., 2016; Matthews, 2019; Szyroka, 2019; Koo et al., 2022), betacellulin (Koo et al., 2020), E-cadherin (Szyroka, 2019), VE-cadherin (Haining et al., 2012; Szyroka, 2019), cellular prion protein (PRP^C) (Seipold et al., 2018), EGF (Tomlinson lab, unpublished data), and RAGE (Tomlinson lab, unpublished data). It is worth noting that although Tspan15/ADAM10 is the dominant GPVI scissor in transfected HEK-293T cells, Tspan33/ADAM10 can also mediate cleavage; the knockout of both Tspan15 and Tspan33 is required to completely abolish GPVI cleavage in HEK-293T and HEL cells (Koo et al., 2022).

Tspan5 and Tspan14 have been implicated in ADAM10-mediated ligand-dependent activation of Notch1 (Figure 6) (Dornier et al., 2012; Jouannet et al., 2016; Saint-Pol et al., 2017a; Eschenbrenner et al., 2020; Xie et al., 2021); the knockdown and overexpression of the TspanC8s reveals that Tspan5 and Tspan14 promote Notch signalling, whereas Tspan15 and Tspan33 act as inhibitors (Dornier et al., 2012; Jouannet et al., 2016; Xie et al., 2021). Tspan5 and Tspan14 likely exhibit functional redundancy. Indeed, the downregulation of both Tspan5 and Tspan14 impairs Notch signalling greater than the knockdown of either TspanC8 in isolation (Dornier et al., 2012; Saint-Pol et al., 2017a). Moreover, the inhibitory effect of Tspan5 antibodies on Notch signalling is further increased in cells depleted of Tspan14 (Saint-Pol et al., 2017a).

By comparison, the TspanC8/ADAM10 scissors involved in the shedding of some substrates remain unclear, despite investigation. Of particular note is APP; different studies reveal varying roles for the TspanC8s, depending on the cell type and validation method used (Prox et al., 2012; Jouannet et al., 2016; Seipold et al., 2018; Brummer et al., 2019). For example, the overexpression of Tspan15 was shown to increase APP cleavage in neuro 2A mouse neuroblastoma cells (Prox et al., 2012), but has the opposite effect in HEK-293 (Brummer et al., 2019) and U2OS-N1 cells (Jouannet et al., 2016). The overexpression of Tspan14 and Tspan33 also decreased APP shedding in the U2OS-N1 cells, unlike the overexpression of Tspan5, which had no effect (Jouannet et al., 2016). Furthermore, the downregulation of Tspan15 expression slightly impaired shedding in a human prostate cancer cell line (Jouannet et al., 2016), in contrast to mouse brains where no effect was observed (Seipold et al., 2018). Taking the mouse model data together with the finding that Tspan15 is upregulated in the brains of Alzheimer's patients (Seipold et al., 2018), it is tempting to speculate that Tspan15 likely does not mediate ADAM10's neuroprotective shedding of APP. However, further investigation is still required to characterise the TspanC8/ADAM10 scissor responsible for APP cleavage.

It is important to note that although ADAM10 is involved in the ectodomain shedding of over 100 substrates, the involvement of specific TspanC8s has only been characterised for a small number of these. Future studies should aim to address this, as specific TspanC8s could be therapeutically targeted to reduce the potential off-target effects associated with treating ADAM10 directly (Smith et al., 2020).

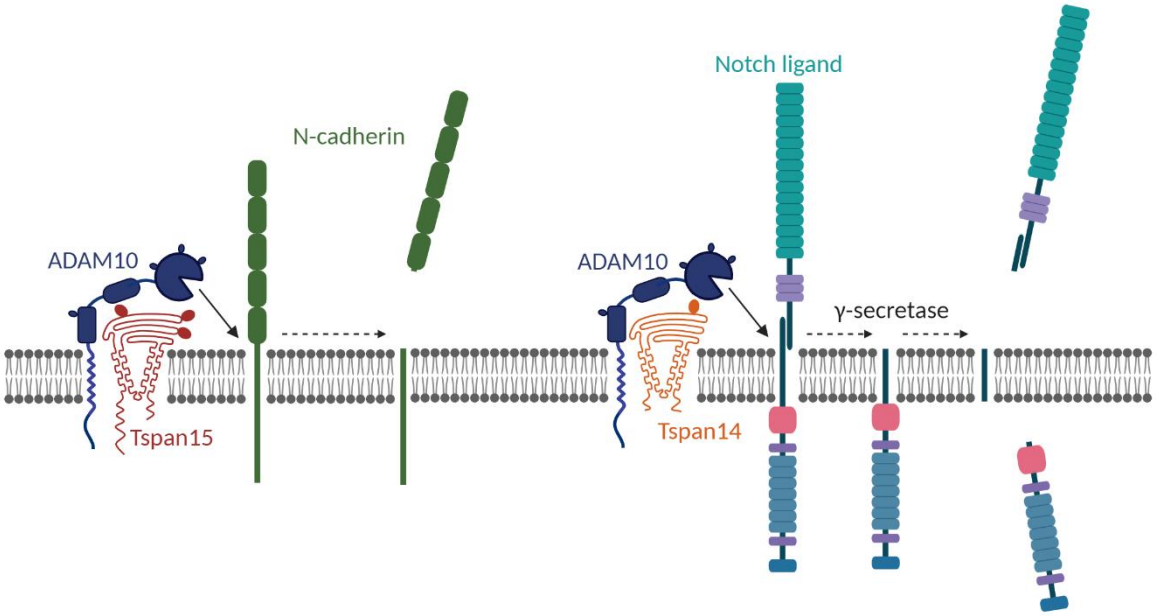


Figure 6: The 'six scissor' hypothesis. The TspanC8s differentially control the specificity of ADAM10 substrate shedding. Whilst Tspan15/ADAM10 cleaves N-cadherin, Tspan14 directs ADAM10-mediated activation of Notch. (Figure created with Biorender.com).

1.5.2.2.1 Potential mechanisms underlying TspanC8/ADAM10 substrate specificity

1.5.2.2.1.1 The TspanC8s regulate the subcellular localisation and dynamics of ADAM10

The TspanC8 tetraspanins have been shown to differentially regulate the subcellular localisation of ADAM10 in multiple cell lines. Initial evidence for this regulatory role came from HeLa cells transfected with GFP-tagged TspanC8s (Dornier et al., 2012). This study showed that ADAM10 surface expression was promoted by the overexpression of Tspan5, Tspan14, Tspan15, or Tspan33; ADAM10 co-localised with these transfected TspanC8s inside the cells and at the cell surface (Figure 5). However, overexpressed Tspan10 and Tspan17 were found to preferentially direct ADAM10 to late endosomes, and as such did not considerably affect its cell surface expression (Figure 5) (Dornier et al., 2012). By comparison, imaging studies revealed that overexpressed Tspan15 and Tspa33 were the only TspanC8s strongly localised to the plasma membrane in mouse kidney cells, with ADAM10 being directed to lateral and apical junctions respectively (Shah et al., 2018). Furthermore, the overexpression of untagged Tspan15, unlike Tspan5, increases ADAM10 surface expression in U2OS

cells (Eschenbrenner et al., 2020). Endogenous Tspan15 also similarly affects ADAM10 localisation (Eschenbrenner et al., 2020; Koo et al., 2020). Although the precise localisation of TspanC8/ADAM10 complexes appears to be cell line-dependent, it remains tempting to speculate that these differences in subcellular localisation may affect substrate specificity by mediating proximity.

Differential regulation of ADAM10 cellular dynamics may also mediate TspanC8/ADAM10 substrate specificity. Indeed, Tspan5 and Tspan15 have opposing effects on ADAM10 endocytosis; Tspan15 better stabilises ADAM10 at the cell surface and reduces endocytosis, whereas Tspan5 promotes ADAM10 endocytosis (Eschenbrenner et al., 2020). Additionally, Tspan15 overexpression, unlike the overexpression of Tspan5, increases the lateral diffusion of ADAM10 (Jouannet et al., 2016).

1.5.2.2.1.2 ADAM10 exists in different conformations depending on the TspanC8 it's in complex with

It has also been proposed that the TspanC8s may differentially modulate the conformation of ADAM10 as a mechanism to regulate substrate specificity. Initial insights for this hypothesis came from co-immunoprecipitation experiments showing that TspanC8s differentially bind to ADAM10 (Noy et al., 2016). Whilst the stalk region of ADAM10 was shown to be sufficient to mediate an interaction with Tspan15, the cysteine-rich region was also required by the other TspanC8s. Furthermore, the disintegrin domain did not improve these interactions and, for Tspan17, had an inhibitory effect (Noy et al., 2016). However, the most striking evidence comes from a recent study that presents the cryo-EM structure of ADAM10 in complex with Tspan15 (Lipper et al., 2023). This structure reveals ADAM10 positioned in an open conformation by Tspan15 (Lipper et al., 2023), a shift from the closed, autoinhibited shape of unbound ADAM10 (Seegar et al., 2017). The large extracellular loop of Tspan15 interacts with ADAM10 at two interfaces, with the first point of contact mediating complex formation (Lipper et al., 2023). This interface is conserved between the TspanC8s, with several conserved motifs required for their interaction with the cysteine-rich region of ADAM10 (Noy et al., 2016; Saint-Pol et al., 2017a; Lipper et al., 2022; Lipper et al., 2023). By comparison, the

residues at the second point of contact, which occurs between the TspanC8 and the ADAM10 metalloprotease domain, vary between the TspanC8s. Although this point of contact is not required for complex formation (Noy et al., 2016), it appears to play an important role in positioning the ADAM10 active site for substrate cleavage (Lipper et al., 2023). Tspan15 positions the catalytic site of ADAM10 ~20 Å from the membrane surface, a distance that would promote cleavage ~10 residues from the membrane (Lipper et al., 2023). In line with this, Tspan15/ADAM10 scissors have been shown to selectively cleave N-cadherin (Uemura et al., 2006; Harrison et al., 2021; Lipper et al., 2023), GPVI (Gardiner et al., 2007; Lipper et al., 2023), and RAGE (Braley et al., 2016; Koo, 2021) at a site that is 10 or 11 amino acids from the plasma membrane. N-cadherin mutation studies have also shown that shifting the cleavage site 4 residues closer to the membrane abolishes Tspan15/ADAM10-mediated shedding (Lipper et al., 2023). In contrast, Tspan5 and Tspan14 promote Notch1 shedding between residues Ala^{1710} and Val^{1711}, 15 residues from the membrane (Mumm et al., 2000; van Tetering et al., 2009; Harrison et al., 2021), suggesting that Tspan5/ADAM10 and Tspan14/ADAM10 may preferentially cleave substrates with higher cut sites. The significance of the second contact interface in substrate specificity is further highlighted using Tspan15-Tspan5 and Tspan15-Tspan14 chimeras. Exchanging the sequences required for the interaction with the ADAM10 metalloprotease domain impairs the cleavage of WT N-cadherin, but increases the cleavage of N-cadherin with a four-residue insertion below the normal cut site (Lipper et al., 2023). Similarly, Tspan15-Tspan14 chimeras in which the Tspan15 extracellular domain is replaced by that of Tspan14 are unable to cleave GPVI (Koo et al., 2022).

Taken together, these studies suggest that the TspanC8s may differentially interact with the ADAM10 metalloprotease domain, modulating the position of the active site relative to the plasma membrane, and as such controlling substrate specificity. However, cryo-EM structures of the other TspanC8/ADAM10 complexes are now required to further validate this ‘molecular ruler’ concept.

1.5.3 Other functions of the TspanC8 tetraspanins

1.5.3.1 Tspan15 promotes the nuclear translocation of NF-κB

In oesophageal squamous cell carcinoma cell lines, Tspan15 positively regulates NF-κB signalling (Zhang et al., 2018). Mechanistically, Tspan15 co-immunoprecipitates with beta-transducin repeat containing E3 ubiquitin protein ligase (β-TrCP), promoting the ubiquitin-mediated degradation of phosphorylated IκB, an inhibitor that sequesters NF-κB in the cytoplasm; NF-κB is a heterodimer composed of p50 and p65. This enables the nuclear translocation of the NF-κB complex and subsequent transcription of various genes associated with metastasis (Figure 7) (Zhang et al., 2018). However, evidence for Tspan15's involvement in this pathway is limited to oesophageal carcinoma cell lines (Zhang et al., 2018). Indeed, β-TrCP has not been identified as a Tspan15 interacting protein in additional cell lines by mass spectrometry (Jouannet et al., 2016; Sidahmed-Adrar et al., 2019; Koo et al., 2020). Furthermore, NF-κB signalling is not modulated by Tspan15 in HEK-293T cells; an NF-κB-luciferase reporter assay demonstrated that transiently transfected Tspan15 could not induce NF-kb luciferase actuation (Tomlinson lab, unpublished data). As such, further experiments are required to confirm the interaction between Tspan15 and β-TrCP, as well as any consequential downstream effects on NF-κB signalling. It is also worth noting that the involvement of ADAM10 and the other TspanC8s is yet to be investigated.

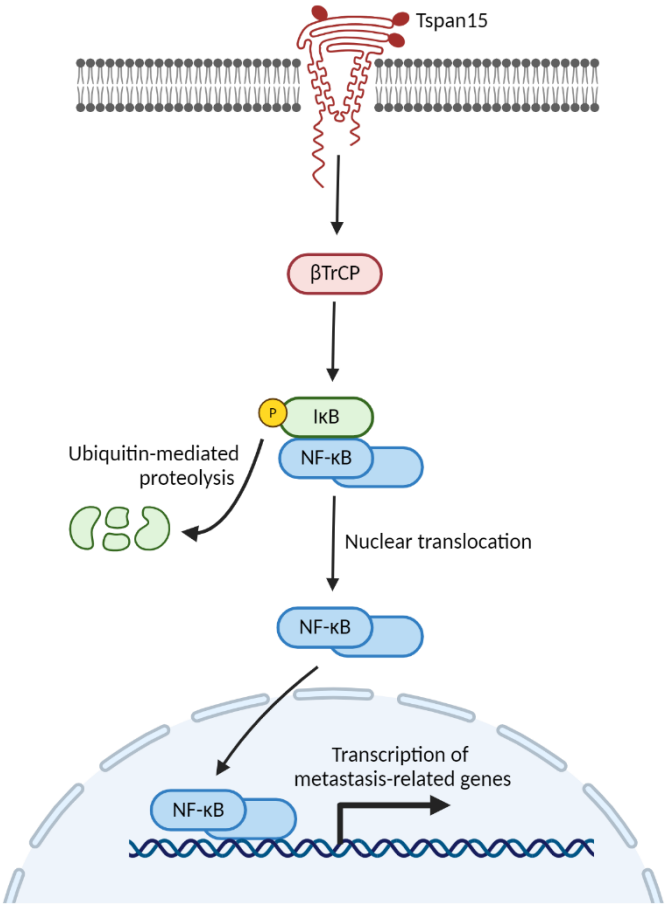


Figure 7: Tspan15 plays a role in the NF-κB signalling pathway. Based on the findings from Zhang et al., 2018, Tspan15 interacts with β-TrCP to promote the degradation of p-IκB and trigger the nuclear translocation of NF-κB, which is composed of two subunits, p50 and p65. (Figure created with BioRender.com).

1.5.4 Tspan15

1.5.4.1 Tspan15 dysregulation in disease

Tspan15 expression is upregulated in various cancers, including oral squamous cell carcinoma (Hiroshima et al., 2019), oesophageal carcinoma (Zhang et al., 2018), hepatocellular carcinoma (Sidahmed-Adrar et al., 2019), and intrahepatic cholangiocarcinoma (Yoshizumi et al., 2023). In both oral squamous cell and oesophageal carcinoma, Tspan15 has a pro-migratory and -invasive role (Zhang et al., 2018; Hiroshima et al., 2019), but the proposed underlying mechanism differs. N-cadherin shedding and β-catenin nuclear localisation were found to be decreased in oral squamous

cell carcinoma cell lines with reduced Tspan15 expression, and although a direct link was not shown, this was proposed to be part of the mechanism underlying Tspan15-mediated invasion (Hiroshima et al., 2019). However, in oesophageal carcinoma, Tspan15 was suggested to drive migration and invasion via its interaction with β-TrCP and subsequent downstream activation of NF-κB signalling (Zhang et al., 2018). Interestingly, the study by Zhang et al. was the only one to investigate the *in vivo* role of Tspan15 in cancer; the upregulation of Tspan15 expression was shown to promote metastasis in a mouse model (Zhang et al., 2018). Taken together, these two studies suggest that Tspan15 likely regulates the migration and invasion of cancer cells via multiple mechanisms. Tspan15 has also been shown to promote cell proliferation and represent a stemness-related marker in hepatocellular carcinoma (Hiroshima et al., 2019), indicating that Tspan15's role in cancer may extend beyond its pro-migratory and -invasive functions. In this instance, the underlying mechanism was proposed to be an ADAM10-dependent increase in ERK phosphorylation and subsequent secretion of connective tissue growth factor (CTGF). However, no direct effect on proliferation or stemness was found (Sidahmed-Adrar et al., 2019). More recently, Tspan15 has been demonstrated to enhance stem cell-like properties and induce chemoresistance in cholangiocarcinoma. This was proposed to be the result of ADAM10-dependent Notch1 activation (Yoshizumi et al., 2023), despite Tspan5 and Tspan14 having been characterised as the regulatory TspanC8s for Notch cleavage (Dornier et al., 2012; Saint-Pol et al., 2017a; Xie et al., 2021). Moreover, Tspan15 has previously been shown to negatively regulate Notch activity (Jouannet et al., 2016) or have no effect (Dornier et al., 2012; Seipold et al., 2018), depending on the cell type and validation method used.

It is also tempting to speculate that Tspan15 may promote the migration and invasion of mesothelioma cells. As a precedent, ADAM10 has been shown to promote the *in vivo* tumour progression of mesothelioma, as well as *in vitro* migration and invasion, with its pro-migratory effect linked to N-cadherin shedding and FGFR signalling (Sépult et al., 2019). Indeed, the migration of mesothelioma cells treated with conditioned media lacking shed N-cadherin was reduced but could

be restored by the addition of a recombinant N-terminal N-cadherin fragment. However, FGFR inhibition blocked this migration-promoting effect (Sépult et al., 2019). Although the role of Tspan15 in malignant pleural mesothelioma was not investigated by Sépult et al., it is likely implicated as the regulatory TspanC8 for ADAM10-mediated shedding of N-cadherin (Prox et al., 2012; Jouannet et al., 2016; Noy et al., 2016; Seipold et al., 2018; Lipper et al., 2023).

Beyond its roles in cancer, Tspan15 is upregulated in the brains of mice and patients with Alzheimer's disease (Seipold et al., 2018) and expressed on arthritis-associated fibroblasts (Croft et al., 2019). Furthermore, single nucleotide polymorphisms within the non-coding region of Tspan15 are associated with venous thromboembolism (Germain et al., 2015; Lindström et al., 2019).

1.6 The cell adhesion protein N-cadherin

1.6.1 N-cadherin regulates various pro-metastatic signalling pathways

Neuronal (N)-cadherin, which is proteolytically cleaved by Tspan15/ADAM10 (Prox et al., 2012; Jouannet et al., 2016; Noy et al., 2016; Seipold et al., 2018; Lipper et al., 2023), belongs to a family of Ca^{2+}-dependent adhesion molecules, which mediate cell-cell interactions (Mrozik et al., 2018). Classical cadherins, like N-cadherin, have a modular structure, which is characterised by five extracellular domains, a single-pass transmembrane region, and a cytoplasmic domain (Figure 8) (Shapiro and Weis, 2009; Mrozik et al., 2018). They interact in trans with cadherins on different cells via contact between their first extracellular domains (EC1), as well as in cis with adjacent cadherin monomers. The latter interaction is mediated by the histidine-alanine-valine (HAV) motif in EC1 and a recognition sequence located within EC2 of a second cadherin molecule (Shapiro and Weis, 2009; Radice, 2013; Mrozik et al., 2018). Furthermore, the cytoplasmic tail of classical cadherins interacts with intracellular proteins, including β-catenin and p120 catenin (Figure 8); whilst β-catenin links cadherins to the cytoskeleton via α-catenin, p120 regulates the activity of Rho GTPases (Shapiro and Weis, 2009; Radice, 2013; Mrozik et al., 2018).

N-cadherin has also been implicated in metastasis; the upregulation of N-cadherin and downregulation of epithelial (E)-cadherin is a marker of the epithelial-to-mesenchymal transition, which facilitates cancer progression (Radice, 2013; Mrozik et al., 2018). It is thought to promote the metastasis of cells via its mediation of cellular adhesion and modulation of signalling pathways (Mrozik et al., 2018). These signalling pathways will be described in Sections 1.6.1.1 and 1.6.1.2.

1.6.1.1 N-cadherin drives the augmentation of FGFR signalling

N-cadherin was first reported to functionally interact with fibroblast growth factor receptors (FGFRs) as a mechanism to promote neurite outgrowth (Williams et al., 1994; Williams et al., 2001), but this interaction has also been shown to play a role in the development and progression of several cancers, including breast (Nieman et al., 1999; Hazan et al., 2000; Suyama et al., 2002; Sanchez-Heras et al., 2006; Hulit et al., 2007; Qian et al., 2014), pancreatic (Rachagani et al., 2012), and non-small cell lung (Quintanal-Villalonga et al., 2020). Several studies have also confirmed a physical interaction by co-immunoprecipitation (Suyama et al., 2002; Sanchez-Heras et al., 2006; Rachagani et al., 2012; Quintanal-Villalonga et al., 2020). Initial findings suggested the interaction was mediated by the fourth extracellular domain of N-cadherin (EC4) and HAV motif within the second Ig-like domain, D2, of FGFR-1 (Williams et al., 1994; Kim et al., 2000; Williams et al., 2001). However, neither mutation of HAV to HEV (Suyama et al., 2002) nor deletion of the HAV motif (Sanchez-Heras et al., 2006) were found to disrupt the interaction. Instead, it is now known that the FGFR acid box, which is located in the linker region between D1 and D2, is critical for its interaction with N-cadherin. Indeed, FGFR-1 does not immunoprecipitate with N-cadherin when this motif is deleted (Sanchez-Heras et al., 2006).

The interaction between N-cadherin and FGFRs has been demonstrated to mediate FGFR activation in a ligand-independent manner (Figure 8) (Williams et al., 2001). Additionally, N-cadherin has been shown to sustain FGF-2-mediated MAPK/ERK signalling (Hazan et al., 2000; Suyama et al., 2002) by preventing the ligand-induced internalisation of FGFRs, and thus stabilising surface expression

(Figure 8) (Suyama et al., 2002). This ultimately led to increased transcription of matrix metalloproteinase-9 (MMP-9) and cellular invasion (Suyama et al., 2002). Whilst other studies have reported a similar effect on the MAPK/ERK pathway (Hulit et al., 2007; Qian et al., 2014), N-cadherin/FGFR can also drive breast cancer cell invasion via the PI3K/Akt pathway (Qian et al., 2014). Given the domain required for N-cadherin to interact with FGFR, it is tempting to speculate that a similar response could be mediated by the extracellular domain released following N-cadherin shedding. Indeed, the soluble form of N-cadherin has been shown to interact with FGFRs in vascular smooth muscle cells (Lyon et al., 2016). Whilst Suyama et al. are cited as showing an effect of shed N-cadherin on FGFR function, no direct link was shown. As such, further studies are required to determine the effect of soluble N-cadherin on FGFR signalling.

FGFRs co-localise with N-cadherin at the plasma membrane except for at sites of cell-cell contact, suggesting that their functional interaction does not regulate N-cadherin's role in cell adhesion (Sanchez-Heras et al., 2006). This is further supported by evidence that an antibody against EC4, the FGFR interacting domain of N-cadherin, impairs the migration but not aggregation of N-cadherin-positive cells (Kim et al., 2000). It can, therefore, be concluded that N-cadherin exhibits two distinct functions that do not occur simultaneously.

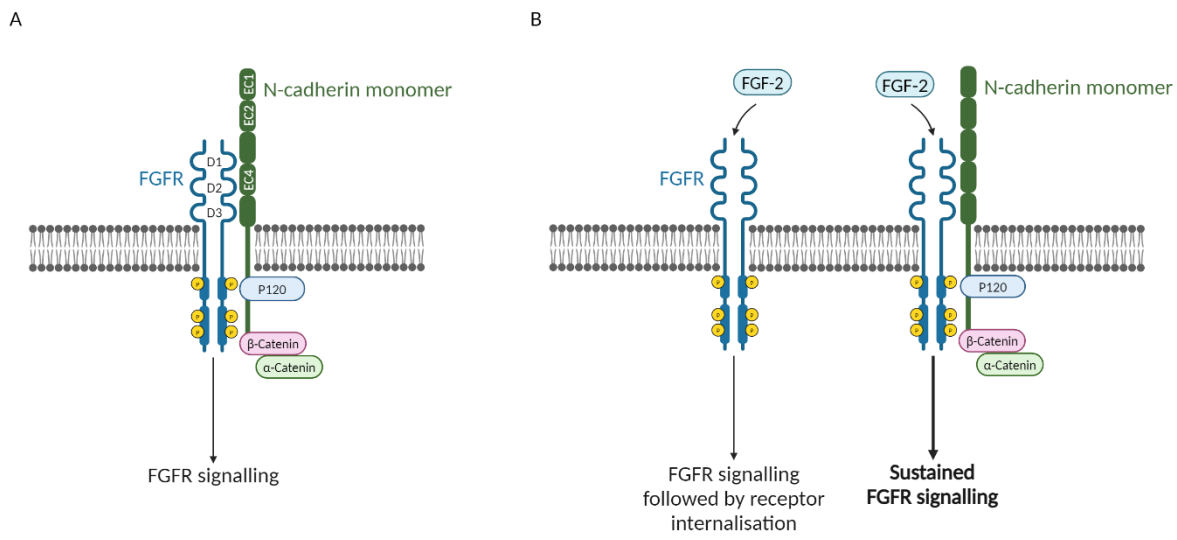


Figure 8: N-cadherin directly interacts with FGFRs to potentiate downstream signalling. N-cadherin interacts with the FGFR acid box via its fourth extracellular domain (EC4). (A) This can promote ligand-independent activation of FGFRs, or (B) sustain MAPK/ERK and PI3/Akt signalling via the stabilisation of FGFR surface expression by preventing FGF-2-mediated internalisation. (Figure created with Biorender.com)

1.6.1.2 Canonical Wnt signalling is modulated by N-cadherin

The canonical Wnt pathway functions to mediate cell proliferation, differentiation, and migration (Liu et al., 2022). As such, its dysregulation is implicated in human diseases, including cancer (Heuberger and Birchmeier, 2010). In the absence of a Wnt ligand, a destruction complex composed of axin, adenomatous polyposis coli (APC), casein kinase 1 (CK1), and glycogen synthase kinase-3 β (GSK-3β) captures β-catenin. The two kinases phosphorylate β-catenin, targeting it for β-TrCP-mediated ubiquitination and subsequent proteasomal degradation (Nelson and Nusse, 2004; Heuberger and Birchmeier, 2010; Amin and Vincan, 2012; Marie and Haÿ, 2013; Li et al., 2021; Liu et al., 2022). Therefore, the level of cytoplasmic β-catenin remains low and the lymphoid enhancer factor (LEF)/T-cell factor (TCF) transcription factors are bound by Groucho, inhibiting the transcription of Wnt-target genes (Heuberger and Birchmeier, 2010; Amin and Vincan, 2012; Liu et al., 2022). Wnt signalling is activated by a Wnt ligand binding to Frizzled and the co-receptor LRP5/6 (Amin and Vincan, 2012; Marie and Haÿ, 2013; Li et al., 2021), which is subsequently phosphorylated by CK1 and GSK-3β (Heuberger and Birchmeier, 2010; Marie and Haÿ, 2013). This leads to the recruitment of Dishevelled and the downstream inhibition of the destruction complex (Heuberger and Birchmeier, 2010; Amin and Vincan, 2012; Marie and Haÿ, 2013; Li et al., 2021). Consequently, cytoplasmic β-catenin is not degraded and instead translocates to the nucleus (Nelson and Nusse, 2004; Heuberger and Birchmeier, 2010; Amin and Vincan, 2012; Marie and Haÿ, 2013; Li et al., 2021; Liu et al., 2022); it displaces Groucho and forms a transcriptionally active complex with LEF/TCF (Heuberger and Birchmeier, 2010; Amin and Vincan, 2012; Marie and Haÿ, 2013; Li et al., 2021). Target genes include c-myc, cyclin D1, and axin-2 (Amin and Vincan, 2012; Li et al., 2021).

In addition to its role within the Wnt signalling pathway, β-catenin functions within the cadherin-catenin adhesion complex; β-catenin interacts with the cytoplasmic tail of N-cadherin connecting it to the actin cytoskeleton via α-catenin (Nelson and Nusse, 2004). Consequently, it has been proposed that these two pathways are linked through a shared pool of β-catenin (Heuberger and Birchmeier, 2010; Mrozik et al., 2018). It is important to note that whilst this section focuses on the role of N-cadherin in the Wnt/β-catenin pathway, other cadherins also interact with β-catenin, and as such functional redundancy is a possibility.

N-cadherin has been shown to sequester β-catenin at the plasma membrane and thus inhibit Wnt signalling (Figure 9) (Heasman et al., 1994; Sanson et al., 1996; Sadot et al., 1998; Mrozik et al., 2018). Indeed, in Xenopus embryos, the overexpression of wild-type N-cadherin, unlike a mutant form lacking the β-catenin-binding site, impairs the formation of dorsal axial structures, similar to the depletion of β-catenin (Heasman et al., 1994). Furthermore, in colon carcinoma cells, the expression of full-length N-cadherin re-directs β-catenin to the plasma membrane and inhibits LEF-1 transactivation (Sadot et al., 1998). N-cadherin has also been proposed to negatively regulate canonical Wnt signalling by interacting with LRP5 (Haÿ et al., 2009a; Haÿ et al., 2009b). In osteoblasts, this interaction promotes β-catenin degradation and decreases LEF/TCF-dependent transcriptional activity, ultimately impairing osteoblast function and bone formation (Haÿ et al., 2009a).

As N-cadherin has been shown to protect β-catenin from degradation (Sadot et al., 1998), other studies have proposed that N-cadherin may positively regulate Wnt signalling by maintaining a stable pool of β-catenin (Figure 9) (Qi et al., 2005; Howard et al., 2011; Zhang et al., 2013). For example, during the transmigration of melanoma cells, despite an increase in N-cadherin expression, β-catenin dissociates from the N-cadherin adhesion complex and translocates to the nucleus, promoting LEF/TCF-mediated transcription (Qi et al., 2005). This release of β-catenin into the cytosol is promoted by Src-mediated phosphorylation of the N-cadherin cytoplasmic domain at Tyr860 (Figure 9) (Qi et al., 2005; Qi et al., 2006). Indeed, overexpression of a dominant-negative Src mutant in

melanoma cells impairs transmigration as a result of inhibiting β-catenin dissociation and signalling (Qi et al., 2006). Additionally, ADAM10-mediated cleavage of the N-cadherin ectodomain and subsequent degradation of the cytoplasmic tail likely disrupts the N-cadherin-β-catenin complex, resulting in the release of β-catenin into the cytosol such that it is available for nuclear translocation; ADAM10 deficiency is associated with increased levels of N-cadherin and β-catenin at the cell surface, as well as reduced expression of β-catenin target genes (Reiss et al., 2005). It has also been suggested that Tspan15/ADAM10-mediated shedding of N-cadherin may induce nuclear localisation of β-catenin to promote the metastasis of oral squamous cell carcinoma (Hiroshima et al., 2019). However, it is important to note that no direct link was shown.

Ultimately, there is evidence to suggest that the direct interaction between N-cadherin and β-catenin regulates Wnt signalling, at least to some extent. However, N-cadherin's involvement is likely complex, with reports of both positive and negative regulation. Although N-cadherin can sequester cytoplasmic β-catenin at the cell membrane, in doing so it maintains a pool of β-catenin, which can be released and become available for nuclear translocation following disruption of the N-cadherin adhesive complex (Figure 9).

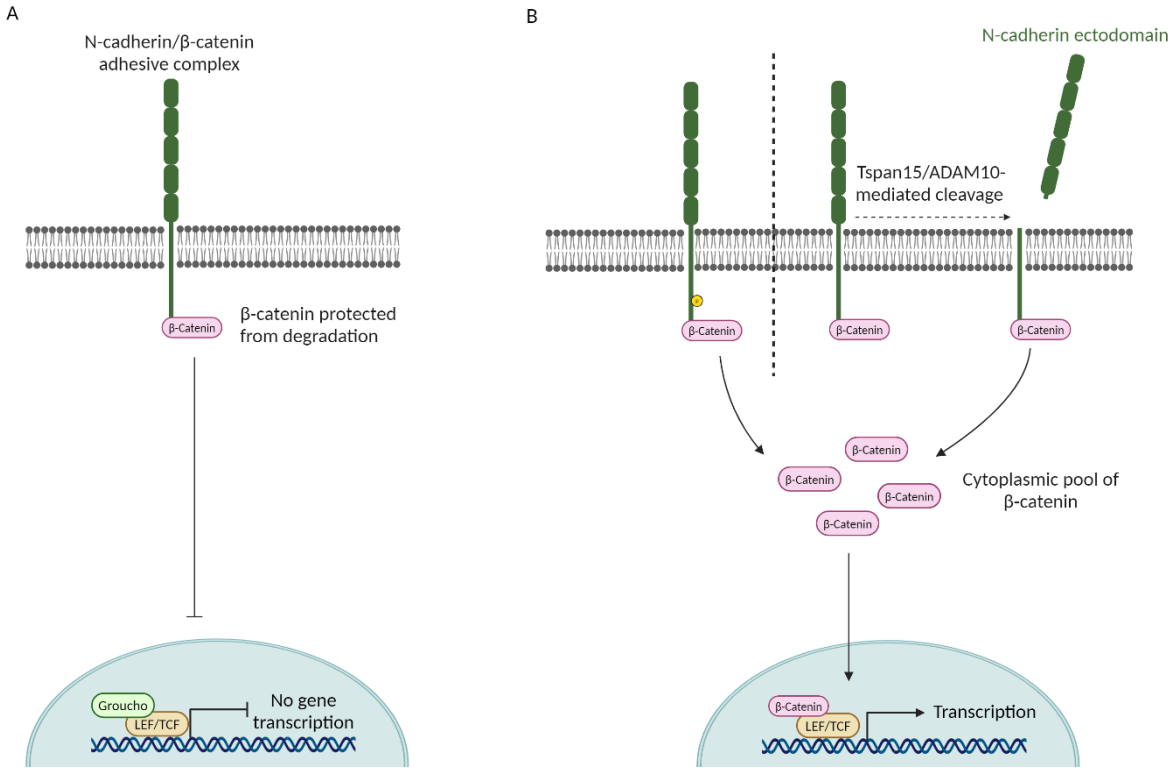


Figure 9: The interaction between N-cadherin and β-catenin regulates Wnt signalling. (A) N-cadherin can sequester β-catenin at the plasma membrane, removing it from the cytosol. As such, N-cadherin protects β-catenin from degradation but also inhibits Wnt signalling. (B) However, phosphorylation of the N-cadherin cytoplasmic tail by Src, or the cleavage of the N-cadherin ectodomain by Tspan15/ADAM10 can result in the release of β-catenin into the cytoplasm, making it available for nuclear translocation. In the nucleus, β-catenin displaces Groucho and binds to LEF/TCF to promote transcription. (Figure created with BioRender.com).

1.7 Project aims and objectives

This thesis aims to characterise the role of Tspan15 in cell proliferation and invasion, as well as establish whether its mechanism of action is ADAM10-dependent and/or -independent. The working hypothesis is that Tspan15 likely promotes cancer cell invasion and, in some cases, proliferation via the regulation of ADAM10-mediated substrate shedding. A clearer understanding of Tspan15's potential involvement in cancer progression will determine whether targeting Tspan15 should be considered as a possible anti-cancer strategy.

The objectives of each chapter are outlined below:

- Chapter 3: To analyse the expression levels of ADAM10 and Tspan15 in different malignancies, as well as the associated effect on patient prognosis.
- Chapter 4: To determine whether the proliferation and invasion of pancreatic cancer cell lines are regulated by the Tspan15/ADAM10 scissor.
- Chapter 5: To explore the role of Tspan15 in HEK-293T cell proliferation and invasion, and subsequently determine its ADAM10-dependent and/or -independent mechanism(s) of action.
- Chapter 6: To investigate the potential role of Tspan15 and ADAM10 in oesophageal carcinoma cell lines.

CHAPTER 2 MATERIALS AND METHODS

2.1 Antibodies

Antibodies for negative cell sorting with Dynabeads (Section 2.2.3.3), fluorescence-activated cell sorting (FACS) (Section 2.2.3.4), flow cytometry (Section 2.3.1), co-immunoprecipitation (Section 2.3.2.2), Western blotting (Section 2.3.3), and immunofluorescence microscopy (Section 2.7.3) are detailed in Table 1.

Table 1: Summary of antibodies. Abbreviations used are as follows – CS: negative cell sorting with Dynabeads; FACS: fluorescence-activated cell sorting; FC: flow cytometry; Co-IP: co-immunoprecipitation; WB: Western blotting; IF: immunofluorescence microscopy; mAb: monoclonal antibody. Unless otherwise stated, antibodies are purified.

	Source and identifier	**Working concentration/dilution**
Primary antibodies		
Mouse IgG1 Kappa mAb (MOPC21)	MP Biomedicals (USA) 0850327	FACS – 10 µg/ml FC – 10 µg/ml Co-IP – 4 µg
Mouse anti-human ADAM10 mAb (11G2)	Dr. Eric Rubinstein (France) (Arduise et al., 2008)	CS – 1 µg per Dynabeads prep FACS – 10 µg/ml FC – 10 µg/ml Co-IP – 1 µg WB – 0.5 µg/ml
Mouse anti-human Tspan15 mAb (1C12)	Abpro (USA) (Koo et al., 2020)	FACS – 10 µg/ml CS – 2.5 µg per cell prep WB – 1:500
Mouse anti-human Tspan15 mAb (1C12); hybridoma supernatant	Abpro (USA) (Koo et al., 2020)	FC - undiluted
Mouse anti-human Tspan15 mAb (4A4)	Abpro (USA) (Koo et al., 2020)	CS – 2.5 µg per cell prep
Mouse anti-human Tspan15 mAb (5D4)	Abpro (USA) (Koo et al., 2020)	CS – 2.5 µg per cell prep Co-IP – 4 µg
Mouse anti-human Tspan15 mAb (5F4)	Abpro (USA) (Koo et al., 2020)	CS – 2.5 µg per cell prep
Rabbit anti-His-Tag mAb	Cell Signalling Technology (UK) (12698S)	Co-IP – 0.65 µg
Rabbit anti-human β-TrCP mAb	Cell Signalling Technology (UK) (4394S)	Co-IP – 0.65 µg WB – 1:000

Mouse anti-p44/42 MAPK (ERK1/2) (3A7) mAb	Cell Signalling Technology (UK) (9107)	WB – 1:1,000
Mouse anti-p-ERK (E-4) mAb	Santa Cruz Biotechnology (UK) (sc-7383)	WB - 1:200
Rabbit anti-NF-kappaB p65 mAb	Cell Signalling Technology (UK) (8242S)	IF - 1:16,000
Secondary antibodies		
Sheep anti-mouse IgG-fluorescein isothiocyanate (FITC)	Sigma-Aldrich (UK) (F2883)	FACS - 1:100 FC - 1:100
Donkey anti-mouse IgG-IRDye® 800CW	LI-COR Biosciences (UK) (926-32212)	WB - 1:10,000
Goat anti-mouse IgG- IRDye® 680RD	LI-COR Biosciences (UK) (926-68070)	WB - 1:10,000
Goat anti-rabbit IgG- IRDye® 800CW	LI-COR Biosciences (UK) (926-32211)	WB - 1:10,000
Goat anti-rabbit Alexa Fluor 647	Invitrogen (UK) (A21244)	IF - 1:300

2.2 Cell biology techniques

Unless otherwise stated, reagents were obtained from Sigma-Aldrich (USA) and plasticware was acquired from Thermo Fisher Scientific (UK).

2.2.1 2D cell culture

Human embryonic kidney cells expressing SV40 large T-antigen (HEK-293T) (Tomlinson lab, UK) and human pancreatic cancer PANC-1 (American Type Culture Collection (ATCC), USA) cells were grown in high glucose Dulbecco's modified Eagle medium (DMEM) (Gibco, UK). AsPC-1 cells (ATCC), a second human pancreatic cancer cell line, were grown in Roswell Park Memorial Institute (RPMI)–1640 medium, and human oesophageal carcinoma KYSE-30 cells (Public Health England (PHE), UK) were grown in a 50:50 mix of RPMI–1640 medium and Ham's F-12 nutrient mix (Gibco, UK). All media was supplemented with 10% (v/v) fetal bovine serum (FBS) (Gibco, USA), 4 mM L-glutamine, 100 U/ml penicillin and 100 μg/ml streptomycin (complete media).

At 80% confluency, cells were washed in sterile Dulbecco's phosphate buffered saline (PBS) without Ca^{2+} and Mg^{2+}, detached using Trypsin-EDTA solution, and cultured at a lower confluency. Cells were grown in 5% (v/v) CO_2 at 37 ^oC.

2.2.2 3D cell culture

Spheroids were established using the hanging drop method. Adherent 2D cell cultures were grown to 80% confluency, trypsinised, and then resuspended in complete media at $2.5x10^4$ cells/ml. Cells were subsequently seeded as 40 µl droplets onto the inverted lid of a 24-well CytoOne plate (Starlab, UK). The lid was then overturned onto a PBS-filled plate, which acts as a hydration chamber to support spheroid formation. After twenty-four hours, the spheroids were transferred to a 24-well plate pre-coated with 1.5% (w/v) agarose (Appleton Wood, UK) diluted in PBS and covered with 1 ml of complete media. Spheroids were grown in 5% (v/v) CO_2 at 37 ^oC with media being exchanged every 3 days.

2.2.3 Generation of knockout cell lines by CRISPR/Cas9

CRISPR/Cas9 genome editing technology was used to generate PANC-1, AsPC-1, HEK-293T, and KYSE-30 cells deficient in ADAM10 or Tspan15 (Ran et al., 2013). The guide oligos for ADAM10 and Tspan15 are detailed in (Table 2) and have been described previously by Koo et al (2020). They were annealed and cloned into the pSpCas9(BB)-2A-Puro (PX459) V2.0 plasmid (Figure A 1, Appendix) (Addgene plasmid # 62988, a gift from Feng Zhang) (Ran et al., 2013; Koo et al., 2020).

Table 2: List of CRISPR/Cas9 ADAM10 and Tspan15 guide oligos.

Gene	Guide oligo (5' to 3')
ADAM10 (guide 1)	5'-CACCGCGTCTAGATTTCCATGCCCA-3' 5'-AAACTGGGCATGGAAATCTAGACGC-3'
ADAM10 (guide 2)	5'-CACCGATACCTCTCATATTTACAC-3' 5'-AAACGTGTAAATATGAGAGGTATC-3'
Tspan15 (guide 1)	5'-CACCGGCGCGCGCTTCTCCTACCTC-3' 5'-AAACGAGGTAGGAGAAGCGCGCGCC-3'
Tspan15 (guide 2)	5'-CACCGAGCGCCCAGGATGCCGCGCG-3'

	5'-AAACCGCGCGGCATCCTGGGCGCTC-3'

2.2.3.1 Transfection of cells with Lipofectamine 2000

Cells were transfected with Lipofectamine 2000 (Invitrogen, UK) as per the manufacturer's protocol. In brief, cells were seeded on a 6-well plate in media supplemented with 10% (v/v) FBS and 4 mM L-glutamine such that they would be between 70 and 80% confluent on the day of transfection. Twenty-four hours post-plating, 10 µl of Lipofectamine 2000 and 2 µg of the relevant plasmid (Section 2.2.3) were diluted in Opti-MEM (Gibco, UK), a reduced serum medium, and incubated at room temperature for 20 minutes. The DNA-lipid complexes were then added dropwise to the cells before incubation at 37 ^{o}C and 5% (v/v) CO_2. For AsPC1 and KYSE-30 cells media was exchanged for fresh penicillin/streptomycin-free media after 4 hours, whilst PANC-1 and HEK-293T cells did not require media replacement.

2.2.3.2 Selection of CRISPR-targeted cells

Forty-eight hours post-transfection, cells were treated with puromycin (Thermo Fisher Scientific, UK) diluted in complete media (Table 3) for 72 hours to select for transfected cells. The relative expression of ADAM10 and Tspan15 was subsequently confirmed by flow cytometry as described in Section 2.3.1, before purification with magnetic Dynabeads or by fluorescence-activated cell sorting (FACS).

Table 3: Optimal puromycin concentration used for each cell line

Cell line	Concentration of puromycin (µg/ml)
AsPC-1	4
HEK-293T	3
KYSE-30	6
PANC-1	5

2.2.3.3 Negative cell sorting with Dynabeads

Knockout (KO) pools of PANC-1, AsPC-1 and HEK-293T cells were purified using magnetic Dynabeads.

2.2.3.3.1 Direct negative cell sorting with Dynabeads

ADAM10 knockout pools were purified via direct negative cell sorting using Dynabeads, with all incubation periods performed at 4 ^{o}C with gentle rotation. First, 25 µl of pan mouse IgG magnetic Dynabeads (Invitrogen, UK) were washed and subsequently resuspended in 1 ml of isolation buffer (0.1% (w/v) Bovine Serum Albumin (BSA) and 2 mM ethylenediaminetetraacetic acid (EDTA) in PBS without Ca^{2+} and Mg^{2+}) with 1 µg of the anti-human ADAM10 11G2 antibody (Table 1). Following incubation overnight, the antibody-bound Dynabeads were washed in isolation buffer to remove any unbound antibody. Impure ADAM10 KO cells within the range of $5x10^6$ to $1x10^7$ were then harvested, pelleted by centrifugation at 270 x g for 5 minutes, and subsequently resuspended in 1 ml of isolation buffer supplemented with the antibody-bound Dynabeads. This solution was incubated for 45 minutes before a magnet was used to separate the ADAM10-positive and -negative cells. The KO population was isolated by collecting the supernatant containing unbound cells. These cells were pelleted by centrifugation at 270 x g for 5 minutes and re-plated in complete media. The relative expression of ADAM10 was confirmed by flow cytometry, with sorting being repeated as required.

2.2.3.3.2 Indirect negative cell sorting with Dynabeads

Tspan15 KO pools were purified via indirect negative cell sorting with Dynabeads, with all incubation periods performed at 4 ^{o}C with gentle rotation. Impure Tspan15 KO cells within the range of $5x10^6$ to $1x10^7$ were harvested, pelleted by centrifugation at 270 x g for 5 minutes, and resuspended in 1 ml of complete media. They were then incubated for 30 minutes with 10 µg of the purified anti-human Tspan15 antibodies, 2.5 µg each of 1C12, 4A4, 5D4, and 5F4 (Koo et al., 2020) (Table 1). Following this incubation period, the antibody-bound cells were washed with isolation buffer to remove any

excess antibody, before resuspension in 1 ml of isolation buffer supplemented with 100 µl of pan mouse IgG magnetic Dynabeads, which were pre-washed in isolation buffer. After incubation for 60 minutes, a magnet was used to separate the Tspan15-positive and -negative cells. The knockout population was isolated by collecting the supernatant containing unbound cells. These cells were pelleted by centrifugation at 270 x g for 5 minutes and re-plated in complete media. The relative expression of Tspan15 was confirmed by flow cytometry, with sorting being repeated as required.

2.2.3.4 Negative cell sorting by fluorescence-activated cell sorting (FACS)

KYSE-30 ADAM10 and Tspan15 knockout pools were purified via fluorescence-activated cell sorting (FACS). This protocol used PBS supplemented with 1% FBS to wash cells and dilute the relevant antibodies. Cells within the range of $2.5x10^6$ to $10x10^6$ were harvested and pelleted by centrifugation at 270 x g for 5 minutes. They were then incubated on ice for 30 minutes with 1.5 µg of primary antibody (Table 1) per $2.5x10^6$ cells, before being washed twice to remove any unbound antibody. The anti-mouse IgG-FITC antibody (Table 1) was then added to the cells at a dilution of 1:100 per $2.5x10^6$ cells. Following incubation on ice for 30 minutes, the cells were washed a further two times. To prepare samples for FACS, PBS supplemented with 1% FBS and 1 mM EDTA was used to resuspend the cells, which were subsequently filtered through a CellTrics mesh filter with 50 µM pores (Sysmex, UK). A two-way sort was performed on the FACSAria Fusion flow cytometer (BD Biosciences, UK) fitted with a 100 µM nozzle. The KO populations were collected, pelleted by centrifugation at 270 x g for 5 minutes, and re-plated in complete media. The relative expression of ADAM10 and Tspan15 was confirmed by flow cytometry, with sorting being repeated as required.

2.2.4 Generation of Tspan15 overexpressing cell lines by Lentiviral transduction

Cells overexpressing Tspan15 were generated from wild-type (WT) and validated ADAM10-knockout cells using lentiviral transduction of pLVX-EF1α-IRES-Puro N-terminal FLAG-tagged human Tspan15, which was generated by subcloning the N-terminal FLAG-Tspan15 sequence into the pLVX-EF1α-IRES-

Puro lentiviral transfer plasmid (Figure A 3, Appendix) (Clontech, USA). This was as described previously by Koo et al. (2020).

2.2.4.1 Transfection with PEI

HEK-293T WT cells were transfected with polyethylenimine (PEI) (Sigma-Aldrich, UK) using a previously described method (Ehrhardt et al., 2006). Cells were seeded in media supplemented with 10% (v/v) FBS and 4 mM L-glutamine on a 6-well plate such that they would be between 50 and 80% confluent on the day of transfection. Twenty-four hours post-plating, 8 µl of a 1 mg/ml PEI stock solution and the required DNA (0.76 µg of the relevant lentiviral transfer vector (Section 2.2.4), 0.55 µg of the psPAX2 packaging vector (Addgene plasmid #12260, a gift from Didier Trono), and 0.22 µg of the pMD2G envelope vector (Addgene plasmid #12259, a gift from Didier Trono)) were diluted in Opti-MEM and incubated at room temperature for 10 minutes. The DNA-PEI complexes were subsequently added dropwise to the cells before incubation overnight at 37 ^{o}C and 5% (v/v) CO_2. Media was then replaced with the normal growth medium without penicillin/streptomycin for the cell lines seeded in Section 2.2.4.2 and incubation for a further 24 hours allowed for virus production.

2.2.4.2 Lentiviral transduction and selection of targeted cells

Cells within the range of $1x10^6$ to $4x10^6$ were seeded in complete media on a 6-well plate. The following day, 2ml of virus-containing media was harvested from the previously transfected HEK-293T cells (Section 2.2.4.1) and supplemented with 5 µg/ml polybrene (Merck, UK), 10% (v/v) FBS, and 0.8 mM L-glutamine. It was then filtered through a 0.45 µm pore filter (Starlab, UK) before being used to replace the media on the previously plated cells. Cells were incubated at 37 ^{o}C and 5% (v/v) CO_2 with media being exchanged after 24 hours for fresh media supplemented with 10% (v/v) FBS, 4 mM L-glutamine, 100 U/ml penicillin and 100 µg/ml streptomycin.

Forty-eight hours post-transduction, cells were treated with fresh media containing the optimal concentration of puromycin (Table 3) for 72 hours to select for transduced cells The relative

expression of ADAM10 and Tspan15 was subsequently confirmed by flow cytometry as described in Section 2.3.1.

2.2.5 Transient transfection of cells with PEI

Polyethylenimine (PEI) was used to transiently transfect HEK-293T cells (Ehrhardt et al., 2006). Cells in media supplemented with 10% (v/v) FBS and 4 mM L-glutamine were plated in a 12-well plate the day before transfection such that they would reach a confluency of 50 to 80%. On the day of transfection, plasmid DNA and PEI were diluted at a ratio of 1:4 in Opti-MEM and subsequently incubated at room temperature for 10 minutes. The formed DNA-PEI complexes were then added dropwise to the cells and incubated overnight.

2.3 Protein biochemistry techniques

Unless otherwise stated, reagents and plasticware were acquired from Thermo Fisher Scientific (UK).

2.3.1 Flow cytometry

For the analysis of cell surface protein expression, $2.5x10^5$ to $5x10^5$ cells were harvested and pelleted by centrifugation at 270 x g for 5 minutes. Cells were subsequently incubated on ice for 30 minutes with 50 µl of primary antibody (Table 1) diluted, where necessary, in buffer (0.2% (w/v) BSA (First Link, UK) and 0.02% (w/v) NaN_3 (Sigma-Aldrich, UK) in PBS (OXOID, UK)). Following this incubation period, cells were washed with the aforementioned buffer to remove any unbound antibody. They were then incubated on ice for 30 minutes with 50 µl of fluorescent secondary antibody (Table 1) diluted in buffer, before being washed again and resuspended in 500 µl of PBS supplemented with 0.2% (w/v) BSA and 0.02% (w/v) NaN_3. For samples requiring storage prior to analysis, cells were instead resuspended and fixed in PBS supplemented with 1% (v/v) formaldehyde (Sigma-Aldrich), 2% (v/v) FBS and 0.02% (w/v) NaN_3. Samples were run on a FACSCalibur (BD Biosciences, UK) or an Attune NxT flow cytometer (Thermo Fisher Scientific, UK); live cells were gated based on size and granularity before fluorescence intensity was measured. Data were subsequently analysed using the

CellQuest Pro software (BD Biosciences, UK) or FlowJo v10.8 (BD Biosciences, UK). Relative surface expression was calculated by dividing the geometric mean fluorescence intensity of the target antibody staining by that of the isotype control. Additionally, quadrants were used to determine the percentage of cells stained by the target antibody.

2.3.2 Protein extraction

2.3.2.1 Whole-cell

Cells were harvested by scraping in PBS and pelleted by centrifugation at 2,655 x g for 3 minutes at 4 ^{o}C. They were subsequently lysed on ice for 30 minutes in 1% Triton X-100 lysis buffer (1% Triton X-100 (v/v) (Sigma-Aldrich), 10 mM Tris, 150 mM NaCl, 1 mM EDTA, 0.02% (w/v) NaN_3 in dH_2O, pH 7.5) supplemented with a 1:100 dilution of 100x protease inhibitor cocktail (Merck, UK). For the analysis of phosphorylated proteins, the lysis buffer was also supplemented with a 1:20 dilution of PhosSTOP (Roche, Germany) to protect against dephosphorylation. Following lysis, insoluble debris was pelleted by centrifugation at 21,000 x g for 10 minutes at 4 ^{o}C. The supernatant was subsequently diluted with an equal volume of 2x sample buffer (non-reducing: 0.1 M Tris, 4% (w/v) sodium dodecyl sulphate (SDS), 20% (v/v) glycerol, 0.01% (w/v) bromophenol blue (Sigma-Aldrich, UK) in dH_2O, pH 6.8; reducing: supplemented with 5% β-mercaptoethanol (Sigma-Aldrich, UK)). All samples were denatured at 95 ^{o}C for 5 minutes before analysis by Western blotting (Section 2.3.3).

2.3.2.2 Co-immunoprecipitation

For each co-immunoprecipitation, 20 µl of Protein G Sepharose beads (50% slurry in PBS) (Generon, UK) were rotated overnight at 4 ^{o}C with the relevant antibody (Table 1) in 1% Triton X-100 (v/v) lysis buffer. The following day, the antibody-coated beads were washed twice in 1% Triton X-100 (v/v) lysis buffer by centrifugation at 2,655 × g for 20 seconds. Next, cells were harvested by scraping and subsequently pelleted by centrifugation at 2,655 x g for 3 minutes at 4 ^{o}C. They were then lysed on ice for 30 minutes in 1% Brij97 lysis buffer (1% Brij97 (w/v) (Sigma-Aldrich, UK), 10 mM Tris, 150 mM

NaCl, 1 mM $CaCl_2$, 1 mM $MgCl_2$, 0.02% (w/v) NaN_3 in dH_2O, pH 7.5) supplemented with a 1:100 dilution of 100x protease inhibitor cocktail (Merck, UK), as well as 5 µM of the ADAM10 inhibitor G1254023X (Merck, UK) to prevent ADAM10 degradation post-lysis (Brummer et al., 2018). Following lysis, insoluble debris was pelleted by centrifugation at 21,000 x g for 10 minutes at 4 ^{o}C. A sample of the supernatant was diluted with 6x sample buffer, whilst the remaining lysate was rotated with the antibody-bound beads for 2 hours at 4 ^{o}C. The beads were subsequently washed four times by centrifugation at 2,655 × g for 20 seconds with 1% (w/v) ice-cold Brij97 and then resuspended in 50 µl of 2x sample buffer. All samples were denatured at 95 ^{o}C for 5 minutes prior to analysis by Western blotting.

ADAM10 and Tspan15 blotting was performed under non-reducing conditions, whilst β-TrCP required reducing conditions due to antibody IgG bands otherwise obscuring protein-specific bands.

2.3.3 Western blotting

SDS-polyacrylamide gel electrophoresis (PAGE) was used to separate proteins with a standard Tris-glycine gel and buffer system. In brief, denatured samples were loaded onto a 10 or 12% Tris-glycine gel alongside the BLUeye ladder (Geneflow, UK) diluted in sample buffer. Samples were run at 125 V for 120 minutes in SDS-PAGE running buffer (25 mM Tris, 192 mM glycine (Sigma-Aldrich, UK), 0.1% SDS (w/v) in dH_2O). Proteins were subsequently transferred from the gel to an activated Immobilon-FL polyvinylidene difluoride (PVDF) membrane (Merck, UK) in transfer buffer (25 mM Tris, 192 mM glycine, 20% (v/v) methanol in dH_2O) using the XCell II™ blot module system (Thermo Fisher Scientific); proteins were transferred at 30 V for 95 minutes. Following transfer, membranes were blocked in 5% (w/v) skimmed milk (Marve, UK) diluted in Tris-buffered saline (TBS) (20 mM Tris, 137 mM NaCl in dH_2O, pH 7.6) or 3% (w/v) BSA (First Link, UK) in TBST (TBS containing 0.1% Tween® 20) for 1 hour at room temperature. Membranes were then washed once in TBST for 5 minutes prior to incubation overnight at 4 ^{o}C with the relevant primary antibodies (Table 1) diluted in 3% (w/v) BSA in

TBST. To remove non-specific antibody binding, membranes were subsequently washed three times with high-salt TBST (TBST supplemented with 500 mM NaCl) for 10 minutes at room temperature. The relevant IRDye®-conjugated fluorescent secondary antibodies (Table 1) diluted in 3% (w/v) BSA in TBST were then incubated with the membrane for 2 hours at room temperature. After 5 washes with high-salt TBST for 5 minutes, excess Tween® 20 was removed from membranes by washing twice in TBS for 5 minutes. Membranes were scanned on an Odyssey® Infrared Imaging System (LI-COR Biosciences, UK) with band intensity quantified following subtraction of background fluorescence.

2.3.4 HiSPECS proteomics

The secretome of previously validated HEK-293T ADAM10 and Tspan15 KO clones (Koo et al., 2020) was analysed by Stefan Lichtenthaler's group using an optimised version of the secretome protein enrichment with click sugars (SPECS) protocol, as outlined previously (Serdaroglu et al., 2017). In summary, $6x10^5$ HEK-293T cells were seeded per well of a Poly-D-Lysine (PDL) coated 6-well plate in DMEM + Glutamax medium (Gibco, Germany) supplemented with 10% FBS (Gibco, Germany) and 1% penicillin/streptomycin (Gibco, Germany). The following day, culture media was replaced with fresh medium supplemented with 1 µmol tetraacetyl-N-azidoacetyl-mannosamine (MaNAz) (kindly provided by Stefan Bräse) solved in DMSO (Roth, Germany) or DMSO as a solvent control; MaNAz is a sialic acid analogue that is incorporated into glycoproteins synthesised de novo. Conditioned media was collected 48 hours post metabolic labelling and filtered through a 0.45 µm PVDF Millex filter. It was then transferred to a 30 kDa Vivaspin column (Sartorius, Germany); samples were centrifuged three times at 4000 x g and 4 ^oC with 2 ml of water being added after each centrifugation step to remove any non-metabolised MaNAz. Click chemistry-mediated biotinylation was subsequently used to label the secreted glycoproteins with 100 nM of Sulfo-DBCO-Biotin (Jena Bioscience, Germany). Following incubation overnight at 4 ^oC, samples were centrifuged three times as before with the water removing any non-reacted DBCO-biotin. A streptavidin affinity purification was then

performed followed by a tryptic in gel digestion of the purified samples. Samples were run on a Q-Exactive Orbitrap LC-MS system (Thermo Fisher Scientific, USA) with a 180-minute gradient. Data were analysed using MaxQuant and Perseus.

2.4 Cell-based assays

2.4.1 Proliferation assay

2.4.1.1 2D proliferation assay

The proliferation of cells in 2D was estimated by counting using a haemocytometer. Cells were plated in triplicate at the density indicated by the 0-hour cell count. At time points of 48- and 96-hours post-plating, cells were trypsinised and resuspended in an appropriate volume of complete media for counting.

2.4.1.2 3D proliferation assay

The proliferation of cells in 3D was estimated by measuring spheroid diameter over a time course. For each condition, six spheroids were cultured as described in Section 2.2.2. Forty-eight hours post transfer to agarose, time t=0 hours phase contrast images were captured on an EVOS M5000 (Thermo Fisher Scientific, UK) with a 10x objective lens. Images were then captured every 24 hours for 96 hours using a 10x or 4x objective lens. ImageJ (Schneider et al., 2012) was used to determine two diameter measurements for each spheroid and data was presented as a fold increase in average diameter from t=0 hours.

2.4.2 Transwell invasion assay

Cell culture inserts (Transwells) with an 8 µm pore transparent polyester (PET) membrane (Falcon, UK) were positioned in a 24-well companion plate (Falcon, UK) and coated with 100 µl of growth factor reduced Matrigel (Corning, UK), which was diluted to 250 µg/ml with ice-cold PBS without Ca^{2+} and Mg^{2+} (Sigma-Aldrich, UK). Plates were incubated at 37 ^{o}C for 2 hours to allow a Matrigel matrix gel to form, after which excess PBS was aspirated. Cells were detached using Accutase solution

(Sigma-Aldrich, UK) before being seeded in FBS-free media on top of the Matrigel matrix in the upper compartment of the Transwell. In some experiments, media was supplemented with 10 µg/ml mouse IgG1k mAb (MOPC-21) (Table 1), 10 µg/ml anti-Tspan15 mAb (1C12, 4A4, 5D4, 5F4) (Table 1), 0.5 µg/ml recombinant human N-terminal N-cadherin (R&D Systems, UK), 25 nM of the FGFR inhibitor PD173074 (Cayman Chemical, USA), or the relevant vehicle control. An equal volume of sterile, deionised water containing 2mM $CaCl_2$ was used as the vehicle control for recombinant human N-cadherin, whilst ethanol was used alongside PD173074. Complete media was added to the bottom of the companion plate with the 10% FBS functioning as a chemoattractant to stimulate invasion. Following incubation for 24 hours at 37 ^{o}C in 5% (v/v) CO_2, non-invasive cells were removed from the upper side of the Matrigel matrix with a cotton swab. Invasive cells on the underside of the Transwell were subsequently washed in PBS, fixed in 4% (v/v) formaldehyde (Sigma-Aldrich, UK), and stained with 0.5% (v/v) crystal violet (Sigma-Aldrich, UK). Cells were then imaged at five fields of view on each Transwell using a Nikon SMZ1000 microscope with a 9.6x magnification. Images were analysed using ilastik (Berg et al., 2019) and ImageJ (Schneider et al., 2012); ilastik was used to classify invasive cells and create a segmentation mask from which the percentage cell coverage was calculated with the following ImageJ Macro:

```
setAutoThreshold("Otsu");
run("Convert to Mask");
run("Area Calculator", "specify=0");
```

2.4.3 Cell viability assay

The Trypan Blue exclusion assay was used to estimate cell viability. Cells were seeded in triplicate in a 6-well plate at a density of 2 x 10^5 cells/well; complete media containing 0.5 µg/ml recombinant human N-cadherin as well as 25 nM PD173074 or ethanol as a vehicle control was used. Twenty-four hours post-plating, media was centrifuged to collect non-adherent cells, before adherent cells were trypsinised. Both populations of cells were then resuspended together in an appropriate volume of

complete media supplemented with a 1:10 dilution of 0.4% Trypan blue (Sigma-Aldrich, UK). The unstained (viable) and stained (non-viable) cells were counted using a haemocytometer with cell viability being calculated:

$$Cell\ viability\ (\%) = \left(1 - \frac{Number\ of\ non-viable\ cells}{Total\ number\ of\ cells}\right) x\ 100$$

2.5 FGFR signalling assay

HEK-293T cells were seeded at a density of 5x10^5 cells/well in a 12-well plate (Thermo Fisher Scientific, UK). The following day, cells were washed twice with PBS, before media was exchanged for Opti-MEM supplemented with ITS+ (formulation: 12.5 mg human recombinant insulin, 12.5 mg human transferrin, 12.5 µg selenium acid, and 10.7 mg linoleic acid) (Corning, UK). After incubation for 1 hour, cells were treated with 0.4 ng/ml human FGF (ACRO Biosystems, UK), 1.2 µg/ml recombinant human N-cadherin, or the two together for 15 minutes, 2 hours, and 8 hours. Where required, an equal volume of sterile PBS was used as a vehicle control for FGF, whilst sterile, deionised water containing 2mM $CaCl_2$ was used for N-cadherin. Cells were subsequently lysed on the plate in 100 µl of 1% (v/v) Triton X-100 lysis buffer, which was supplemented with a 1:100 dilution of 100x protease inhibitor cocktail and a 1:20 dilution of PhosSTOP (see Section 2.3.2.1). Lysate samples were assessed by Western blotting as described in, Section 2.3.3, with antibodies against ERK and P-ERK (Table 1). Band intensities of ERK and P-ERK were quantitated and the percentage of total ERK that had been phosphorylated was calculated.

2.6 NF-kB luciferase reporter assay

HEK-293T cells were transfected, as described in Section 2.2.5, with 0.2 µg of the NF-κB-luciferase reporter plasmid (Shapiro et al., 1996). Following incubation overnight, positive control wells were stimulated for 6 hours with 50 ng/ml phorbol myristate acetate (PMA) (Merck) and 1 µM ionomycin (SLS, UK) for maximal activation. Matched control wells were left unstimulated and treated with an equal volume of vehicle control (DMSO + ethanol). Cells were subsequently lysed for 5 minutes at

room temperature in 1% (v/v) Triton X-100 supplemented with 0.1 mM dithiothreitol (DTT) (Merck, UK) and 20 mM KH_2PO, pH 7.8 (Thermo Fisher Scientific, UK). Post lysis, lysates were plated in triplicate 100 µl volumes in a 96-well plate with an equal volume of luciferase assay buffer (20 mM adenosine triphosphate (ATP) (Sigma-Aldrich, UK), 40 mM $MgCl_2$ (Thermo Fisher Scientific, UK), 40 mM KH_2PO in dH_20, pH 7.8). Luciferase activity was measured following injection of 1 mM D-luciferin (Cambridge Bioscience, UK) on a Mithras LB 940 luminometer (Berthold Technologies, Germany). Luminescence was quantitated for each condition as a percentage of PMA- and ionomycin-treated cells.

2.7 Microscopy

2.7.1 Light microscopy

HEK-293T cells were seeded on a 6-well plate (Thermo Fisher Scientific, UK) at a density of $1x10^5$ cells/well. Cells were imaged 96 hours post-plating on an EVOS M5000 imaging system (Thermo Fisher Scientific, UK) equipped with a 20x objective lens and brightfield phase ring.

2.7.2 Live cell imaging

HEK-293T cells were seeded on a 24-well plate (Corning, UK) at a density of $8x10^4$ cells/well. The following day, live cell images were captured at two fields of view every 15 minutes for 24 hours on a Livecyte microscope (Phasefocus, UK) equipped with a 20x objective lens. Throughout imaging, cells were maintained in 5% (v/v) CO_2 at 37 ^oC.

The integrated analysis software was used to segment cells and assess their behaviour, including morphology (perimeter and sphericity), proliferation, and random motility (instantaneous velocity and confinement ratio).

2.7.3 Fluorescence microscopy

2.7.3.1 Immunostaining

Cells were cultured on 13 mm glass coverslip (VWR, UK) in a 24-well plate. Twenty-four hours post-plating, cells were washed in PBS, fixed in 4% (v/v) formaldehyde for 15 minutes, and subsequently washed a further three times. To enable the staining of intracellular proteins, cells were permeabilised for 5 minutes with 0.1% (v/v) Triton X-100 diluted in PBS, before being washed again. Cells were then incubated with block buffer (1% (w/v) high-purity BSA (Sigma-Aldrich, UK) and 2% (v/v) goat serum (Merck, UK) diluted in PBS) for at least 20 minutes to prevent non-specific antibody binding. The anti-NF-kappaB p65 antibody (Table 1) diluted in block buffer was next added to the coverslips. Following incubation for 1 hour, the cells were washed three times with PBS to remove any unbound antibody. They were then incubated for 1 hour in the dark with the Alexa Fluor 647 secondary antibody (Table 1) and 1 µg/ml Hoechst trihydrochloride (Invitrogen) diluted in block buffer, before being washed a further four times. To prepare samples for imaging, coverslips were mounted onto glass cover slides (Thermo Fisher Scientific, UK) with Hydromount (National Diagnostics, USA). Slides were stored in the dark at 4 ^{o}C.

2.7.3.2 Airyscan confocal microscopy

Dual colour confocal images were acquired in super-resolution mode on a Zeiss LSM 900 microscope (Zeiss, Germany) with a 63× 1.4 NA oil objective and Airyscan 2 detector. For the antibodies and dyes outlined in Section 2.7.3.1, the 640 nm and 405 nm laser lines were used. Post-capture, images were processed on the Zen Blue software (Zeiss, Germany) to obtain Airyscan images with improved resolution and signal-to-noise (Huff et al., 2017).

The colocalisation of proteins was analysed on Fiji software (Schindelin et al., 2012; Pike et al., 2017). Images were processed by median filtering for noise removal, rolling-ball background subtraction, and threshold adjustment. Post-processing, Manders' coefficients were used to determine the localisation of proteins (Manders et al., 1993).

2.8 Analysis of cancer samples using GEPIA2

2.8.1 Gene expression analysis

ADAM10 and Tspan15 RNA-seq data from cancer and corresponding control tissues were analysed using the Gene Expression Profiling Interactive Analysis 2 (GEPIA2) portal (Tang et al., 2019), which combines datasets from The Cancer Genome Atlas (TCGA) and the Genotype-Tissue Expression (GTEx) project. The data were $\log_2$(TPM+1) transformed and the $\log_2$fold_change ($\log_2$FC) was calculated by subtracting the median non-tumour control expression from that of the tumour sample. Statistical significance was analysed by a one-way analysis of variance (ANOVA); the $\log_2$FC threshold was set to 1 and the p-value cutoff was 0.01.

2.8.2 Patient survival analysis

The clinical significance of ADAM10 and Tspan15 tumour expression on patient survival was analysed using GEPIA2 (Tang et al., 2019). Patients were stratified into 'high'- and 'low'-expression cohorts with the respective impact on overall survival being assessed; the exact cutoff threshold is detailed in each figure. The cox proportional hazard ratio (HR) was calculated and differences between cohorts were analysed by a log-rank test with the p-value cutoff set at 0.05.

2.9 Statistical analysis

Statistical analyses were conducted using GraphPad Prism® version 10.0.3 for Windows (GraphPad Software, USA), unless otherwise stated. Non-parametric data were normalised prior to statistical analysis either by log or arcsine square root transformation. Differences in means were analysed by an unpaired t-test or a one- or two-way analysis of variance (ANOVA). For ANOVA tests, a Dunnett's or Tukey's multiple comparisons post hoc test was also completed. With the exception of data obtained from GEPIA2: ns = non-significant; * $p < 0.05$; ** $p < 0.01$; *** $p < 0.001$; **** $p < 0.0001$. The precise statistical analyses are outlined in each figure legend.

CHAPTER 3 THE EXPRESSION OF ADAM10 AND TSPAN15 HAS THE POTENTIAL TO BE CLINICALLY SIGNIFICANT IN MULTIPLE DIFFERENT CANCERS

3.1 Introduction

ADAM10 and Tspan15 have been reported to play a role in various malignancies (Guo et al., 2012; Fu et al., 2014; Liu et al., 2015; Mullooly et al., 2015; You et al., 2015; Ma et al., 2016; Tsang et al., 2018; Zhang et al., 2018; Hiroshima et al., 2019; Sépult et al., 2019; Sidahmed-Adrar et al., 2019; Yuan et al., 2020b). However, Tspan15's role has only been explored in several cancer types, and very few studies consider the role of Tspan15 and ADAM10 as a functional complex. This chapter, therefore, aimed to investigate the expression profiles of ADAM10 and Tspan15 in prevalent cancers, as well as the respective impact on patient survival. A secondary aim of this chapter was also to explore the differential expression and potential prognostic implications of other members of the ADAM and TspanC8 family; the significance of interplay between closely related proteins is rarely considered. To address these aims, a bioinformatics approach was used to analyse datasets publicly available on the Gene Expression Profiling Interactive Analysis 2 (GEPIA2) server (Tang et al., 2019).

Taken together, these findings will inform biological follow-up studies that aim to further understand the cancer-associated roles of these proteins.

3.2 Results

3.2.1 Pancreatic adenocarcinoma tumours exhibit increased expression of ADAM10 in addition to Tspan15; high tumour expression of both proteins is associated with a reduced survival rate

The GEPIA2 web server (Tang et al., 2019), which integrates datasets from The Cancer Genome Atlas (TCGA) and the Genotype-Tissue Expression (GTEx) project, was used to analyse ADAM10 and Tspan15 RNA-seq data from pancreatic adenocarcinoma tumour samples and corresponding control tissues. The data were $\log_2$(TPM+1) transformed and the $\log_2$fold_change ($\log_2$FC) was calculated by subtracting the median non-tumour control expression from the tumour value. Analysis of the data revealed differential expression profiles for ADAM10 and Tspan15 in pancreatic adenocarcinoma

tumours compared to normal tissues (Figure 10A); the two proteins were co-upregulated with respective log_2FC values of 2.47 (FC: 5.540) and 3.48 (FC: 11.158). Kaplan-Meier survival curves were subsequently analysed using the same online server. Patients were stratified into those with high-level (above the indicated cutoff point) and low-level (below the indicated cutoff point) tumour expression with the associated effect on overall survival being assessed; a range of cutoff points were tested to identify any cohorts of patients for which ADAM10 and Tspan15 expression may be a potential prognostic biomarker. This showed that pancreatic adenocarcinoma patients with an ADAM10 expression above the median tumour value had a reduced survival rate (Figure 10B). Indeed, a hazard ratio of 2.1 was observed for patients with high expression compared to those expressing ADAM10 below the median cutoff. Similarly, the patients expressing Tspan15 above the 70% cutoff point had a worse prognosis than those with expression below the 30% value (Figure 10B); the hazard ratio for high Tspan15 expression was 1.9.

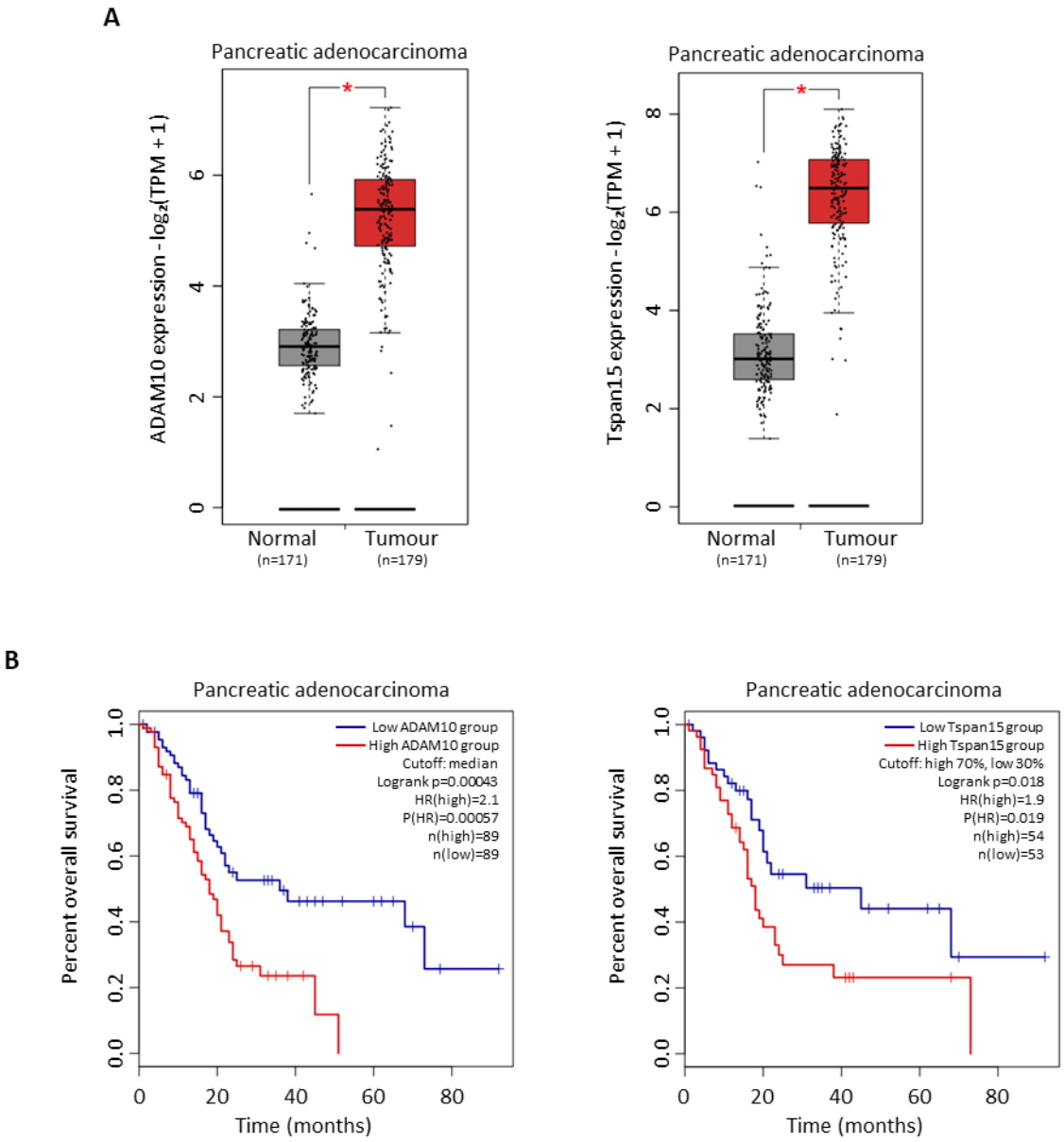


Figure 10: ADAM10 and Tspan15 are co-upregulated in pancreatic adenocarcinoma and patient survival is impaired by high tumour expression. Gene expression and survival data for pancreatic adenocarcinoma patients were assessed using publicly available databases on the GEPIA2 server (Tang et al., 2019). (A) ADAM10 and Tspan15 expression data were presented as boxplots comparing expression between tumour and corresponding control tissues. Data were $\log_2$(TPM+1) transformed and analysed by a one-way ANOVA; the $|\log_2 FC|$ threshold was set to 1 and the significance threshold was $p<0.01$. (B) Kaplan-Meier survival curves presented the survival probabilities of patients stratified into those with 'high level' (above the median value for ADAM10 and the 70% cutoff point for Tspan15) and 'low level' (below the median value for ADAM10 and the 30% cutoff point for Tspan15) tumour expression. Statistical differences were analysed by a log-rank test (* $p<0.05$).

3.2.2 ADAM10 and Tspan15 are co-upregulated in oesophageal carcinoma, but high tumour expression of neither protein affects patient prognosis.

Gene expression and survival data for oesophageal carcinoma were analysed using the GEPIA2 server (Tang et al., 2019). This indicated that oesophageal carcinoma patients exhibited increased expression of both ADAM10 and Tspan15 (Figure 11A); compared to corresponding control tissues tumour samples had a log_2FC of 1.65 (FC: 3.138) for ADAM10 expression and 1.8 (FC: 3.482) for Tspan15 expression. However, high tumour expression of neither protein had an effect on the probability of patient survival (Figure 11B).

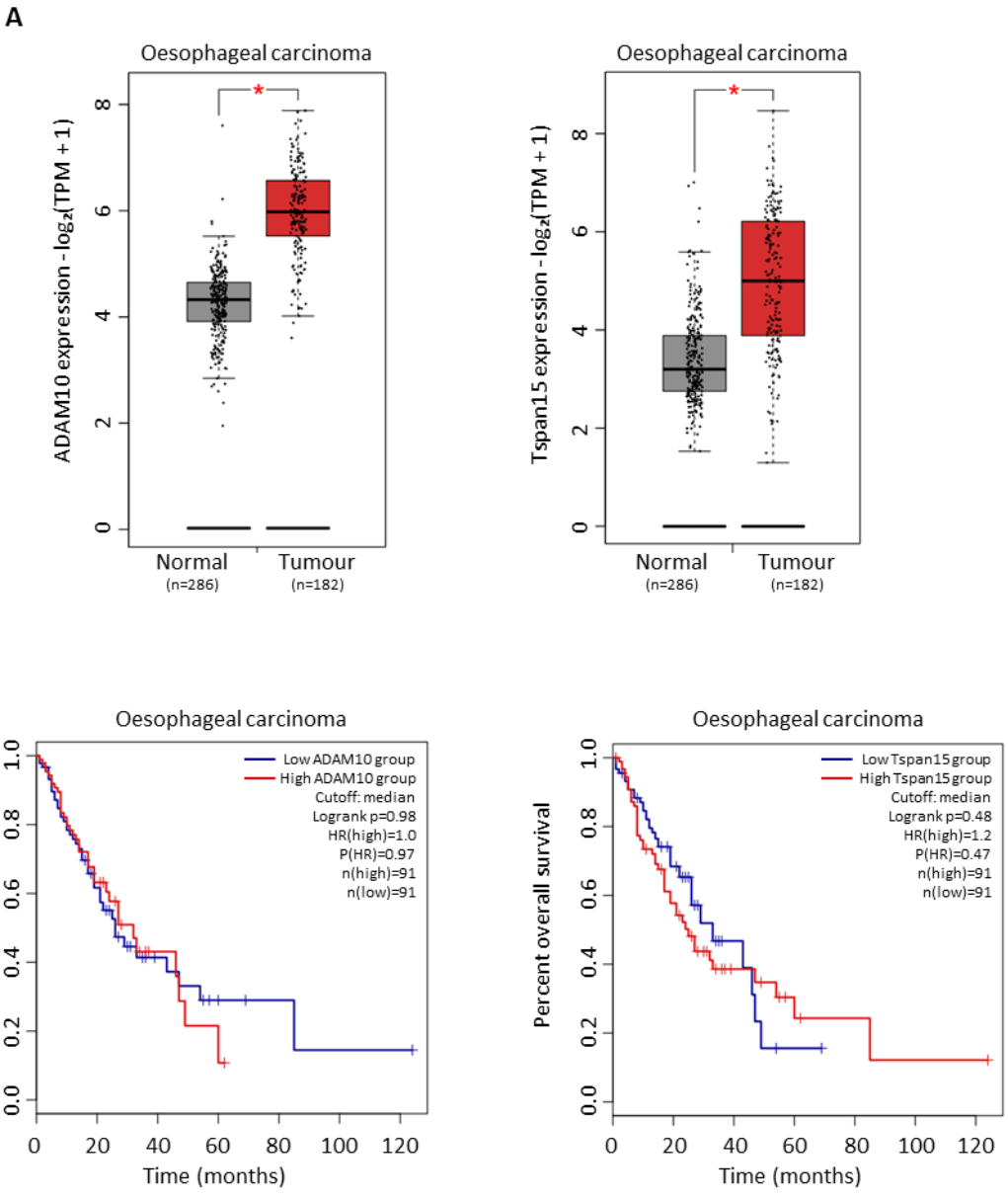


Figure 11: The gene expression of both ADAM10 and Tspan15 is increased in oesophageal carcinoma, but high tumour expression is not associated with unfavourable patient survival. Gene expression and survival data for oesophageal carcinoma patients were assessed using publicly available databases on the GEPIA2 server (Tang et al., 2019). (A) ADAM10 and Tspan15 expression data were presented as boxplots comparing expression between tumour and corresponding control tissues. Data were $\log_2$(TPM+1) transformed and analysed by a one-way ANOVA; the $|\log_2 FC|$ threshold was set to 1 and the significance threshold was $p<0.01$. (B) Kaplan-Meier survival curves presented the survival probabilities of patients stratified into those with 'high level' (above the median cutoff point) and 'low level' (below the median cutoff point) tumour expression. Statistical differences were analysed by a log-rank test (* $p<0.05$).

3.2.3 The gene expression of both ADAM10 and Tspan15 is increased in cholangiocarcinoma

The GEPIA2 server (Tang et al., 2019) was used to assess the expression levels of ADAM10 and Tspan15 in cholangiocarcinoma, as well as the associated effect on prognosis. This showed that both ADAM10 and Tspan15 were significantly upregulated (Figure 12A); cholangiocarcinoma tumours had a 2.41 $\log_2$FC (FC: 5.315) in ADAM10 expression compared to corresponding non-tumour tissues, in addition to a 5.14 $\log_2$FC (FC: 35.261) in Tspan15 expression. Despite this, patient survival was not dependent on Tspan15 tumour expression with no significant difference seen between those with expression above or below the median cutoff point (Figure 12B). In contrast, high ADAM10 tumour expression was unexpectedly associated with an improved prognosis (Figure 12B); a hazard ratio (HR) of 0.23 was indicative of a reduced risk of death for patients with high expression. Given the small sample size, however, more tumour samples are required to confirm this.

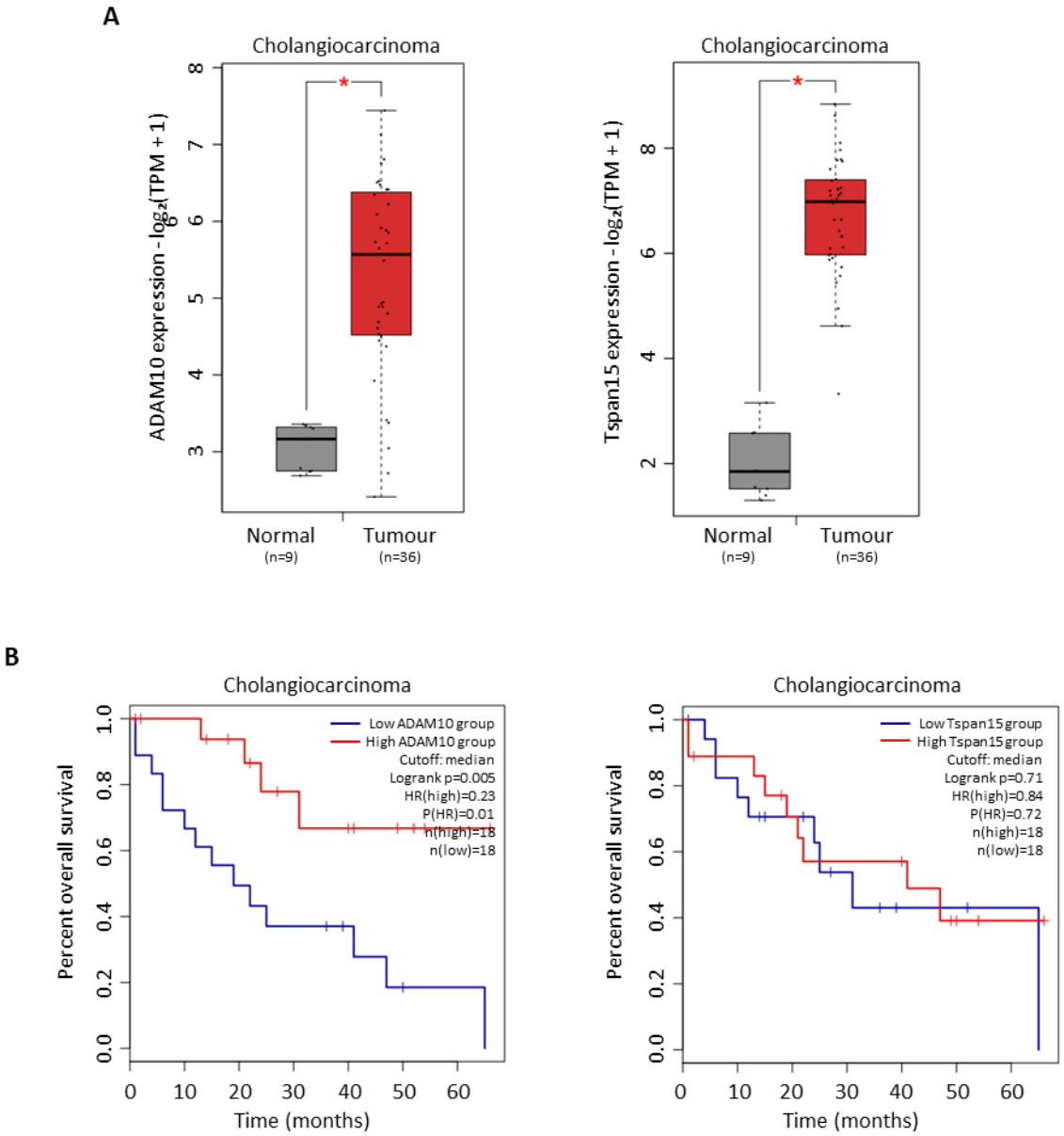


Figure 12: ADAM10 and Tspan15 gene expression is co-upregulated in cholangiocarcinoma tumours. Gene expression and survival data for cholangiocarcinoma patients were assessed using publicly available databases on the GEPIA2 server (Tang et al., 2019). (A) ADAM10 and Tspan15 expression data were presented as boxplots comparing expression between tumour and corresponding control tissues. Data were $\log_2$(TPM+1) transformed and analysed by a one-way ANOVA; the $|\log_2 FC|$ threshold was set to 1 and the significance threshold was $p<0.01$. (B) Kaplan-Meier survival curves presented the survival probabilities of patients stratified into those with 'high level' (above the median cutoff point) and 'low level' (below the median cutoff point) tumour expression. Statistical differences were analysed by a log-rank test (* $p<0.05$).

3.2.4 Tspan15 is upregulated in liver hepatocellular carcinoma and high tumour expression is associated with unfavourable patient survival

Liver hepatocellular carcinoma data available on the GEPIA2 server (Tang et al., 2019) was analysed to explore the clinical significance of ADAM10 and Tspan15 gene expression. It was shown that Tspan15 was overexpressed in tumour samples with a log_2FC of 1.08 (FC: 2.114) (Figure 13A). Furthermore, high Tspan15 tumour expression was associated with an adverse prognosis; patients with expression above the median had a hazard ratio of 1.5 compared to those with expression below the median (Figure 13B). ADAM10 expression was also found to be moderately increased in liver hepatocellular carcinoma tumours (Figure 13A); the log_2FC was 0.94 (FC: 1.919) between tumour samples and corresponding control tissues. However, the probability of patient survival was not affected by the expression levels of ADAM10 (Figure 13B).

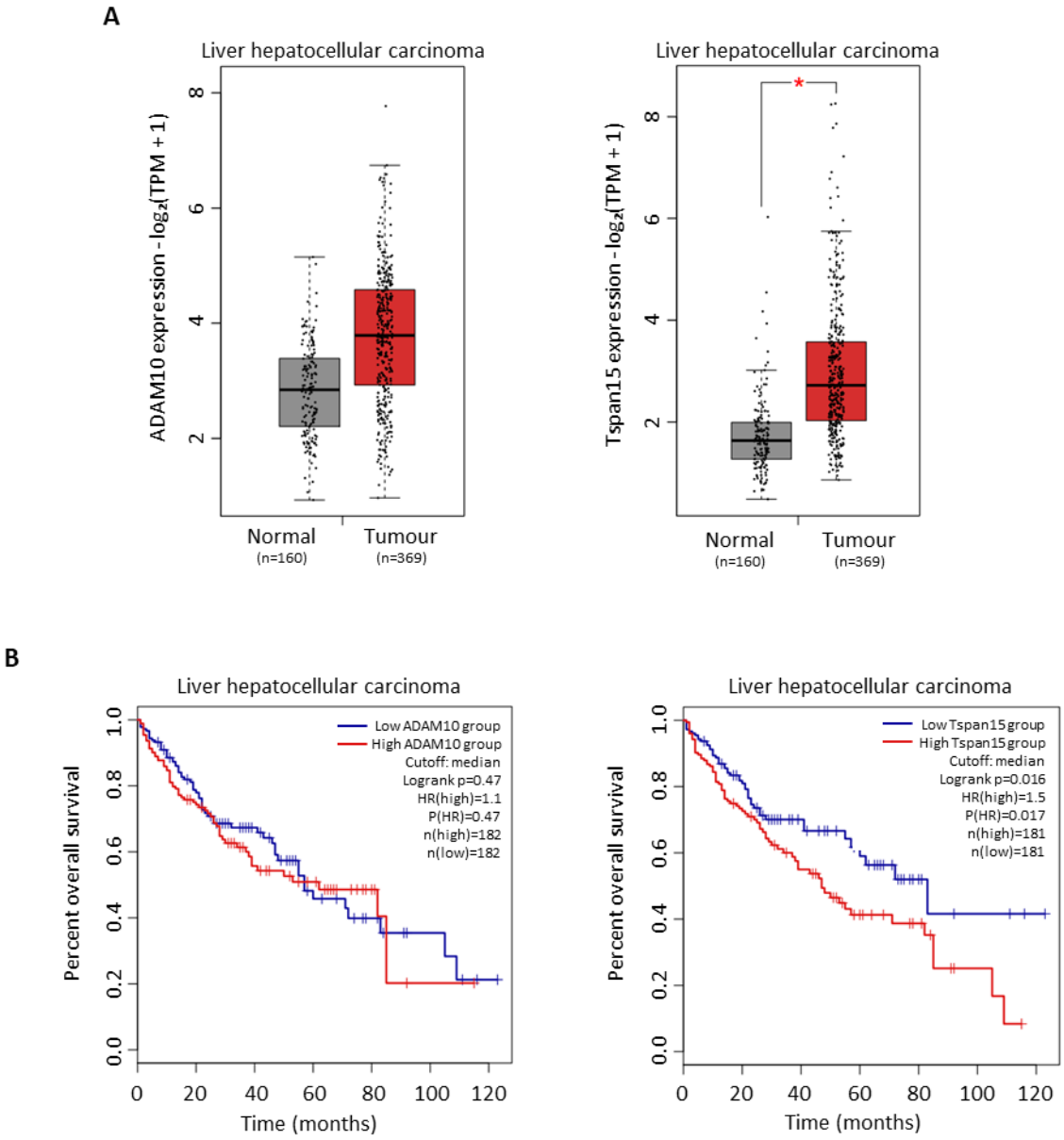


Figure 13: The gene expression of Tspan15 is elevated in liver hepatocellular and high tumour expression is a potential prognostic biomarker. Gene expression and survival data for liver hepatocellular carcinoma patients were assessed using publicly available databases on the GEPIA2 server (Tang et al., 2019). (A) ADAM10 and Tspan15 expression data were presented as boxplots comparing expression between tumour and corresponding control tissues. Data were $\log_2$(TPM+1) transformed and analysed by a one-way ANOVA; the $|\log_2 FC|$ threshold was set to 1 and the significance threshold was $p<0.01$. (B) Kaplan-Meier survival curves presented the survival probabilities of patients stratified into those with 'high level' (above the median cutoff point) and 'low level' (below the median cutoff point) tumour expression. Statistical differences were analysed by a log-rank test (* $p<0.05$).

3.2.5 Tspan15, unlike ADAM10, is upregulated in ovarian serous cystadenocarcinoma, but high Tspan15 tumour expression does not affect patient survival, whereas high ADAM10 expression is a potential prognostic biomarker

The GEPIA2 server (Tang et al., 2019) was used to investigate the potential clinical significance of ADAM10 and Tspan15 in ovarian serous cystadenocarcinoma. Analysis of the data revealed that ADAM10 gene expression was not significantly increased in tumours compared to corresponding control tissues (Figure 14A); the $\log_2$FC was 0.51 (FC: 1.424). High-level ADAM10 tumour expression, however, was found to be unfavourable for patient survival with a hazard ratio of 1.3 (Figure 14B). By comparison, RNA-seq data showed that Tspan15 was upregulated in ovarian serous cystadenocarcinoma tumours by a $\log_2$FC of 3.49 (FC: 11.236) (Figure 14A), but high tumour expression did not affect patient prognosis (Figure 14B).

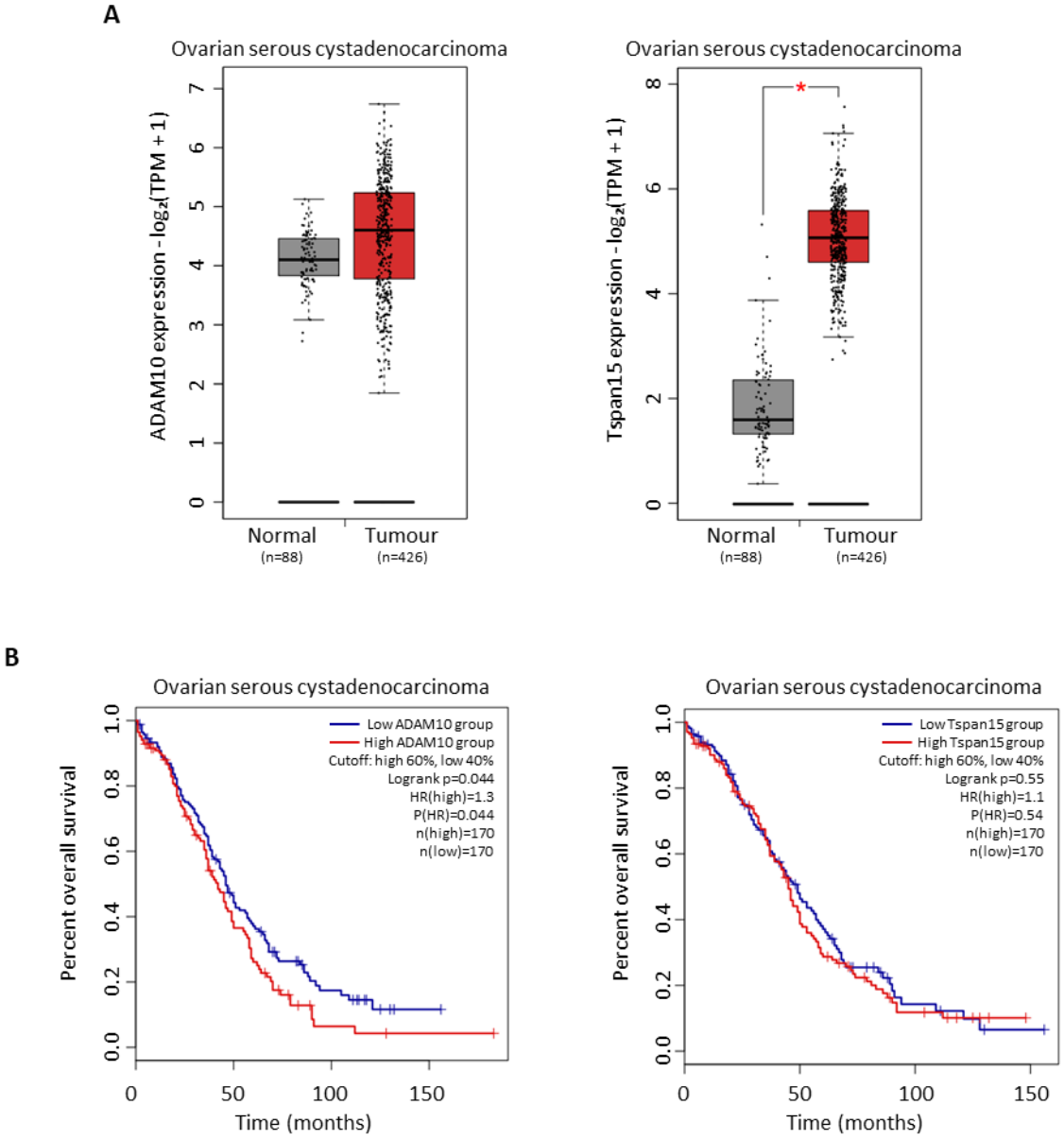


Figure 14: The gene expression of Tspan15 is increased independently of ADAM10 in ovarian serous cystadenocarcinoma tumours, but high Tspan15 tumour expression is not unfavourable for patient survival, whereas high ADAM10 expression is. Gene expression and survival data for ovarian serous cystadenocarcinoma patients were assessed using publicly available databases on the GEPIA2 server (Tang et al., 2019). (A) ADAM10 and Tspan15 expression data were presented as boxplots comparing expression between tumour and corresponding control tissues. Data were $\log_2$(TPM+1) transformed and analysed by a one-way ANOVA; the $|\log_2 FC|$ threshold was set to 1 and the significance threshold was $p<0.01$. (B) Kaplan-Meier survival curves presented the survival probabilities of patients stratified into those with 'high level' (above the 60% cutoff point) and 'low level' (below the 40% cutoff point) tumour expression. Statistical differences were analysed by a log-rank test (* $p<0.05$).

3.2.6 The gene expression of ADAM10 but not Tspan15 is upregulated in prostate adenocarcinoma tumours

The expression profiles of ADAM10 and Tspan15 in prostate adenocarcinoma tumours compared to matched TCGA normal and GTEx data were analysed using GEPIA2 (Tang et al., 2019), as described in Section 3.2.1. It was shown that ADAM10, unlike Tspan15, was overexpressed in tumour samples with a $\log_2$FC of 1.03 (FC: 2.042) (Figure 15A). However, analysis of patient survival data using the same online server indicated that high (above the median cutoff point) ADAM10 expression was not associated with a worse prognosis (Figure 15B). Similarly, Tspan15 expression did not affect the overall survival of prostate adenocarcinoma patients with no difference observed between those with high (above the median cutoff point) and low (below the median cutoff point) expression (Figure 15B).

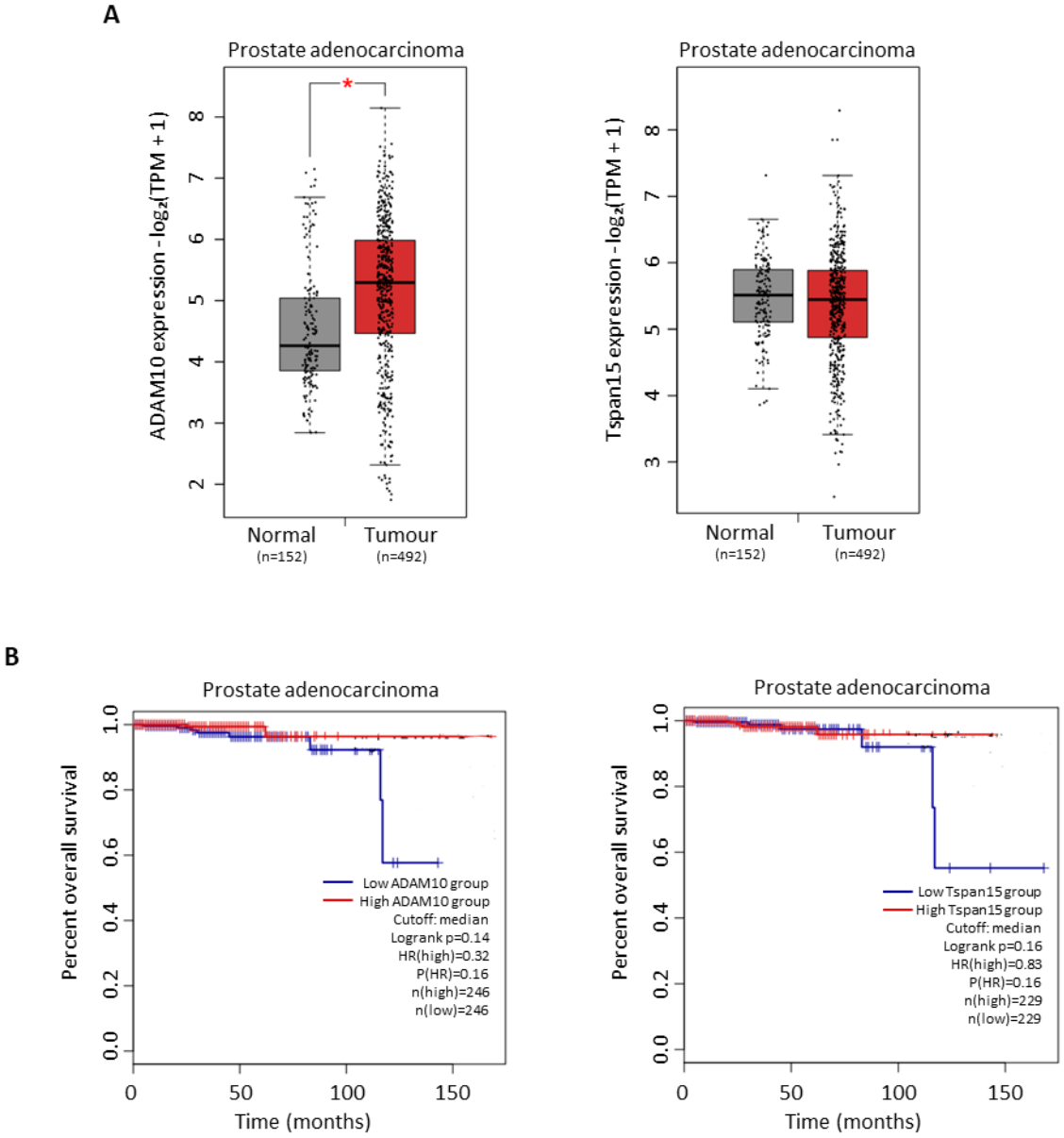


Figure 15: ADAM10 is upregulated independently of Tspan15 in prostate adenocarcinoma tumours. Gene expression and survival data for prostate adenocarcinoma patients were assessed using publicly available databases on the GEPIA2 server (Tang et al., 2019). (A) ADAM10 and Tspan15 expression data were presented as boxplots comparing expression between tumour and corresponding control tissues. Data were $\log_2$(TPM+1) transformed and analysed by a one-way ANOVA; the $|\log_2 FC|$ threshold was set to 1 and the significance threshold was $p<0.01$. (B) Kaplan-Meier survival curves presented the survival probabilities of patients stratified into those with 'high level' (above the median cutoff point) and 'low level' (below the median cutoff point) tumour expression. Statistical differences were analysed by a log-rank test (* $p<0.05$).

3.2.7 Colon adenocarcinoma patients exhibit an upregulation of ADAM10 expression that is Tspan15-independent

The GEPIA2 server (Tang et al., 2019) was used to assess the expression levels of ADAM10 and Tspan15 in colon adenocarcinoma, as well as the associated impact on patient survival. Analysis of the data revealed that colon adenocarcinoma patients exhibited increased ADAM10 but not Tspan15 expression (Figure 16A); the log_2FC for ADAM10 expression was 1.08 (FC: 2.114) between tumour samples and corresponding control tissues. Despite this, ADAM10 expression, similar to Tspan15 expression, had no associated effect on patient survival (Figure 16B).

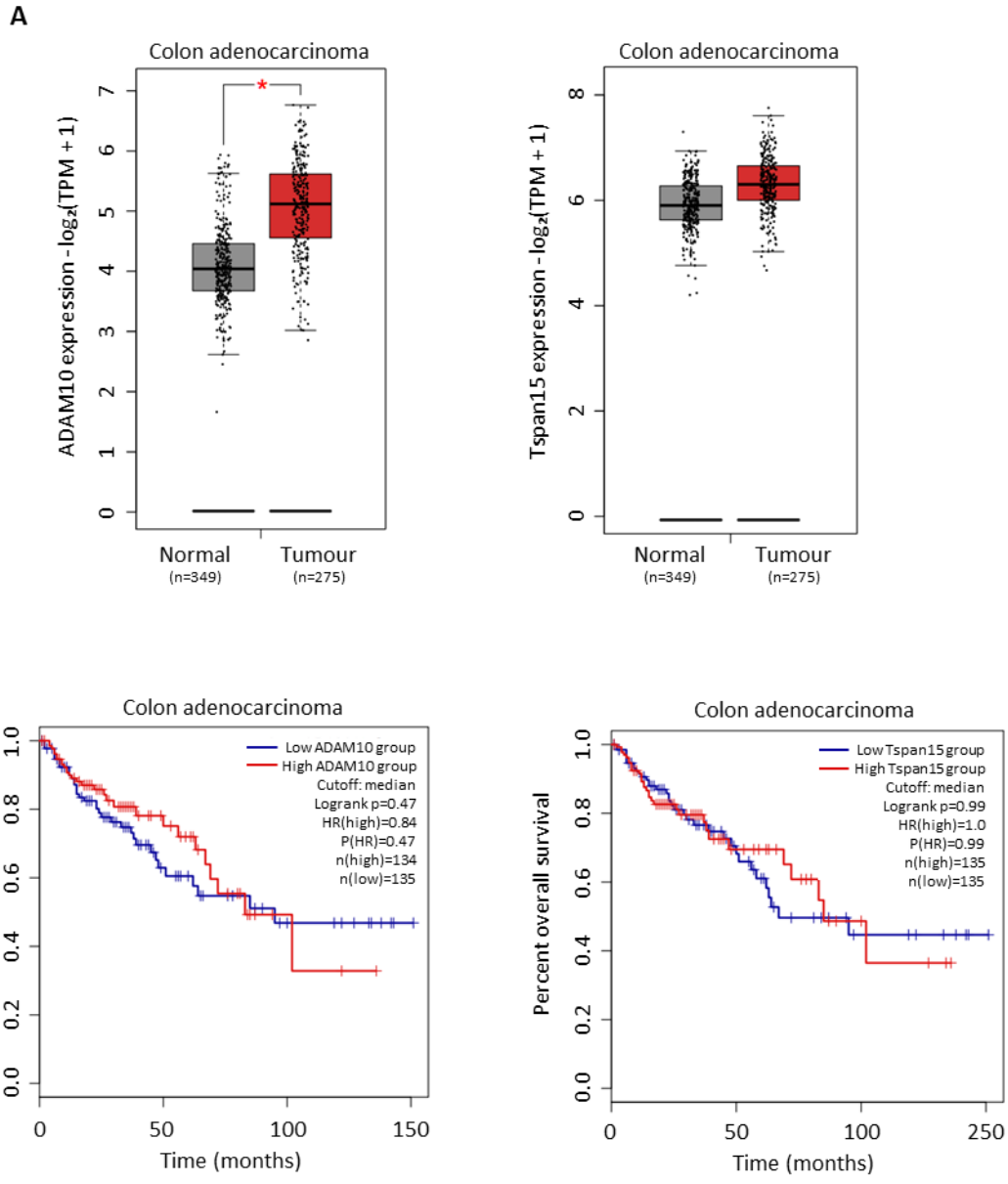


Figure 16: ADAM10, unlike Tspan15, is overexpressed in colon adenocarcinoma; neither protein though is a potential prognostic biomarker. Gene expression and survival data for colon adenocarcinoma patients were assessed using publicly available databases on the GEPIA2 server (Tang et al., 2019). (A) ADAM10 and Tspan15 expression data were presented as boxplots comparing expression between tumour and corresponding control tissues. Data were $\log_2$(TPM+1) transformed and analysed by a one-way ANOVA; the $|\log_2 FC|$ threshold was set to 1 and the significance threshold was $p<0.01$. (B) Kaplan-Meier survival curves presented the survival probabilities of patients stratified into those with 'high level' (above the median cutoff point) and 'low level' (below the median cutoff point) tumour expression. Statistical differences were analysed by a log-rank test (* $p<0.05$).

3.2.8 ADAM10 is differentially expressed in glioblastoma multiforme tumours but does not affect patient survival

Gene expression and survival data for glioblastoma multiforme were assessed using GEPIA2 (Tang et al., 2019) as outlined in Section 3.2.1. This showed that ADAM10 expression was significantly upregulated (Figure 17A); glioblastoma multiforme tumours had a 1.94 $\log_2$FC (FC: 3.837) in ADAM10 expression compared to corresponding control tissues. Additionally, glioblastoma multiforme tumours exhibited a moderate upregulation of Tspan15 expression with a $\log_2$FC of 0.97 (FC: 1.959) (Figure 17A). Despite this, the expression levels of neither ADAM10 nor Tspan15 affected patient survival (Figure 17B).

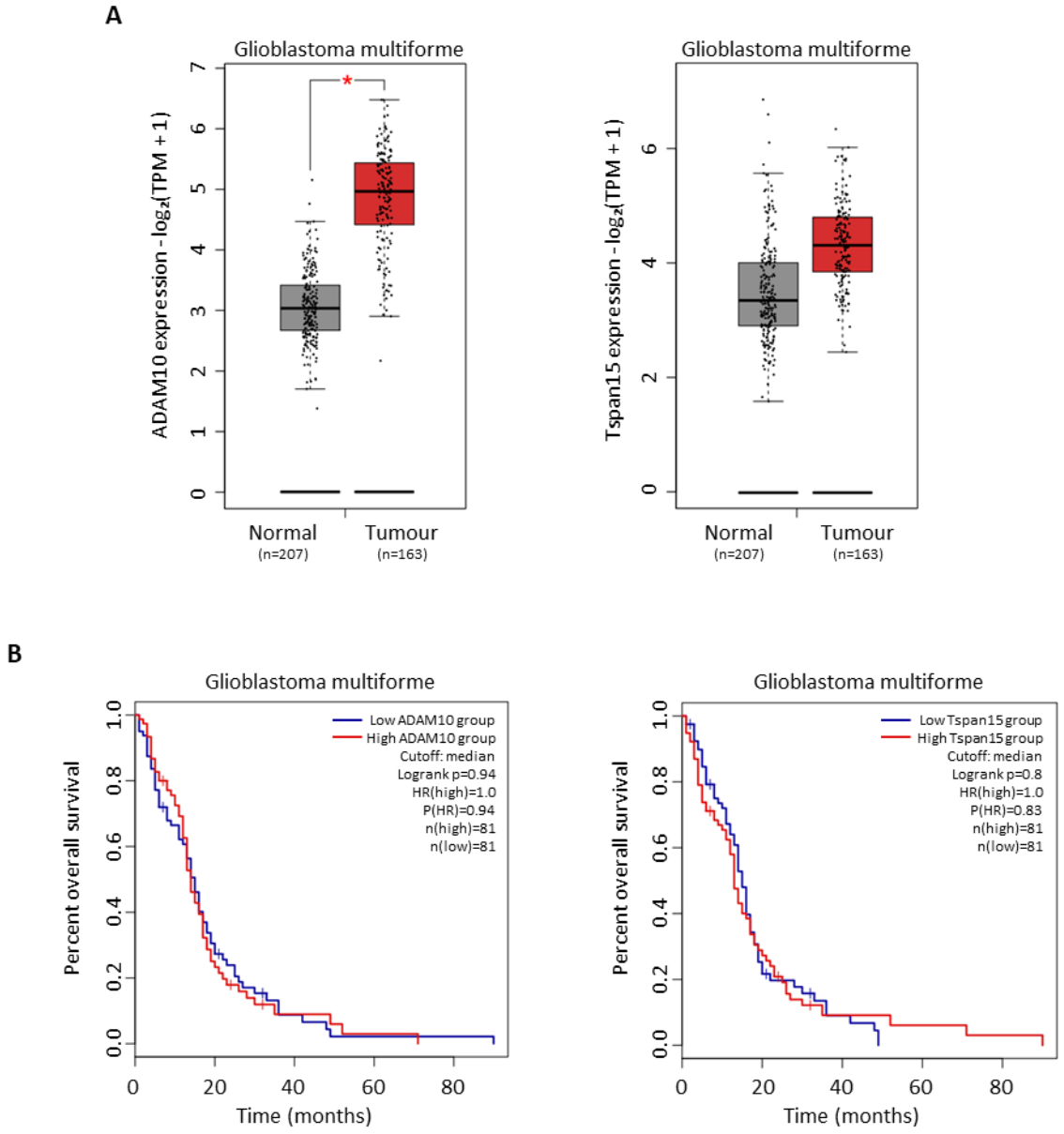


Figure 17: ADAM10 is overexpressed in glioblastoma multiforme tumours, but expression levels are not associated with an altered patient prognosis. Gene expression and survival data for glioblastoma multiforme patients were assessed using publicly available databases on the GEPIA2 server (Tang et al., 2019). (A) ADAM10 and Tspan15 expression data were presented as boxplots comparing expression between tumour and corresponding control tissues. Data were $\log_2$(TPM+1) transformed and analysed by a one-way ANOVA; the $|\log_2 FC|$ threshold was set to 1 and the significance threshold was $p<0.01$. (B) Kaplan-Meier survival curves presented the survival probabilities of patients stratified into those with 'high level' (above the median cutoff point) and 'low level' (below the median cutoff point) tumour expression. Statistical differences were analysed by a log-rank test (* $p<0.05$).

3.2.9 Skin cutaneous melanoma tumours exhibit increased ADAM10 gene expression, but this is not a prognostic biomarker

The GEPIA2 server (Tang et al., 2019) was used to analyse publicly available datasets for skin cutaneous melanoma, as per Section 3.2.1. Evaluation of RNA-seq data from tumour samples and corresponding controls revealed that ADAM10 is upregulated independently of Tspan15 in skin cutaneous melanoma (Figure 18A). Indeed, ADAM10 expression had a $\log_2$FC of 1.98 (FC: 3.945) for tumour samples compared to normal tissues, whereas 0.18 was the $\log_2$FC (FC: 1.133) for Tspan15 expression in skin cutaneous melanoma. Subsequent analysis of Kaplan-Meier survival curves, however, indicated that patients stratified into those with 'high level' (above the median cutoff point) and 'low level' (below the median cutoff point) ADAM10 expression did not exhibit an altered survival probability (Figure 18B). As such, ADAM10 expression is not likely a potential prognostic biomarker for skin cutaneous melanoma patients. Likewise, Tspan15 tumour expression was not shown to be correlated with the probability of patient survival (Figure 18B).

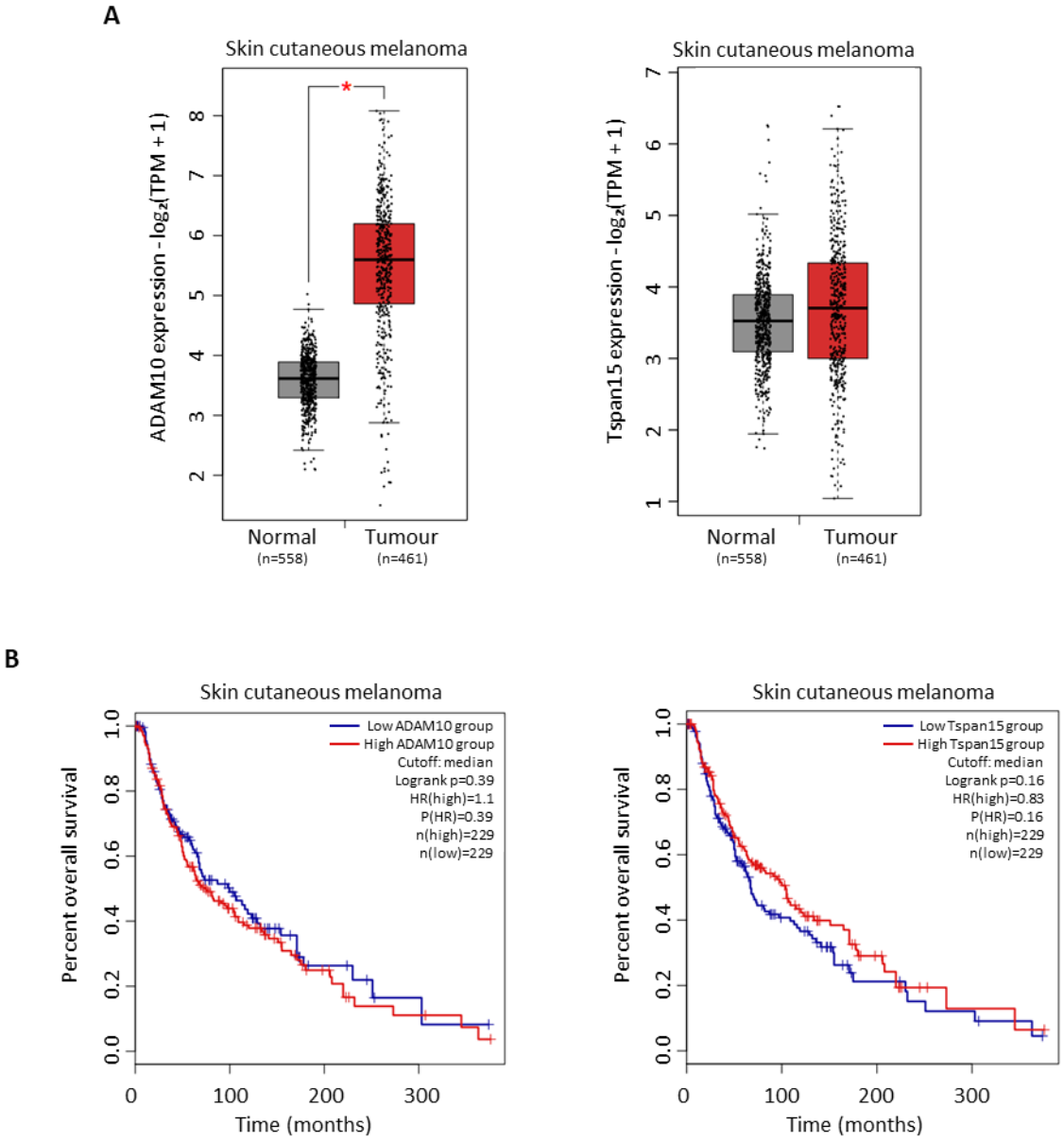


Figure 18: Skin cutaneous melanoma patients exhibit increased ADAM10 gene expression, but high tumour expression is not associated with an adverse prognosis. Gene expression and survival data for skin cutaneous melanoma patients were assessed using publicly available databases on the GEPIA2 server (Tang et al., 2019). (A) ADAM10 and Tspan15 expression data were presented as boxplots comparing expression between tumour and corresponding control tissues. Data were $\log_2$(TPM+1) transformed and analysed by a one-way ANOVA; the $|\log_2 FC|$ threshold was set to 1 and the significance threshold was $p<0.01$. (B) Kaplan-Meier survival curves presented the survival probabilities of patients stratified into those with 'high level' (above the median cutoff point) and 'low level' (below the median cutoff point) tumour expression. Statistical differences were analysed by a log-rank test (* $p<0.05$).

3.2.10 ADAM10 gene expression is increased in stomach adenocarcinoma

The expression profiles of ADAM10 and Tspan15 in stomach adenocarcinoma tumours were analysed using the GEPIA2 server (Tang et al., 2019). It was shown that the gene expression of ADAM10, unlike Tspan15, was significantly upregulated (Figure 19A); the log_2FC for ADAM10 expression was 2.32 (FC: 4.993) between tumour samples and corresponding non-tumour tissues. Nevertheless, analysis of patient survival probabilities revealed that neither ADAM10 nor Tspan15 likely modulates prognosis in this malignancy (Figure 19B).

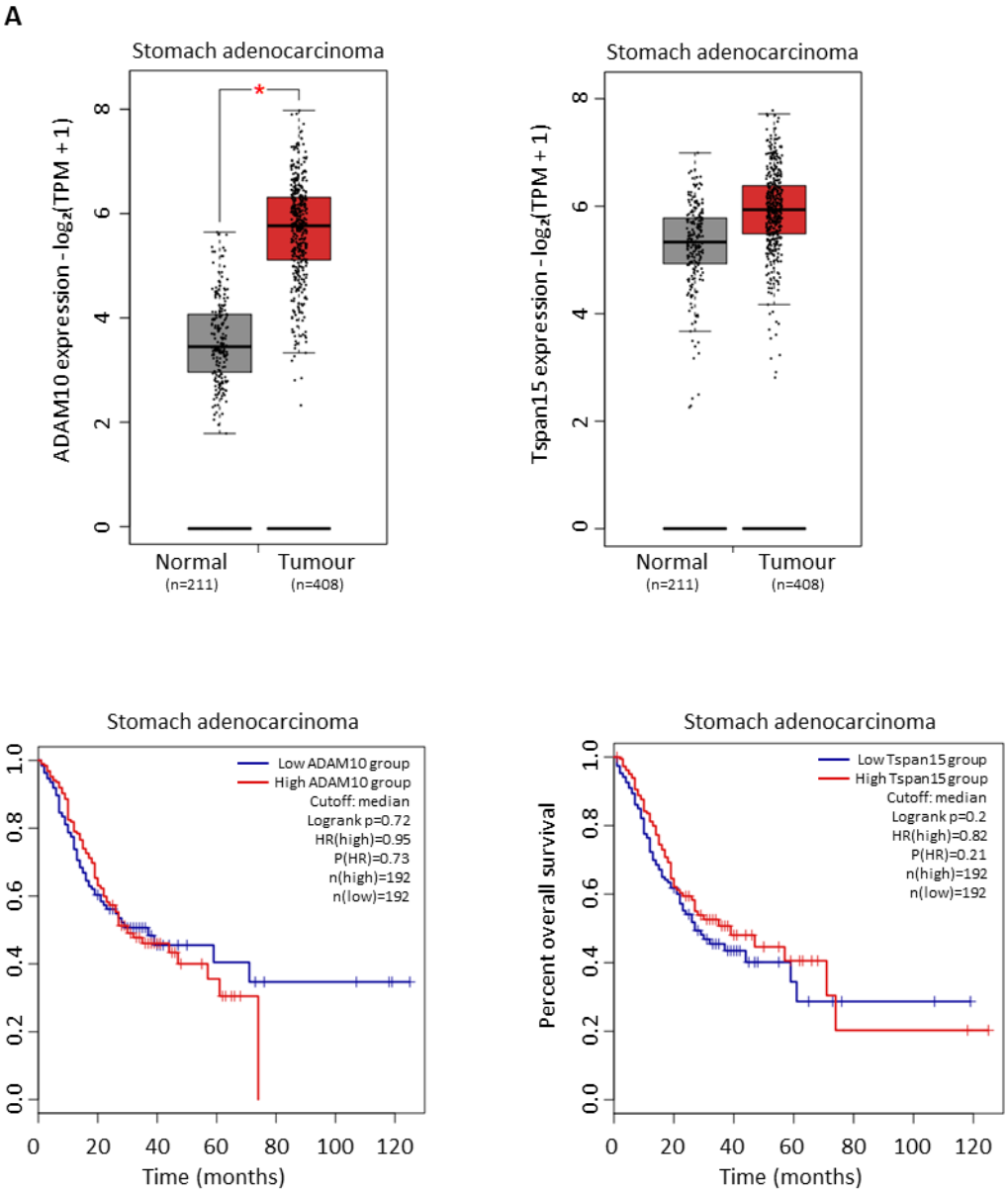


Figure 19: Stomach adenocarcinoma patients exhibit an upregulation in ADAM10 gene expression, but high tumour expression does not affect overall survival. Gene expression and survival data for stomach adenocarcinoma patients were assessed using publicly available databases on the GEPIA2 server (Tang et al., 2019). (A) ADAM10 and Tspan15 expression data were presented as boxplots comparing expression between tumour and corresponding control tissues. Data were $\log_2$(TPM+1) transformed and analysed by a one-way ANOVA; the $|\log_2 FC|$ threshold was set to 1 and the significance threshold was $p<0.01$. (B) Kaplan-Meier survival curves presented the survival probabilities of patients stratified into those with 'high level' (above the median cutoff point) and 'low level' (below the median cutoff point) tumour expression. Statistical differences were analysed by a log-rank test (* $p<0.05$).

3.2.11 ADAM10 and Tspan15 gene expression is subtly upregulated in breast cancer tumours compared to corresponding non-tumour tissues and high ADAM10 tumour expression is unfavourable for patient survival

The potential clinical significance of ADAM10 and Tspan15 expression in breast cancer was evaluated using data publicly available on the GEPIA2 server (Tang et al., 2019), as described in Section 3.2.1. This revealed a subtle upregulation of both ADAM10 and Tspan15 gene expression in breast cancer tumours compared to corresponding control tissues (Figure 20A). However, this increase in expression did not reach significance; tumour samples had a $\log_2$FC of 0.88 (FC: 1.840) for ADAM10 and 0.78 (FC: 1.717) for Tspan15. Interestingly though, breast cancer patients with an ADAM10 tumour expression above the upper quartile level had a lower survival probability (Figure 20B). Indeed, a hazard ratio of 1.6 was observed for patients with high tumour expression compared to those expressing ADAM10 below the lower quartile cutoff. By comparison, Tspan15 expression had no effect on patient survival (Figure 20B).

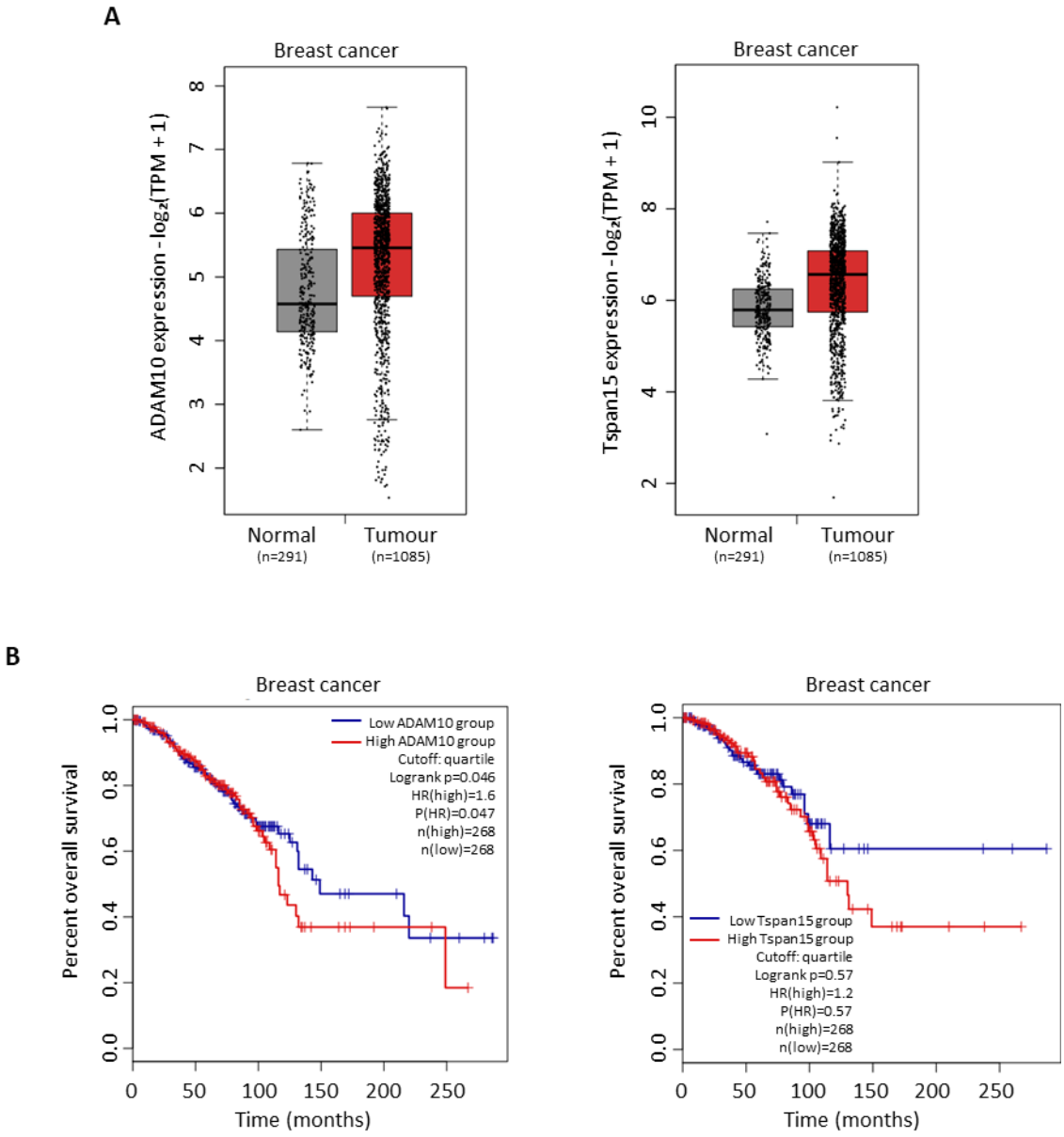


Figure 20: A slight differential expression of ADAM10 and Tspan15 is observed in breast cancer tumours and the probability of patient survival is negatively correlated with high ADAM10 tumour expression. Gene expression and survival data for breast cancer patients were assessed using publicly available databases on the GEPIA2 server (Tang et al., 2019). (A) ADAM10 and Tspan15 expression data were presented as boxplots comparing expression between tumour and corresponding control tissues. Data were $\log_2$(TPM+1) transformed and analysed by a one-way ANOVA; the $|\log_2 FC|$ threshold was set to 1 and the significance threshold was $p<0.01$. (B) Kaplan-Meier survival curves presented the survival probabilities of patients stratified into those with 'high level' (above the upper quartile cutoff point) and 'low level' (below the lower quartile cutoff point) tumour expression. Statistical differences were analysed by a log-rank test (* $p<0.05$).

3.2.12 Lung squamous cell carcinoma tumours do not exhibit significantly altered expression of either ADAM10 or Tspan15, but the overall survival rate is reduced when ADAM10 tumour expression is high

The GEPIA2 server (Tang et al., 2019) was used to assess the expression profiles of ADAM10 and Tspan15 in lung squamous cell carcinoma tumours compared to corresponding non-tumour tissues. Analysis of the RNA-seq data showed that neither ADAM10 nor Tspan15 expression was significantly different in tumour samples (Figure 21A). However, there was a slight increase in ADAM10 expression with a $\log_2$FC of 0.83 (FC: 1.778), as well as a subtle decrease in Tspan15 expression. Subsequent analysis of survival probabilities indicated that high-level ADAM10 tumour expression above the quartile cutoff point, unlike that of Tspan15, may be unfavourable for patient survival (Figure 21B).

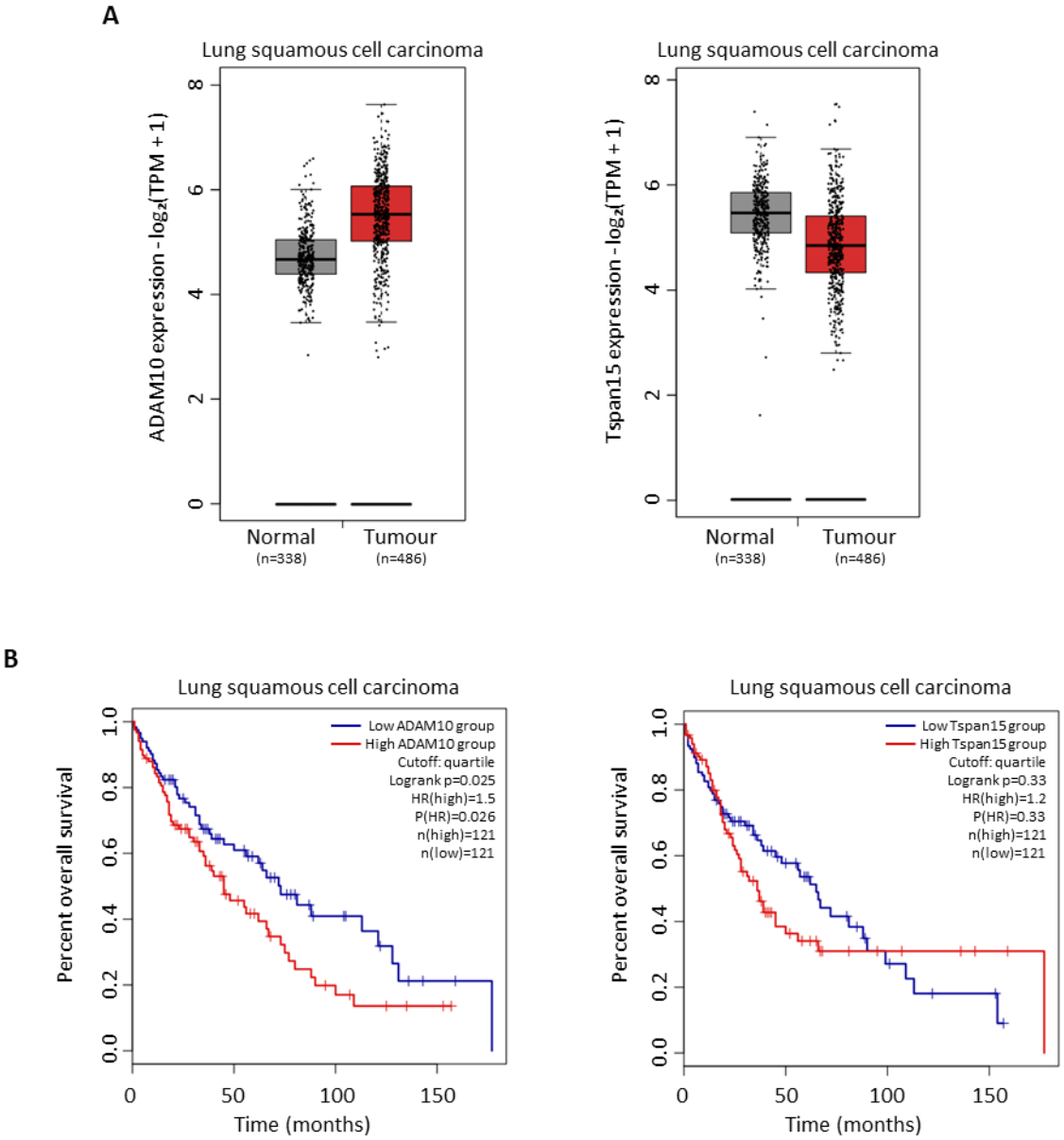


Figure 21: Neither ADAM10 nor Tspan15 gene expression is significantly changed in lung squamous cell carcinoma tumours compared to control samples, but high ADAM10 tumour expression is associated with a worse prognosis. Gene expression and survival data for lung squamous cell carcinoma patients were assessed using publicly available databases on the GEPIA2 server (Tang et al., 2019). (A) ADAM10 and Tspan15 expression data were presented as boxplots comparing expression between tumour and corresponding control tissues. Data were $\log_2$(TPM+1) transformed and analysed by a one-way ANOVA; the $|\log_2 FC|$ threshold was set to 1 and the significance threshold was $p<0.01$. (B) Kaplan-Meier survival curves presented the survival probabilities of patients stratified into those with 'high level' (above the upper quartile cutoff point) and 'low level' (below the lower quartile cutoff point) tumour expression. Statistical differences were analysed by a log-rank test (* $p<0.05$).

3.2.13 Neither ADAM10 nor Tspan15 gene expression is upregulated in lung adenocarcinoma tumours and tumour expression is not associated with patient survival

Lung adenocarcinoma data available on the GEPIA2 server (Tang et al., 2019) was also analysed to assess the potential clinical significance of ADAM10 and Tspan15 gene expression in this malignancy. However, it was shown that neither protein was upregulated in lung adenocarcinoma tumours (Figure 22A); ADAM10 expression had a log_2FC of 0.41 (FC: 1.329) for tumour samples compared to normal tissues, whereas 0.48 was the log_2FC (FC: 1.395) for Tspan15. Furthermore, no evidence was found that patient survival was associated with the tumour expression of ADAM10 or Tspan15 (Figure 22B). Taken together with the data from the previous section, this suggests that ADAM10 may exhibit a subtype-specific role in lung cancer.

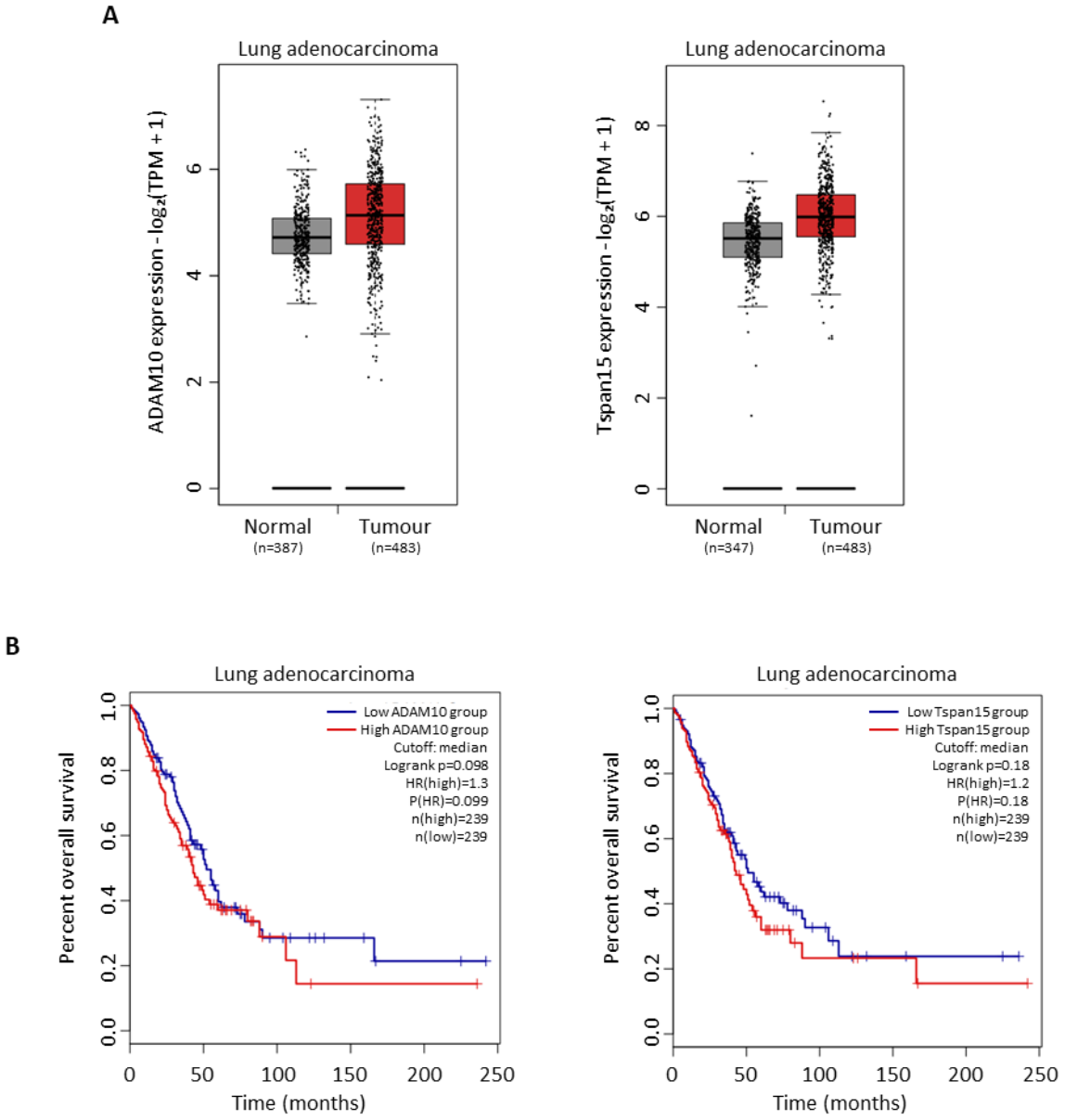
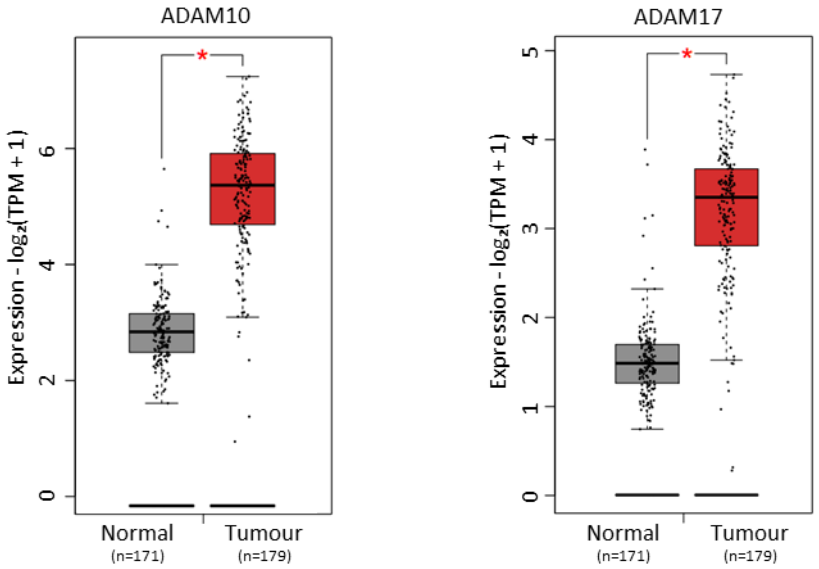


Figure 22: Lung adenocarcinoma patients do not exhibit a differential expression of either ADAM10 or Tspan15 and patient prognosis is not affected by tumour expression. Gene expression and survival data for lung adenocarcinoma patients were assessed using publicly available databases on the GEPIA2 server (Tang et al., 2019). (A) ADAM10 and Tspan15 expression data were presented as boxplots comparing expression between tumour and corresponding control tissues. Data were $\log_2$(TPM+1) transformed and analysed by a one-way ANOVA; the $|\log_2 FC|$ threshold was set to 1 and the significance threshold was $p<0.01$. (B) Kaplan-Meier survival curves presented the survival probabilities of patients stratified into those with 'high level' (above the median cutoff point) and 'low level' (below the median cutoff point) tumour expression. Statistical differences were analysed by a log-rank test (* $p<0.05$).

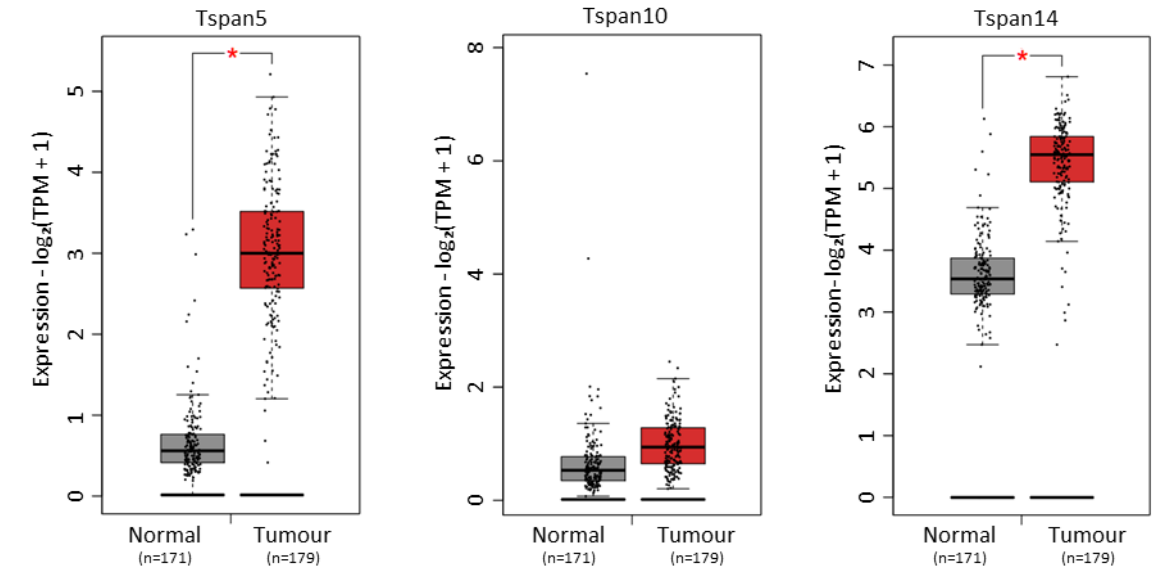
3.2.14 Other members of the ADAM and TspanC8 families are upregulated in pancreatic adenocarcinoma tumours

Given that both ADAM10 and Tspan15 gene expression was upregulated in pancreatic adenocarcinoma and high tumour expression was associated with unfavourable patient prognosis (Section 3.2.1), pancreatic adenocarcinoma was selected as the model malignancy for biological follow-up studies, which aimed to further characterise the cancer-associated roles of these proteins. However, due to possible functional overlap with other members of the ADAM10 and TspanC8 families, the expression levels of ADAM17, Tspan5, Tspan10, Tspan14, Tspan17, and Tspan33 were first assessed using the GEPIA2 server (Tang et al., 2019). The data were $\log_2$(TPM+1) transformed and the $\log_2$fold_change ($\log_2$FC) was calculated by subtracting the median non-tumour control expression from the tumour value. Analysis of the RNA-seq data showed that ADAM17, similar to ADAM10, was significantly upregulated in pancreatic adenocarcinoma tumours compared to corresponding non-tumour samples (Figure 23A, which includes ADAM10 data previously shown in Figure 10A for ease of comparison); the $\log_2$FC was 1.87 (FC: 3.655) for ADAM17 and 2.47 (FC: 5.540) for ADAM10. Furthermore, in addition to Tspan15, differential expression was observed in three other TspanC8s, namely Tspan5, Tspan14, and Tspan17 (Figure 23B, which includes Tspan15 data previously shown in Figure 10A for ease of comparison). Indeed, pancreatic adenocarcinoma tumours vs normal samples had a $\log_2$FC of 2.44 (FC: 5.426) for Tspan5, 2.01 (FC: 4.028) for Tspan14, and 1.49 (FC: 2.809) for Tspan17. By comparison, the gene expression of Tspan10 and Tspan33 was not significantly upregulated in this malignancy (Figure 23B).

A


ADAM10
Expression - log2(TPM + 1)
Normal
(n=171)
Tumour
(n=179)
ADAM17
Expression - log2(TPM + 1)
Normal
(n=171)
Tumour
(n=179)

B


Tspan5
Expression - log2(TPM + 1)
Normal
(n=171)
Tumour
(n=179)
Tspan10
Expression - log2(TPM + 1)
Normal
(n=171)
Tumour
(n=179)
Tspan14
Expression - log2(TPM + 1)
Normal
(n=171)
Tumour
(n=179)

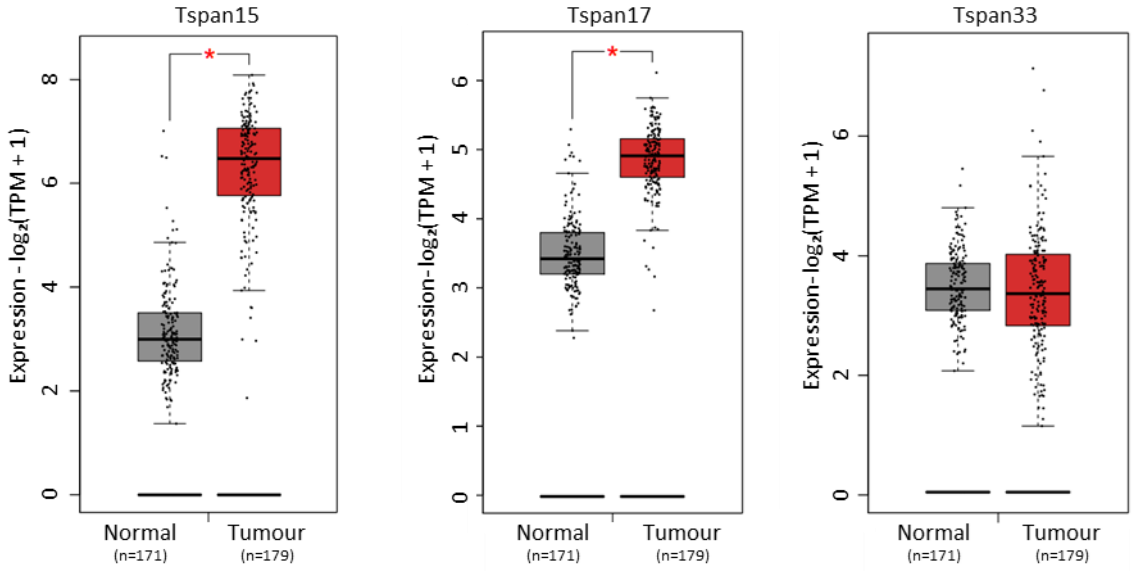


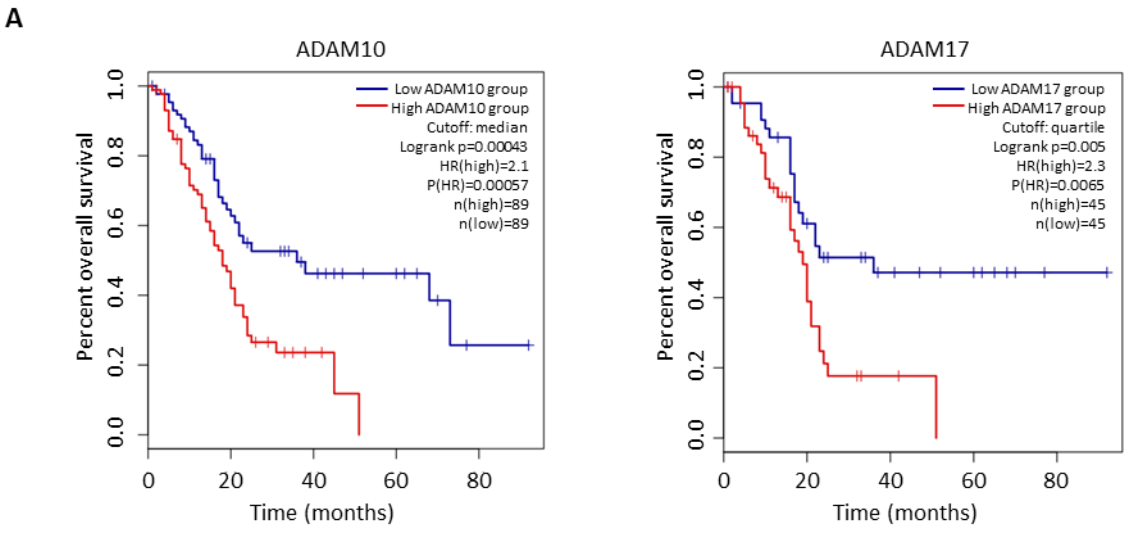
Figure 23: Multiple members of the ADAM and TspanC8 families are upregulated in pancreatic adenocarcinoma tumours. RNA sequencing data from pancreatic adenocarcinoma tumours and normal pancreas samples were analysed using the GEPIA2 portal (Tang et al., 2019), which combines datasets from the TCGA and GTEx. (A) Boxplots were used to summarise the differential gene expression of ADAM10 and ADAM17 in tumour vs normal samples. Data were $\log_2$(TPM+1) transformed and analysed by a one-way ANOVA. The $|\log_2 FC|$ threshold was set to 1 and the p-value cutoff was 0.01. (B) As described in A, but for members of the TspanC8 family, including Tspan5, Tspan10, Tspan14, Tspan15, Tspan17, and Tspan33.

3.2.15 High expression of multiple ADAM and TspanC8 family members has an effect on pancreatic adenocarcinoma patient prognosis

To assess the potential clinical significance of ADAM17 and TspanC8 family member (Tspan5, Tspan10, Tspan14, Tspan17, and Tspan33) expression levels in pancreatic adenocarcinoma, Kaplan-Meier survival curves were analysed using GEPIA2 (Tang et al., 2019). Patients were stratified into those with high-level (above the indicated cutoff point) and low-level (below the indicated cutoff point) tumour expression with the associated effect on overall survival being assessed; a range of cutoff points were tested to identify any cohorts of patients for which expression may be a potential prognostic biomarker. This showed that high ADAM17 expression, similar to high expression of ADAM10, was unfavourable for patient survival with a hazard ratio of 2.3 (Figure 24A, which includes ADAM10 data previously shown in Figure 10B for ease of comparison). However, it is worth noting

that ADAM10 tumour expression has the potential to be a prognostic biomarker for a greater number of patients; ADAM10 expression above the median cutoff point was correlated with reduced survival, whereas for ADAM17, a reduction in patient prognosis was associated with expression higher than the upper quartile value. Moreover, several members of the TspanC8 family, in addition to Tspan15, were also implicated in pancreatic adenocarcinoma patient survival (Figure 24B, which includes Tspan15 data previously shown in Figure 10B for ease of comparison). Indeed, pancreatic adenocarcinoma patients expressing Tspan5 or Tspan10 above the upper quartile cutoff point had a reduced survival rate compared to those with expression below the lower quartile value; the hazard ratio was 1.9 for highTspan5 expression and 2.0 for Tspan10. In contrast, high-level Tspan33 expression had the opposite effect and was associated with an improved prognosis, suggesting that it may act as a tumour suppressor. Unlike these three TspanC8s, however, patient survival was not dependent on the expression of Tspan14 or Tspan17; no significant difference in prognosis was observed between those with high-level (above the upper quartile cutoff point) and low-level (below the lower quartile cutoff point) tumour expression.

These data provide further evidence that multiple members of the ADAM and TspanC8 families likely promote pancreatic adenocarcinoma progression, but with the extent of their involvement differing.



B

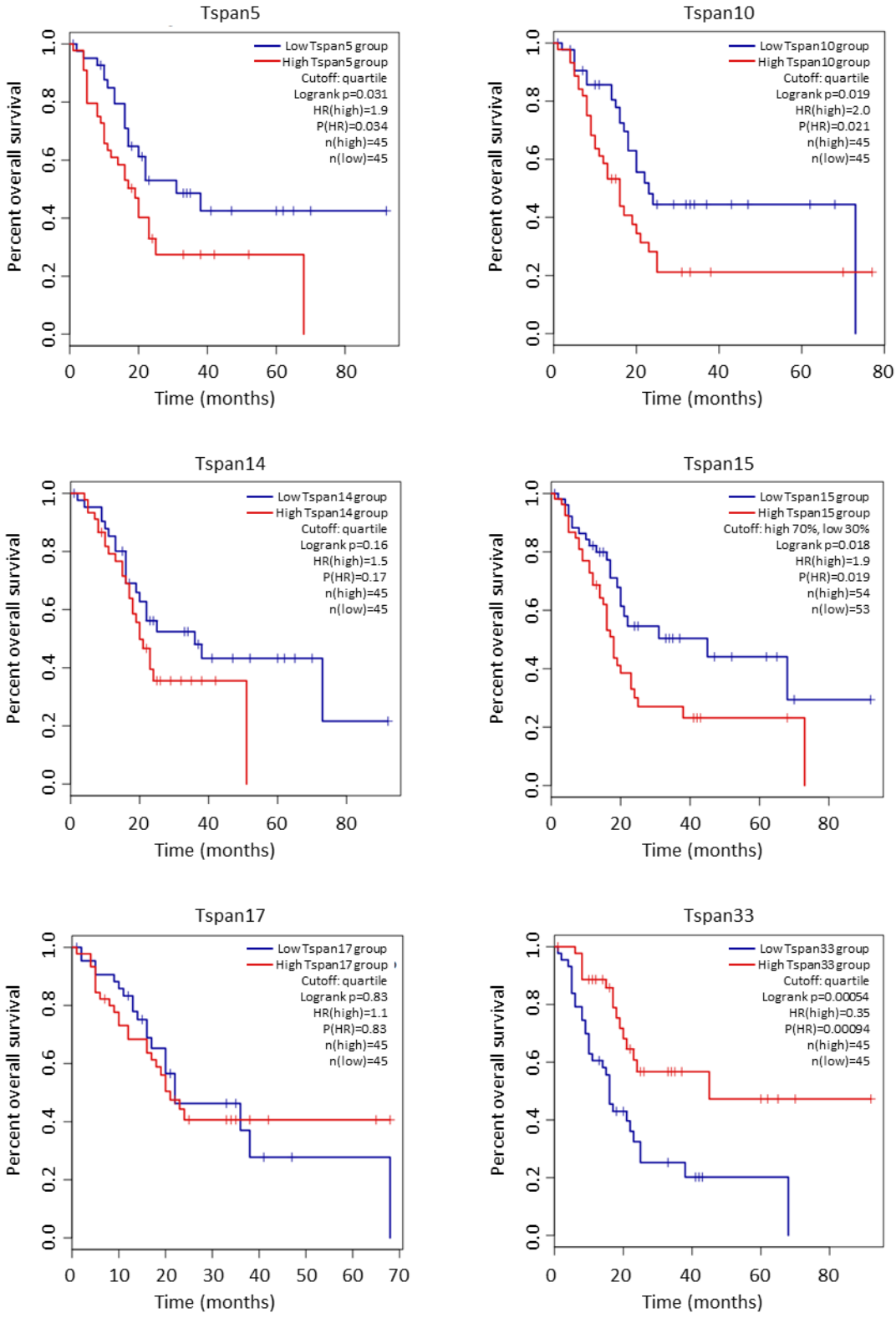

Tspan5
Low Tspan5 group
High Tspan5 group
Cutoff: quartile
Logrank p=0.031
HR(high)=1.9
P(HR)=0.034
n(high)=45
n(low)=45
Tspan10
Low Tspan10 group
High Tspan10 group
Cutoff: quartile
Logrank p=0.019
HR(high)=2.0
P(HR)=0.021
n(high)=45
n(low)=45
Tspan14
Low Tspan14 group
High Tspan14 group
Cutoff: quartile
Logrank p=0.16
HR(high)=1.5
P(HR)=0.17
n(high)=45
n(low)=45
Tspan15
Low Tspan15 group
High Tspan15 group
Cutoff: high 70%, low 30%
Logrank p=0.018
HR(high)=1.9
P(HR)=0.019
n(high)=54
n(low)=53
Tspan17
Low Tspan17 group
High Tspan17 group
Cutoff: quartile
Logrank p=0.83
HR(high)=1.1
P(HR)=0.83
n(high)=45
n(low)=45
Tspan33
Low Tspan33 group
High Tspan33 group
Cutoff: quartile
Logrank p=0.00054
HR(high)=0.35
P(HR)=0.00094
n(high)=45
n(low)=45
Percent overall survival
Time (months)

Figure 24: Pancreatic adenocarcinoma patient survival is affected by the high expression of multiple members of the ADAM and TspanC8 families. Survival data for pancreatic cancer patients were analysed by assessing public databases available on the GEPIA2 portal (Tang et al., 2019). (A) Kaplan-Meier survival curves showed the survival probabilities of patients stratified into those with 'high level' (above the indicated cutoff point) and 'low level' (below the indicated cutoff point) ADAM expression. The log-rank test implemented within the GEPIA2 portal was used to assess statistical differences (* $p<0.05$). (B) As described in A, but for members of the TspanC8 family, including Tspan5, Tspan10, Tspan14, Tspan15, Tspan17, and Tspan33.

3.3 Discussion

This chapter explored the expression profiles of ADAM10 and Tspan15 in a number of prevalent malignancies, as well as the associated effect on patient prognosis. It was shown that ADAM10 and Tspan15 were co-upregulated in various tumours, whilst in others a significant increase in expression was only observed for one of the two proteins. Furthermore, although high tumour expression was not always associated with altered survival outcomes, there were several examples in which the expression of ADAM10 and/or Tspan15 could be considered a potential prognostic biomarker.

The role of ADAM10 in cancer is relatively well-studied, especially compared to other members of the ADAM family (Rosenbaum and Saftig, 2023). As such, analysis of patient data within this chapter was able to provide evidence supporting ADAM10's previously reported involvement in malignancies of the pancreas (Gaida et al., 2010; Woods and Padmanabhan, 2013; Woods et al., 2015; Lin et al., 2016; Liu et al., 2020; Mueller et al., 2021; Hossen et al., 2023), oesophagus (Ma et al., 2016), prostate (Cai et al., 2022), colon (Gavert et al., 2007), glial brain cells (Kohutek et al., 2009; Wolpert et al., 2014; Venkatesh et al., 2017; Liu et al., 2018), skin (Lee et al., 2010), ovaries (Buchanan et al., 2017), breast (Feldinger et al., 2014; Mullooly et al., 2015; Tsang et al., 2018), and lungs (Guo et al., 2012; Sépult et al., 2019). Interestingly, despite some tumours showing no differential expression of ADAM10 compared to corresponding control samples, high tumour expression was still associated with unfavourable patient survival. This suggests that high ADAM10 expression within a patient population may be sufficient to act as a prognostic biomarker.

In contrast to ADAM10, there are very few studies exploring the role of Tspan15 in cancer. However, Tspan15 has been implicated in hepatocellular (Sidahmed-Adrar et al., 2019) and oesophageal carcinoma (Zhang et al., 2018), as well as intrahepatic cholangiocarcinoma (Yoshizumi et al., 2023). The findings of this chapter support a role for Tspan15 in these malignancies with gene expression found to be upregulated. Additionally, high tumour expression was found to be a potential prognostic biomarker for liver hepatocellular carcinoma. It is worth noting that Tspan15 has also been proposed to promote the metastasis of oral squamous cell carcinoma (Hiroshima et al., 2019). However, as datasets for this malignancy were not available on GEPIA2 (Tang et al., 2019), the clinical significance of Tspan15 could not be validated.

The analysis of oesophageal carcinoma data available on the GEPIA2 server (Tang et al., 2019) showed that ADAM10 and Tspan15 were co-upregulated in oesophageal carcinoma, suggesting that they may be acting as a functional complex. Previous publications, however, report distinct mechanisms by which ADAM10 and Tspan15 promote the invasion and metastasis of oesophageal carcinoma (Ma et al., 2016; Zhang et al., 2018). For example, ADAM10 has been proposed to drive the progression of this malignancy via E-cadherin shedding. It is important to note, though, that no direct link was shown, nor were the downstream effects of ectodomain cleavage explored (Ma et al., 2016). By comparison, Tspan15 has been proposed to mediate oesophageal carcinoma metastasis through its interaction with β-TrCP and subsequent activation of NF-κB signalling (Zhang et al., 2018). Although Ma et al. explored the role of ADAM10 in isolation from its regulatory TspanC8, Tspan15/ADAM10 has been shown to cleave E-cadherin (Szyroka, 2019), and thus Tspan15 likely has at least two pro-metastatic functions within oesophageal carcinoma. Equally, Zhang et al. did not consider whether ADAM10 is required for Tspan15's activity within the NF-κB pathway. As such, ADAM10 has the potential to promote oesophageal carcinoma metastasis in this capacity.

This chapter also indicates that Tspan15's role in cancer likely extends beyond the previously reported malignancies. For example, the analysis of patient data revealed a potential role for

Tspan15 in pancreatic cancer; Tspan15 gene expression was shown to be upregulated in pancreatic adenocarcinoma tumours, and high tumour expression was associated with a worse prognosis. Furthermore, pancreatic adenocarcinoma patients exhibited increased ADAM10 expression, which was unfavourable for patient survival. Although this is a novel finding for Tspan15, previous studies indicate that ADAM10 exhibits pro-tumorigenic activity in pancreatic cancer (Gaida et al., 2010; Woods and Padmanabhan, 2013; Woods et al., 2015; Lin et al., 2016; Liu et al., 2020; Mueller et al., 2021; Hossen et al., 2023). The importance of ADAM10's sheddase activity is evident within these studies. Indeed, ADAM10-mediated shedding of ULBP2 promotes immune evasion (Lin et al., 2016), whereas metastasis following radiation treatment is driven by ephrinB2 cleavage (Mueller et al., 2021). As the specific TspanC8/ADAM10 complex required for the shedding of ULBP2 and ephrinB2 has not been investigated, Tspan15 may affect patient prognosis through the regulation of ADAM10-mediated shedding of one or both of these substrates. Moreover, the growth and survival of pancreatic cancer cells are positively regulated by ADAM10 cleavage of APP (Woods and Padmanabhan, 2013). Despite investigation, the regulatory TspanC8 for APP shedding remains unclear, with *in vitro* results varying based on the model system and validation approach used (Prox et al., 2012; Woods and Padmanabhan, 2013; Jouannet et al., 2016; Brummer et al., 2019). However, as Tspan15 knockout mice do not exhibit impaired APP shedding in the brain (Seipold et al., 2018), it is likely that one of the other TspanC8 tetraspanins is important for this pro-tumorigenic function of ADAM10. Consequently, distinct mechanisms of tumourigenesis may be mediated by different TspanC8/ADAM10 complexes. Interestingly, Tspan5, Tspan14, and Tspan17 were also found to be upregulated in pancreatic adenocarcinoma tumours, with patient survival affected by high-level Tspan5, Tspan10, and Tspan33 tumour expression. This further suggests that Tspan15 may not be the only TspanC8 with a role in pancreatic cancer. Furthermore, pancreatic adenocarcinoma tumours exhibited an increase in ADAM17 expression and patient prognosis was reduced by expression above the upper quartile cut-off point. Consequently, ADAM17, similar to ADAM10, has the potential to

impact upon the tumorigenesis of pancreatic cancer. Whilst not explored further in this thesis, it is worth noting that ADAM17 has previously been reported to play a role in this malignancy (Ringel et al., 2006; Liu et al., 2023). For example, Liu et al. showed that ADAM17 overexpression promoted the proliferation, invasion, and immune evasion of pancreatic cancer cells, as well as inhibited apoptosis. Moreover, pancreatic cancer tumour growth was revealed to be positively regulated by ADAM17 expression in mice (Liu et al., 2023).

In addition to pancreatic cancer, the findings from this chapter revealed a potential novel role for Tspan15 in ovarian serous cystadenocarcinoma; tumours of this malignancy were found to exhibit increased levels of Tspan15 gene expression. ADAM10 has previously been proposed to promote ovarian cancer progression via the cleavage of Nectin-4 and subsequent activation of various signalling cascades, including the Akt pathway (Buchanan et al., 2017). As the regulatory TspanC8 for ADAM10-mediated shedding of Nectin-4 has not been investigated, it is tempting to speculate that Tspan15 could modulate this cleavage, and thus contribute to ovarian cancer progression through this pathway. Interestingly, whilst high-level ADAM10 expression in ovarian serous cystadenocarcinoma tumours represented a potential prognostic biomarker, this was not the case for Tspan15. Although the exact reasoning for this is unclear, it is possible that increased Tspan15 expression is required to mediate cleavage of Nectin-4 by ADAM10 but is not independently sufficient to affect patient survival. Nevertheless, Tspan15's role in ovarian cancer would be an interesting and important avenue for future research.

Moreover, this work identified another cancer, namely cholangiocarcinoma, within which both ADAM10 and Tspan15 may be implicated. Indeed, the gene expression of these two proteins was found to be increased in cholangiocarcinoma compared to corresponding non-tumour tissues. Immunohistochemistry from a previous study also confirms that this differential expression occurs at the protein level (Yoshizumi et al., 2023). Subsequent analysis of Kaplan-Meier survival plots showed that although prognosis was likely unrelated to Tspan15 expression, low-level ADAM10 tumour

expression was correlated with unfavourable patient survival. This suggests that unlike in the other 12 cancers investigated, ADAM10 may exhibit tumour suppressive activity in cholangiocarcinoma. However, as the dataset available on GEPIA2 (Tang et al., 2019) only included 36 tumour samples, additional data is required to validate this association between expression and prognosis. Nevertheless, initial evidence for ADAM10 functioning as a tumour suppressor has been reported in ovarian cancer; metastasis was attenuated via ADAM10-mediated downregulation of N-cadherin expression (Chen et al., 2023). Further evidence that ADA10 may exhibit both oncogenic and tumour-suppressive activity comes from its substrate Notch, which has a dual role in cancer (South et al., 2012). For example, gain-of-function mutations in the Notch receptor have a clear oncogenic role in T-cell acute lymphoblastic leukaemia (T-ALL) (Weng et al., 2004; Aster et al., 2008; Tosello and Ferrando, 2013). Additionally, oncogenic Notch signalling has also been demonstrated in breast cancer (Robinson et al., 2011; Stoeck et al., 2014; Edwards and Brennan, 2021). In contrast, emerging evidence suggests that Notch functions as a tumour suppressor within skin cancer (Nicolas et al., 2003; Proweller et al., 2006; South et al., 2012). Indeed, the inactivation of Notch1 in the epidermis layer of the skin resulted in mice developing spontaneous basal cell carcinoma lesions (Nicolas et al., 2003). Furthermore, the inhibition of Notch signalling in mice is linked to the onset of squamous cell carcinoma (Proweller et al., 2006).

Despite the findings of this chapter identifying exciting avenues for future research, it is important to consider the limitations of the investigation. Firstly, only mRNA expression data was assessed, and as such it will be beneficial to confirm whether differential expression also occurs at the protein level, as well as the associated effects on patient prognosis. Secondly, the purity of patient samples is affected by stromal cells, including fibroblasts (Yoshihara et al., 2013), which are a key component of the tumour microenvironment (Hanahan and Weinberg, 2011). As such, it is possible that the differential gene expression observed within this chapter was not associated with tumour cells and was instead caused by infiltrating stromal cells. Moving forward, these limitations could be addressed using

immunohistochemistry. This would enable the analysis of protein expression, as well as the characterisation of contributing cell types. It is worth noting, however, that although effective antibodies are available for ADAM10, ADAM17, and Tspan15, they are limited for the other TspanC8s.

To summarise, this chapter demonstrated that ADAM10 and Tspan15 likely exhibit pro-tumorigenic functions. However, biological follow-up studies are required to confirm this and characterise their specific roles. As such, Chapter 4 will explore the potential functions of ADAM10 and Tspan15 in pancreatic cancer.

CHAPTER 4 ADAM10 AND TSPAN15 DO NOT REGULATE THE IN VITRO PROLIFERATION OR INVASION OF PANCREATIC CANCER CELL LINES

4.1 Introduction

As outlined in the previous chapter, the gene expression levels of ADAM10 and Tspan15 are upregulated in pancreatic adenocarcinoma, and high tumour expression is associated with a worse prognosis (Chapter 3). This suggests that these two proteins likely play a role in pancreatic cancer progression. Indeed, several studies provide evidence supporting a pro-tumorigenic function of ADAM10 within this malignancy (Gaida et al., 2010; Woods and Padmanabhan, 2013; Woods et al., 2015; Lin et al., 2016; Liu et al., 2020; Mueller et al., 2021; Hossen et al., 2023). For example, the cleavage of APP by ADAM10 promotes the anchorage-independent growth and survival of pancreatic cancer cells (Woods and Padmanabhan, 2013). By comparison, ADAM10-mediated shedding of ULBP2, a ligand for the immune-activating receptor NKG2D, facilitates immune evasion (Lin et al., 2016). Treatment of pancreatic cancer cell lines with gemcitabine, a chemotherapy drug, has been shown to downregulate ADAM10 expression, leading to increased levels of membrane-bound ULBP2 due to impaired ectodomain shedding. This was then demonstrated to correlate with an enhanced cytotoxic effect of natural killer cells (Lin et al., 2016). Furthermore, ADAM10 has been proposed to mediate resistance to radiotherapy in pancreatic cancer tumours via cleavage of ephrinB2, a receptor tyrosine kinase (Mueller et al., 2021). Following radiation therapy, ADAM10 expression is upregulated, which increases the proteolytic processing of ephrinB2 and likely promotes the metastatic potential of tumour cells (Mueller et al., 2021). Taken together, these studies suggest that ADAM10-mediated cleavage likely supports multiple pro-tumourigenic functions. It is worth noting, however, that the signalling pathways activated following this ectodomain shedding remain largely uncharacterised. Nevertheless, efforts have been made to understand the role of ADAM10 in pancreatic cancer, which is not the case for Tspan15 nor the Tspan15/ADAM10 complex. However, Servage et al. demonstrated that Tspan15 is contained within extracellular vesicles (EVs) released

from pancreatic cancer cells but not normal pancreatic epithelial cells (Servage et al., 2020). As cancer cell-derived EVs have been shown to promote cancer progression (Chang et al., 2021), this further supports the potential importance of Tspan15 in pancreatic cancer.

Beyond contributing to pancreatic cancer tumour progression, ADAM10 also promotes the migration and invasion of various malignancies, including breast cancer, hepatocellular carcinoma, oesophageal carcinoma, and bladder cancer, as well as others (Guo et al., 2012; Fu et al., 2014; Liu et al., 2015; Mullooly et al., 2015; You et al., 2015; Ma et al., 2016; Tsang et al., 2018; Sépult et al., 2019; Yuan et al., 2020b). In some cases, ADAM10's role extends to the mediation of proliferation (Fu et al., 2014; Liu et al., 2015; You et al., 2015; Ma et al., 2016; Tsang et al., 2018; Yuan et al., 2020b). Previous studies have also shown that Tspan15 positively regulates migration and invasion in oral squamous cell carcinoma (Hiroshima et al., 2019) and oesophageal carcinoma (Zhang et al., 2018). Moreover, in hepatocellular carcinoma, Tspan15 represents a stemness-related marker that can drive proliferation (Sidahmed-Adrar et al., 2019). More recently, Tspan15 has additionally been shown to promote stemness in cholangiocarcinoma (Yoshizumi et al., 2023)

Given the limitations of existing studies in understanding the role of ADAM10 and Tspan15 in pancreatic cancer patient survival, this chapter aimed to explore their involvement, focusing on whether the Tspan15/ADAM10 complex can mediate pancreatic cancer cell proliferation and/or invasion.

4.2 Results

4.2.1 The generation and validation of ADAM10 and Tspan15 KO pancreatic cancer cell lines

Bioinformatics data from the previous chapter suggests that ADAM10 and Tspan15 may promote the progression of pancreatic adenocarcinoma. To confirm this and characterise their specific roles, cells lines depleted of ADAM10 and Tspan15 were required. Two human pancreatic cancer-derived cell lines, PANC-1 and AsPC-1, were selected as model systems (Lieber et al., 1975; Chen et al., 1982).

Both of these cell lines exhibit mutations in K-RAS, TP53 and CDKN2A/p16, three of the most commonly mutated genes in pancreatic ductal carcinoma (Deer et al., 2010). An additional tumour suppressor protein, SMAD4/DPC4, is inactivated in 48 to 55% of invasive pancreatic adenocarcinomas. Although PANC-1 cells have been found to exhibit no sequence alterations in the SMAD4/DPC4 gene, the data for AsPC-1 cells is inconsistent. Whilst some studies detect the wild-type sequence, others report alterations, including a point mutation or homozygous deletion (Deer et al., 2010).

CRISPR/Cas9 genome editing technology was used to generate ADAM10 and Tspan15 knockout (KO) cells. PANC-1 and AsPC-1 WT cells were transfected with ADAM10 and Tspan15 guide oligos (Table 2) cloned into the pSpCas9(BB)-2A-Puro vector (plasmid map available in Figure A 1, Appendix) (Koo et al., 2020) using Lipofectamine 2000. To select for transfected cells, the culture media was replaced with complete DMEM supplemented with puromycin (Table 3) 48 hours post-transfection. Following incubation for 72 hours, the surface expression of ADAM10 and Tspan15 was analysed by flow cytometry. This revealed two distinct cell populations in most of the PANC-1 and AsPC-1 KO pools (Figure 25A-B); both cells deficient for and still expressing the protein of interest were present. Consequently, purification was required prior to use in functional assays. However, as variability between clones derived from single cells can be significant (Giuliano et al., 2019), a new methodology was developed to purify the heterogeneous KO pools using magnetic Dynabeads. The AsPC-1 ADAM10 guide 1 KO pool was excluded from this purification and subsequent functional assays due to an absence of ADAM10-negative cells to purify (Figure 25B). Additionally, the PANC-1 Tspan15 guide 1 KO pool exhibited significant morphological changes and was thus discounted.

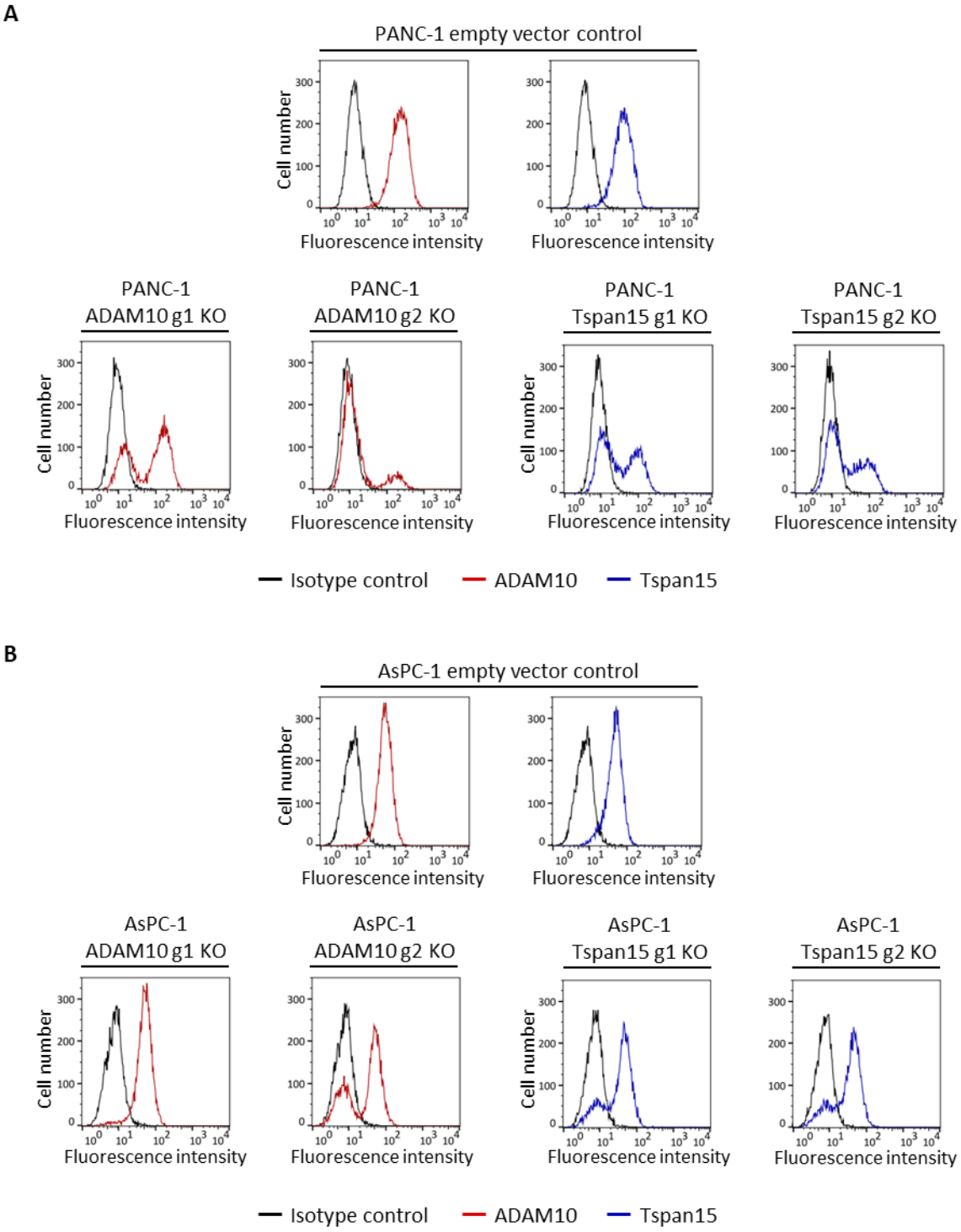
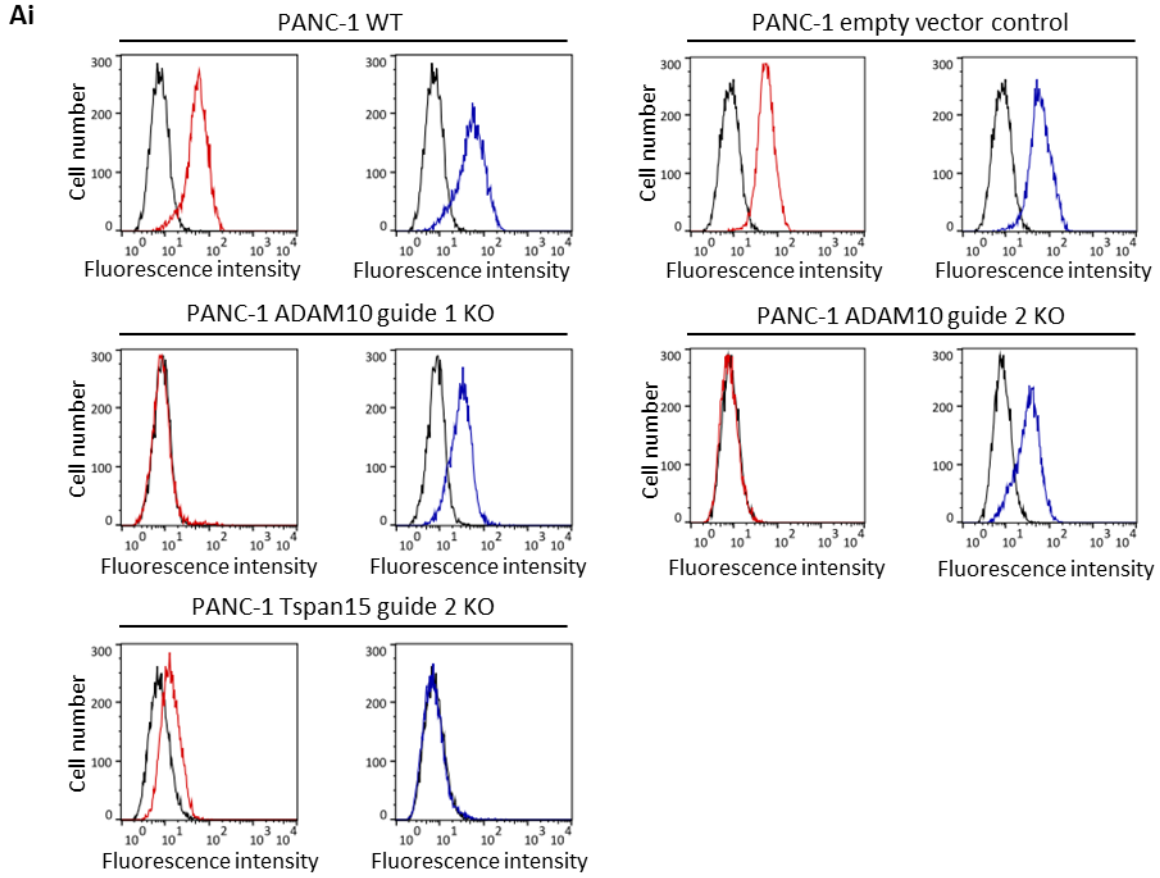


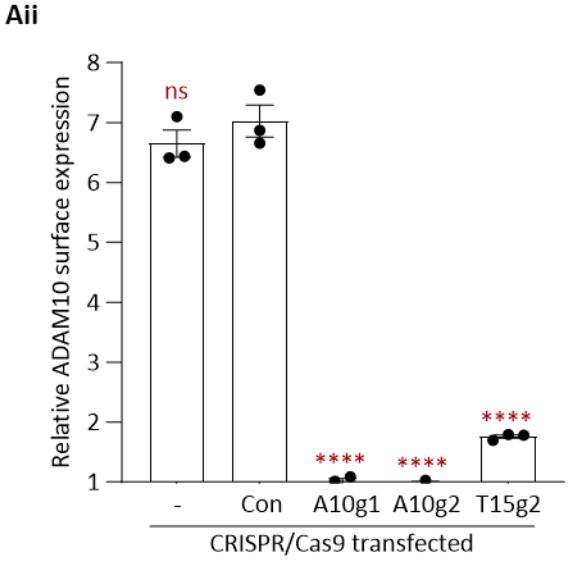
Figure 25: Generation and validation of PANC-1 and AsPC-1 ADAM10 and Tspan15 KO pools. (A) CRISPR/Cas9 gene editing technology was used to generate ADAM10 and Tspan15 KO pools. PANC-1 cells were transfected with ADAM10 and Tspan15 guide oligos (guide 1 (g1) and guide 2 (g2)) cloned into the pSpCas9(BB)-2A-Puro vector, as well as an empty vector control. The resulting surface expression of ADAM10 and Tspan15 was validated by flow cytometry. N=1. (B) Experiment was as described in A, but for AsPC-1 cells.

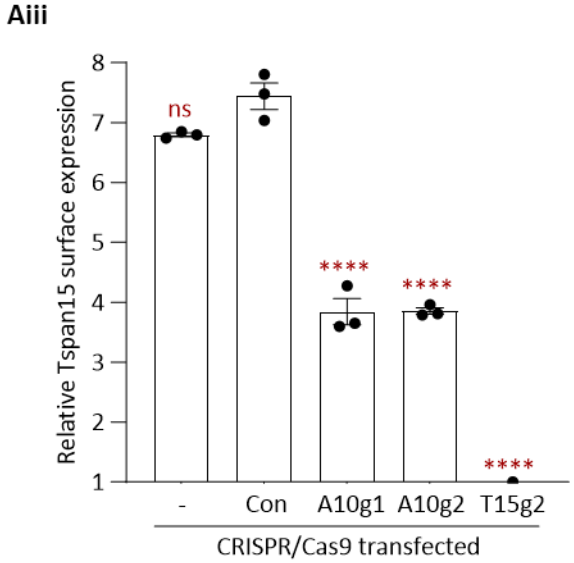
4.2.2 ADAM10 and Tspan15 KO pools can be purified using magnetic Dynabeads

Instead of generating KO clones from single cells, a negative cell sorting protocol was developed to purify the heterogenous KO pools, with the aim of producing a homogenous population of cells deficient for the protein of interest. Antibody-coated, magnetic Dynabeads were used to deplete cells still expressing the protein of interest. However, optimisation of the methodology revealed that modifications were required for ADAM10 vs Tspan15 knockouts. ADAM10 KO pools were purified via direct negative cell sorting. Pan mouse IgG magnetic Dynabeads were rotated overnight at 4 ^{o}C with 1 µg of the anti-ADAM10 11G2 antibody (Table 1) diluted in isolation buffer. Impure ADAM10 KO cells were then added to the antibody-bound Dynabeads and rotated for 45 minutes at 4 ^{o}C, before a magnet was used to separate the ADAM10-positive and -negative cells. The supernatant, containing unbound cells, was collected to isolate the negative population. As this protocol was insufficient to capture Tspan15-positive cells and thus purify the heterogenous population (data not shown), Tspan15 KO pools were instead sorted via indirect negative cell sorting. In brief, impure Tspan15 KO cells were harvested and rotated for 30 minutes at 4 ^{o}C with 2.5 µg of each of the 4 purified anti-Tspan15 antibodies (Table 1). The antibody-bound cells were then washed prior to rotation with pan mouse IgG Dynabeads for 60 minutes at 4 ^{o}C. As in the direct protocol, a magnet was subsequently used to isolate the Tspan15-negative cells from the positive ones.

Flow cytometry analysis confirmed the successful purification of both PANC-1 and AsPC-1 KO pools; the pools were observed to be deficient for ADAM10 or Tspan15 at the cell surface following negative cell sorting (Figure 26A-B). Further to this, in PANC-1 and AsPC-1 ADAM10 KO cells, Tspan15 surface expression was reduced by ~53% and ~87% respectively (Figure 26Aiii, Figure 26Biii). Similarly, ADAM10 surface expression was decreased in the Tspan15 KO cells; the reduction was ~87% in PANC-1 (Figure 26Aii) cells and ~81% in AsPC-1 (Figure 26Bii) cells. This is as expected given previous studies showing that ADAM10 expression mediates Tspan15 expression and vice versa (Eschenbrenner et al., 2020; Koo et al., 2020).


Ai
PANC-1 WT
PANC-1 empty vector control
PANC-1 ADAM10 guide 1 KO
PANC-1 ADAM10 guide 2 KO
PANC-1 Tspan15 guide 2 KO
Cell number
Fluorescence intensity
Isotype control
ADAM10
Tspan15


Aii
Relative ADAM10 surface expression
ns
****
-
Con
A10g1
A10g2
T15g2
CRISPR/Cas9 transfected


Aiii
Relative Tspan15 surface expression
ns
****
-
Con
A10g1
A10g2
T15g2
CRISPR/Cas9 transfected

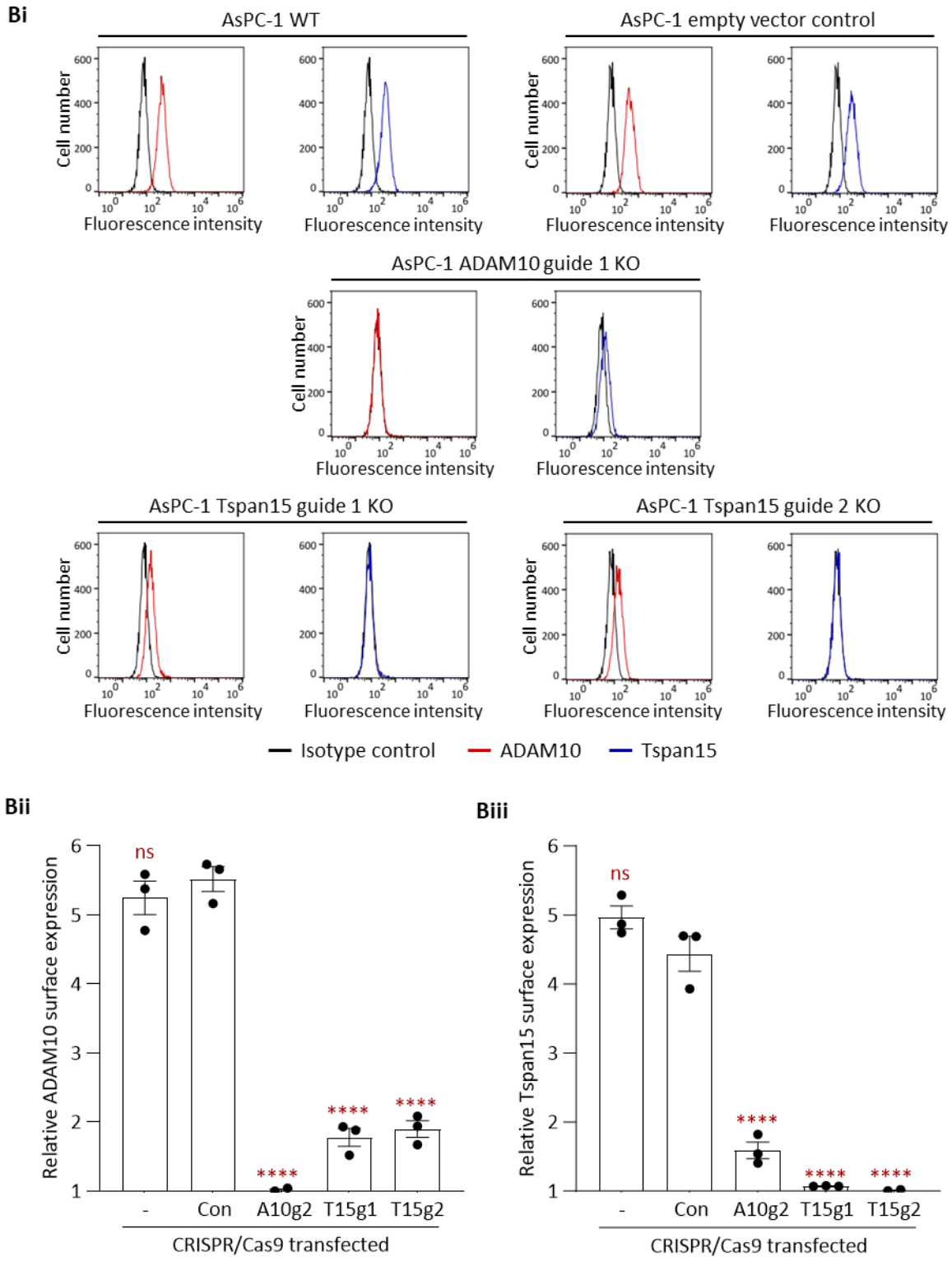


Figure 26: Validation of PANC-1 and AsPC-1 ADAM10 and Tspan15 KO pools following purification with magnetic Dynabeads. (Ai) Impure ADAM10 (A10) and Tspan15 (T15) (guide 1 (g1) and guide 2 (g2)) KO pools underwent negative cell sorting with antibody-coated, magnetic Dynabeads. The expression of ADAM10 and Tspan15 on the cell surface was then validated by flow cytometry; cells

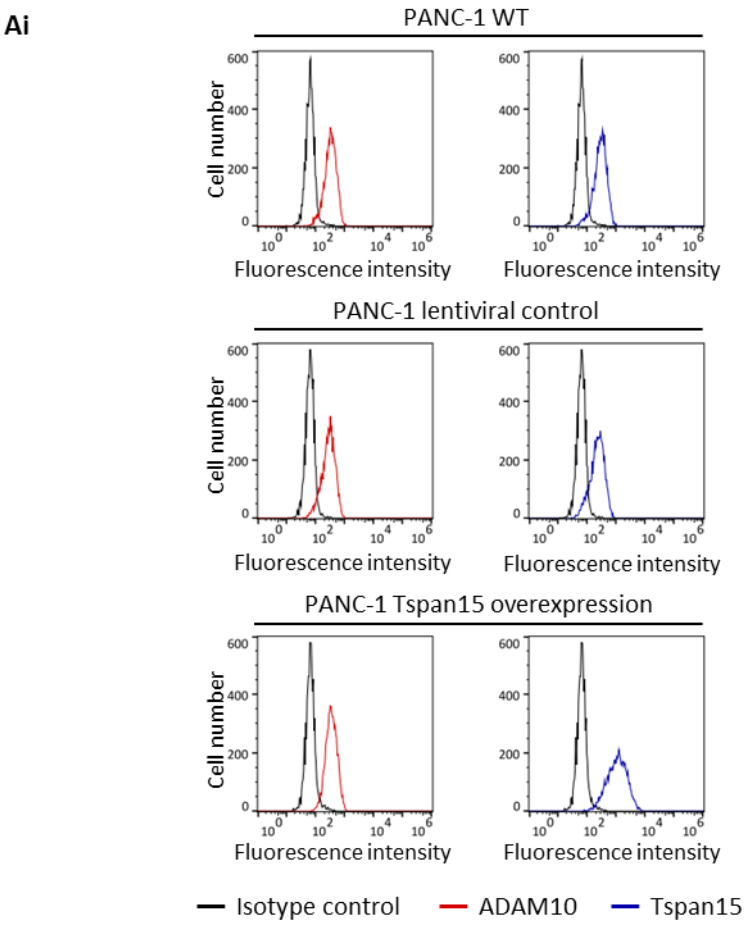
were stained for ADAM10 (red) or Tspan15 (blue) and an isotype control (black). (Aii) ADAM10 and (Aiii) Tspan15 surface expression was quantified and presented as the geometric mean fluorescence intensity relative to the isotype control. Data were log-transformed and analysed by a one-way ANOVA with a Tukey's multiple comparisons test. Statistics shown are compared to the empty vector control (con) transfected cells, with other comparisons not shown. N=3; data represents mean relative surface expression ± SEM. (Bi-iii) Experiment was as described in panel Ai-iii but for AsPC-1 cells.

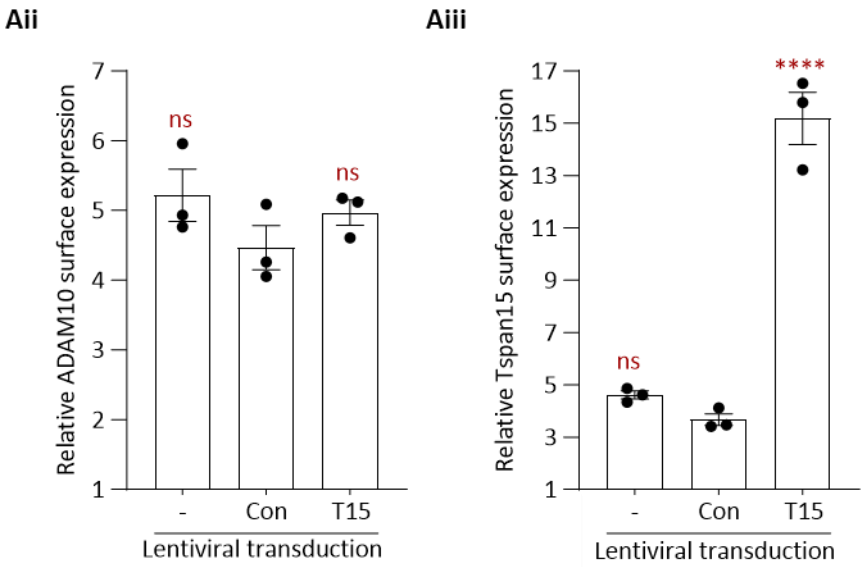
4.2.3 The generation and validation of pancreatic cancer cell lines overexpressing Tspan15

Given that Tspan15 expression is upregulated in pancreatic adenocarcinoma (Section 3.2.1) (Tang et al., 2019), cell lines overexpressing Tspan15 were also a valuable tool to explore the role of this tetraspanin. As such, HEK-293T cells were transfected with N-terminal FLAG-tagged Tspan15 in the pLVX-EF1α-IRES-Puro lentiviral vector or a control lentiviral plasmid (plasmid map available in Figure A 2, Appendix), as well as the psPAX2 packaging vector and pMD2G envelope vector. Following incubation for 24 hours, virus-containing media was harvested from the HEK-293T cells and supplemented with polybrene, FBS, and L-glutamine. It was then added to PANC-1 or AsPC-1 cells to transduce stable Tspan15 overexpression or generate lentiviral control cells, both of which were selected for using puromycin. The resulting surface expression of Tspan15 and ADAM10 was validated by flow cytometry.

Analysis of the data revealed that transduction with the FLAG-tagged Tspan15 lentiviral vector increased Tspan15 surface expression 4.5-fold in PANC-1 cells (Figure 27Aiii) and 5.1-fold in AsPC-1 cells (Figure 27Biii), compared to the relevant cells transduced with a lentiviral control. ADAM10 surface expression was also increased by ~13% in AsPC-1 cells overexpressing Tspan15 (Figure 27Bii), which is as expected given that ADAM10 and Tspan15 are normally required for the expression of each other (Eschenbrenner et al., 2020; Koo et al., 2020). However, Tspan15 overexpression was not associated with an increase in ADAM10 surface expression in PANC-1 cells (Figure 27Aii), further supporting the idea that Tspan15 may have an additional partner protein in this cell line.

In the remainder of this chapter, the newly generated cell lines were characterised in functional assays to determine the involvement of ADAM10 and Tspan15 in pancreatic cancer progression.





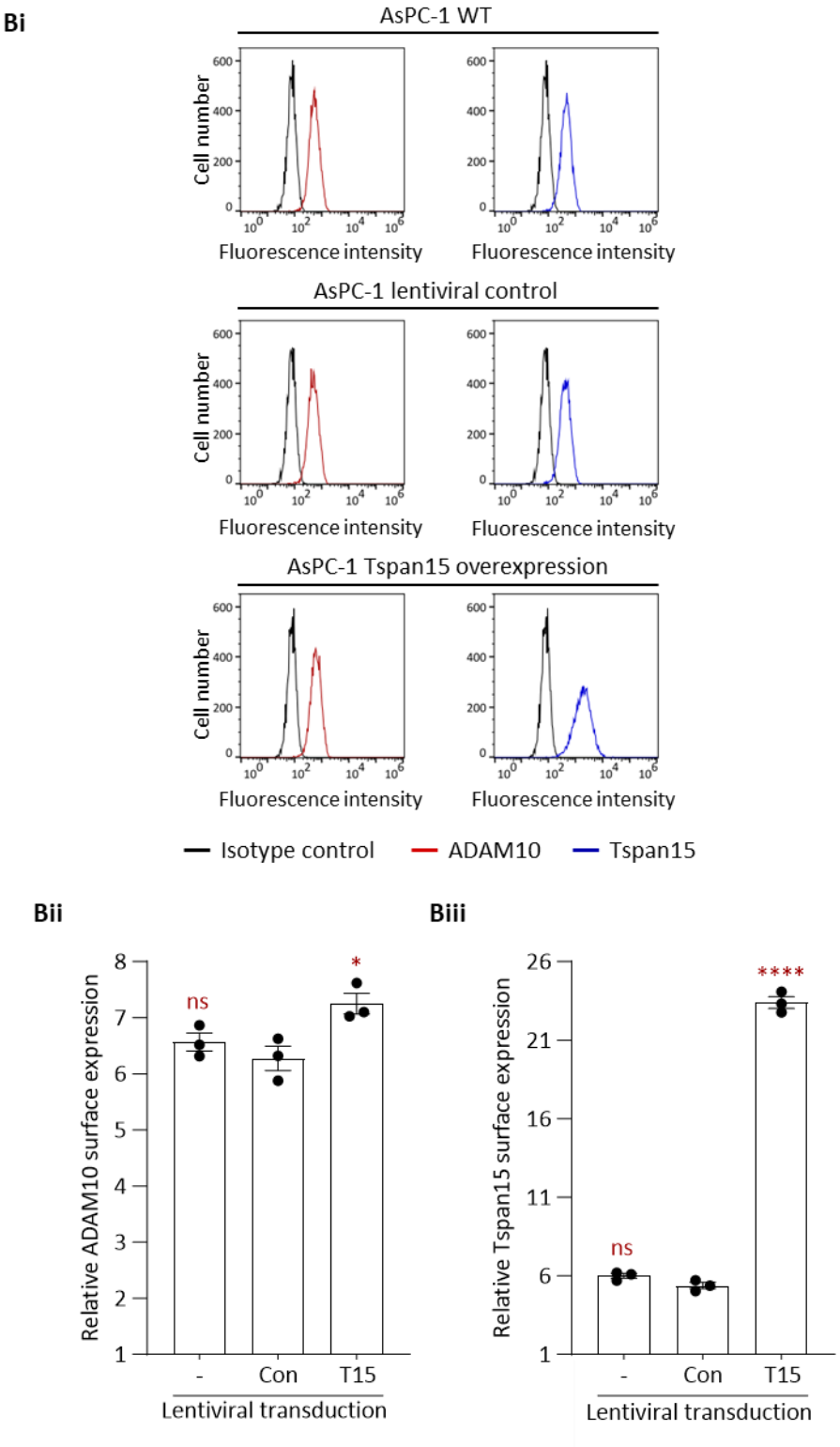


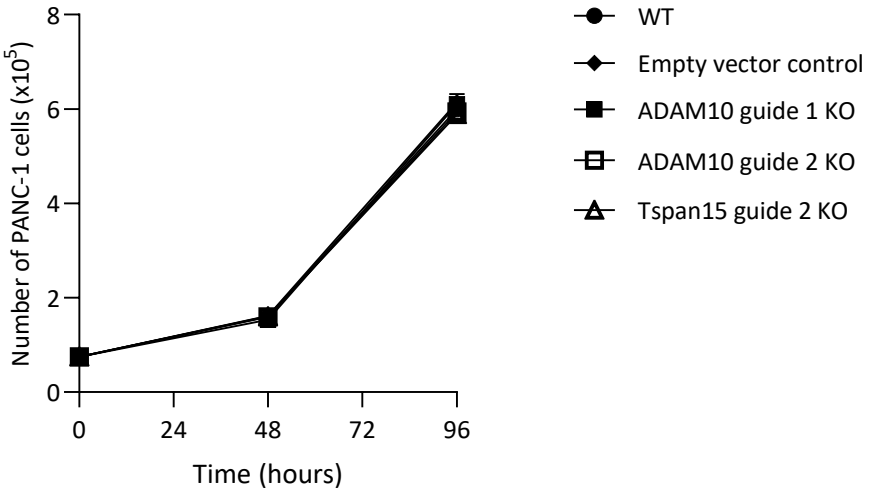
Figure 27: Validation of PANC-1 and AsPC-1 cells overexpressing Tspan15. (Ai) PANC-1 WT cells were transduced with a N-terminal FLAG-tagged Tspan15 (T15) or control (con) lentiviral vector before validation by flow cytometry. The surface expression of (Aii) ADAM10 and (Aiii) Tspan15 was quantitated and presented as the geometric mean fluorescence intensity relative to isotype control staining. Data were log-transformed and analysed by a one-way ANOVA with a Tukey's multiple

comparisons test. Statistics shown are compared to lentiviral control cells. N=3; data represents mean relative surface expression ± SEM. (Bi-iii) Experiment was as described in panel Ai-iii, but for AsPC-1 cells.

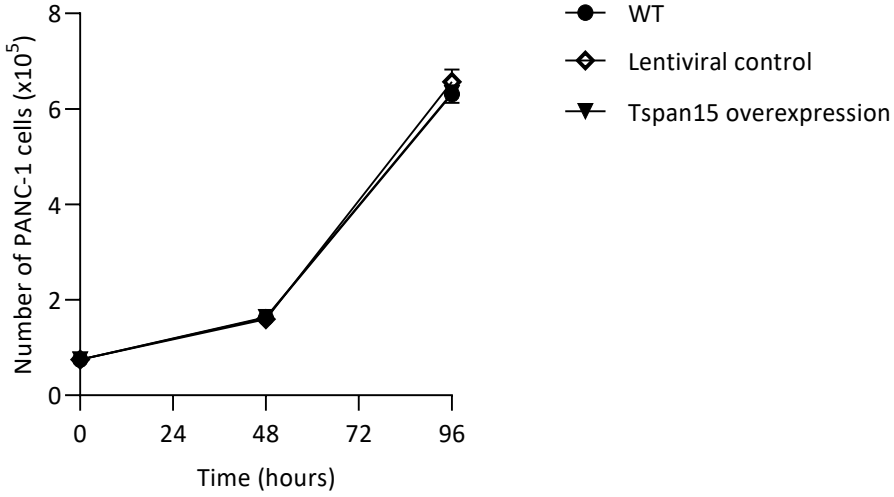
4.2.4 ADAM10 and Tspan15 do not regulate the 2D proliferation of PANC-1 and AsPC-1 cells

ADAM10 and Tspan15 have been shown to promote proliferation in some cancers (Arima et al., 2007; Fu et al., 2014; Liu et al., 2015; You et al., 2015; Tsang et al., 2018; Sidahmed-Adrar et al., 2019; Yuan et al., 2020b) but not others (Mullooly et al., 2015; Zhang et al., 2018; Sépult et al., 2019), suggesting a tumour-specific role. Further to this despite previous studies, it is unclear whether ADAM10 regulates pancreatic cancer proliferation due to conflicting observations (Gaida et al., 2010; Woods et al., 2015; Lin et al., 2016; Mueller et al., 2021). As such, it was important to further characterise the role of ADAM10 and explore the involvement of Tspan15 in pancreatic cancer cell proliferation. An estimation of PANC-1 and AsPC-1 cell proliferation was determined from cell counts at 48- and 96-hours post-plating. In PANC-1 cells, proliferation was unaffected at both time points by the knockout of ADAM10 or Tspan15 (Figure 28Ai), as well as Tspan15 overexpression (Figure 28Aii). Over 96 hours, the doubling rate of the newly generated cell lines was between 31 and 32 hours. Similarly, the expression of ADAM10 and Tspan15 did not influence AsPC-1 proliferation (Figure 28B) with cells doubling every 42 to 46 hours over a 96-hour period.

Ai


Number of PANC-1 cells (x10^5)
8
6
4
2
0
0
24
48
72
96
Time (hours)
WT
Empty vector control
ADAM10 guide 1 KO
ADAM10 guide 2 KO
Tspan15 guide 2 KO

Aii


Number of PANC-1 cells (x10^5)
8
6
4
2
0
0
24
48
72
96
Time (hours)
WT
Lentiviral control
Tspan15 overexpression

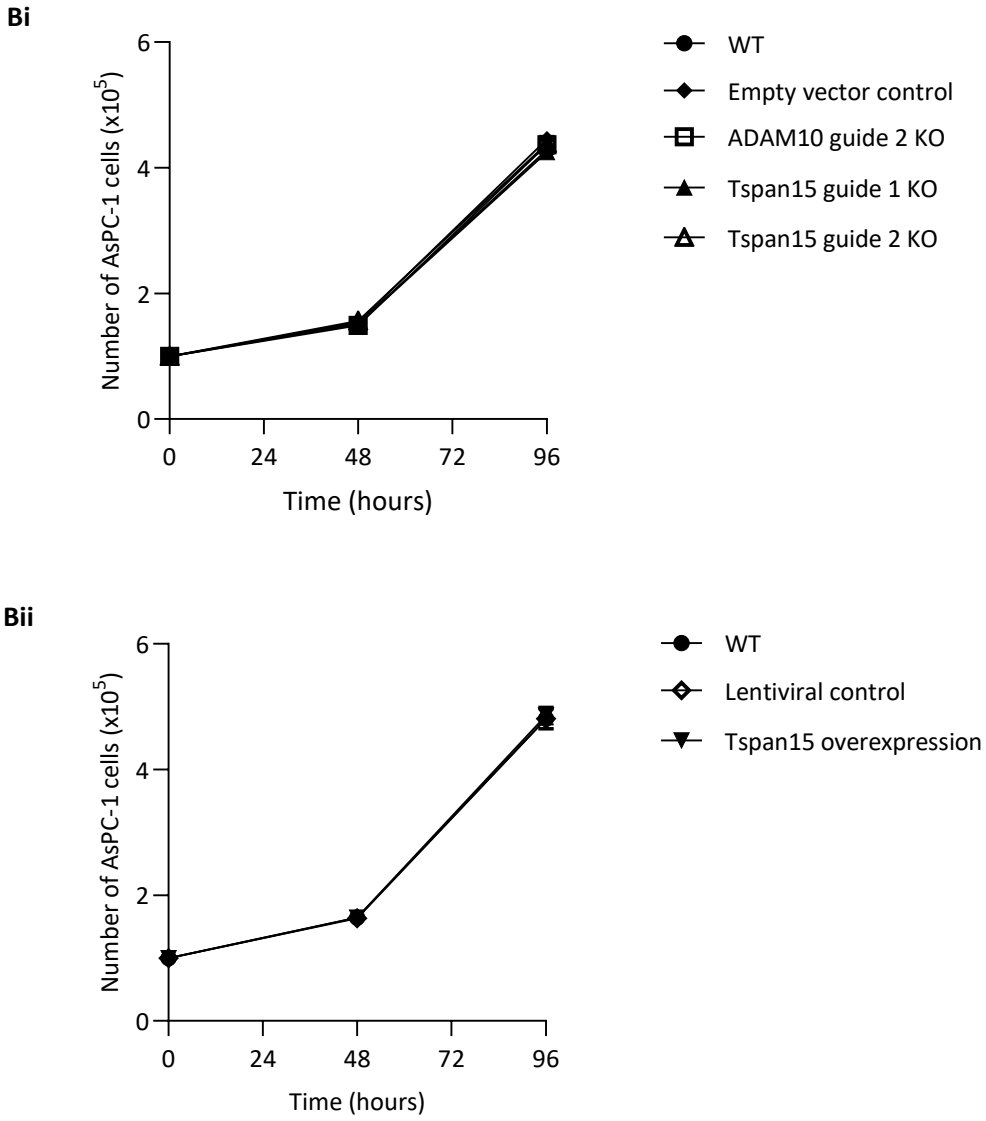


Figure 28: The proliferation of PANC-1 and AsPC-1 cells is unaffected by ADAM10 or Tspan15 knockout, and Tspan15 overexpression. (Ai) PANC-1 ADAM10 and Tspan15 KO pools, as well as (Aii) Tspan15 overexpression cells were trypsinised and counted 48- and 96-hours post-plating to estimate proliferation. Data were statistically analysed by a two-way ANOVA with a Tukey's multiple comparisons test. N=3; data represents mean number of cells ± SEM. The experiment described in panel A was performed for (Bi) AsPC-1 ADAM10 and Tspan15 KO pools and (Bii) Tspan15 overexpressing cells.

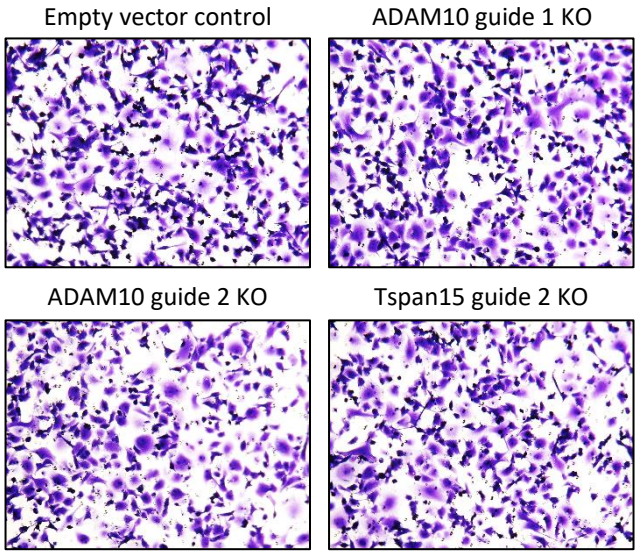
4.2.5 Loss of neither ADAM10 nor Tspan15 affects the invasive capabilities of pancreatic cancer cell lines

ADAM10 and Tspan15 have been shown to regulate the invasion of various cancer types (Guo et al.,

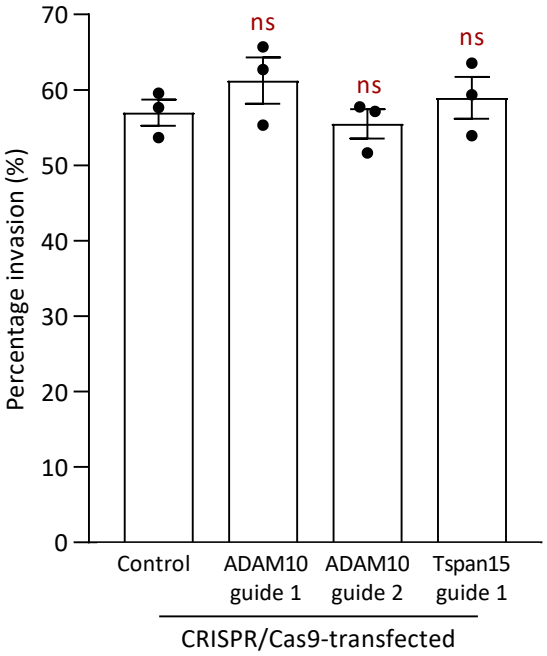
2012; Fu et al., 2014; Liu et al., 2015; Mullooly et al., 2015; Ma et al., 2016; Zhang et al., 2018;

Hiroshima et al., 2019; Sépult et al., 2019; Sidahmed-Adrar et al., 2019; Yuan et al., 2020b), with several studies presenting a potential role for ADAM10 in pancreatic cancer invasion (Gaida et al., 2010; Woods et al., 2015; Mueller et al., 2021). To further validate this role and investigate the involvement of Tspan15, a Transwell invasion assay was used to measure the invasive capabilities of PANC-1 and AsPC-1 cells through a Matrigel matrix. ADAM10 and Tspan15 KO cells, as well as control transfected cells, were seeded on Matrigel-coated, 8 µm pore Transwells in FBS-free media. To stimulate invasion, complete media containing 10% FBS was added to the bottom of the companion plate as a chemoattractant. Following incubation for 24 hours, the invasive cells, those on the underside of the Transwell membrane, were fixed, stained with crystal violet, and imaged using a Nikon SMZ1000 microscope. The images were then quantified with ilastik (Berg et al., 2019) and ImageJ (Schneider et al., 2012). This showed that loss of neither ADAM10 nor Tspan15 impaired the invasive capabilities of PANC-1 cells (Figure 29A); a percentage invasion of ~58% was observed in both control transfected and KO cells. Similarly, AsPC-1 cell invasion was not dependent on the expression levels of ADAM10 or Tspan15 (Figure 29B). Indeed, cells depleted of ADAM10 or Tspan15, as well as those with unmodified expression levels, covered ~12% of the Transwell membrane after 24 hours. These results, therefore, indicate that within this *in vitro* assay, ADAM10 and Tspan15 are not critical for invasion. However, this contradicts the previous studies demonstrating that ADAM10 regulates the invasion of human (Gaida et al., 2010; Woods et al., 2015) and mouse (Mueller et al., 2021) pancreatic cancer cell lines. The differences between these studies and their findings will be discussed relative to the current study in Section 4.3.

Ai


Empty vector control
ADAM10 guide 1 KO
ADAM10 guide 2 KO
Tspan15 guide 2 KO

Aii


Percentage invasion (%)
70
60
50
40
30
20
10
0
ns
ns
ns
Control
ADAM10 guide 1
ADAM10 guide 2
Tspan15 guide 1
CRISPR/Cas9-transfected

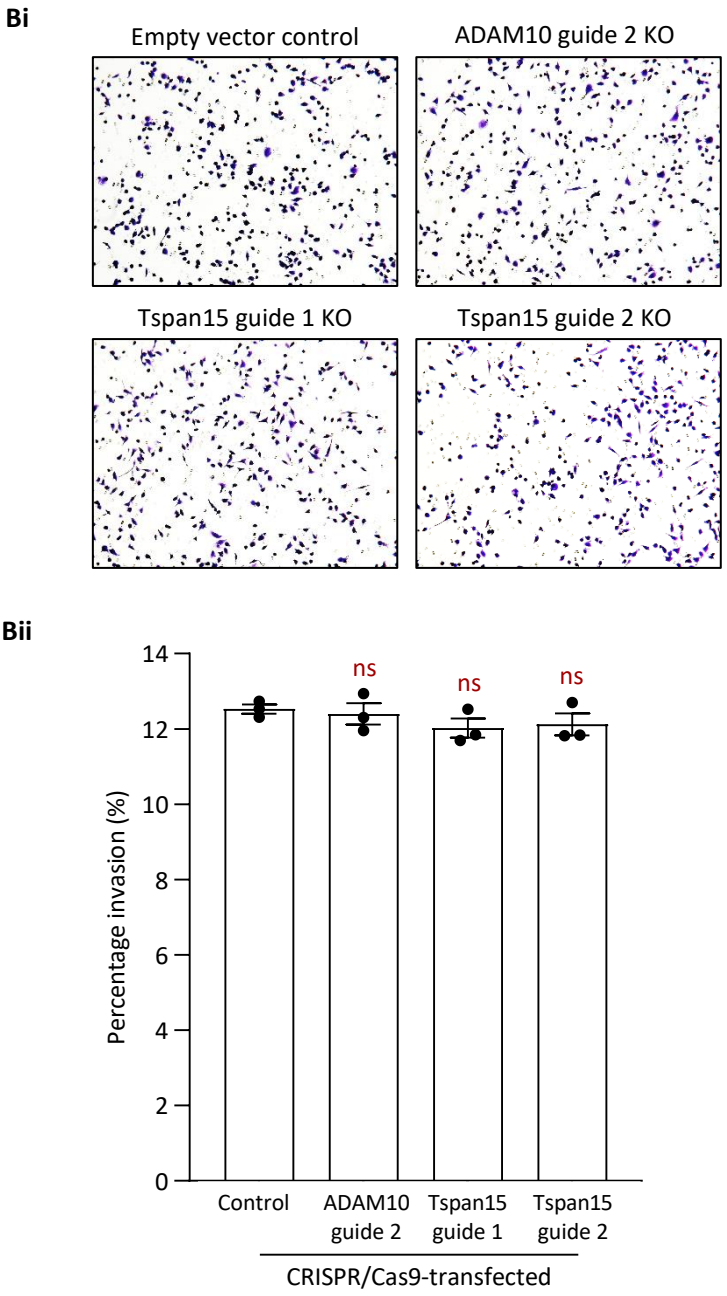
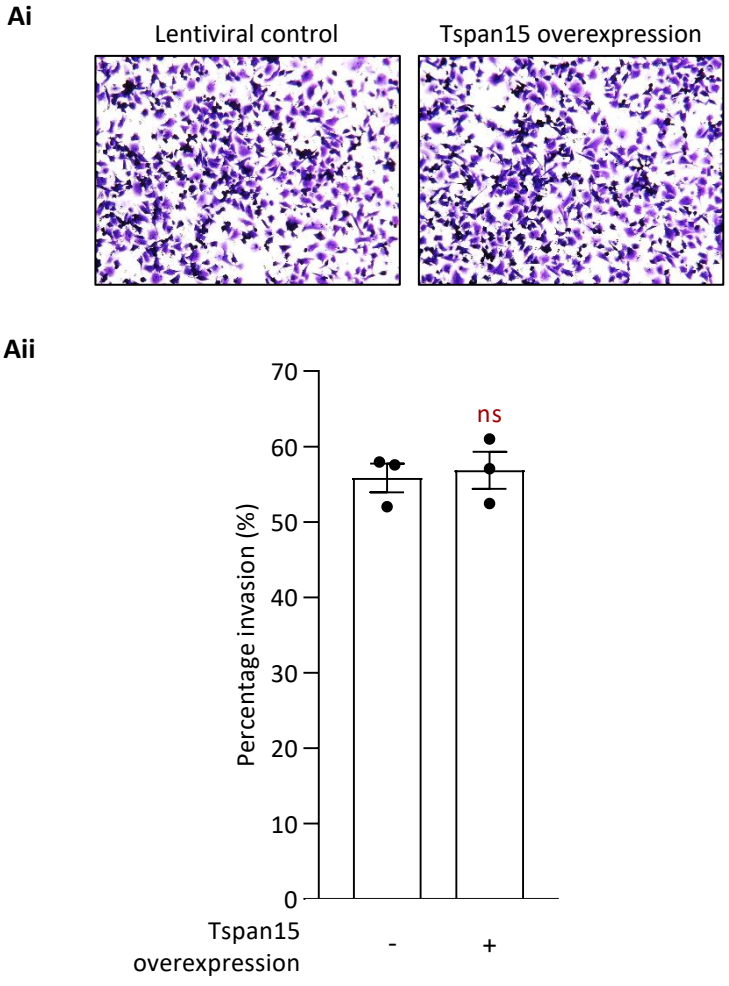


Figure 29: The invasive capabilities of PANC-1 and AsPC-1 cells are unaffected by the loss of ADAM10 or Tspan15. (Ai) PANC-1 ADAM10 and Tspan15 KO cells, as well as empty vector control transfected cells, were seeded on Transwells coated with 25 µg of Matrigel at a density of $1.5x10^5$ cells in 500 µl of FBS-free media. Complete media was added to the bottom of the companion plate with the 10% FBS functioning as a chemoattractant to stimulate invasion. Following incubation for 24 hours, invasive cells were fixed, stained with 0.05% crystal violet, and imaged using a Nikon SMZ1000 microscope. Images are representative of 5 fields of view per experiment. (Aii) Percentage cell coverage of the Transwell membrane, as a measure of invasion, was quantitated, arcsine-transformed, and statistically analysed by a one-way ANOVA with a Tukey's multiple comparisons test. Statistics shown are compared to control transfected cells. N=3; data represents mean percentage invasion ± SEM. (Bi-Bii) Experiment was as described in panel Ai-Aii, but for AsPC-1 cells, which were seeded at a density of $2x10^5$ cells in 500 µl.

4.2.6 The invasion of pancreatic cancer cell lines is unaffected by Tspan15 overexpression

To further validate the role of Tspan15 in pancreatic cancer cell invasion, the newly generated Tspan15 overexpression cell lines were used. The invasive capabilities of PANC-1 and AsPC-1 cells overexpressing Tspan15 4.5-fold and 5.1-fold, respectively, were assessed in a Transwell invasion assay, as described in Section 4.2.5. In both cell lines, the upregulation of Tspan15 surface expression did not affect invasion through a Matrigel matrix (Figure 30A-B); PANC-1 lentiviral control and Tspan15 overexpression cells covered ~56% of the Transwell membrane, and AsPC-1 cells exhibited a percentage invasion of ~15% regardless of Tspan15 surface expression. Taken together with the data from the previous section, this suggests that Tspan15 and ADAM10 likely do not have a role in pancreatic cancer invasion under these conditions.



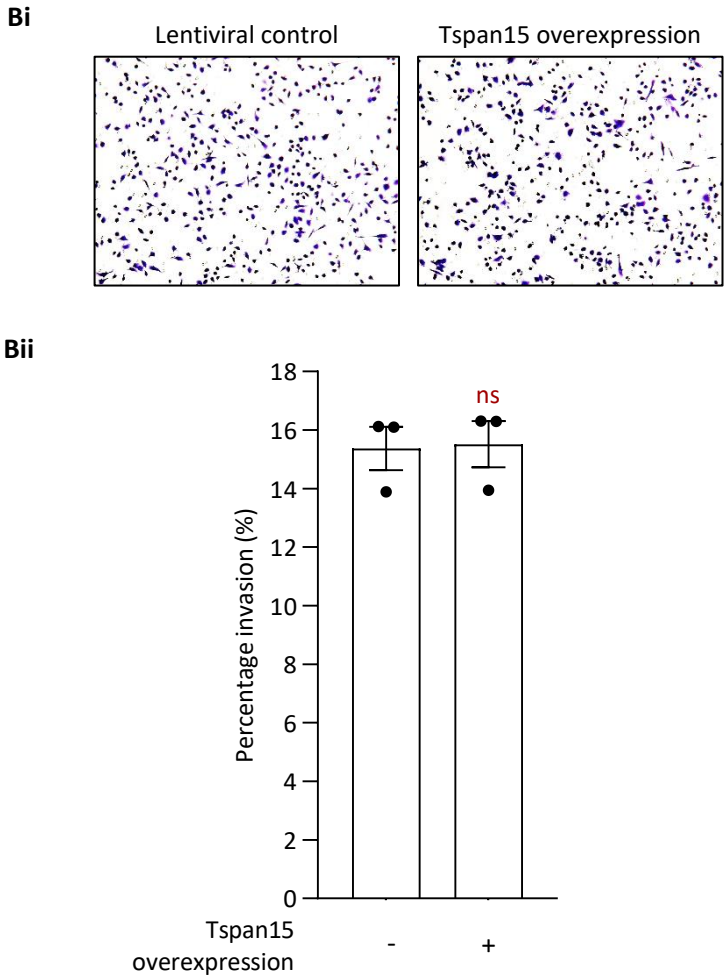


Figure 30: Tspan15 overexpression does not alter PANC-1 or AsPC-1 invasion through a Matrigel matrix. (Ai) PANC-1 lentiviral control and Tspan15 overexpressing cells were seeded at a density of $1.5x10^5$ cells per 500 µl of FBS-free media on Matrigel-coated Transwells. To stimulate invasion, complete media containing 10% FBS was added to the companion plate as a chemoattractant. After 24 hours, invasive cells were fixed, stained with 0.05% crystal violet, and imaged using a Nikon SMZ1000 microscope. Images are representative of 5 fields from each experiment. (Aii) Percentage cell coverage of the Transwell membrane was quantified using Ilastik and ImageJ. Data were arcsine-transformed and analysed by an unpaired, two-tailed t-test. N=3; data represents mean percentage invasion ± SEM. (Bi-Bii) Experiment was as described in panel Ai-Aii, but for AsPC-1 cells, which were seeded at a density of $2x10^5$ cells in 500 µl.

4.3 Discussion

As ADAM10 and Tspan15 have been shown to be upregulated in pancreatic adenocarcinoma, with high-tumour expression a potential marker of poor prognosis (Chapter 3), this chapter aimed to

establish whether ADAM10 and Tspan15 mediate the proliferation and/or invasion of pancreatic cancer. However, no evidence was found to support this potential involvement.

The first section of this chapter focused on the generation of ADAM10 and Tspan15 KO pancreatic cancer cell lines, as well as those overexpressing Tspan15. Interestingly, validation of the newly generated PANC-1 cells revealed that Tspan15 may interact with other proteins in addition to ADAM10. Previous studies have shown that ADAM10 is the main Tspan15 interactor (Jouannet et al., 2016; Sidahmed-Adrar et al., 2019; Koo et al., 2020), with the two proteins being observed to form an intimate heterodimer (Lipper et al., 2023). Their protein expression is also reciprocally regulated independently of mRNA levels (Eschenbrenner et al., 2020; Koo et al., 2020). Nevertheless, in PANC-1 cells, Tspan15 surface expression appeared to be unrelated to the expression of ADAM10. Tspan15 surface expression is typically reduced by ~80% in ADAM10 KO cells (Koo et al., 2020). However, in PANC-1 cells depleted of ADAM10, Tspan15 expression was better retained, with a reduction of ~53% observed. Further to this, the overexpression of Tspan15 in PANC-1 cells was not accompanied by an increase in ADAM10 surface expression, contrasting data from AsPC-1 (Section 4.2.3) and HEK-293T (Section 5.2.4) cells. Taken together, these findings provide preliminary evidence that the expression of Tspan15 at the cell surface may be supported by alternative interactors. Although follow-up experiments fell outside the scope of this project, future studies should aim to identify these proteins. This could be achieved using mass spectrometry to analyse proteins biotinylated during proximity-dependent labelling (Susa et al., 2023), a method that is particularly useful for identifying weak interactions that may be lost during an immunoprecipitation. It will also be important to determine the impact of any novel binding partners on Tspan15's pro-tumorigenic functions in pancreatic cancer, especially as AsPC-1 cells showed no evidence of a novel Tspan15 interactor.

Functional characterisation of these cells did not support a role for ADAM10 or Tspan15 in promoting the proliferation or invasion of pancreatic cancer cell lines. This could be due to the mutational

signature of PANC-1 and AsPC-1 cells; both cell lines exhibit mutations in K-RAS, TP53 and CDKN2A/p16 (Deer et al., 2010), which could be driving proliferation and invasion irrespective of the expression of ADAM10 and Tspan15. However, compared to this chapter's findings, a previous study, also using a Matrigel invasion assay, showed that ADAM10 knockdown decreased the invasive capabilities of two pancreatic cancer cell lines (Gaida et al., 2010). The disparity between these findings could be due to differences in the experimental setup. For example, Gaida et al. used siRNA to transiently decrease the expression of ADAM10 in AsPC-1 and COLO-357 cells, whereas this study utilised CRISPR/Cas9 generated ADAM10 KO PANC-1 and AsPC-1 cells. It is interesting to consider that stably knocking out ADAM10, unlike transient downregulation, may result in the acquisition of compensatory mutations. Furthermore, whilst two previous studies support the data from this thesis showing that ADAM10 does not regulate pancreatic cancer cell proliferation (Gaida et al., 2010; Mueller et al., 2021), other studies present opposing findings (Woods and Padmanabhan, 2013; Woods et al., 2015). As different cell lines were used (Gaida et al., 2010; Woods and Padmanabhan, 2013; Woods et al., 2015; Mueller et al., 2021), this inconsistency may be due to ADAM10's contribution to proliferation varying between different pancreatic cancer cell lines. It is also worth noting that no direct link was shown between ADAM10 and proliferation by Woods et al. (2015). Instead, the calcium channel blocker fendiline, which inhibited ADAM10 functioning, was demonstrated to impair the proliferation of pancreatic cancer cells (Woods et al., 2015). Future studies investigating the role of ADAM10 and Tspan15 in pancreatic cancer cell proliferation and invasion should be completed using spheroids, organoids, and/or mouse models, all of which more accurately represent the disease state of pancreatic adenocarcinoma tumours than 2D cell lines. Although the generation of PANC-1 spheroids was attempted during this project, the formation of 3D cultures was unsuccessful.

ADAM10 and Tspan15 may also exhibit other roles in pancreatic cancer. One consideration relates to the inclusion of ADAM10 and Tspan15 within EVs released from pancreatic cancer cells (Servage et

al., 2020), and thus their potential to modulate the tumour microenvironment and drive metastasis via trans cleavage of substrates. Alternatively, Tspan15 has the potential to promote immune evasion or resistance to radiotherapy. Indeed, ADAM10-mediated shedding of ULBP2 is thought to impair the activation of natural killer cells (Lin et al., 2016), whereas cleavage of ephrinB2 by ADAM10 drives radiation-induced metastasis (Mueller et al., 2021). As the TspanC8/ADAM10 complex for these substrates has not been determined, Tspan15 has the potential to mediate one or both of these pro-tumorigenic functions. Ultimately, future studies are required to obtain additional evidence to fully understand the role of ADAM10 and Tspan15 in pancreatic cancer.

In summary, this chapter showed that ADAM10 and Tspan15 may not mediate pancreatic cancer proliferation or invasion. Nevertheless, these two proteins have been reported to positively regulate the proliferation and invasion of other malignancies (Arima et al., 2007; Guo et al., 2012; Fu et al., 2014; Liu et al., 2015; Mullooly et al., 2015; You et al., 2015; Ma et al., 2016; Tsang et al., 2018; Zhang et al., 2018; Hiroshima et al., 2019; Sépult et al., 2019; Sidahmed-Adrar et al., 2019; Yuan et al., 2020a). However, whether Tspan15's involvement is ADAM10-dependent or -independent remains unclear. As such, this will be investigated further in the following chapter using a non-cancerous cell line to eliminate the potential effect of relatively strong oncogenic mutations, which may mask any more subtle roles of Tspan15 in an *in vitro* proliferation or invasion assay.

CHAPTER 5 TSPAN15 PROMOTES THE INVASION OF HEK-293T CELLS IN AN ADAM10-DEPENDENT MANNER VIA N-CADHERIN SHEDDING AND FGF RECEPTOR SIGNALLING

5.1 Introduction

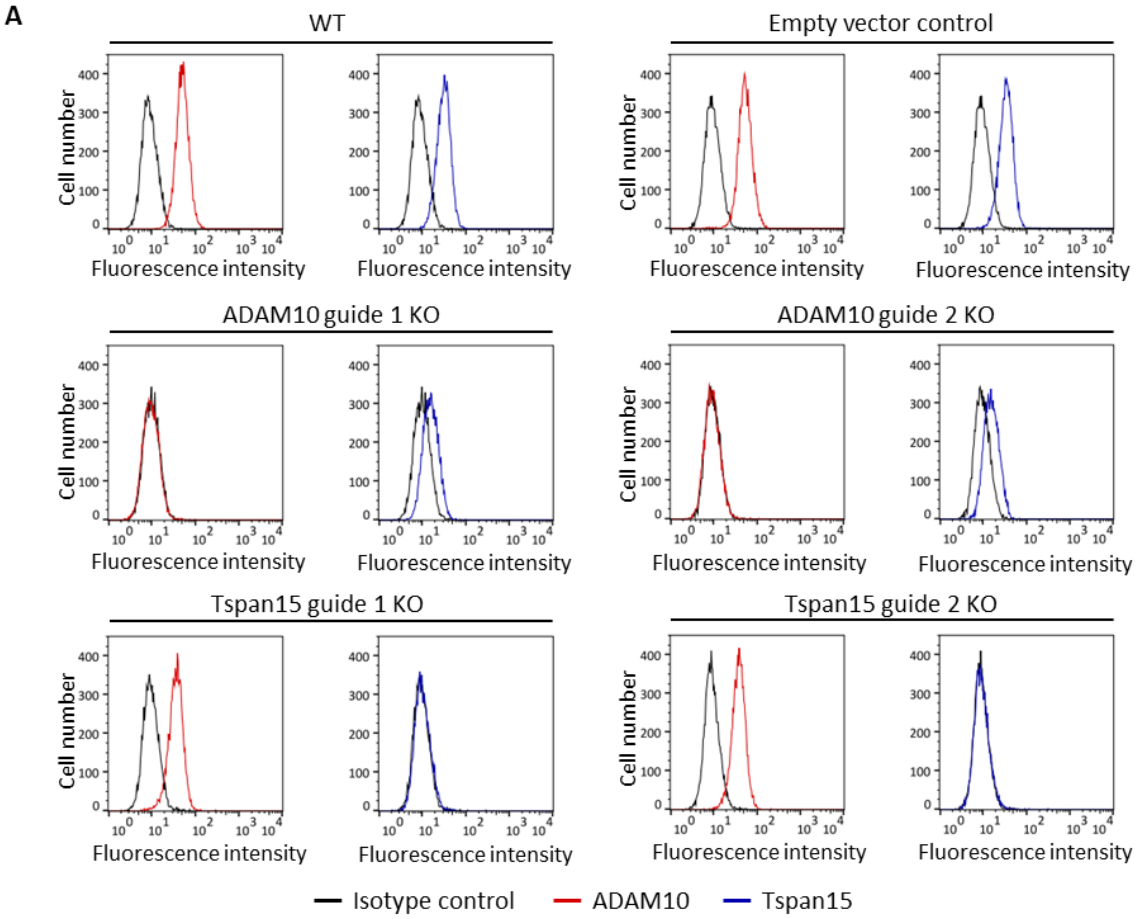
ADAM10 and Tspan15 have been shown to promote the invasion and proliferation of various cancers (Guo et al., 2012; Fu et al., 2014; Liu et al., 2015; Mullooly et al., 2015; You et al., 2015; Ma et al., 2016; Tsang et al., 2018; Zhang et al., 2018; Hiroshima et al., 2019; Sépult et al., 2019; Sidahmed-Adrar et al., 2019; Yuan et al., 2020b). However, despite patient data suggesting a potential role for both ADAM10 and Tspan15 in pancreatic cancer (Chapter 3), two pancreatic cancer cell lines, PANC-1 and AsPC-1, showed no growth or invasive phenotypes related to the expression of either protein (Chapter 4). It is tempting to speculate that the strong oncogenic mutations present in these cell lines (Deer et al., 2010) may have masked any more subtle effects of ADAM10 and Tspan15 within an *in vitro* proliferation or invasion assay. As such, this chapter aimed to investigate the role of Tspan15 in proliferation and invasion using a non-cancerous cell line.

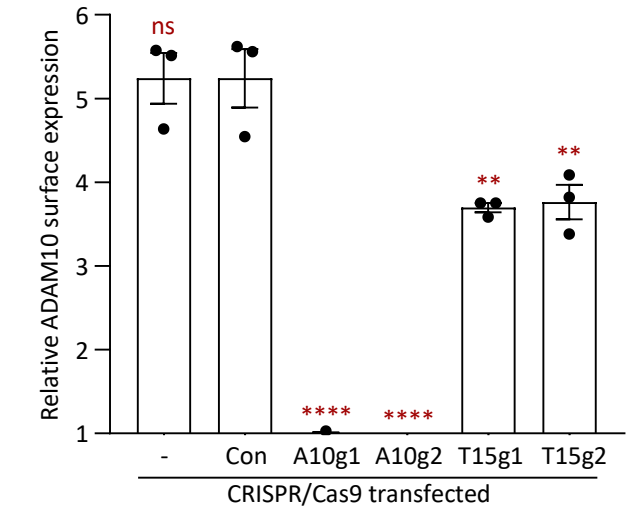
Furthermore, a secondary aim of this chapter was to explore the potential mechanism(s) underpinning Tspan15's role in cell growth and invasion, as whether this is ADAM10-dependent or -independent remains largely unstudied (Zhang et al., 2018; Hiroshima et al., 2019; Sidahmed-Adrar et al., 2019). Since the involvement of ADAM10-mediated cleavage in tumourigenesis is well-established (Guo et al., 2012; Woods and Padmanabhan, 2013; Lin et al., 2016; Ma et al., 2016; Tsang et al., 2018; Sépult et al., 2019; Yuan et al., 2020b; Garcia Garcia et al., 2021; Mueller et al., 2021), the first mechanism of interest was Tspan15's role in directing ADAM10 substrate specificity (Jouannet et al., 2016; Noy et al., 2016; Matthews et al., 2017a; Matthews et al., 2017b; Saint-Pol et al., 2017b; Matthews et al., 2018). Additionally, the proposed mechanism of action for Tspan15 in promoting NF-κB signalling via its interaction with β-TrCP (Zhang et al., 2018) was of interest.

5.2 Results

5.2.1 The generation and validation of ADAM10 and Tspan15 KO HEK-293T cells

To address the aforementioned aims of this chapter (Section 5.1), HEK-293T ADAM10 and Tspan15 knockout (KO) cells were generated using CRISPR/Cas9 genome editing technology, as per Chapter 4. HEK-293T WT cells were transfected with ADAM10 and Tspan15 guide oligos (Table 2) cloned into a pSpCas9(BB)-2A-Puro vector (plasmid map available in Figure A 1, Appendix). After 48 hours, cells were treated with puromycin to select for transfected cells and subsequently purified using antibody-coated magnetic Dynabeads. Flow cytometry analysis confirmed that the newly generated KO pools were deficient for ADAM10 or Tspan15 at the cell surface (Figure 31). Further to this, in line with previous studies showing that ADAM10 and Tspan15 are required for the expression of each other (Eschenbrenner et al., 2020; Koo et al., 2020), ADAM10 surface expression was decreased by ~36% in Tspan15 KO cells (Figure 31Bi). Similarly, ADAM10 KO cells exhibited a ~71% reduction in Tspan15 surface expression (Figure 31Bii).


A
WT
Empty vector control
ADAM10 guide 1 KO
ADAM10 guide 2 KO
Tspan15 guide 1 KO
Tspan15 guide 2 KO
Cell number
Fluorescence intensity
Isotype control
ADAM10
Tspan15


Bi
Relative ADAM10 surface expression
ns
**
**
****
****
-
Con
A10g1
A10g2
T15g1
T15g2
CRISPR/Cas9 transfected

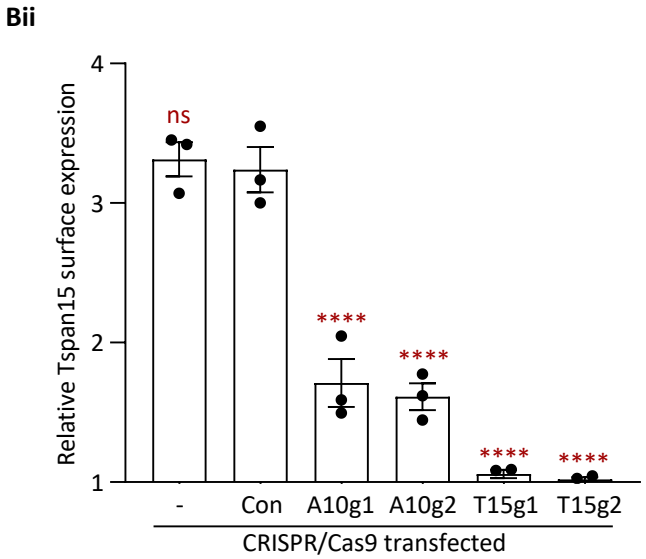


Figure 31: Validation of HEK-293T ADAM10 and Tspan15 KO pools. (A) CRISPR/Cas9 gene editing technology was used to generate ADAM10 (A10) and Tspan15 (T15) KO pools. HEK-293T cells were transfected with ADAM10 and Tspan15 guide oligos (guide 1 (g1) and guide 2 (g2)) cloned into the pSpCas9(BB)-2A-Puro vector, as well as an empty vector control (con). The impure KO pools were purified using antibody-coated, magnetic Dynabeads, and the resulting ADAM10 and Tspan15 surface expression was validated by flow cytometry. The surface expression of (Bi) ADAM10 and (Bii) Tspan15 was quantified and presented as the geometric mean fluorescence intensity of the target protein staining relative to isotype control staining. Data were log-transformed and analysed by a one-way ANOVA with a Tukey's multiple comparisons test. Statistics shown are compared to the control (con) transfected cells, with other comparisons not shown. N=3; data represents mean relative surface expression ± SEM.

5.2.2 The morphology of HEK-293T cells is unaffected by the loss of ADAM10 or Tspan15

The morphology of the newly generated ADAM10- and Tspan15-knockout HEK-293T cells was characterised in this section. This was to ensure that cellular behaviour would be unaffected by morphological differences. To do so, a Livecyte microscope was used to image the HEK-293T cells every 15 minutes for 24 hours. The automated single-cell tracking and integrated analysis enabled the perimeter and sphericity of individual cells to be measured at each time point. However, these morphological characteristics were unaffected by the loss of ADAM10 or Tspan15 (Figure 32), indicating that these two proteins are likely not important for the morphology of HEK-293T cells.

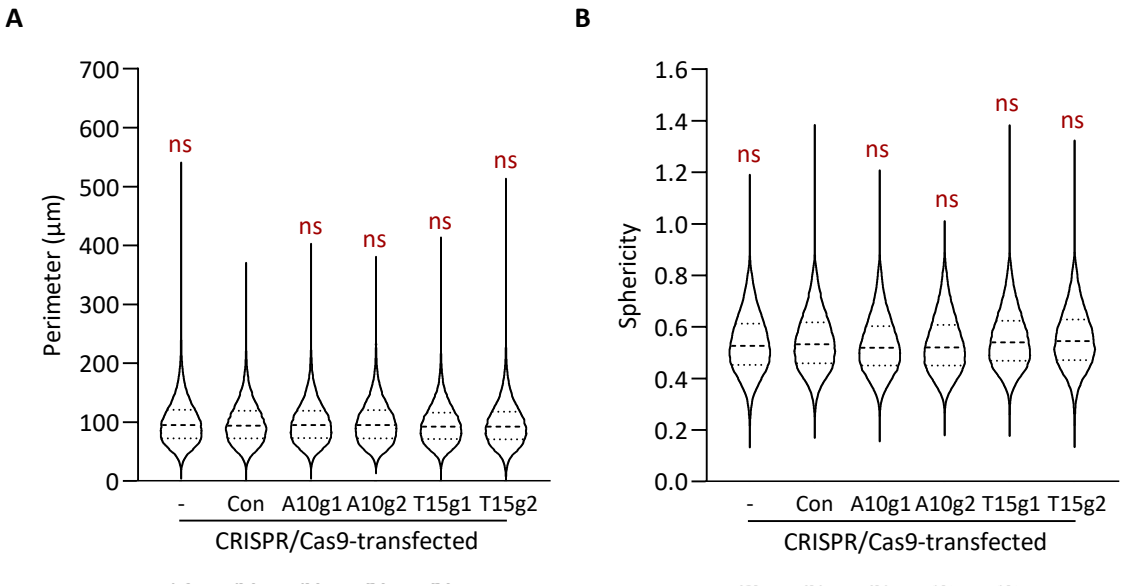


Figure 32: Morphological characterisation of ADAM10 and Tspan15 KO HEK-293T cells. Live cell imaging was used to characterise the morphology of HEK-293T ADAM10 (A10) and Tspan15 (T15) (guide 1 (g1) and guide 2 (g2)) KO cells as well as wild-type (WT) and empty vector control (con) transfected cells. Images were captured at two fields of view every 15 minutes for 24 hours using a Livecyte microscope equipped with a 20x objective lens. The integrated analysis was then used to segment cells and measure their (A) perimeter and (B) sphericity at each time point. Mean data points were analysed by a one-way ANOVA with a Tukey's multiple comparisons test. Statistics shown are compared to CRISPR/Cas9 control (con) transfected cells, with other comparisons not shown but also non-significant. N=3; data represents a minimum of 17,000 measurements from each repeat; the dashed line denotes the median, whilst the dotted lines indicate the upper and lower quartiles.

5.2.3 The loss of ADAM10 and Tspan15 does not affect the motility of HEK-293T cells

Further to the morphological characterisation of the HEK-293T ADAM10- and Tspan15-knockout cells (Section 5.2.2), their motility was also assessed via live cell imaging. Images of the cells were captured every 15 minutes for 24 hours using a Livecyte microscope. The automated single-cell tracking and integrated analysis enabled the instantaneous velocity and confinement ratio, a measure of how directly or indirectly the cells move, to be quantified at each time point. However, over 24 hours, the loss of neither ADAM10 nor Tspan15 affected the cellular velocity or path confinement of HEK-293T cells (Figure 33), suggesting that these two proteins are not required for

the motility of this cell line. As such, any differences in cellular behaviour will not be due to differences in motility.

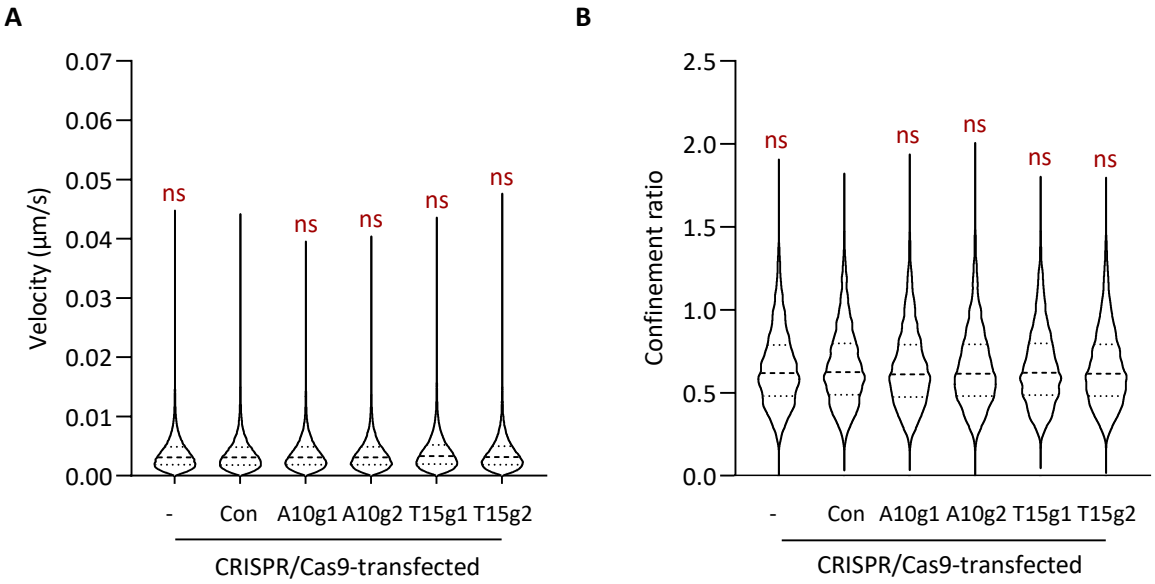


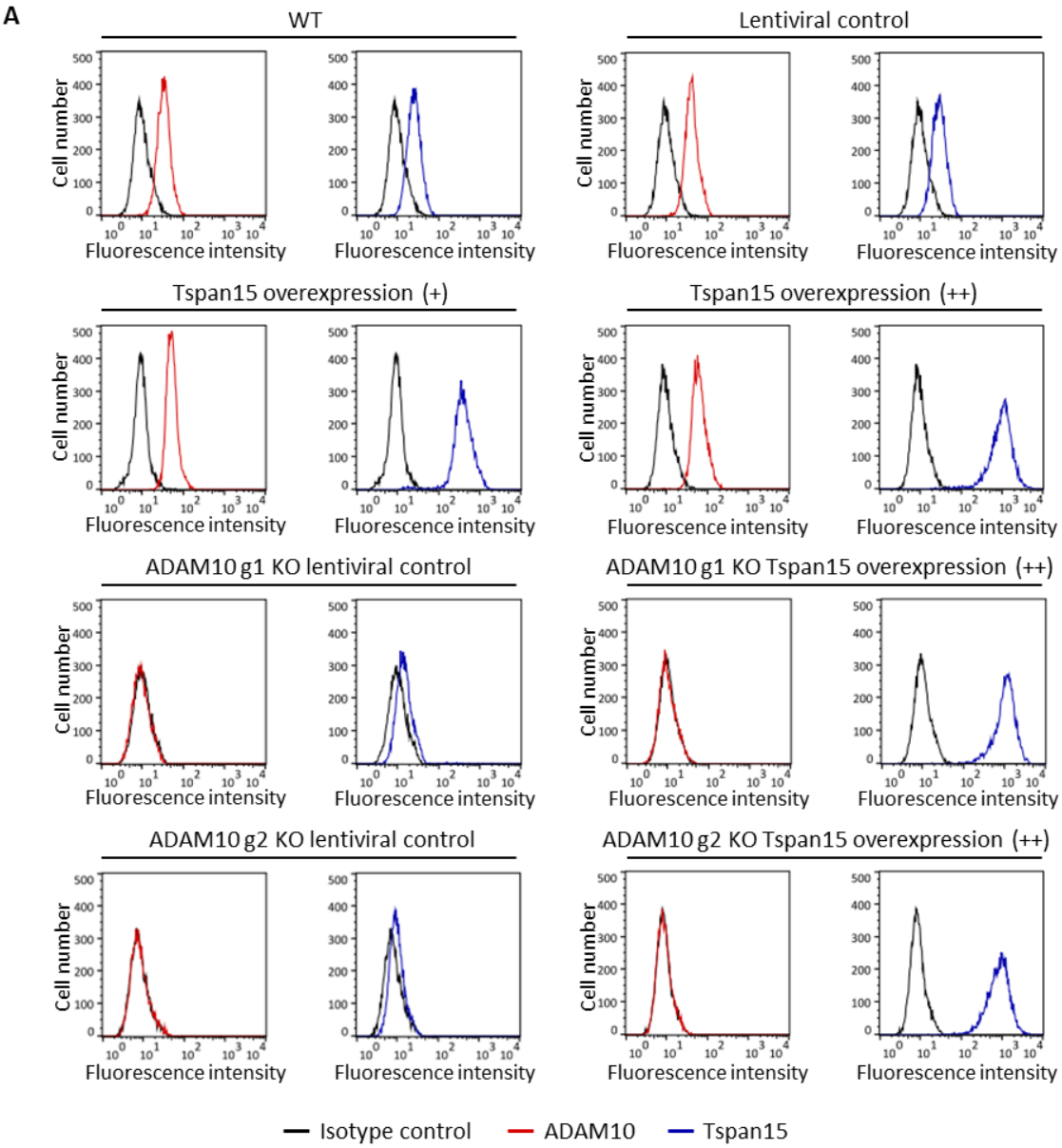
Figure 33: Loss of ADAM10 and Tspan15 does not affect the motility of HEK-293T cells. HEK-293T ADAM10 (A10) and Tspan15 (T15) (guide 1 (g1) and guide 2 (g2)) KO cells as well as wild-type (WT) and empty vector control (con) transfected cells were subjected to live cell imaging. Over a 24-hour period, a Livecyte microscope equipped with a 20x objective lens was used to capture images at two fields of view every 15 minutes. The integrated analysis was then used to segment cells and measure their (A) instantaneous velocity and (B) confinement ratio at each time point. Mean data points were analysed by a one-way ANOVA with a Tukey's multiple comparisons test. Statistics shown are compared to CRISPR/Cas9 control (con) transfected cells, with other comparisons not shown but also non-significant. N=3; data represents a minimum of 15,500 measurements for velocity and 880 measurements for the confinement ratio from each repeat; the dashed line denotes the median, whilst the dotted lines indicate the upper and lower quartiles

5.2.4 The generation and validation of HEK-293T cells overexpressing Tspan15

To further increase the resources available to address the aims of this chapter, HEK-293T cells overexpressing Tspan15 in both the presence and absence of ADAM10 surface expression were generated. HEK-293T WT and ADAM10 KO cells were transduced with N-terminal FLAG-tagged Tspan15 in the pLVX-EF1α-IRES-Puro lentiviral plasmid or a control lentiviral vector (plasmid map available in Figure A 2, Appendix) before selection with puromycin, as described in Section 4.2.3. Flow cytometry was then used to assess the expression of ADAM10 and Tspan15 at the cell surface.

The resulting analysis revealed that Tspan15 surface expression was upregulated 27- and 50-fold, + and ++ respectively, in HEK-293T WT cells transduced with the FLAG-tagged Tspan15 lentiviral vector, compared with WT cells transduced with a lentiviral control (Figure 34Bii). Additionally, in ADAM10 KO pools transduced with FLAG-tagged Tspan15 in the pLVX-EF1α-IRES-Puro lentiviral plasmid, surface expression of Tspan15 was increased 50-fold (++), relative to expression in WT lentiviral control cells (Figure 34Bii). ADAM10 surface expression was also increased by ~95%, when Tspan15 was overexpressed both 27- and 50-fold in HEK-293T WT cells (Figure 34Bi), providing further evidence that ADAM10 is required for Tspan15 expression (Eschenbrenner et al., 2020; Koo et al., 2020).

Throughout this chapter, the newly generated cell lines were used to investigate the role of Tspan15 in cell proliferation and invasion, as well as the associated mechanism of action.


A
WT
Lentiviral control
Tspan15 overexpression (+)
Tspan15 overexpression (++)
ADAM10 g1 KO lentiviral control
ADAM10 g1 KO Tspan15 overexpression (++)
ADAM10 g2 KO lentiviral control
ADAM10 g2 KO Tspan15 overexpression (++)
Cell number
Fluorescence intensity
Isotype control
ADAM10
Tspan15

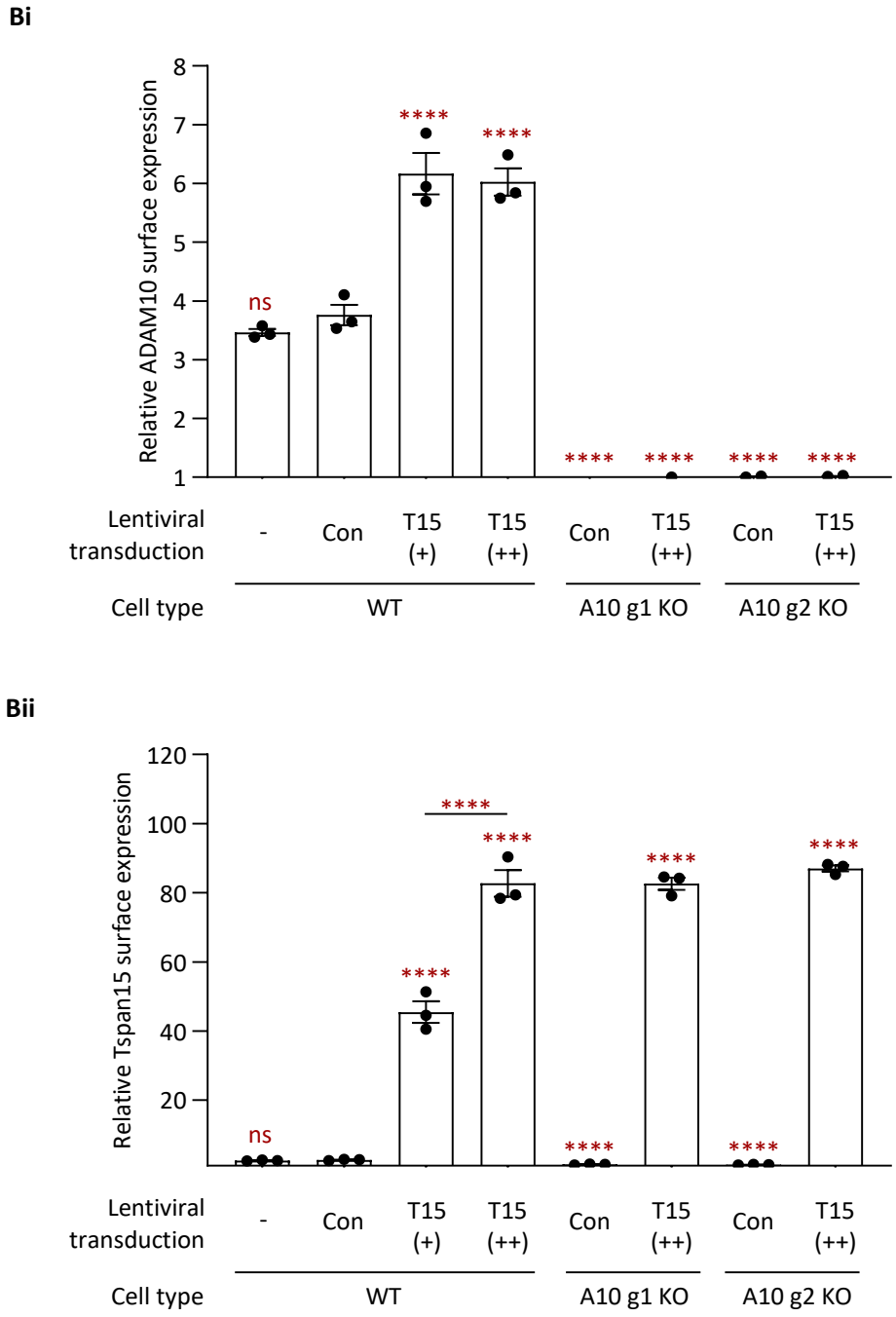


Figure 34: Validation of HEK-293T WT and ADAM10 KO cells overexpressing Tspan15. (A) HEK-293T WT and ADAM10 (A10) (guide 1 (g1) and guide 2 (g2)) KO cells were transduced with a N-terminal FLAG-tagged Tspan15 (T15) or control (con) lentiviral vector before validation by flow cytometry. (B) The surface expression of (i) ADAM10 and (ii) Tspan15 was quantified and presented as geometric mean fluorescence intensity relative to isotype control staining. Data were log-transformed and analysed by a one-way ANOVA with a Tukey's multiple comparisons test. Statistics shown are compared to the WT lentiviral control cells unless otherwise stated. N=3; data represents mean relative surface expression ± SEM.

5.2.5 The morphology of HEK-293T cells is unaffected by the overexpression of Tspan15

Prior to use in functional assays, the morphology of the Tspan15 overexpressing HEK-293T cells was characterised. This was to ensure that cellular behaviour would not be impacted by differences in morphology. The perimeter and sphericity of the aforementioned cell lines were quantified as per the experimental setup in Section 5.2.2; images of the cells were captured on a Livecyte microscope with automated single-cell tracking and integrated analysis enabling morphological characterisation. Over 24 hours, the size and shape of HEK-293T cells were unaffected by the upregulation of Tspan15 surface expression irrespective of ADAM10 expression (Figure 35). Therefore, this provides further evidence that ADAM10 and Tspan15 do not regulate the morphology of HEK-293T cells.

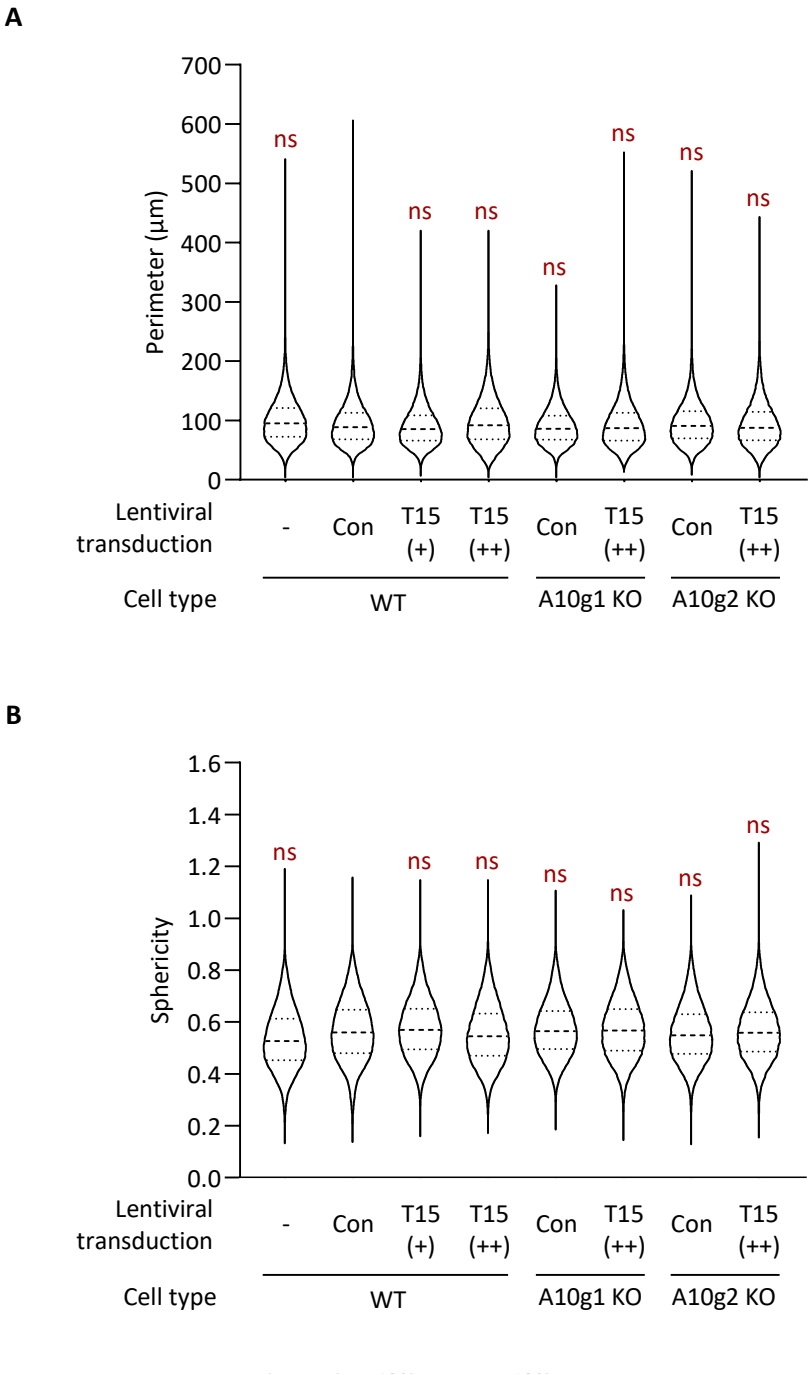


Figure 35: Morphological characterisation of HEK-293T cells overexpressing Tspan15 in the presence and absence of ADAM10 expression. A Livecyte microscope equipped with a 20x objective lens was used to image HEK-293T WT and ADAM10 (A10) (guide 1 (g1) and guide 2 (g2)) KO lentiviral control (con) cells, as well as cells overexpressing Tspan15 27- (+) and 50-fold (++). Images from two fields of view were captured every 15 minutes for 24 hours. The automated analysis was then used to segment cells before measuring their (A) perimeter and (B) sphericity at each time point. Mean data points were analysed by a one-way ANOVA with a Tukey's multiple comparisons test. Statistics shown are compared to WT lentiviral control (con) cells, with other comparisons not shown but also non-significant. N=3; data represents a minimum of 14,000 measurements from each repeat; the dashed line denotes the median, whilst the dotted lines indicate the upper and lower quartiles.

5.2.6 A striking clumping phenotype is observed in HEK-293T cells overexpressing Tspan15 50-fold, irrespective of ADAM10 expression

As HEK-293T cells approached confluency 96 hours post-plating at a density of $1x10^5$ cells in a 6-well plate, an EVOS M5000 microscope was used to capture images at five fields of view. Analysis of these images revealed a striking clumping phenotype in HEK-293T WT and ADAM10 KO cells overexpressing Tspan15 50-fold (++) (Figure 36). However, since a similar phenotype was not observed when Tspan15 expression was upregulated 27-fold (+) (Figure 36), this may be an artefact of extreme Tspan15 overexpression. Alternatively, the clumping morphology may be indicative of Tspan15 exhibiting ADAM10-independent activity in HEK-293T cells, which is explored further in Section 5.2.8.

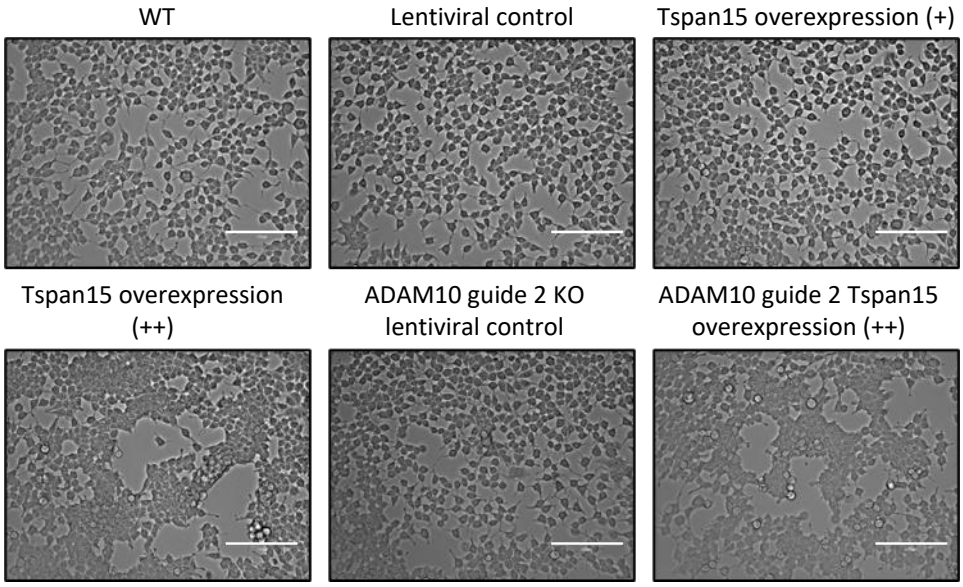


Figure 36: The overexpression of Tspan15 50-fold is associated with a striking clumping phenotype that is independent of ADAM10 expression. HEK-293T WT and ADAM10 guide 2 KO lentiviral control and Tspan15 overexpressing (27-fold (+) and 50-fold (++)) cells were plated at a density of $1x10^5$ cells in a 6-well plate. An EVOS M5000 equipped with a 20x objective lens and a brightfield phase ring was used to image the cells 96 hours post-plating as they approached confluency. Images are representative of 5 fields of view per experiment and the scale bar represents 150 µm. N=2.

5.2.7 The overexpression of Tspan15 regulates the path confinement of HEK-293T cells in an ADAM10-dependent manner

In addition to their morphological characterisation, the motility of the newly generated HEK-293T cells overexpressing Tspan15 was analysed via live cell imaging, as per the experimental setup in Section 5.2.3. In brief, a Livecyte microscope was used to capture images of the cells every 15 minutes for 24 hours. The automated single-cell tracking and integrated analysis then enabled the assessment of their motility, including the instantaneous velocity and confinement ratio at each time point. Consistent with the findings from Section 5.2.3, Tspan15 expression was not shown to regulate cellular velocity (Figure 37A); the overexpression of Tspan15 27- (+) and 50-fold (++) did not affect this motion parameter in HEK-293T cells, irrespective of ADAM10 expression. By comparison, 50-fold (++) overexpression of Tspan15 in both WT and ADAM10 KO cells was associated with an increased confinement ratio (Figure 37B), indicative of more direct movement. As a similar shift in path confinement was not seen in HEK-293T cells overexpressing Tspan15 27-fold (+) (Figure 37B), this phenotype is likely expression level-dependent, similar to the cell clumping phenotype observed in the previous section (Section 5.2.6). It is tempting to speculate that extreme Tspan15 overexpression (++) may result in reduced cell meandering due to movement within the respective clumps.

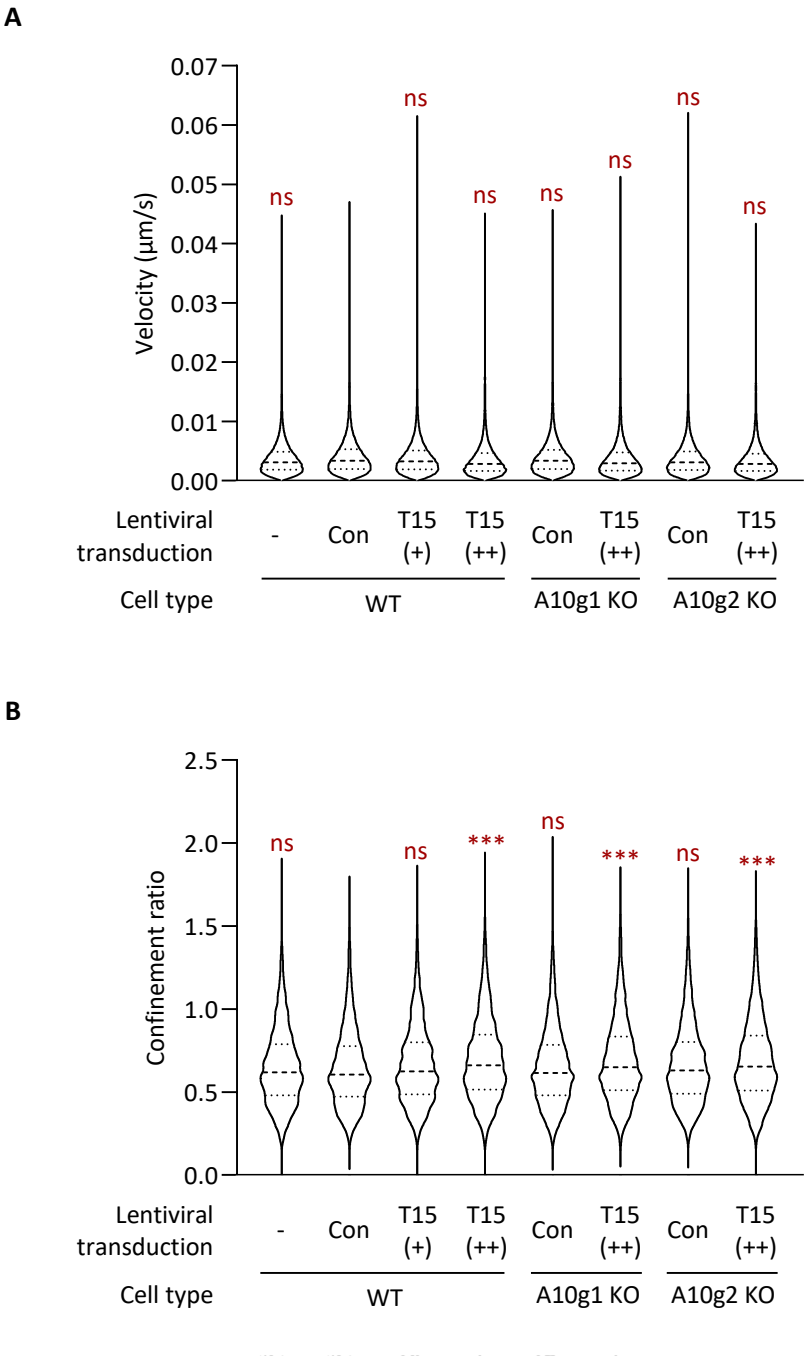


Figure 37: Elevated levels of Tspan15 expression affect how directly HEK-293T cells move but not their velocity. HEK-293T WT and ADAM10 (A10) (guide 1 (g1) and guide 2 (g2)) KO lentiviral control (con) cells, as well as cells overexpressing Tspan15 27- (+) and 50-fold (++) were subjected to live cell imaging. A Livecyte microscope equipped with a 20x objective lens was used to capture images at two fields of view every 15 minutes for 24 hours. The integrated analysis was then used to segment cells and measure the (A) instantaneous velocity and (B) confinement ratio at each time point. Mean data points were analysed by a one-way ANOVA with a Tukey's multiple comparisons test. Statistics shown are compared to WT lentiviral control (con) cells, with other comparisons not shown. N=3; data represents a minimum of 12,000 measurements for velocity and 1,050 measurements for the confinement ratio from each repeat; the dashed line denotes the median, whilst the dotted lines indicate the upper and lower quartiles

5.2.8 Tspan15 does not activate NF-κB signalling in HEK-293T cells

Tspan15 has been shown to drive metastasis in oesophageal carcinoma cell lines via its interaction with β-TrCP and subsequent downstream activation of NF-κB signalling, but the requirement for ADAM10 was not investigated (Zhang et al., 2018). Nevertheless, it remains possible that Tspan15-induced NF-κB activation is ADAM10-independent and may be responsible for Tspan15's effects on motility and cell clumping, as reported in Section 5.2.6 and Section 5.2.7. To determine whether Tspan15 promotes NF-κB signalling in HEK-293T cells, an NF-κB luciferase reporter assay was used in which luciferase expression is driven by NF-κB activity (Shapiro et al., 1996). For this assay, Tspan15 knockout and overexpressing cells were transfected with the NF-kB luciferase reporter construct. The following day, positive control wells were stimulated for 6 hours with PMA, a protein kinase C activator, and ionomycin, a Ca^{2+} ionophore, to maximally activate the reporter, while matched wells were treated with an equal volume of DMSO and ethanol. Cells were subsequently lysed in 1% Triton X-100 lysis buffer and NF-κB luciferase activity was measured. However, NF-κB-luciferase activation was unaffected by Tspan15 knockout (Figure 38A) or overexpression (Figure 38B), suggesting that Tspan15 does not promote NF-κB signalling in HEK-293T cells. As such, the potential ADAM10-independent activity of Tspan15, especially that associated with the clumping morphology and altered motility observed in HEK-293T cells overexpressing Tspan15 50-fold, requires further investigation, but was not addressed further in this thesis.

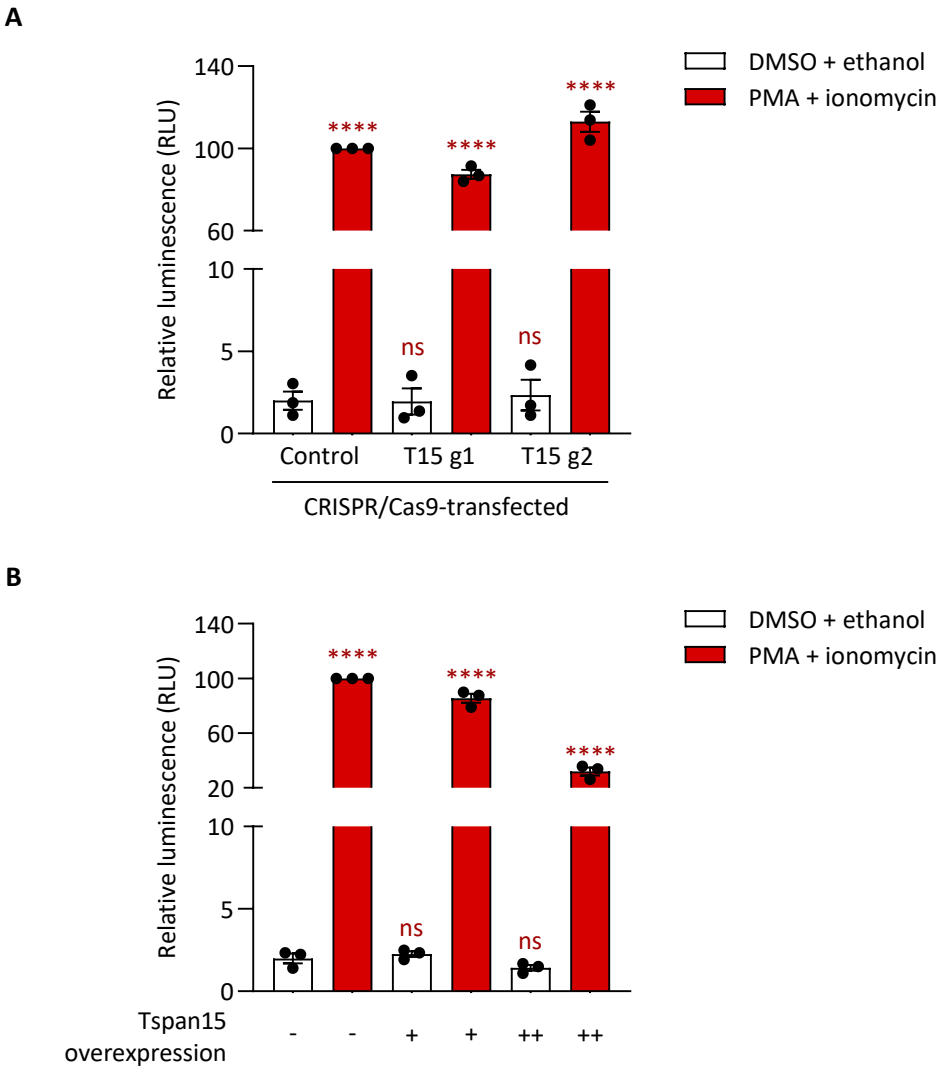


Figure 38: NF-κB signalling is not mediated by Tspan15 in HEK-293T cells. (A) Tspan15 guide 1 (g1) and guide 2 (g2) KO HEK-293T cells, as well as empty vector control transfected cells, were transfected with an NF-κB-luciferase reporter construct for 24 hours. Cells were then stimulated with 50 ng/ml PMA and 1 µM ionomycin, or left unstimulated and treated with DMSO and ethanol as a vehicle control. After 6 hours, the cells were lysed in 1% Triton X-100 lysis buffer and NF-κB luciferase activity was assessed in triplicate. Luminescence was quantitated as a percentage of PMA- and ionomycin-treated cells and presented relative to control cells. Data were arcsine-transformed and analysed by a one-way ANOVA with a Dunnett's multiple comparisons test compared to unstimulated control cells. N=3; data represents mean relative luminescence ± SEM. (B) Experiment was as described in A but for HEK-293T cells overexpressing Tspan15 27- (+) and 50-fold (++).

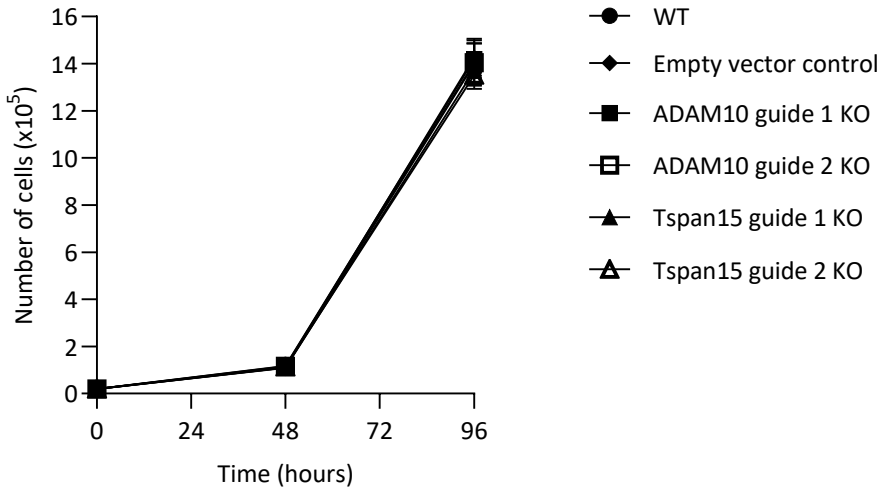
5.2.9 The expression levels of ADAM10 and Tspan15 do not affect the proliferation of HEK-293T cells

The findings from the previous chapter showed that ADAM10 and Tspan15 do not regulate the *in vitro* proliferation of two pancreatic cancer cell lines (Section 4.2.4). However, these two proteins have been previously reported to drive the cellular proliferation of other malignancies (Arima et al., 2007; Fu et al., 2014; Liu et al., 2015; You et al., 2015; Tsang et al., 2018; Sidahmed-Adrar et al., 2019; Yuan et al., 2020b). As such, to investigate whether ADAM10 and Tspan15 regulate the proliferation of HEK-293T cells, an estimation of proliferation was determined from cell counts 48- and 96-hours post-plating at a density of $2x10^4$ cells in a 6-well plate, as outlined in Section 4.2.4. Consistent with the data from PANC-1 and AsPC-1 cells, the rate of HEK-293T cell proliferation was not significantly altered at either timepoint by the loss of ADAM10 or Tspan15 (Figure 39Ai). Additionally, the overexpression of Tspan15 27- (+) or 50-fold (++) did not affect cell growth, irrespective of ADAM10 expression (Figure 39Aii). Regardless of the ADAM10 and Tspan15 expression levels, the HEK-293T cells had a doubling time of between 15 and 16 hours over 96 hours.

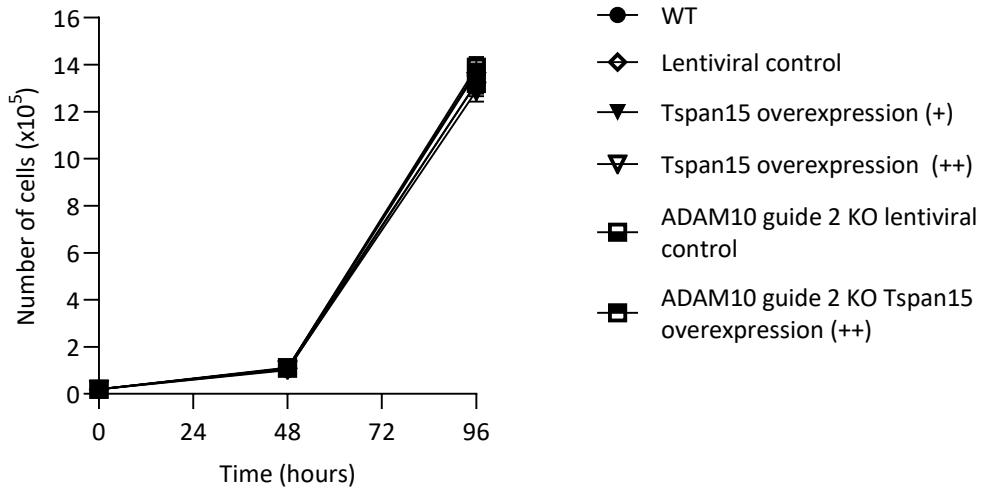
This finding was further validated by live cell imaging using a Livecyte microscope. HEK-293T cells, which were plated at a density of $8x10^4$ cells a day prior, were imaged at two fields of view every 15 minutes for 24 hours. The doubling rate of the cells was then determined by the microscope's automated single-cell tracking together with the integrated analysis. Similar to the observation in the previous experiment, the proliferation rate of HEK-293T cells was unaffected by the expression levels of ADAM10 and Tspan15 (Figure 39B).

Taken together, these two experiments provide strong evidence to suggest that ADAM10 and Tspan15 do not mediate the 2D proliferation of HEK-293T cells.

Ai


Number of cells (x10^5)
16
14
12
10
8
6
4
2
0
0
24
48
72
96
Time (hours)
WT
Empty vector control
ADAM10 guide 1 KO
ADAM10 guide 2 KO
Tspan15 guide 1 KO
Tspan15 guide 2 KO

Aii


Number of cells (x10^5)
16
14
12
10
8
6
4
2
0
0
24
48
72
96
Time (hours)
WT
Lentiviral control
Tspan15 overexpression (+)
Tspan15 overexpression (++)
ADAM10 guide 2 KO lentiviral control
ADAM10 guide 2 KO Tspan15 overexpression (++)

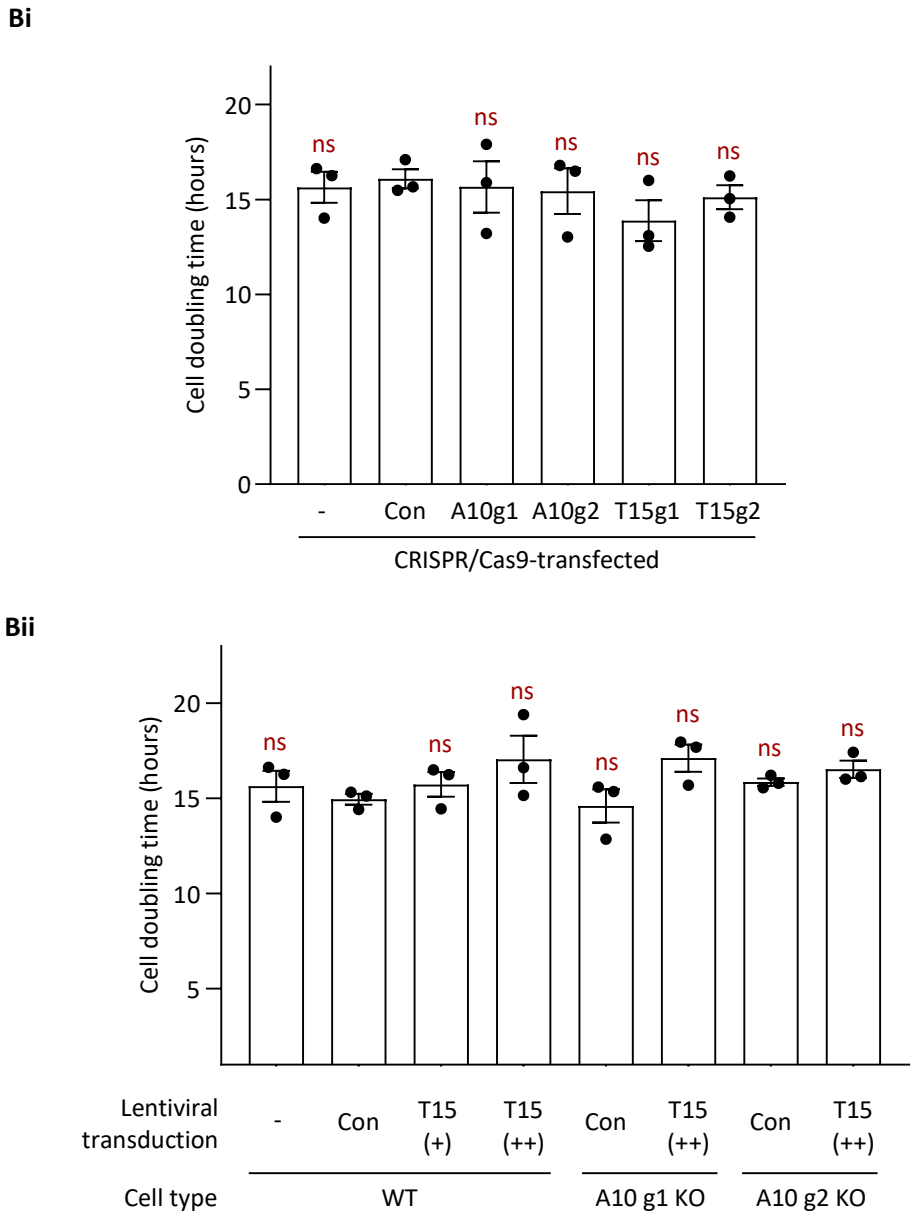


Figure 39: ADAM10 and Tspan15 do not regulate the 2D proliferation of HEK-293T cells. (A) The proliferation rate of (i) HEK-293T wild-type (WT), empty vector control (con) transfected, ADAM10 (A10) and Tspan15 (T15) (guide 1 (g1) and guide 2 (g2)) KO, as well as (ii) HEK-293T WT and ADAM10 (A10) KO lentiviral control (con) and Tspan15 overexpressing (27- (+) and 50-fold (++)) cells was estimated from cell counts 48- and 96-hours post-plating; cells were trypsinised at each time point and counted using a haemocytometer. Data were statistically analysed by a two-way ANOVA with a Tukey's multiple comparisons test and all results were non-significant. N=3; data represents the mean number of cells ± SEM. (Bi) HEK-293T ADAM10 and Tspan15 KO cells, as well as (ii) HEK-293T WT and ADAM10 (guide 1 (g1) and guide 2 (g2)) KO cells overexpressing Tspan15 were plated at a density of $8x10^4$ cells in a 24-well plate. Twenty-four hours post-plating, a Livecyte microscope was used to image the cells; images were captured every 15 minutes for 24 hours at two fields of view. The integrated analysis was then used to segment the cells and calculate their doubling time. Data were analysed by a one-way ANOVA with a Tukey's multiple comparisons test. N=3; data represents the mean doubling time ± SEM.

5.2.10 ADAM10 and Tspan15 do not mediate the proliferation of HEK-293T spheroids

The 2D proliferation of HEK-293T cells was not shown to be regulated by ADAM10 or Tspan15 (Section 5.2.9). However, to fully understand the role of these proteins in cellular proliferation, 3D cultures should be used, as they more accurately model the *in vivo* microenvironment (Baker and Chen, 2012; Cacciamali et al., 2022). As such, HEK-293T ADAM10 and Tspan15 KO spheroids were established using the hanging drop method and transferred to a 24-well plate coated with agarose. Forty-eight hours post-transfer, an EVOS M5000 microscope was used to capture time t=0 hours images. Subsequent images were then captured every 24 hours for 96 hours and an estimation of proliferation was determined from the changes in spheroid diameter, which were measured using the straight-line selection tool on ImageJ. Consistent with the data from 2D cultures, 3D proliferation was unaffected by the loss of ADAM10 or Tspan15 over a 96-hour period (Figure 40). Together, this data strongly suggests that ADAM10 and Tspan15 are not required for the proliferation of HEK-293T cells.

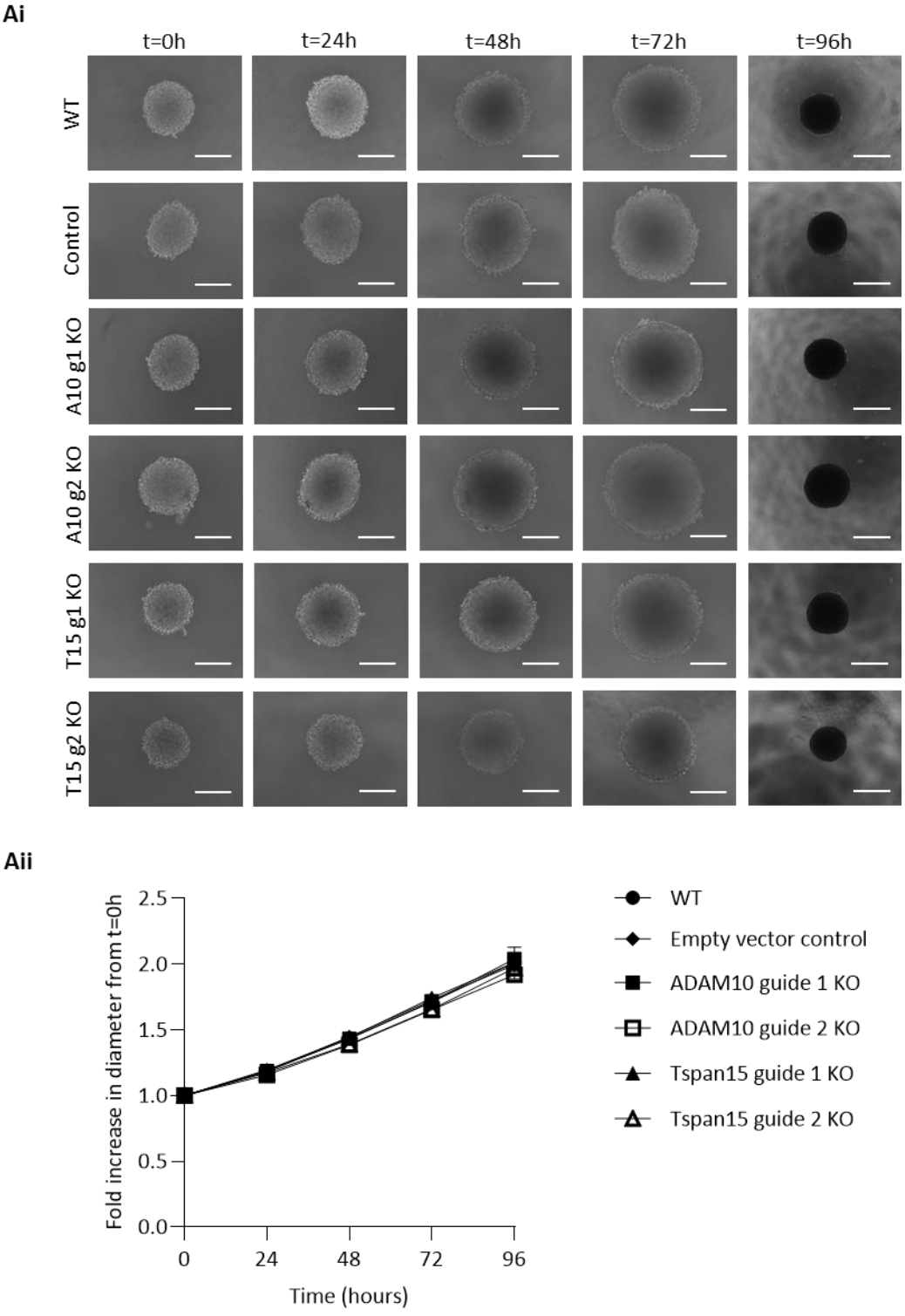


Figure 40: The proliferation of HEK-293T spheroids is not regulated by ADAM10 or Tspan15. (Ai) HEK-293T ADAM10 and Tspan15 KO spheroids were generated via the hanging drop method and transferred to a 24-well plate coated with 1.5% agarose. Following incubation in 5% CO_2 at 37 ^{o}C for 48 hours, the spheroids were imaged every 24 hours for 96 hours using an EVOS M5000 equipped

with a 10x or 4x objective lens. Representative images are shown. Scale bars represent 300 µm for time (t)=0 to 72 hours (h) and 750 µm for t=96h. (Aii) Proliferation was estimated from spheroid diameter measurements taken at each time point and presented as the fold increase from t=0h. N=2; data represents the mean fold diameter increase ± SEM.

5.2.11 Loss of ADAM10 or Tspan15 impairs the invasive capabilities of HEK-293T cells

Although this study has shown that ADAM10 and Tspan15 may not mediate pancreatic cancer cell invasion (Chapter 4), these two proteins have been reported to play a role in the invasion of various other tumours (Guo et al., 2012; Fu et al., 2014; Liu et al., 2015; Mullooly et al., 2015; Ma et al., 2016; Zhang et al., 2018; Hiroshima et al., 2019; Sépult et al., 2019; Sidahmed-Adrar et al., 2019; Yuan et al., 2020b). As such, the invasive capabilities of HEK-293T cells depleted of ADAM10 or Tspan15 were assessed in a Transwell invasion assay. ADAM10 and Tspan15 KO cells, as well as empty vector control transfected cells, were seeded in FBS-free DMEM on 8 µm pore Transwells coated with Matrigel. The cells were then incubated in 5% CO_2 at 37 ^{o}C and allowed to invade through the Matrigel towards the complete DMEM in the bottom of the companion plate; the complete DMEM contains 10% FBS, which acts as a chemoattractant to stimulate invasion. After 24 hours, the invasive cells were fixed, stained with crystal violet, and then imaged using a Nikon SMZ1000 microscope. Quantification of the images revealed that loss of ADAM10 or Tspan15 significantly impaired the invasive capabilities of HEK-293T cells, with invasion being reduced in the knockout cells by ~67% compared to control cells (Figure 41). While this suggests that ADAM10 and Tspan15 regulate HEK-293T cell invasion, it does not confirm whether Tspan15's mechanism of action is ADAM10-dependent or -independent, as Tspan15 surface expression is decreased by ~71% in the ADAM10 KO cells (Section 5.2.1).

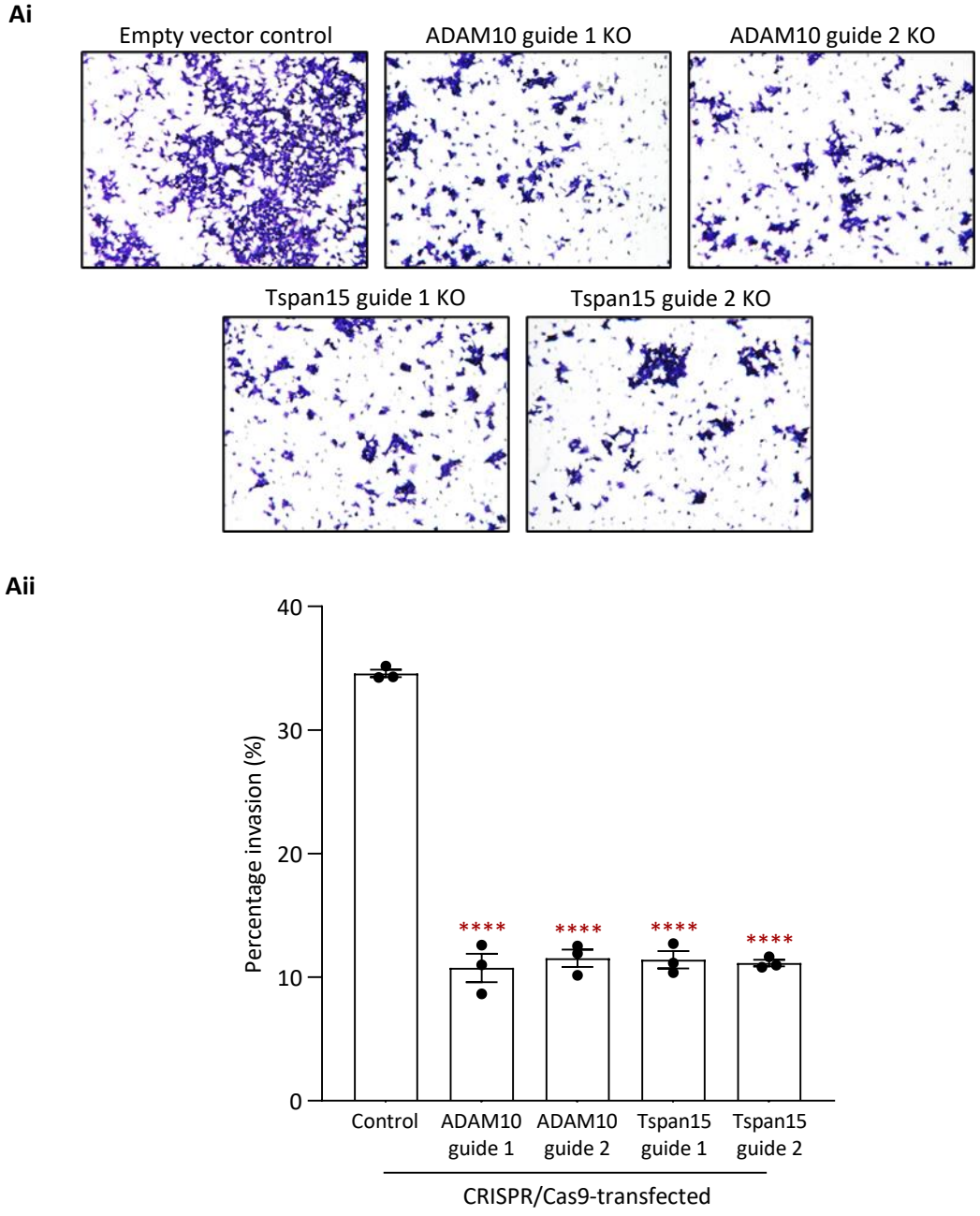


Figure 41: ADAM10- and Tspan15-knockout HEK-293T cells exhibit impaired invasive capabilities. (Ai) ADAM10 and Tspan15 KO HEK-293T cells together with empty vector control transfected cells were seeded on Transwells coated with 25 µg of Matrigel; $2x10^5$ cells were seeded in 500 µl of FBS-free DMEM. To stimulate invasion, complete DMEM, which contained 10% FBS, was added to the companion plate as a chemoattractant. Following incubation for 24 hours, invasive cells were fixed, stained with 0.05% crystal violet, and then imaged using a Nikon SMZ1000 microscope. Images are representative of 5 fields of view captured per experiment. (Aii) Ilastik and ImageJ were used to quantify percentage cell coverage of the Transwell membrane. Data were arcsine-transformed and analysed by a one-way ANOVA with a Tukey's multiple comparisons test. Statistics shown are compared to empty vector control transfected cells. N=3; data represents mean percentage invasion ± SEM.

5.2.12 Increasing levels of Tspan15 surface expression promotes HEK-293T cell invasion

Findings from the previous section demonstrate that Tspan15 is a likely regulator of HEK-293T cell invasion. To further validate this, the invasive capabilities of HEK-293T WT cells overexpressing Tspan15 were assessed in a Transwell invasion assay, as described in the previous section (Section 5.2.11). Analysis of the data revealed that increasing Tspan15 surface expression was associated with elevated invasion. Indeed, a 27- (+) and 50-fold (++) overexpression of Tspan15 resulted in a respective invasion increase of ~57% and ~139% compared to lentiviral control cells (Figure 42).

Taken together with the data from the previous section (Section 5.2.11), this finding strongly suggests that Tspan15 has a role in mediating the invasion of HEK-293T cells.

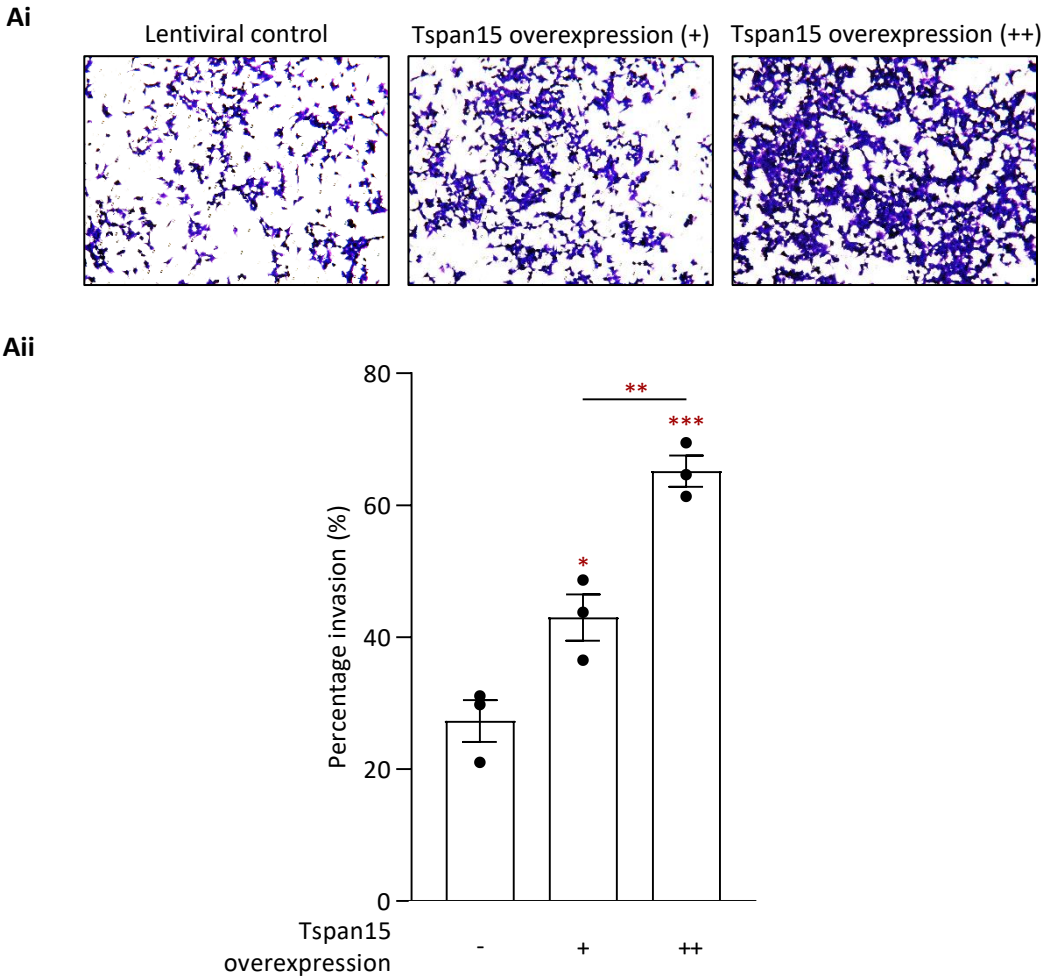


Figure 42: Overexpression of Tspan15 in HEK-293T WT cells increases invasion. (Ai) HEK-293T lentiviral control (-) cells and cells overexpressing Tspan15 27- (+) and 50-fold (++) were resuspended at a density of $2x10^5$ cells in 500 µl of FBS-free DMEM. They were then seeded on Transwells coated with 25 µg of Matrigel. To stimulate invasion, complete media containing 10% FBS was added to the bottom of the companion plate as a chemoattractant. After 24 hours, invasive cells were fixed, stained with 0.05% crystal violet, and imaged using a Nikon SMZ1000 microscope. Images are representative of 5 fields of view from each experiment. (Aii) Percentage cell coverage of the Transwell membrane was quantified using Ilastik and ImageJ. Data were arcsine-transformed and analysed by a one-way ANOVA with a Tukey's multiple comparisons test. Unless otherwise stated statistics shown are compared to WT lentiviral control (-) cells. N=3; data represents mean percentage invasion ± SEM.

5.2.13 Tspan15 promotes the invasion of HEK-293T cells in an ADAM10-dependent manner

To investigate whether Tspan15 promotes HEK-293T cell invasion in an ADAM10-dependent or

-independent manner, HEK-293T cells deficient for ADAM10 and overexpressing Tspan15 50-fold (++)

were used. A Transwell invasion assay, as described in Section 5.2.11, enabled the invasive capabilities of the aforementioned cell lines alongside ADAM10 KO lentiviral controls to be assessed. In brief, the cells were seeded on Matrigel-coated Transwells in FBS-free DMEM. To stimulate invasion, complete DMEM, containing 10% FBS as a chemoattractant, was then added to the bottom of the companion plate. Following incubation for 24 hours, the invasive cells, those on the underside of the Transwell membrane, were fixed, stained with crystal violet, imaged, and quantified. In contrast to the findings from the previous section (Section 5.2.12) in which ADAM10-expressing cells were used, the upregulation of Tspan15 surface expression in ADAM10-deficient cells did not increase invasion compared to ADAM10 KO lentiviral control cells (Figure 43). This suggests that Tspan15 requires ADAM10 surface expression in order to promote invasion.

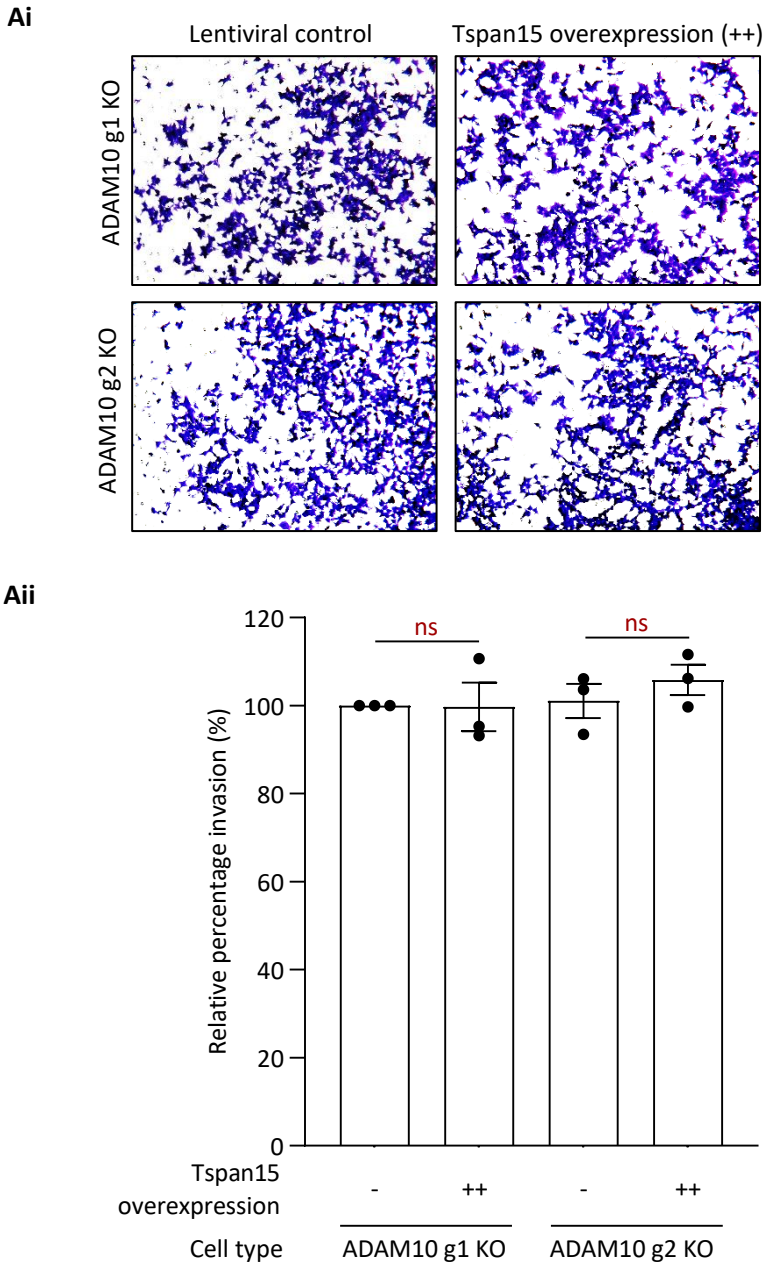


Figure 43: Overexpression of Tspan15 in the absence of ADAM10 surface expression does not alter the invasive capabilities of HEK-293T cells. (Ai) The invasive capabilities of HEK-293T ADAM10 (guide 1 (g1) and guide 2 (g2)) lentiviral control cells (-), as well as cells overexpressing Tspan15 50-fold (++) were assessed in a Transwell invasion assay. Cells were seeded on Matrigel-coated Transwells at a density of $2x10^5$ cells in 500 µl of FBS-free DMEM. Complete DMEM containing 10% FBS was added to the companion plate as a chemoattractant to stimulate invasion. Following incubation for 24 hours, invasive cells were fixed, stained with 0.05% crystal violet, and then imaged using a Nikon SMZ1000 microscope. Images are representative of 5 fields of view per experiment. (Aii) Percentage cell coverage of the Transwell membrane was quantitated and presented relative to ADAM10 guide 1 lentiviral control cells. Data were arcsine-transformed and analysed by a one-way ANOVA with a Tukey's multiple comparisons test. N=3; data represents mean percentage invasion ± SEM.

5.2.14 N-cadherin is a substrate of the Tspan15/ADAM10 'molecular scissor'

Data from the previous section suggests that the invasion of HEK-293T cells is mediated by the Tspan15/ADAM10 complex. As such, the secretome of previously validated HEK-293T ADAM10 and Tspan15 KO clones (Koo et al., 2020) was analysed to identify potential substrates that could promote invasion following cleavage. This experiment was performed by Stefan Lichtenthaler's group using a high-performance secretome protein enrichment with click sugars (hiSPECS) protocol, as outlined previously (Serdaroglu et al., 2017). Analysis of hits that were significantly reduced in both knockouts compared to WT cells revealed eight genes (Figure 44; Table A 1, Appendix), including three encoding transmembrane proteins, namely N-cadherin (CDH2), β-1,4-galactosyltransferase 5 (B4GALT5), and cache domain containing 1 (CACHD1) (Figure 44; Table A 1, Appendix). Of these proteins, N-cadherin is a known substrate of the Tspan15/ADAM10 complex (Prox et al., 2012; Jouannet et al., 2016; Noy et al., 2016; Seipold et al., 2018; Lipper et al., 2023) and has been shown to play a role in cancer cell invasion (Hazan et al., 2000; Tanaka et al., 2010; Choi et al., 2013; Gao et al., 2013; Zhang et al., 2013; Wang et al., 2016; Labernadie et al., 2017; Ciołczyk-Wierzbicka and Laidler, 2018; Hiroshima et al., 2019; Sépult et al., 2019). As such, it is tempting to consider that Tspan15/ADAM10-mediated cleavage of N-cadherin may be driving invasion in HEK-293T cells. By comparison, there is less evidence to support a role for the other two proteins. For example, ADAM10 has not previously been reported to shed the ectodomains of B4GALT5 and CACHD1. Furthermore, although B4GALT5 has been implicated in cancer (Shirane et al., 1999; Sato et al., 2000; Xu et al., 2001; Jiang et al., 2006; Zhou et al., 2013; Tang et al., 2020; Han et al., 2022) and demonstrated to exhibit pro-invasive functions in glioma (Jiang et al., 2006) and hepatocellular carcinoma (Han et al., 2022) cell lines, the role of the soluble N-terminal fragment has not been investigated. CACHD1 also has no known roles in tumorigenesis and is instead thought to regulate the nervous system (Cottrell et al., 2018; Rudan Njavro et al., 2020; Tian et al., 2021; Ablinger et al.,

2022; Powell et al., 2022). Consequently, the effect of the shed N-terminal N-cadherin fragment on HEK-293T cell invasion was selected for further investigation (Section 5.2.15).

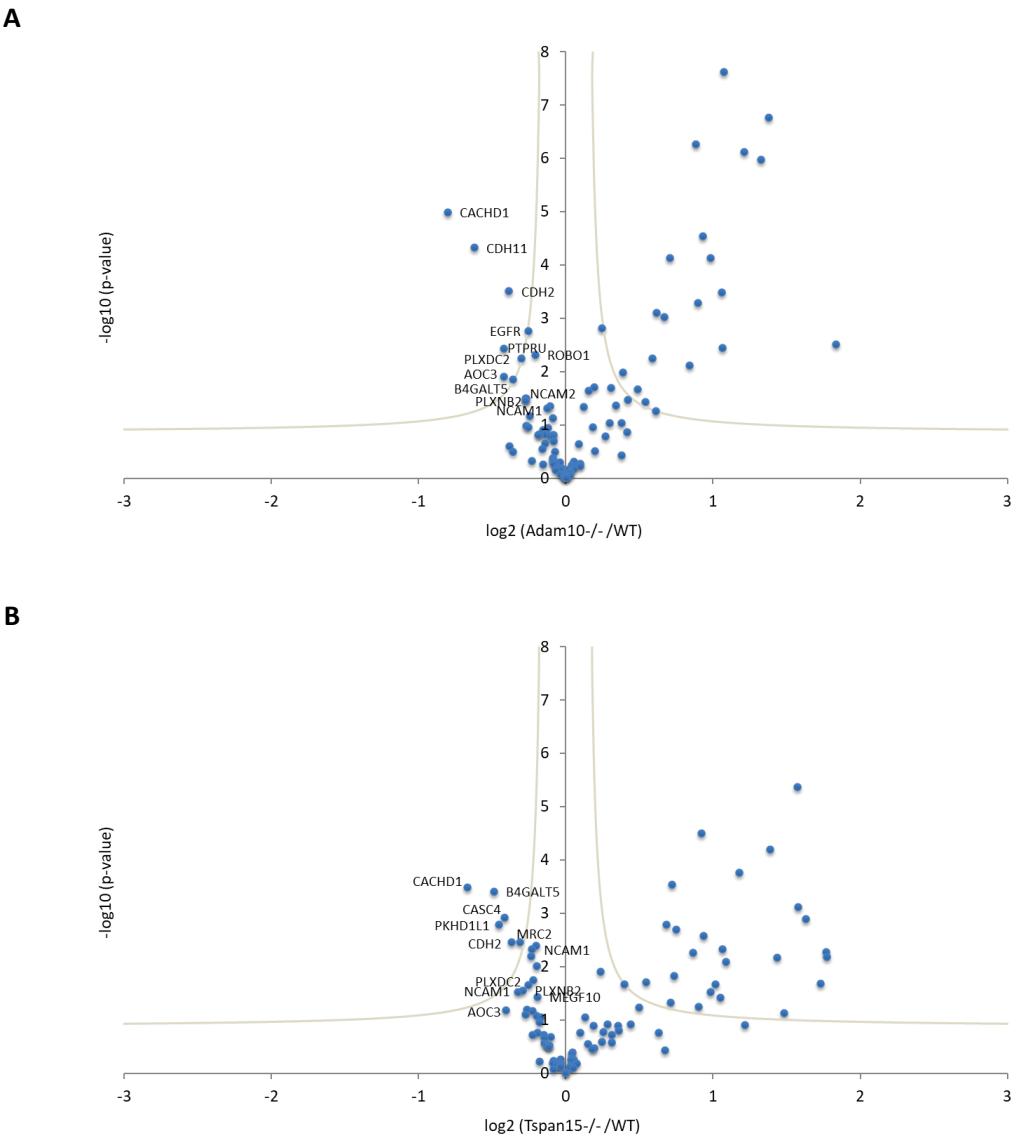


Figure 44: N-cadherin (CDH2) shedding is significantly reduced in both ADAM10 and Tspan15 KO HEK-293T cells. A high-performance secretome protein enrichment with click sugars (hiSPECS) protocol was used to analyse the secretome of HEK-293T cells; ADAM10 (Adam10-/-) and Tspan15 (Tspan15-/-) KO cells were compared to wild-type (WT). (A) Volcano plot showing the quantitative comparison of the shed transmembrane proteins identified between ADAM10 KO and WT cells. A false discovery rate estimation was applied and is indicated by the grey curve. N=3; significantly changed proteins: $p \leq 0.05$ ($-\log_{10} \geq 1.3$). (B) Experiment was as described in panel A but for Tspan15 KO cells compared to WT. (Experiments kindly performed by Stefan Lichtenthaler's group).

5.2.15 The N-terminal fragment of N-cadherin promotes the invasion of HEK-293T cells

As a precedent for N-cadherin cleavage driving invasion in HEK-293T cells, ADAM10 has been shown to promote mesothelioma cell migration and invasion, with N-cadherin cleavage underlying its pro-migratory capabilities (Sépult et al., 2019). Indeed, mesothelioma cells treated with conditioned media lacking the shed fragment of N-cadherin exhibited reduced migration, which was restored by the addition of the recombinant N-terminal N-cadherin fragment (Sépult et al., 2019). It is worth noting that the underlying mechanism for ADAM10's pro-invasive functions was not investigated (Sépult et al., 2019), and as such may also be dependent on N-cadherin cleavage. Therefore, this section investigated the potential of Tspan15/ADAM10-mediated shedding of N-cadherin to drive invasion in HEK-293T cells. A Transwell invasion assay was used to assess the invasive capabilities of control transfected and Tspan15-knockout cells treated with 0.5 μg/ml recombinant N-terminal N-cadherin. The cells were seeded in FBS-free DMEM on 8 μm pore Transwells coated with Matrigel. To stimulate invasion, DMEM containing 10% FBS as a chemoattractant was added to the bottom of the companion plate. Following incubation in 5% CO_2 at 37 ^{o}C for 24 hours, the invasive cells were fixed, stained with crystal violet and imaged. Quantification of the images revealed that the addition of the N-cadherin ectodomain increased invasion by ~43% in control cells and restored Tspan15 KO cell invasion to the level observed in untreated control cells (Figure 45). As such, this experiment provided strong evidence that the N-terminal N-cadherin fragment released following cleavage by Tspan15/ADAM10 plays a role in the invasion of HEK-293T cells.

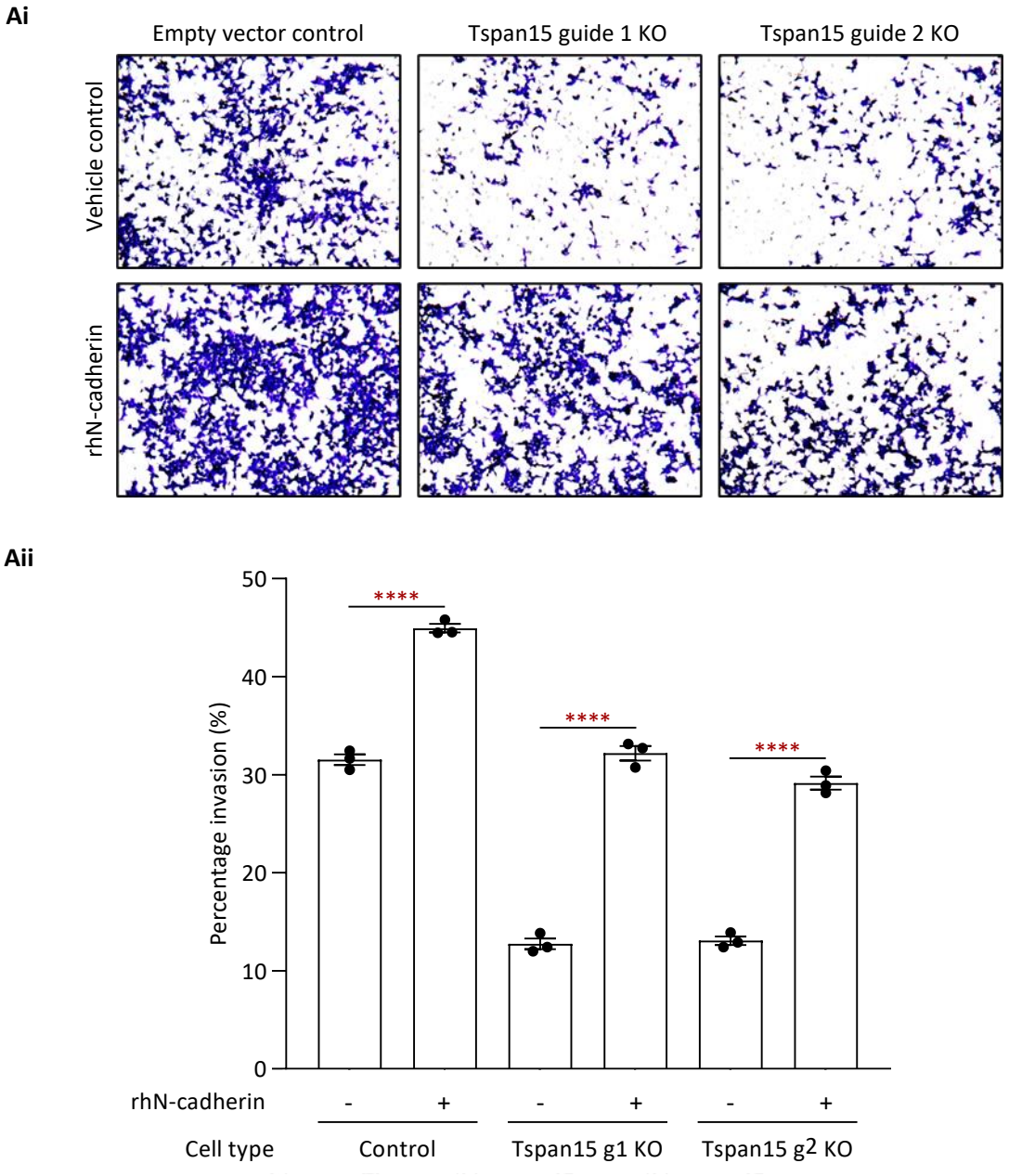


Figure 45: The N-cadherin ectodomain increases the invasive capabilities of HEK-293T control and Tspan15 KO cells. (Ai) HEK-293T empty vector control and Tspan15 (guide 1 (g1) and guide 2 (g2)) KO cells were resuspended at a density of $2x10^5$ cells in FBS-free DMEM, which was supplemented with 0.5 µg/ml recombinant human (rh)N-cadherin (+), or 2mM $CaCl_2$ as a vehicle control (-). Cells were then seeded on Transwells coated with 25 µg of Matrigel. Complete DMEM was added to the bottom of the companion plate with the 10% FBS functioning as a chemoattractant to stimulate invasion. After 24 hours, invasive cells were fixed, stained with 0.05% crystal violet, and imaged using a Nikon SMZ1000 microscope. Images are representative of 5 fields of view captured per experiment. (Aii) Percentage cell coverage of the Transwell membrane was quantitated, arcsine-transformed, and statistically analysed by a one-way ANOVA with a Tukey's multiple comparisons test. N=3; data represents mean percentage invasion ± SEM.

5.2.16 The N-cadherin ectodomain promotes invasion via FGF receptors

The soluble N-cadherin fragment has been proposed to promote mesothelioma cell migration via fibroblast growth factor receptor (FGFR) activation (Sépult et al., 2019). As such, this section aimed to determine whether the N-terminal N-cadherin fragment requires FGFR activity to promote HEK-293T cell invasion. The invasive capabilities of Tspan15 knockout cells treated with the N-terminal fragment of N-cadherin and the FGFR-specific inhibitor PD170374, which inhibits the autophosphorylation of the tyrosine kinase domain, were assessed in a Transwell invasion assay, as outlined in Section 5.2.11. In HEK-293T Tspan15 KO cells supplemented with soluble N-cadherin, the inhibition of FGFR activity impaired invasion by ~69% (Figure 46), suggesting that the pro-invasive effect of the N-cadherin ectodomain requires FGFR activity.

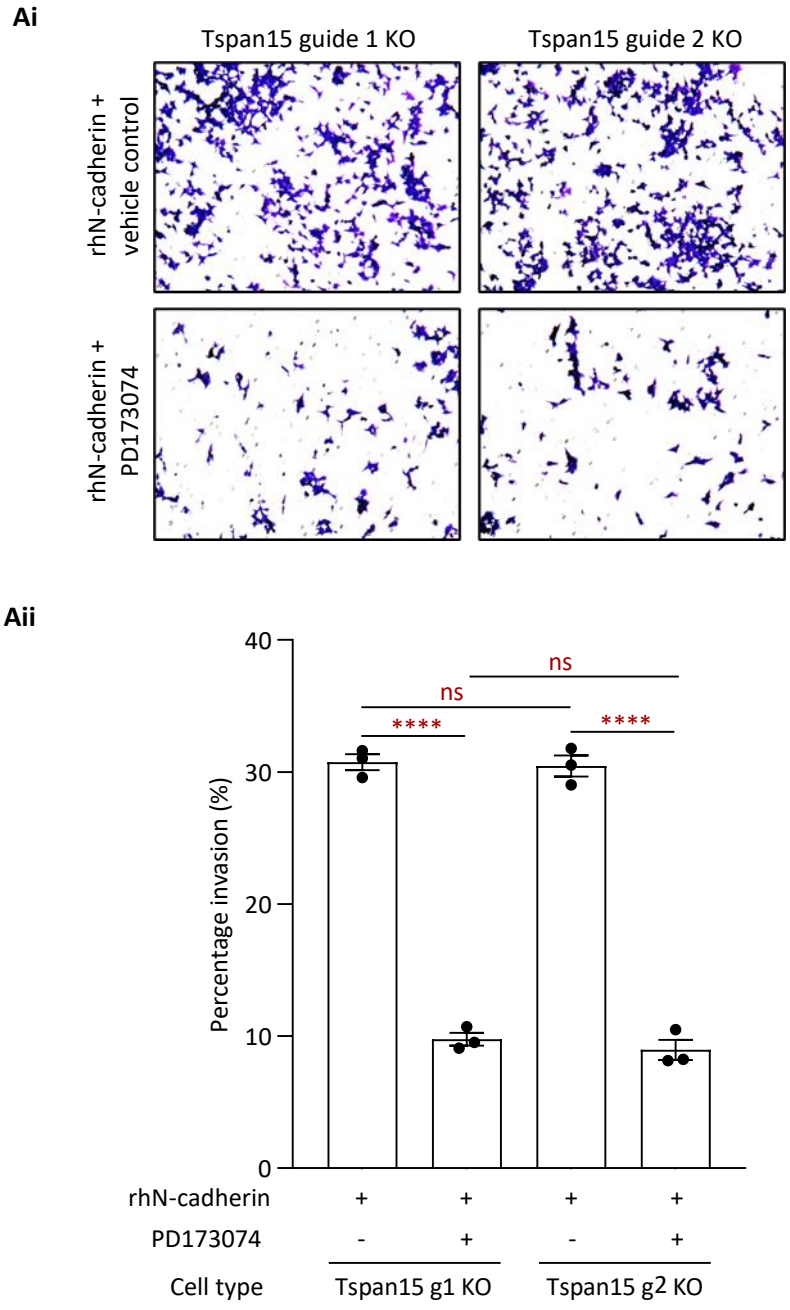


Figure 46: The pro-invasive effect of the N-cadherin ectodomain requires FGFR activity. (Ai) Tspan15 (guide 1 (g1) and guide 2 (g2)) KO HEK-293T cells were seeded on Matrigel-coated Transwells at a density of $2x10^5$ in 500 µl of FBS-free DMEM. Media was supplemented with 0.5 µg/ml rhN-cadherin, in addition to 25 nM of a FGFR inhibitor (PD173074) (+) or ethanol as a vehicle control (-). To stimulate invasion, complete DMEM, containing 10% FBS, was added to the companion plate as a chemoattractant. Following a 24-hour incubation period, invasive cells were fixed, stained with 0.05% crystal violet, and imaged using a Nikon SMZ1000 microscope. Images are representative of 5 fields of view from each experiment. (Aii) Ilastik and ImageJ were used to quantify percentage cell coverage of the Transwell membrane. Data were arcsine-transformed and analysed by a one-way ANOVA with a Tukey's multiple comparisons test. N=3; data represents mean percentage invasion ± SEM.

5.2.17 Inhibition of FGF receptors impairs proliferation but not cell viability

To assess whether the FGFR inhibitor PD173074 used in Section 5.2.16 affects proliferation or cell viability, Tspan15 KO cells were treated with 25 nM PD173074 or ethanol as a vehicle control, in addition to 0.5 μg/ml of the N-terminal N-cadherin fragment. After 24 hours, the cells were counted using trypan blue to distinguish between live and dead cells. Analysis of the counts revealed that inhibition of FGFRs in the presence of rhN-cadherin impaired proliferation by ~33% (Figure 47A) but did not affect cell viability (Figure 47B). This suggests that under the treatment conditions used in Section 5.2.16, PD173074 is not toxic to cells. Additionally, although a growth defect is associated with FGFR inhibition, the conclusions from the previous section do not need to be revised, as invasion and proliferation are mutually exclusive.

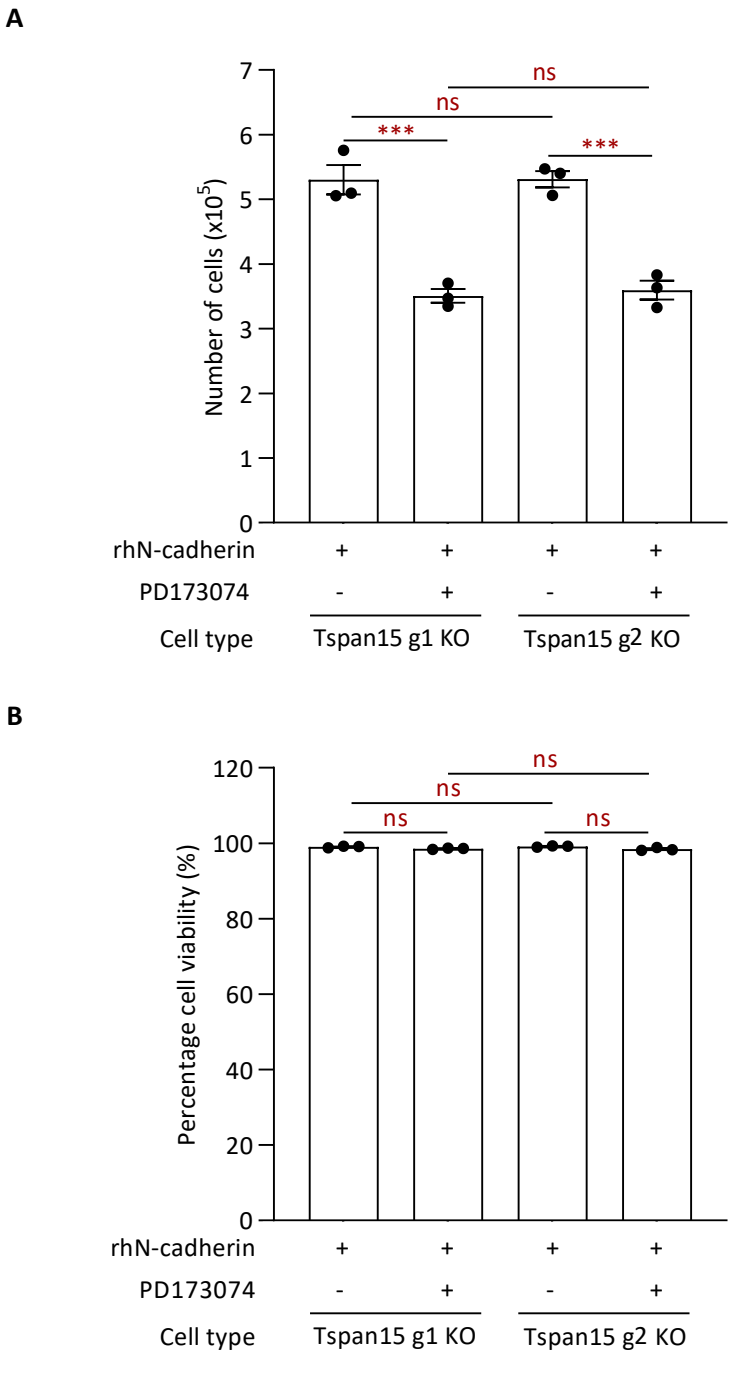


Figure 47: PD173074 reduces proliferation but not cell viability. HEK-293T cells deficient in Tspan15 were treated with 25 nM PD173074 (+) or ethanol as a vehicle control (-), as well as 0.5 µg/ml rhN-cadherin. After 24 hours, cells were trypsinised and counted. To differentiate between live and dead cells, trypan blue was added to the cell suspension. (A) Proliferation was estimated from the live cell counts. Data were statistically analysed by a one-way ANOVA with a Tukey's multiple comparisons test. N=3; data represents the mean number of cells ± SEM. (B) Percentage cell viability was calculated as the number of live cells relative to the total number of cells. Data were log-transformed and analysed by a one-way ANOVA with a Tukey's multiple comparisons test. N=3; data represents mean percentage cell viability ± SEM.

5.2.18 Recombinant N-cadherin ectodomain does not sustain FGF-induced MAPK/ERK activation in HEK-293T cells

Full-length N-cadherin has been proposed to promote invasion via the stabilisation of FGFRs and subsequent sustained activation of FGF-induced MAPK/ERK signalling (Suyama et al., 2002). Since this chapter has shown that the N-terminal N-cadherin fragment likely promotes the invasion of HEK-293T cells in an FGFR-dependent manner (Section 5.2.16), the potential for soluble N-cadherin to promote sustained FGF-mediated ERK phosphorylation was assessed in this section. HEK-293T wild-type cells were stimulated with 1.2 µg/ml human recombinant N-cadherin ectodomain in the presence and absence of 0.4 ng/ml human FGF for 0.25, 2, and 8 hours. Cells were subsequently lysed in 1% Triton X-100 lysis buffer and the amount of phosphorylated and total ERK was assessed by Western blotting. FGF was shown to induce the phosphorylation of ERK in HEK-293T cells with maximal activation observed after 0.25 hours (Figure 48B). However, co-treatment with soluble N-cadherin did not further increase the level of phosphorylated ERK at any time point (Figure 48B), suggesting that the N-terminal N-cadherin fragment is unable to stabilise FGFRs and sustain downstream MAPK/ERK signalling. Additionally, the N-cadherin ectodomain could not activate the MAPK/ERK pathway in the absence of FGF; stimulation with soluble N-cadherin alone was not associated with increased ERK phosphorylation (Figure 48B). Importantly, total levels of ERK were unaffected by the different stimulation conditions, indicating that stimulation with the N-terminal N-cadherin fragment and FGF did not alter ERK expression (Figure 48A).

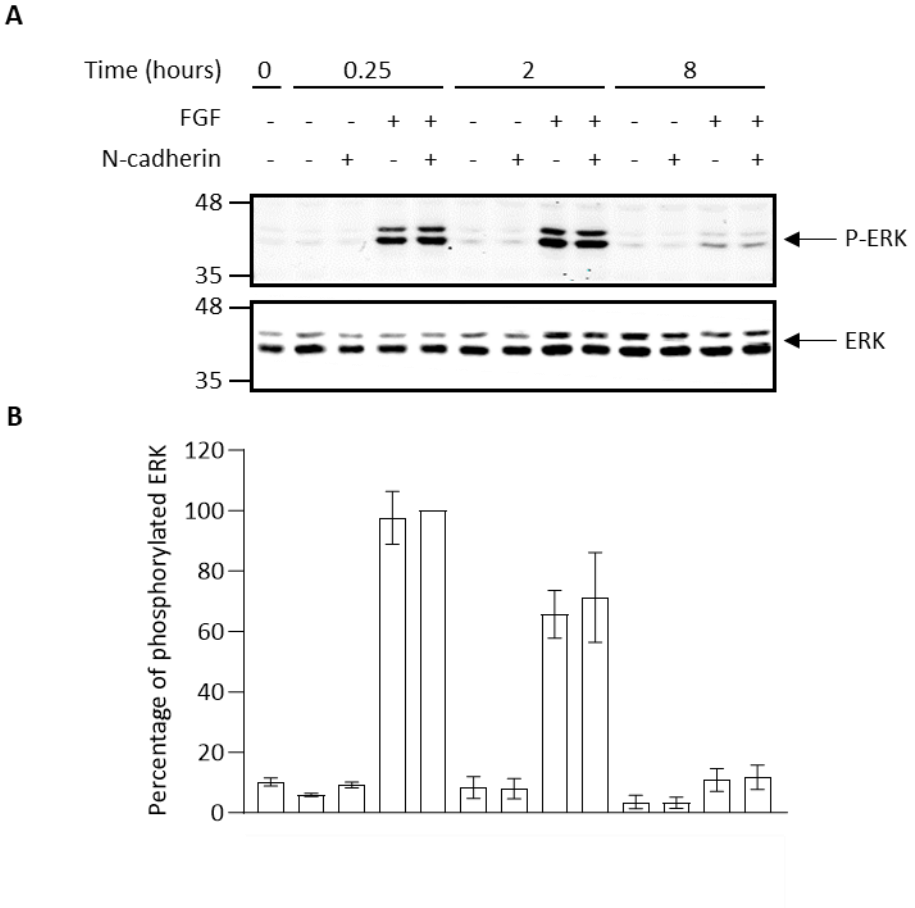


Figure 48: FGF-mediated activation of MAPK/ERK signalling is not sustained by recombinant N-terminal N-cadherin. (A) Wild-type HEK-293T cells were stimulated with 0.4 ng/ml human FGF, 1.2 µg/ml recombinant human N-cadherin ectodomain, or both together for 0.25, 2, and 8 hours. Vehicle controls included an equal volume of PBS for FGF and an equivalent volume of sterile, deionised water containing 2 mM $CaCl_2$ for N-cadherin. Cells were subsequently lysed in 1% Triton X-100 lysis buffer, which was supplemented with a 1:100 dilution of 100x protease inhibitor cocktail and a 1:20 dilution of PhosSTOP. Lysates were assessed by Western blotting using antibodies against phosphorylated ERK (P-ERK) and ERK. (B) The percentage of phosphorylated ERK was quantified and presented relative to cells treated with FGF and N-cadherin for 0.25 hours. N=2; data represents the mean percentage of phosphorylated ERK ± SEM.

5.2.19 The upregulation of Tspan15 expression increases MAPK/ERK signalling

Following on from the previous section, the phosphorylation of ERK was assessed in HEK-293T cells overexpressing Tspan15 50-fold (++), in which N-cadherin is likely shed constitutively. Cells were stimulated with 0.4 ng/ml human FGF for 0.25, 2, and 8 hours, prior to lysis in 1% Triton X-100 lysis buffer. Western blotting was then used to assess the amount of phosphorylated and total ERK in the resulting lysates. Strikingly, the percentage of phosphorylated ERK was increased at all three time

points in cells overexpressing Tspan15 compared to lentiviral control cells (Figure 49B), with the greatest difference observed after 2 hours. Total levels of ERK, however, were comparable irrespective of Tspan15 expression levels (Figure 49A).

Taken together with findings from the previous section, these data indicate that Tspan15 overexpression is associated with increased FGF-induced ERK activation, but do not prove that stabilisation of FGFRs by the N-cadherin ectodomain is responsible for this.

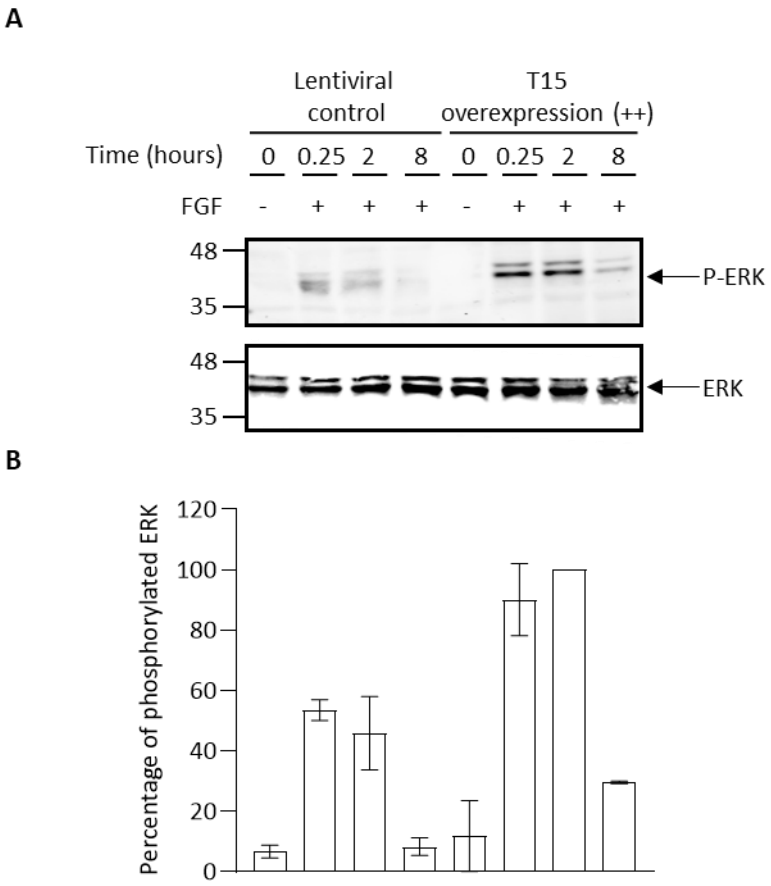


Figure 49: MAPK/ERK signalling is increased in HEK-293T cells overexpressing Tspan15. (A) HEK-293T lentiviral control cells and cells overexpressing Tspan15 50-fold (++) were stimulated with 0.4 ng/ml human FGF for 0.25, 2, or 8 hours. Cells were subsequently lysed in 1% Triton X-100 lysis buffer, which was supplemented with a 1:100 dilution of protease inhibitor cocktail and a 1:20 dilution of PhosSTOP. Lysates were Western blotted for phosphorylated ERK (P-ERK) and ERK. (B) The percentage of phosphorylated ERK was quantified and presented relative to Tspan15 overexpression cells treated with FGF for 2 hours. N=2; data represents the mean percentage of phosphorylated ERK ± SEM.

5.2.20 Treatment with Tspan15 antibodies does not impair the invasion of HEK-293T cells

A previous study in the Tomlinson lab resulted in the generation of the first anti-Tspan15 monoclonal antibodies (1C12, 4A4, 5D4, 5F4). Two of these, 1C12 and 4A4, have been shown to inhibit Tspan15/ADAM10 activity; 1C12 and 4A4 reduced the cleavage of transfected VE-cadherin (Koo et al., 2020) and betacellulin (Tomlinson lab, unpublished data) by ~50%, whereas 5D4 and 5F4 had no inhibitory effect (Koo et al., 2020; Tomlinson lab, unpublished data). As such, the potential for these antibodies to impair HEK-293T cell invasion was investigated. To do so, a Transwell invasion assay, as described in Section 5.2.11, was used to assess the invasive capabilities of HEK-293T cells treated with 10 µg/ml of an anti-Tspan15 (1C12, 4A4, 5D4, 5F4) or control IgG1 antibody. The cells were seeded in FBS-free DMEM on 8 µm pore Matrigel-coated Transwells. To stimulate invasion, complete DMEM containing 10% FBS was added to the bottom of the companion plate as a chemoattractant. Following incubation for 24 hours, the invasive cells were fixed, stained with crystal violet, and imaged with a light microscope. Quantification of the invasive cells indicated that none of the Tspan15 antibodies had an inhibitory effect on HEK-293T cell invasion (Figure 50); percentage cell coverage was around 34% for cells treated with an anti-Tspan15 or control IgG1 antibody, as well as untreated cells. This suggests that the subtle effects of the Tspan15 antibodies on substrate cleavage do not translate to an effect on cell invasion.

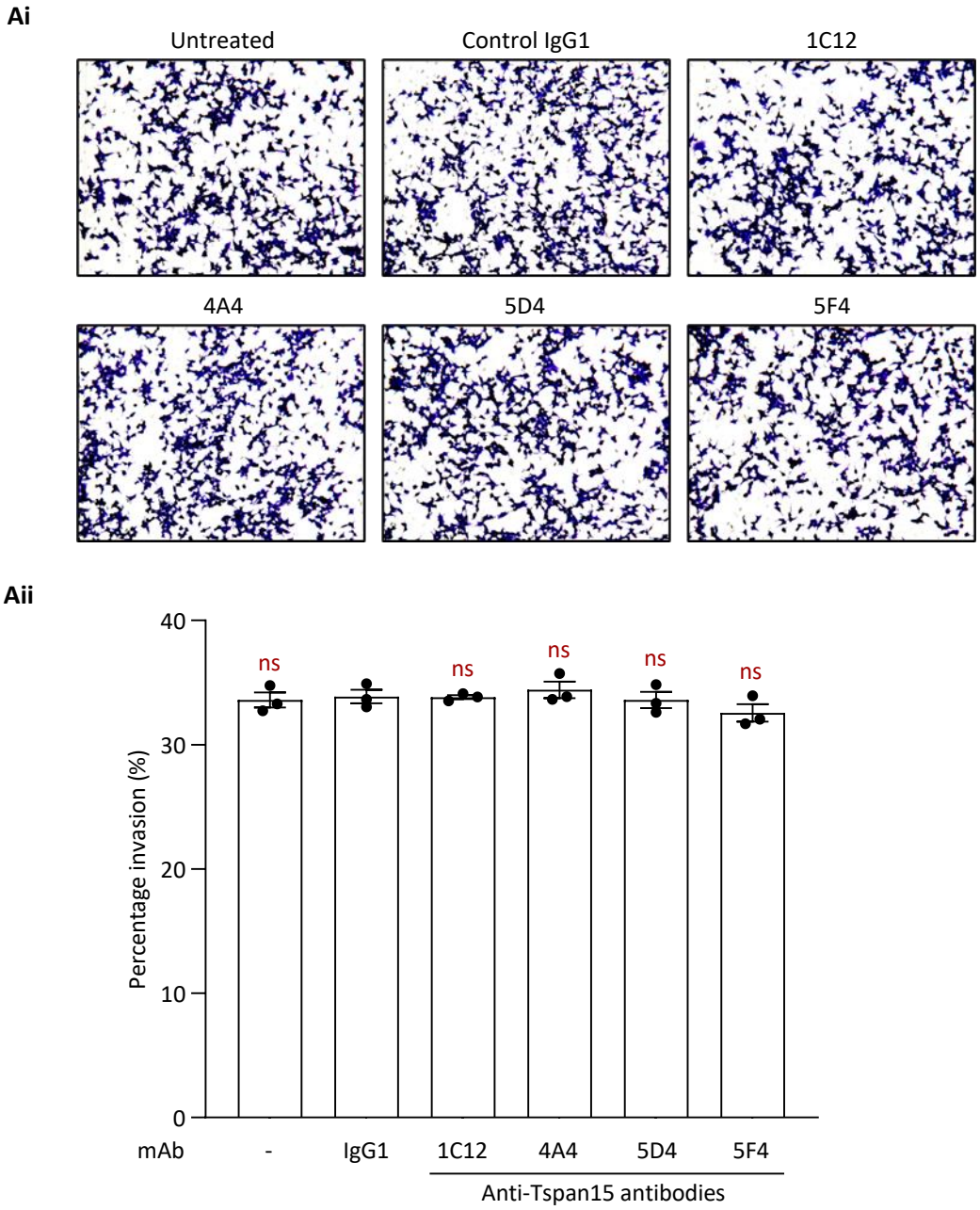


Figure 50: The invasive capabilities of HEK-293T cells are not impaired by treatment with Tspan15 mAbs. (Ai) HEK-293T WT cells were treated with 10 µg/ml of an anti-Tspan15 antibody (1C12, 4A4, 5D4, or 5F4) or control mouse IgG1. Together with untreated control (-) cells, they were then seeded on Transwells coated with 25 µg of Matrigel at a density of $2x10^5$ cells in 500 µl of FBS-free DMEM. To stimulate invasion, complete DMEM containing 10% FBS was added to the bottom of the companion plate. Cells were left to invade towards the chemoattractant for 24 hours, before being fixed, stained with 0.05% crystal violet, and imaged using a Nikon SMZ1000 microscope. Images are representative of 5 fields of view from each experiment. (Aii) Percentage cell coverage of the Transwell membrane, as a measure of invasion, was quantitated, arcsine-transformed, and statistically analysed by a one-way ANOVA with a Tukey's multiple comparisons test. Statistics shown are compared to control IgG1-treated cells with other comparisons not shown. N=3; data represents mean percentage invasion ± SEM.

5.3 Discussion

This chapter aimed to characterise Tspan15's role in mediating cell proliferation and invasion. Using HEK-293T cells as a model system, the findings suggest that Tspan15 can drive invasion in an ADAM10-dependent manner via N-cadherin cleavage and FGFR signalling.

The first major finding of this chapter was that Tspan15 promoted the invasion but not the proliferation of HEK-293T cells, which is consistent with previous observations in oesophageal and oral squamous cell carcinoma (Zhang et al., 2018; Hiroshima et al., 2019). However, Sidahmed-Adrar et al. showed that Tspan15 mediates the proliferation of hepatocellular carcinoma cells (Sidahmed-Adrar et al., 2019), suggesting that Tspan15 may regulate proliferation in a cell type-dependent manner.

This chapter also demonstrated that the depletion of ADAM10 expression impairs the invasive capabilities of HEK-293T cells, indicating that ADAM10, similar to Tspan15, exhibits pro-invasive activity. However, although Tspan15 and ADAM10 act as a functional scissor complex (Prox et al., 2012; Jouannet et al., 2016; Noy et al., 2016; Seipold et al., 2018; 2020; Lipper et al., 2023), this finding was insufficient to confirm an ADAM10-dependent mechanism of action for Tspan15, as Tspan15 surface expression was reduced by ~71% in the ADAM10 KO cells. As such, to enable the analysis of ADAM10 dependence, HEK-293T cells overexpressing Tspan15 in the absence of ADAM10 expression were generated. Interestingly, Tspan15 was unable to promote invasion in these cells, providing the first definitive evidence that the Tspan15/ADAM10 complex can mediate invasion (Figure 51). This observation highlighted the potential importance of ADAM10 sheddase activity, which is regulated by the TspanC8s, including Tspan15 (Prox et al., 2012; Jouannet et al., 2016; Noy et al., 2016; Seipold et al., 2018; Lipper et al., 2023). Subsequent analysis of HEK-293T secretome data generated by the Tomlinson and Lichtenthaler labs revealed three substrates, namely N-cadherin, B4GALT5, and CACHD1, that have the potential to promote invasion via their cleaved

ectodomains. Whilst N-cadherin is a well-characterised substrate of Tspan15/ADAM10 (Prox et al., 2012; Jouannet et al., 2016; Noy et al., 2016; Seipold et al., 2018; Lipper et al., 2023), B4GALT5 and CACHD1 have not previously been reported to be cleaved by ADAM10. As such, only N-cadherin shedding was investigated within this study with regard to its potential effects on invasion. Interestingly, the impaired invasion observed in Tspan15 KO cells was rescued by the addition of a recombinant N-terminal N-cadherin fragment. This soluble fragment has also been observed to promote migration in a mesothelioma cell line (Sépult et al., 2019), suggesting that the pro-metastatic role of shed N-cadherin is not specific to HEK-293T cells. Although the role of Tspan15 in mesothelioma cell migration and invasion was not investigated, it is likely involved as the regulatory TspanC8 for ADAM10-mediated cleavage of N-cadherin. Indeed, Tspan15 is the only TspanC8 that has been shown to direct the ectodomain shedding of N-cadherin by ADAM10 (Prox et al., 2012; Jouannet et al., 2016; Noy et al., 2016; Seipold et al., 2018; Lipper et al., 2023). Hiroshima et al. also proposed Tspan15/ADAM10-mediated N-cadherin shedding as the underlying mechanism for Tspan15's role in oral squamous cell carcinoma invasion. However, whilst the depletion of Tspan15 and ADAM10 was shown to decrease the secretion of soluble N-cadherin, the effect on invasion was not assessed (Hiroshima et al., 2019). Even so, there is strong evidence to suggest that Tspan15/ADAM10 plays a key role in promoting invasion via N-cadherin shedding.

The next section of this chapter aimed to characterise the downstream effects of N-cadherin shedding that may contribute to the invasive capabilities of cells. Remarkably, the pro-invasive activity of soluble N-cadherin was abolished by inhibition of FGFR signalling, suggesting that cleaved N-cadherin requires FGFR activity to promote invasion (Figure 51), which has also been shown for malignant pleural mesothelioma migration (Sépult et al., 2019). However, it is important to note that the effect of FGFR inhibition alone was not tested, and as such it is possible that FGFR signalling promotes invasion independently of N-cadherin shedding with a greater effect. Additional experiments are, therefore, required to confirm that the pro-invasive function of N-cadherin

shedding is actually dependent on downstream FGFR activity. Regardless, since the soluble N-terminal N-cadherin fragment can interact with FGFRs (Lyon et al., 2016), similar to full-length N-cadherin (Suyama et al., 2002), it is tempting to speculate that cleaved N-cadherin may have the same functional capabilities, and thus be able to sustain MAPK/ERK signalling induced by FGF. However, although Tspan15 overexpression was shown to be associated with an increase in FGF-mediated ERK phosphorylation, a similar effect was not observed following the addition of the soluble N-cadherin fragment to wild-type cells. The exact reasoning for this disparity is unknown, but the addition of soluble N-cadherin at a single time-point may be insufficient to sustain signalling. By comparison, the upregulation of Tspan15 expression likely increases constitutive N-cadherin shedding, which could be required to effectively stabilise FGFRs and maintain downstream signalling. Alternatively, Tspan15 overexpression may be associated with an increase in FGFR expression that augments MAPK/ERK signalling.

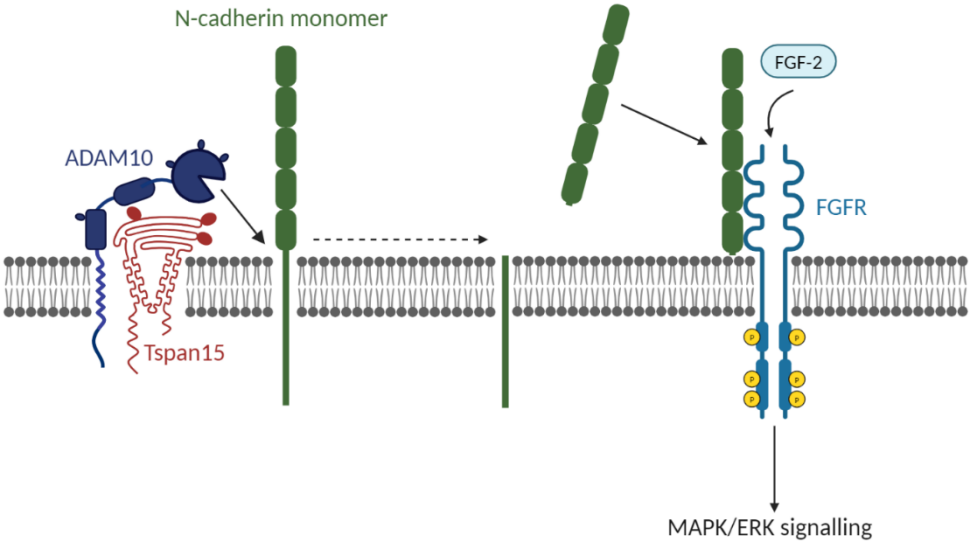


Figure 51: Tspan15 promotes the invasion of HEK-293T cells in an ADAM10-dependent manner. In this model, Tspan15/ADAM10-mediated shedding of N-cadherin promotes HEK-293T cell invasion, likely via FGFR signalling (figure created with Biorender.com).

Although not addressed by this study, a pro-invasive effect of Wnt/β-catenin signalling downstream of N-cadherin shedding is also possible. As a precedence, ADAM10-mediated cleavage of N-cadherin has been proposed to promote Wnt signalling via the redistribution of β-catenin. Indeed, in ADAM10-deficient cells, β-catenin predominantly localises with N-cadherin at the cell surface, impairing its ability to promote Wnt signalling (Reiss et al., 2005). Furthermore, Tspan15 knockdown was shown to inhibit the nuclear localisation of β-catenin in oral squamous cell carcinoma cell lines. Although Tspan15 overexpression was proposed to drive metastasis, at least in part, through the β-catenin pathway, a direct link was not demonstrated (Hiroshima et al., 2019). Nevertheless, it is possible that cleavage of N-cadherin by Tspan15/ADAM10 promotes invasion via multiple mechanisms, including augmentation of FGFR signalling and activation of the Wnt/β-catenin pathway.

Although this chapter identifies Tspan15 as a potential anti-invasion therapeutic target, the four Tspan15 antibodies generated by the Tomlinson lab (Koo et al., 2020) did not inhibit HEK-293T cell invasion, despite binding being confirmed by flow cytometry (Koo et al., 2020). This suggests that they are unable to modulate the required Tspan15/ADAM10-mediated activity. However, two of the four antibodies, 1C12 and 4A4, have been shown to diminish the cleavage of transfected VE-cadherin (Koo et al., 2020) and betacellulin (Tomlinson lab, unpublished data) by ~50%. As a functional effect has only been observed for overexpressed substrates (Koo et al., 2020; Tomlinson lab, unpublished data), it is possible that these Tspan15 antibodies do not affect the cleavage of endogenous substrates. Alternatively, a 50% reduction in shedding may not translate to a functional effect on cell invasion. Further experiments are now required to examine whether Tspan15/ADAM10-mediated shedding of endogenous N-cadherin can be inhibited, for example with an increased concentration of the existing Tspan15 antibodies or with novel Tspan15 antibodies that would disrupt the Tspan15/ADAM10 complex. Such targeting of Tspan15 could be a promising anti-cancer treatment that blocks tumour cell invasion.

Lastly, this chapter showed that 50-fold overexpression of Tspan15 caused a striking clumping phenotype and altered directionality irrespective of ADAM10 expression, suggesting that Tspan15 may also act independently of ADAM10 in HEK-293T cells. However, as similar phenotypes were not observed when Tspan15 was upregulated 27-fold, it is possible that these findings are an artefact of extremely high Tspan15 expression. Alternatively, this Tspan15 activity may be expression level dependent. It is tempting to speculate that 50-fold Tspan15 overexpression may promote cell-cell interactions via the formation of adhesion-containing nanodomains, ultimately resulting in cell clumping. Whilst this hypothesis was not explored further, the potential ADAM10-independent involvement of Tspan15 within the NF-κB pathway was investigated. A previous study has reported that Tspan15 interacts with β-TrCP to promote the downstream activation of NF-kB signalling (Zhang et al., 2018), but as the involvement of ADAM10 was not investigated, it is possible that Tspan15 may be acting independently of ADAM10. However, an NF-κB luciferase assay provided no evidence to suggest that Tspan15 induces NF-κB activation in HEK-293T cells. Consequently, the observed changes in HEK-293T cell morphology and directionality are unlikely caused by Tspan15's proposed role in NF-κB signalling.

In summary, this chapter demonstrated that the Tspan15/ADAM10 complex can promote invasion and provided insight into a possible underlying mechanism. Moreover, preliminary evidence was obtained to suggest that Tspan15 may function independently of ADAM10.

CHAPTER 6 INVESTIGATING THE ROLE OF TSPAN15 AND ADAM10 IN ACTIVATING NF-ΚB IN AN OESOPHAGEAL CARCINOMA CELL LINE

6.1 Introduction

Tspan15 has been reported to promote NF-κB signalling in oesophageal cancer cell lines via an interaction with βTrCP. This is an E3 ubiquitin ligase, which is involved in the signalling pathway through the recognition and degradation of phosphorylated IκBα, an inhibitor of NF-κB (Zhang et al., 2018). However, other studies have failed to validate this Tspan15 function. For example, β-TrCP has not been identified as a binding partner of Tspan15 in proteomic studies (Sidahmed-Adrar et al., 2019; Koo et al., 2020). Additionally, no evidence has been found using an NF-κB luciferase reporter assay that Tspan15 can promote NF-κB signalling in HEK-293T cells, including those transiently transfected with Tspan15 and β-TrCP (Tomlinson lab, unpublished data), as well as the Tspan15 KO and overexpressing cells generated within this project, as shown in Chapter 5 (Section 5.2.8). Therefore, this chapter aimed to investigate Tspan15's proposed regulatory role within the NF-κB signalling pathway in an oesophageal carcinoma cell line. It is also important to note that Zhang et al. did not investigate whether ADAM10 is required for Tspan15's interaction with β-TrCP or the subsequent activation of NF-κB signalling. As such, a secondary aim of this chapter was to characterise ADAM10's involvement or lack thereof.

6.2 Results

6.2.1 KYSE-30 cells express Tspan15 and ADAM10

Given that Tspan15 has been reported to be upregulated in ten oesophageal carcinoma (OSCC) cell lines compared to a non-cancerous oesophagus cell line (Zhang et al., 2018), it was important to first confirm that KYSE-30 cells, the chosen OSCC cell line from the previous study, expressed Tspan15 at the cell surface. Further to this, the expression of ADAM10, which was not explored previously (Zhang et al., 2018), should also be considered due to its potential contribution to Tspan15's role in these cells. As such, the surface expression of both proteins was assessed by flow cytometry and data

analysis confirmed that the KYSE-30 cells expressed Tspan15 and ADAM10 at the cell surface (Figure 52).

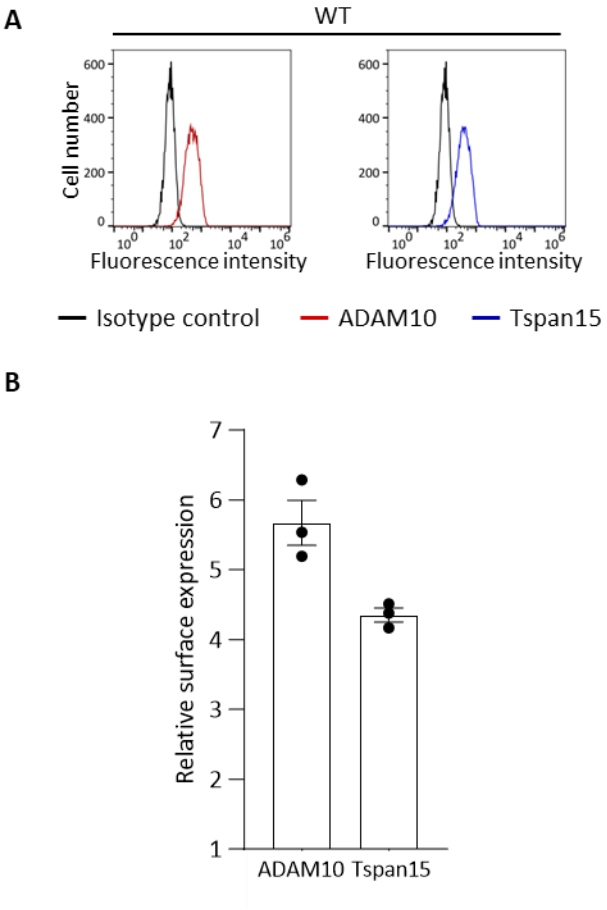


Figure 52: Tspan15 and ADAM10 are expressed on the surface of KYSE-30 cells. (A) The expression of Tspan15 and ADAM10 on the surface of KYSE-30 WT cells was confirmed by flow cytometry; cells were stained for Tspan15 (blue) or ADAM10 (red) and an isotype control (black). (B) Tspan15 and ADAM10 surface expression was quantified and presented as geometric mean fluorescence intensity relative to isotype control staining. N=3; data represents mean relative surface expression ± SEM.

6.2.2 Tspan15 does not appear to interact with β-TrCP in KYSE-30 cells

Tspan15 has previously been shown to interact with β-TrCP in KYSE-30 cells (Zhang et al., 2018). However, the experiment was not without limitations. For example, the interaction was demonstrated by co-immunoprecipitation using antibodies to Tspan15 and β-TrCP, but the specificity of the Tspan15 antibody was not validated in the authors' Tspan15-knockdown cells. It has also since

been discontinued by the manufacturer. Furthermore, the negative control immunoprecipitation was with a non-binding IgG antibody; potentially better controls would have been the authors' Tspan15 and β-TrCP-knockdown cells. Given these limitations, it was important to repeat the experiment and confirm the proposed interaction using one of our Tspan15 antibodies, which has been Tspan15-knockout cell validated (Koo et al., 2020).

Lysates from KYSE-30 WT cells were generated using the relatively low stringency 1% Brij97 lysis buffer. A whole cell lysate sample was diluted with 6x sample buffer, whilst the remaining sample was subjected to immunoprecipitation. It was rotated for 2 hours at 4 ^{o}C with G Sepharose beads coated with an antibody against Tspan15, β-TrCP, ADAM10, or IgG. The beads were subsequently washed four times in 1% Brij97 and then resuspended in 50 µl of 2x sample buffer. Western blotting was used to measure the level of Tspan15, β-TrCP, and ADAM10, as well as assess their interactions with each other. Due to antibody IgG bands obscuring protein-specific bands, β-TrCP blotting was performed under reducing conditions, whereas ADAM10 and Tspan15 were detected under non-reducing conditions. Analysis of the blots revealed that both ADAM10 and Tspan15 were detected in the whole cell lysate controls (Figure 53A; Figure 53Bi-ii), but contradictory to the previous study (Zhang et al., 2018), β-TrCP was not (Figure 53A). As such, to prove the functionality of the β-TrCP antibody, HEK-293T cells were transiently transfected with β-TrCP using PEI. These cells were then lysed and blotted under the same conditions as the KYSE-30 cells. Given that β-TrCP was detected in the transfected HEK-293T cells (Figure 53A), expression in KYSE-30 cells is likely below the level of detection for Western blotting. Moreover, in contrast to the previous study (Zhang et al., 2018), analysis of the immunoprecipitations revealed no evidence of an interaction between Tspan15 and β-TrCP (Figure 53A; Figure 53Bi). β-TrCP was also not detected in its own immunoprecipitates (Figure 53A), further suggesting that KYSE-30 cells may not express β-TrCP at detectable levels. As such, qPCR is required to assess whether KYSE-30 cells are likely producing any protein.

However, the immunoprecipitations did show that Tspan15 interacted with ADAM10 in KYSE-30 cells. Additionally, it was shown for the first time that the ADAM10 immunoprecipitation was more efficient in capturing Tspan15 than the Tspan15 immunoprecipitation itself (Figure 53A; Figure 53Bi-ii). This finding may be explained by the structure of the ADAM10-Tspan15 complex in which the ADAM10 ectodomain is located over the top of Tspan15. Although 1C12, an anti-Tspan15 antibody that binds to a similar epitope as the antibody used for this immunoprecipitation, was able to bind Tspan15 when in complex with ADAM10, antibody access may still be partially restricted (Lipper et al., 2023).

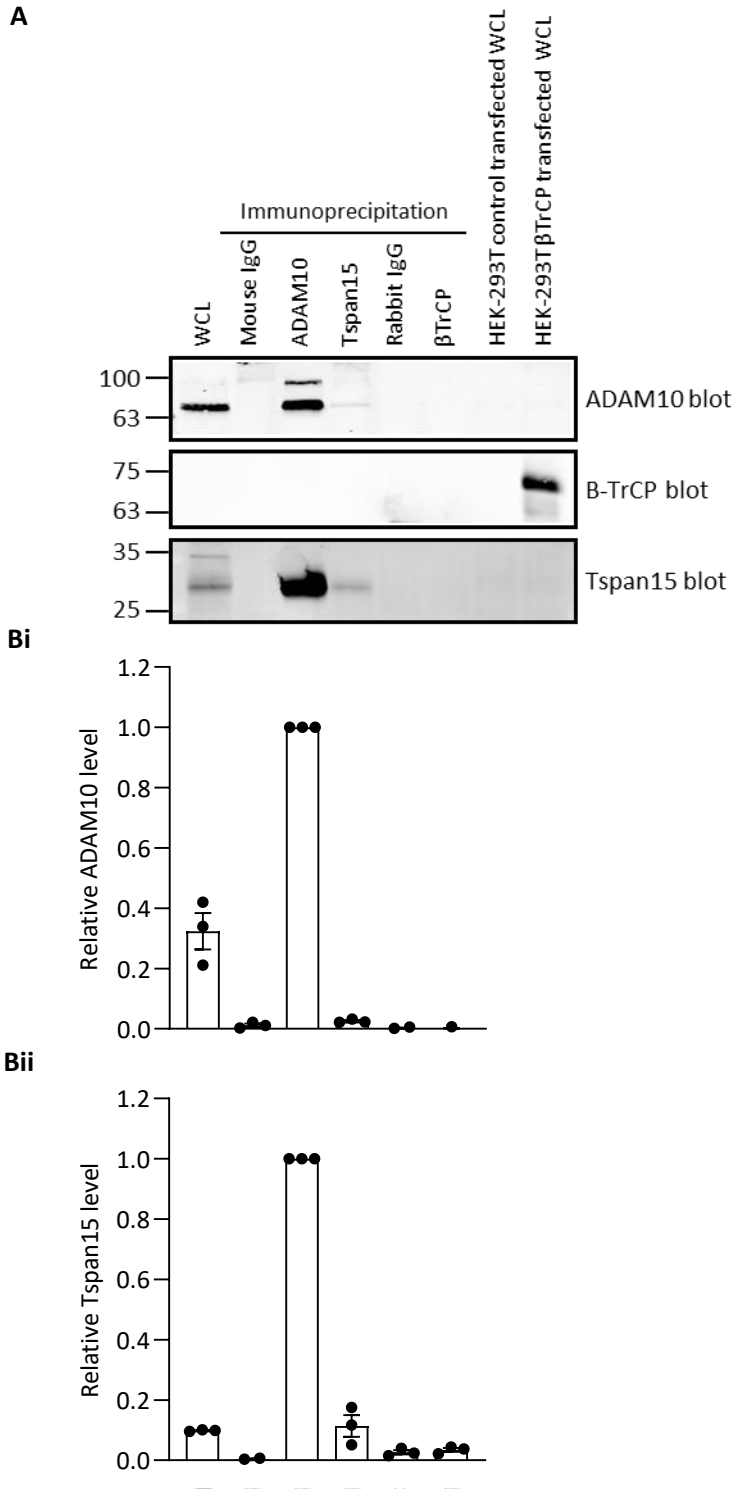


Figure 53: ADAM10 but not βTrCP co-immunoprecipitates with Tspan15 in KYSE-30 cells. (A) KYSE-30 WT cells were lysed in 1% Brij97 lysis buffer supplemented with a protease inhibitor cocktail and 5 µM of the ADAM10 inhibitor G1254023X. A sample of the whole cell lysate (WCL) was diluted with 6x sample buffer, whilst the remaining supernatant was subject to immunoprecipitation with antibodies against ADAM10, Tspan15, and βTrCP, as well as negative control mouse and rabbit IgG antibodies. Immunoprecipitated proteins were subsequently Western blotted for ADAM10, βTrCP, and Tspan15.

Blotting was performed under non-reducing conditions, apart from for β-TrCP, which required reducing conditions. Transfected HEK-293T cells were included in the Western blot as a control for the β-TrCP antibody; cells were lysed in the same lysis buffer and blotted under the same conditions. (B) For KYSE-30 samples, the amount of (i) ADAM10 and (ii) Tspan15 was quantitated and presented relative to the ADAM10 co-immunoprecipitation. N=3; data represents the mean protein level ± SEM.

6.2.3 Tspan15 does not promote the nuclear translocation of NF-κB

The study by Zhang et al. showed that the localisation of the NF-κB p65 correlated with Tspan15 expression; in control transfected cells p65 was predominantly nuclear, whereas the knockdown of Tspan15 resulted in a cytoplasmic localisation (Zhang et al., 2018). To confirm these findings, dual-colour confocal microscopy, using a nuclear dye and an antibody against the p65 subunit of NF-κB, was used to quantify the amount of NF-κB located in the nucleus. However, in contrast to the previous findings, our study revealed that p65 was primarily cytoplasmic in KYSE-30 WT cells; the median colocalisation between p65 and the nucleus was 4.4% (Figure 54).

.

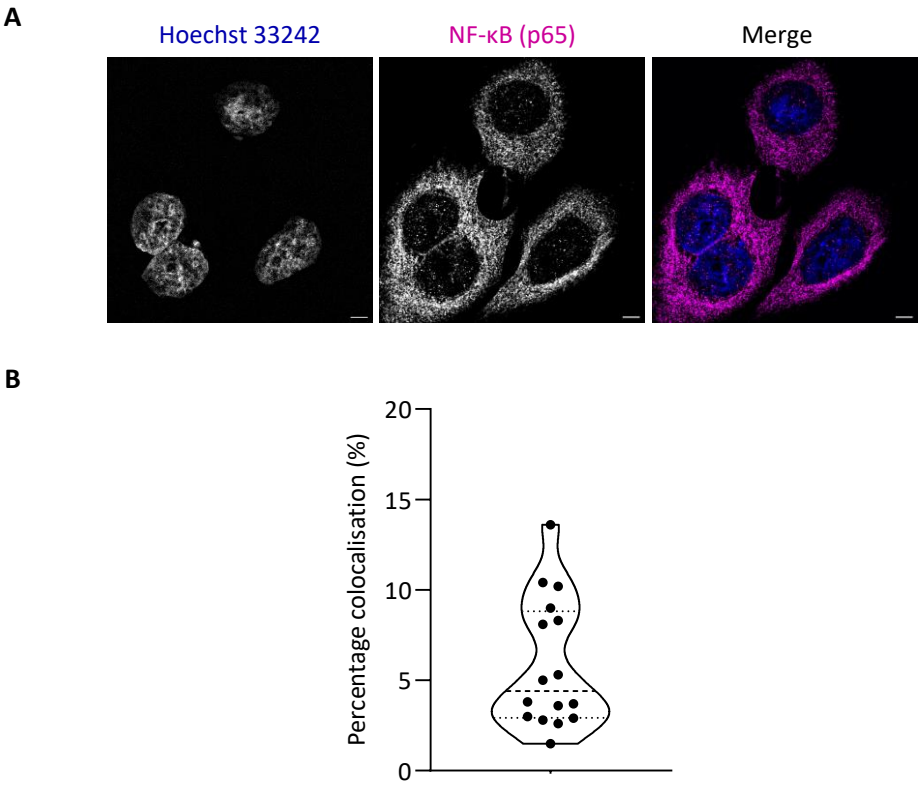


Figure 54: NF-κB is predominantly localised within the cytoplasm of KYSE-30 cells. (A) KYSE-30 WT cells were fixed, permeabilised, and stained for DNA (blue) with Hoechst 33242, as well as the p65 subunit of NF-κB (magenta). An Airyscan confocal microscope in super-resolution mode was then used to image the middle plane of the cells. No signal was detected in the magenta channel of cells stained with a control rabbit IgG antibody (images not shown). Images are representative of 5 fields of view per experiment and the scale bar represents 11 µm. (B) The degree of NF-κB located within the nucleus was presented as the percentage of overlapping pixels within the magenta (p65) channel. N=3.

6.2.4 The generation and validation of Tspan15 and ADAM10 KO oesophageal carcinoma cell lines

Impaired invasion was observed in Tspan15-knockdown KYSE-30 cells by Zhang et al., but the effect of ADAM10 was not considered (Zhang et al., 2018). To further characterise the role of Tspan15 and explore the involvement of ADAM10 in oesophageal carcinoma cell invasion, CRISPR/Cas9 genome editing was used to generate Tspan15 and ADAM10 knockout KYSE-30 cell lines. The cells were transfected with Tspan15 and ADAM10 guide oligos cloned into the pSpCas9(BB)-2A-Puro vector (plasmid map available in Figure A 1, Appendix) (Koo et al., 2020). Puromycin was used to select transfected cells, which then had their Tspan15 and ADAM10 surface expression validated by flow

cytometry (Figure 55). Three of the KO pools (ADAM10 guide 1, Tspan15 guide 1, and Tspan15 guide 2) were heterogeneous populations, with cells deficient for and still expressing the protein of interest. Consequently, purification was required before use in functional assays. The ADAM10 guide 2 KO pool, however, was completely deficient for ADAM10 at the cell surface (Figure 55) and as such did not require purification.

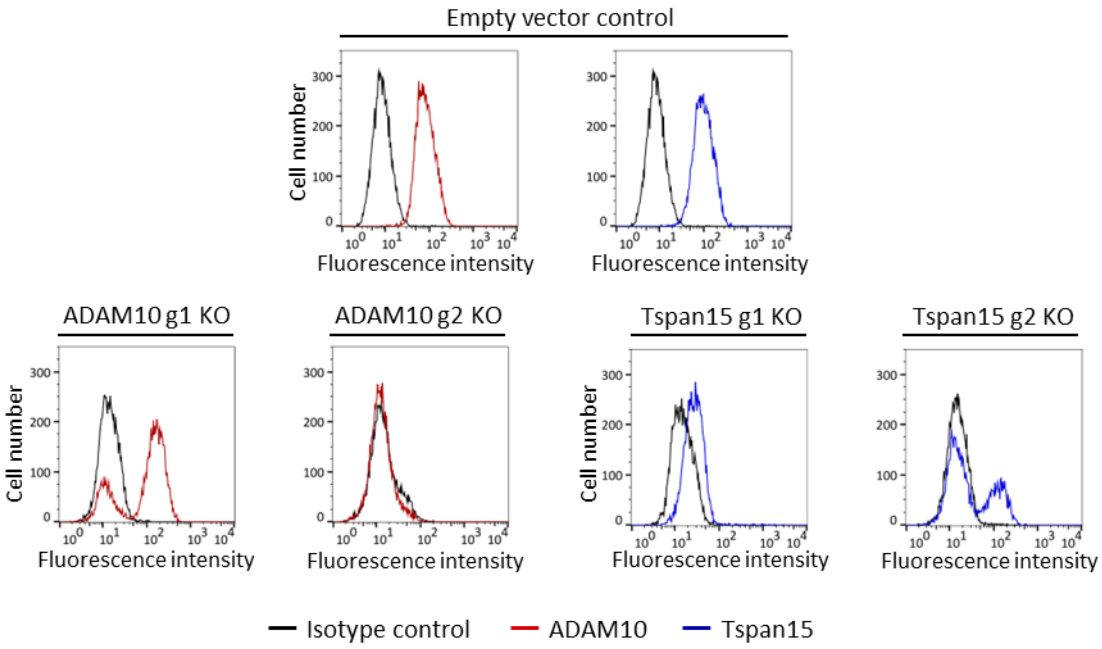


Figure 55: Generation and validation of KYSE-30 Tspan15 and ADAM10 KO pools. Tspan15 and ADAM10 KO pools were generated using CRISPR/Cas9 gene editing technology. KYSE-30 cells were transfected with Tspan15 and ADAM10 guide oligos (guide 1 (g1) and guide 2 (g2)) cloned into the pSpCas9(BB)-2A-Puro vector, as well as an empty vector control. The surface expression of Tspan15 and ADAM10 was subsequently validated by flow cytometry. N=1.

6.2.5 Purification using magnetic Dynabeads is insufficient to generate pure KYSE-30 Tspan15 and ADAM10 KO pools

Prior to use in functional assays, the KYSE-30 Tspan15 and ADAM10 KO pools generated in Section 6.2.4 required purification, except for the ADAM10 guide 2 KO pool, which was a homogenous population of ADAM10 negative cells (Figure 55). As per the newly developed protocol outlined in Section 4.2.2, antibody-coated magnetic Dynabeads were used for the required negative cell sorting. However, flow cytometry analysis of ADAM10 and Tspan15 surface expression showed that the

sorting was insufficient to generate pure KYSE-30 KO pools (Figure 56). The purity of the ADAM10 guide 1 KO pool was increased, but it remained a heterogeneous population with some cells still expressing ADAM10 at the cell surface. In contrast, the Tspan15 KO pools appeared to have an increased population of Tspan15 positive cells post-sorting, suggesting the possibility of positive cell outgrowth.

This experiment also confirmed the purity of the ADAM10 guide 2 KO pool (Figure 56), which was shown to be completely ADAM10 deficient following treatment with puromycin (Figure 55).

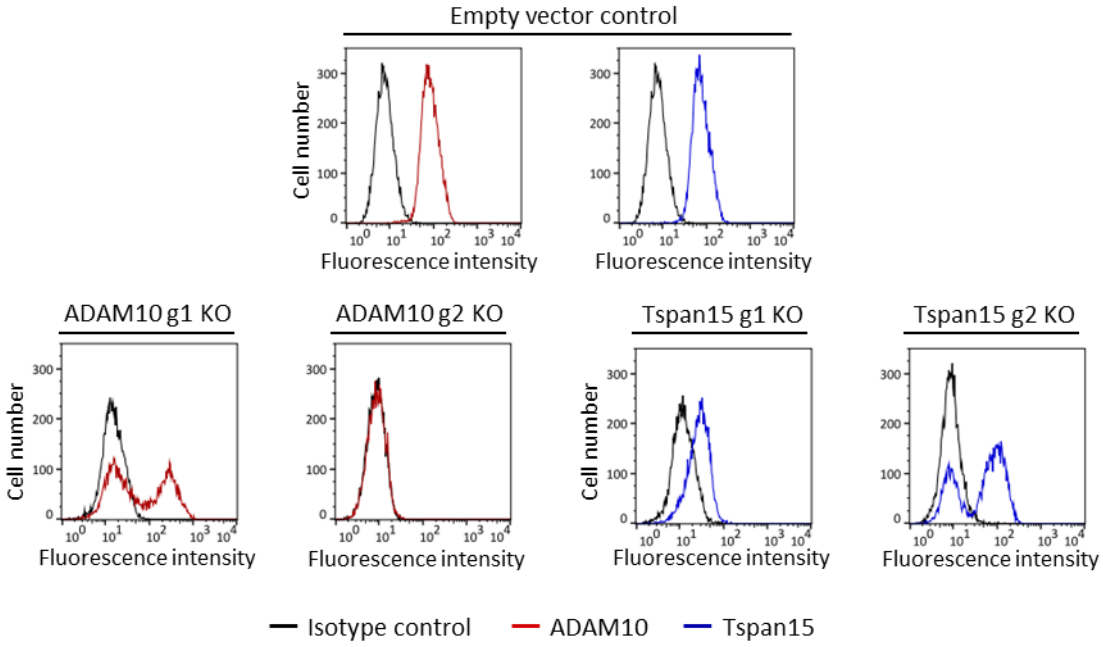


Figure 56: Validation of KYSE-30 Tspan15 and ADAM10 KO pools following purification with magnetic Dynabeads. Heterogenous Tspan15 (guide 1 (g1) and guide 2 (g2)) and ADAM10 (guide 1 (g1)) KO pools underwent negative cell sorting with antibody-coated, magnetic Dynabeads. The resulting purity of the pools was validated by flow cytometry; cells were stained with antibodies against Tspan15 (blue) or ADAM10 (red) and an isotype control (black). The ADAM10 guide 2 (g2) KO pool was included in the flow cytometry analysis but was not purified by negative cell sorting. N=1.

6.2.6 Purification using fluorescence-activated cell sorting was sufficient to purify KYSE-30 Tspan15 and ADAM10 KO pools

Fluorescence-activated cell sorting (FACS) was then employed as an alternative method to purify the three impure KYSE-30 KO pools. In brief, a two-way sort of cells stained with an antibody against

Tspan15 or ADAM10 was performed on the FACSAria Fusion flow cytometer. The negative population was collected and the resulting expression of Tspan15 and ADAM10 was assessed by flow cytometry. Analysis of the data confirmed successful purification of the knockout pools by FACS; a single population of cells deficient for Tspan15 or ADAM10 was visualised for each pool (Figure 57). Unfortunately, this was achieved at the end of the project, but future experiments should aim to determine whether there is an invasion defect in the absence of Tspan15 or ADAM10 in KYSE-30 cells.

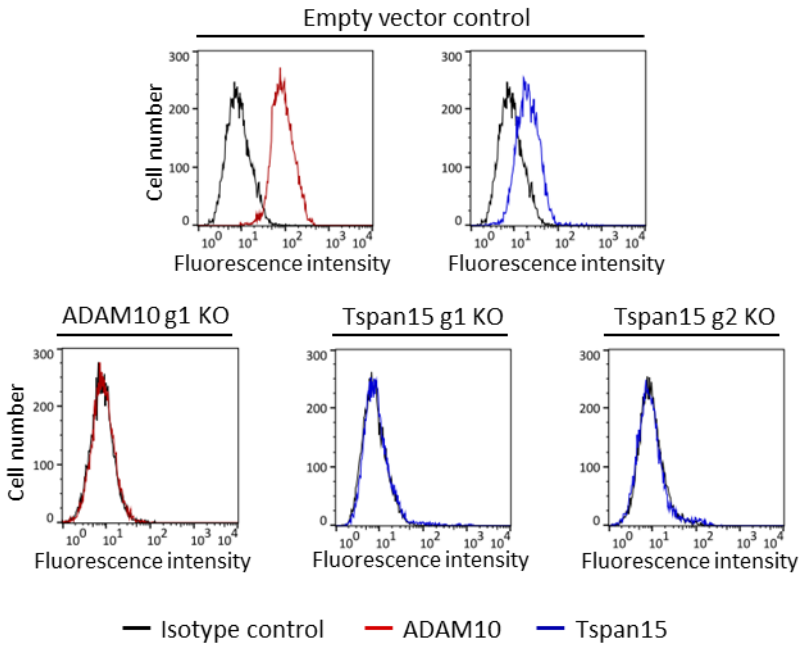


Figure 57: Validation of KYSE-30 Tspan15 and ADAM10 KO pools following purification by FACS. The Tspan15 (guide 1 (g1) and guide 2 (g2)) and ADAM10 (guide 1 (g1)) KO pools, which were insufficiently purified following negative cell sorting with magnetic Dynabeads, were sorted by FACS. Flow cytometry was then used to validate the resulting purity by assessing the expression of ADAM10 and Tspan15 at the cell surface. N=1.

6.3 Discussion

Whilst Tspan15 has been reported to activate NF-κB signalling in oesophageal carcinoma cell lines (Zhang et al., 2018), a potential role for ADAM10 has not yet been explored. Therefore, this chapter aimed to reproduce two key findings from the Zhang et al. study using the same cell line, before

extending this to explore ADAM10's involvement or lack thereof. This work, however, contradicted the aforementioned study and provided no evidence that Tspan15 could interact with β-TrCP or promote the nuclear translocation of NF-κB.

The first major finding of this chapter revealed no interaction between Tspan15 and β-TrCP, which is inconsistent with previous findings (Zhang et al., 2018). Further to this, although both studies used the same cell line and anti-β-TrCP antibody, this work, unlike that by Zhang et al., showed that β-TrCP was not expressed at detectable levels in KYSE-30 cells. Although the reason for these inconsistencies is unclear, there are several potential underlying causes. Firstly, differences in KYSE-30 growth conditions, possibly caused by disparities in FBS formulation, could affect β-TrCP expression, and thus explain the differences in detection by Western blotting. Secondly, the anti-Tspan15 antibody used by Zhang et al. may have been binding non-specifically; it was not validated in their Tspan15-knockdown cells (Zhang et al., 2018) and has since been discontinued by the manufacturer. By comparison, this study utilised a knockout cell validated Tspan15 antibody generated by the Tomlinson group (Koo et al., 2020). Lastly, different lysis buffers were used, which may have affected the lysate proteomes. For example, in the previous study cells were lysed in RIPA buffer (Zhang et al., 2018), a highly stringent detergent that solubilises nuclear proteins and may disrupt antibody binding or protein-protein interactions due to the inclusion of SDS. In contrast, the much weaker Brij97 lysis buffer was used in this study to maximise the chance of detecting a potentially weak interaction. As such, it is possible that the observed interactions from the Zhang et al. study could be due to their antibodies co-immunoprecipitating nuclear proteins. Future studies should overexpress β-TrCP and Tspan15 or identify cell lines with robust expression of these proteins to enable definitive characterisation of their potential interaction.

This chapter also presented no evidence to support the hypothesis that Tspan15 promotes the nuclear translocation of NF-κB, further contradicting the Zhang et al. study. Whilst this thesis found NF-κB predominantly localised within the cytoplasm of KYSE-30 cells, Zhang et al. reported a strong

nuclear localisation. It is worth noting that Zhang et al. failed to quantify their data with only representative cell images being shown. Nevertheless, their images were highly convincing and included two additional oesophageal carcinoma cell lines. Although these cell lines exhibited weaker NF-κB nuclear staining, Tspan15 overexpression promoted strong nuclear translocation (Zhang et al., 2018). This disparity in KYSE-30 cells, similar to the interaction between Tspan15 and β-TrCP, may arise due to differences in growth conditions caused by unique FBS formulations. For example, it is possible that the FBS used in the previous study, unlike this thesis, contained a key growth factor that can drive NF-κB to the nucleus. Alternatively, the inconsistent results may be caused by distinct imaging planes; cells should be imaged at the middle plane to detect differences in subcellular localisation. Whilst this protocol was followed for the current study, a specific imaging plane was not referenced by Zhang et al. However, a limitation of the current study was the lack of positive control for NF-κB nuclear localisation. To address this, the experiment should be repeated using stimuli that promote NF-κB nuclear translocation, such as TNFα, or with KYSE-30 cells overexpressing Tspan15.

Furthermore, despite Zhang et al. showing that overexpression of Tspan15 did not affect oesophageal carcinoma cell proliferation, the findings from this chapter suggest that Tspan15 may promote the growth of KYSE-30 cells. Indeed, it was difficult to generate a pure population of Tspan15 CRISPR/Cas9 knockout cells, presumably due to Tspan15 positive cells exhibiting a faster growth rate. Interestingly, ADAM10 has previously been reported to positively regulate the proliferation of an oesophageal carcinoma cell line, and E-cadherin shedding was proposed as the underlying mechanism (Ma et al., 2016). As Tspan15 is the regulatory TspanC8 for ADAM10-mediated cleavage of E-cadherin, this further supports a potential role for Tspan15 in oesophageal carcinoma proliferation. To investigate how changes in Tspan15 expression directly affect proliferation, the pure knockout cells, generated at the end of this thesis, could be tested in a proliferation assay.

It is, however, important to address the limitations of this chapter, especially with regard to scope. Although the reproducibility of two key findings from the previous. study was assessed, Zhang et al. further investigated the involvement of Tspan15 within the NF-κB signalling pathway. For example, they also explored whether Tspan15 expression affected the degradation of phosphorylated-IκBα (p-IκBα); it was shown that Tspan15 enhances β-TrCP-mediated ubiquitination of p-IκBα to promote degradation (Zhang et al., 2018). Additionally, qRT-PCR and Western blotting were used to investigate the effect of Tspan15 on the expression of several NF-κB target genes, which are known to promote metastasis (Zhang et al., 2018). As such, future studies should aim to reproduce these findings to better understand Tspan15's role, or lack thereof, in promoting NF-κB signalling.

To summarise, this chapter failed to reproduce two key findings from a previous study (Zhang et al., 2018); no evidence was found that Tspan15 could interact with β-TrCP or promote the nuclear translocation of NF-κB in KYSE-30 cells. As such, the role of Tspan15 and the potential involvement of ADAM10 in the activation of NF-κB signalling remains unclear.

CHAPTER 7 GENERAL DISCUSSION

7.1 Overview

The primary aim of this project was to further characterise Tspan15's role in cell proliferation and invasion, with a particular focus on the underlying mechanism and whether this is likely ADAM10-dependent and/or -independent. Chapter 3 highlighted the clinical importance of the project, revealing that Tspan15 and ADAM10 are upregulated, either individually or together, in a number of different cancers, with an associated prognostic effect in some cases. Pancreatic cancer was of particular note, as both proteins were upregulated, and 'high' tumour expression was unfavourable for patient survival. However, the data from Chapter 4 provided no evidence that Tspan15 or ADAM10 could mediate the *in vitro* proliferation or invasion of human pancreatic cancer cell lines. Nevertheless, Chapter 5 showed that Tspan15 promoted the invasion of HEK-293T cells in an ADAM10-dependent manner via N-cadherin shedding and FGFR signalling. However, aside from the invasion phenotype, preliminary evidence also suggested that Tspan15 may exhibit ADAM10-independent activity. Finally, Tspan15's involvement within the NF-κB signalling pathway was explored in Chapter 6, but the findings failed to validate the previously proposed mechanism (Zhang et al., 2018).

This study is the first to conclusively show that Tspan15 can promote invasion in an ADAM10-dependent manner and presents one of the possible mechanisms of action. The following sections will discuss these findings and the suggested follow-up investigations in more detail.

7.2 Tspan15 promotes invasion in an ADAM10-dependent manner and the underlying mechanism likely involves the interplay between different signalling pathways

Tspan15 and ADAM10 have previously been implicated in cancer cell invasion (Gaida et al., 2010; Guo et al., 2012; Fu et al., 2014; Ma et al., 2016; Zhang et al., 2018; Hiroshima et al., 2019; Sépult et al., 2019; Sidahmed-Adrar et al., 2019; Yuan et al., 2020b; Mueller et al., 2021). However, this study provides the first evidence that Tspan15 can promote invasion in an ADAM10-dependent manner

(Section 5.2.13); Tspan15 was unable to promote invasion in the absence of ADAM10 expression in HEK-293T cells. Furthermore, it was demonstrated that the Tspan15/ADAM10 complex can promote invasion via N-cadherin shedding and FGFR signalling. Indeed, soluble N-cadherin was shown to restore invasion in Tspan15 KO cells (Section 5.2.15), but this effect was counteracted by FGFR inhibition (Section 5.2.16). Shed N-cadherin has also been determined to similarly promote the migration of a malignant pleural mesothelioma cell line, with activation of FGFRs proposed as the underlying mechanism (Sépult et al., 2019). However, it is important to note that the role of Tspan15 was not investigated by Sépult et al., as ADAM10 was considered in isolation from its regulatory TspanC8.

Taking these findings together with evidence from other studies (Suyama et al., 2002; Lyon et al., 2016), it was hypothesised that cleaved N-cadherin could sustain FGF-induced MAPK/ERK activation, similar to full-length N-cadherin. However, although the upregulation of Tspan15 expression was associated with increased FGF-induced ERK activation (Section 5.2.19), the recombinant N-terminal N-cadherin fragment was unable to sustain MAPK/ERK signalling (Section 5.2.18). The underlying cause of these seemingly contradictory results is yet to be determined but could be due to differences in the duration of FGFR stabilisation. It is interesting to consider that constitutive N-cadherin shedding, which is likely increased by Tspan15 upregulation, is required to induce persistent ERK phosphorylation and downstream signalling. As such, the addition of a soluble N-cadherin ectodomain fragment at a single time point may only facilitate a short-term increase in ERK phosphorylation. Suyama et al. showed that increased N-cadherin expression resulted in sustained FGF-induced MAPK/ERK phosphorylation, further suggesting that endogenous shedding over time may be important for a functional effect. Alternatively, Tspan15 overexpression may be associated with an increase in FGFR expression, driving downstream MAPK/ERK activation.

Moving forward, the proposed Tspan15/ADAM10/N-cadherin/FGFR axis should be investigated in cancer cell lines, with the individual proteins being knocked out by CRISPR/Cas9 and overexpressed

by lentiviral transduction. Additionally, a cleavage-site N-cadherin mutant (Uemura et al., 2006) would enable specific inhibition of N-cadherin shedding to assess the direct effects on FGFR signalling and invasion. These cells should also be grown in 3D spheroid models, such that invasion can be assessed in a more representative tumour model. Mechanistically, advanced fluorescence microscopy could be used to determine the co-localisation of Tspan15, ADAM10, N-cadherin, and FGFR on the surface of invading cells, as well as visualise the release of the N-cadherin ectodomain and subsequent binding to FGFRs.

Whilst this study focused on MAPK/ERK signalling downstream of FGFRs, another important downstream pathway is the PI3/Akt signalling cascade, which has also been implicated in cancer cell invasion (Weber et al., 2011a; Jia et al., 2018; Starska et al., 2018; Liu et al., 2019; Mueller et al., 2021; Rascio et al., 2021). As such, future studies should investigate the involvement of PI3K/Akt signalling in promoting invasion downstream of N-cadherin shedding. It is also important to consider the possible involvement of the Wnt/β-catenin pathway, especially as ADAM10-mediated shedding of N-cadherin has been proposed to disrupt the N-cadherin/β-catenin adhesion complex, enabling β-catenin to activate Wnt signalling (Reiss et al., 2005). Moreover, in oral squamous cell carcinoma cell lines, Tspan15 knockdown was associated with a decrease in the expression of ADAM10 and N-cadherin, as well as a reduction in the release of soluble N-cadherin and diminished β-catenin nuclear localisation (Hiroshima et al., 2019). Although Tspan15 was proposed to promote metastasis via this pathway, no direct link was shown. Regardless, it is tempting to speculate that Tspan15/ADAM10-mediated shedding of N-cadherin may also promote invasion via activation of the Wnt/β-catenin signalling pathway (Figure 58).

Analysis of hiSPECs mass spectrometry data from the Tomlinson and Lichtenthaler labs (Section 5.2.14) also revealed two other potential Tspan15/ADAM10 substrates in HEK-293T cells, namely β-1,4-galactosyltransferase 5 (B4GALT5) and cache domain containing 1 (CACHD1), which could also have pro-invasive capabilities following cleavage. However, as these proteins have not previously

been reported as ADAM10 substrates, cell-based shedding assays should first confirm their ectodomain shedding by the Tspan15/ADAM10 complex. B4GALT5 is of particular interest as it has been implicated in cancer (Shirane et al., 1999; Sato et al., 2000; Xu et al., 2001; Jiang et al., 2006; Zhou et al., 2013; Tang et al., 2020; Han et al., 2022) and shown to promote invasion in glioma (Jiang et al., 2006) and hepatocellular carcinoma (Han et al., 2022) cell lines. It is worth noting though that neither study determined the underlying mechanism for this role nor considered B4GALT5 cleavage. As such, Tspan15/ADAM10-mediated shedding of B4GALT5 and its implications on invasion would be an interesting avenue for future research. By comparison, there is no evidence to suggest that CACHD1 exhibits pro-tumourigenic capabilities, with its reported functions related to the regulation of the nervous system (Cottrell et al., 2018; Rudan Njavro et al., 2020; Tian et al., 2021; Ablinger et al., 2022; Powell et al., 2022). However, CACHD1 has been implicated in Wnt signalling within the brain to regulate neurogenesis and neural identity (Powell et al., 2022), and as such has the potential to promote invasion via modulation of Wnt signalling in other contexts.

In summary, Tspan15 is expected to promote cancer cell invasion in an ADAM10-dependent manner, but the underlying mechanism likely involves the interplay between different signalling pathways, especially given the complex nature of tumourigenesis.

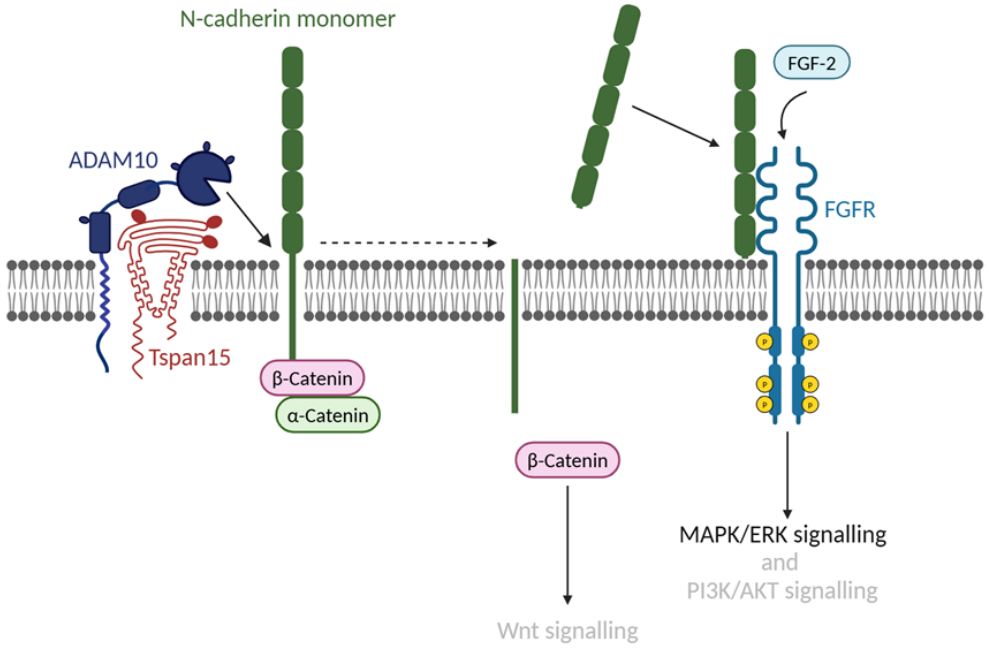


Figure 58: Proposed model of the mechanisms by which the Tspan15/ADAM10 complex can promote invasion. Tspan15/ADAM can promote invasion via N-cadherin shedding and likely the subsequent interplay between downstream signalling pathways. This thesis provides evidence for a Tspan15/ADAM10/N-cadherin/FGFR axis, which likely drives invasion via downstream MAPK/ERK signalling. The literature also suggests that β-catenin/Wnt and PI3K/Akt signalling may positively regulate invasion downstream of N-cadherin cleavage (figure created with Biorender.com).

7.3 Tspan15 and ADAM10 are implicated in cancer and their role may extend beyond promoting invasion

Chapter 3 revealed that Tspan15 and ADAM10 are upregulated in various cancers compared to corresponding control tissues, and high tumour expression may be linked to unfavourable patient survival. There is strong evidence to support a pro-invasive role for Tspan15 and ADAM10 in cancer, as discussed in the previous section. However, the findings from Chapter 4 suggest that this does not extend to pancreatic adenocarcinoma, and thus Tspan15/ADAM10 likely exhibits other pro-tumourigenic roles. Nevertheless, it is important to note that in contrast to the data from this thesis, a previous study proposes a role for ADAM10 in pancreatic cancer invasion; the silencing of ADAM10 was shown to impair the invasive capabilities of AsPC-1 and COLO-357 cells in a Matrigel invasion assay (Gaida et al., 2010). Despite both studies including AsPC-1 cells, there were a number of key

differences between the experiments that could be the cause of the inconsistent results. Firstly, whilst ADAM10 KO pancreatic cancer cell lines were utilised within this study, Gaida et al. transiently downregulated ADAM10 expression using siRNA. It is possible that stable knockout of ADAM10, unlike siRNA-induced knockdown, is associated with compensatory mutations. Alternatively, the siRNAs used may have had off-target effects that impaired invasion. A second difference was the duration of the invasion assays; in the previous study, cells were left to invade for 48 hours (Gaida et al., 2010), compared to 24 hours in this study. It is also worth mentioning that Gaida et al. failed to indicate the concentration of Matrigel used, and as such this could be a vital difference. Future studies should use more physiologically relevant models to explore the role of Tspan15 and ADAM10 in pancreatic cancer invasion. For example, spheroids embedded in matrigel could be used to examine invasion in 3D. However, pancreatic cancer mouse models will ultimately be required to prove an *in vivo* role; mice could be injected with luciferase-expressing pancreatic cancer cells depleted of ADAM10 or Tspan15. Biphotonic imaging would then allow the assessment of tumour progression, whilst immunohistochemistry could be used to quantify the degree of tumour invasion.

It is also important to consider alternative roles for Tspan15 and ADAM10 in pancreatic cancer. Since Tspan15 and ADAM10 are included in EVs secreted from pancreatic cancer cells (Servage et al., 2020), they have the potential to promote metastasis via modulation of the tumour microenvironment. It is tempting to speculate that the substrate repertoire of the Tspan15/ADAM10 scissor may be altered on EVs. For example, even though Tspan15 is unable to promote ADAM10-mediated shedding of Notch in cis (Dornier et al., 2012), it may facilitate trans cleavage on EVs, resulting in downstream signalling. Interestingly, Notch signalling has been implicated in pancreatic cancer (Plentz et al., 2009; Mazur et al., 2010; Abel et al., 2014). Moving forward, the effects of EVs containing Tspan15 and ADAM10 released from pancreatic cancer cells should be determined. To do so, EVs will need to be isolated from cell cultures by ultrafiltration and subsequent size exclusion

chromatography (Guerreiro et al., 2018). These could then be added to cell lines to investigate their effect on Notch activation.

Tspan15 also has the potential to mediate resistance to radiotherapy in pancreatic adenocarcinoma tumours. As a precedent, ADAM10 expression is upregulated in pancreatic cancer tumours following radiation therapy, leading to ephrinB2 cleavage, which promotes fibrosis, metastasis, and tumour survival (Mueller et al., 2021). However, the regulatory TspanC8 for ephrinB2 cleavage has yet to be investigated. Therefore, Tspan15 could play a role in this mechanism of acquired resistance. Confirming this hypothesis would require the analysis of Tspan15/ADAM10 substrates in pancreatic cancer cells by hiSPECS mass spectrometry, as outlined previously (Serdaroglu et al., 2017), and subsequent cell-based shedding assays.

7.4 Tspan15 may exhibit ADAM10-independent activity

Another notable finding from Chapter 5 was the effect of Tspan15 overexpression on the morphology (Section 5.2.6) and directionality (Section 5.2.7) of HEK-293T cells; a striking clumping phenotype and increased confinement ratio were observed when Tspan15 was upregulated 50-fold in both WT and ADAM10 KO cells. Whilst not addressed in detail within this study, these observations are the first evidence that Tspan15 may exhibit ADAM10-independent activity. However, it is important to consider the possibility that the aforementioned phenotypes may be an artefact of extreme overexpression, especially as similar phenotypes were not observed when Tspan15 was upregulated 27-fold, and Tspan15 downregulation did not have the reverse effect. Furthermore, proteomic analysis reveals that ADAM10 is the main interactor with endogenous Tspan15 in HEK-293T cells, and the only other protein identified above the false discovery rate is Tspan15 itself (Koo et al., 2020). Despite this, it cannot be excluded that Tspan15's activity may be concentration-dependent. It is possible that exceptionally high Tspan15 expression may promote the formation of Tspan15-organised nanodomains containing adhesion molecules. Alternatively,

expression at this level has the potential to facilitate transient association with other tetraspanin-enriched nanodomains that play a role in cell adhesion. Both would have the potential to increase cell-cell interactions promoting cell clumping. As a precedent, a proteomic approach shows that Tspan15-GFP interacts with several adhesion molecules within U2OS and HepG2 cells, including integrin α6β1, integrin α2β1, EWI-2, and neogenin (Jouannet et al., 2016; Sidahmed-Adrar et al., 2019). Additionally, Tspan15 has been indicated to associate with β-catenin, which is integral for adherens junctions, as well as with several proteins involved in the formation and integrity of tight junctions (Sidahmed-Adrar et al., 2019). Although this provides preliminary evidence that Tspan15 may play a role in cell-cell interactions, it is worth noting that in both studies cells were lysed in the relatively low stringency 1% Brij97 lysis buffer (Jouannet et al., 2016; Sidahmed-Adrar et al., 2019), and thus the majority of proteins identified likely associate with Tspan15 indirectly. Furthermore, biochemical assays have not been performed to validate these interactors. As such, the prospect of ADAM10-independent activity remains highly speculative and requires further investigation.

7.5 The binding partners of Tspan15 may extend beyond ADAM10

ADAM10 is regarded as the principal Tspan15-interacting protein (Jouannet et al., 2016; Sidahmed-Adrar et al., 2019; Koo et al., 2020). The importance of this interaction is highlighted by the observation that ADAM10 and Tspan15 form an intimate heterodimer (Lipper et al., 2023) and reciprocally regulate the expression of each other (Eschenbrenner et al., 2020; Koo et al., 2020). However, preliminary evidence, including that from Chapter 4, presents the possibility that Tspan15 may form complexes with additional proteins.

Chapter 4 revealed that the level of Tspan15 surface expression is relatively independent of ADAM10 in PANC-1 cells. Indeed, the knockout of ADAM10 only reduced Tspan15 surface expression by ~53% (Section 4.2.2), whereas a decrease of ~80% is typically observed in other cell lines. Furthermore, in contrast to previous data from AsPC-1 and HEK-293T cells, the upregulation of Tspan15 surface

expression by a fold of 4.5 was not associated with a significant increase in ADAM10 expression (Section 4.2.3). In AsPC-1 cells, a 5.1-fold increase in Tspan15 expression resulted in the upregulation of ADAM10 expression by ~13%, whereas in HEK-293T cells, an increase in ADAM10 surface expression of ~95% was observed when Tspan15 was overexpressed 30- or 50-fold. Given these findings, it is intriguing to speculate that Tspan15 may interact with additional proteins in PANC-1 cells, ultimately supporting expression at the cell surface. Future studies should aim to identify these proteins, for example, by immunoprecipitation with an anti-Tspan15 antibody followed by liquid chromatography-mass spectrometry. Alternatively, proximity-dependent labelling methods involving biotinylation enzymes, such as APEX2 or TurboID, could be used, with mass spectrometry used to identify the proteins (Susa et al., 2023). From this, it would also be important to determine the extent of an interaction between ADAM10 and Tspan15. Whilst Tspan15/ADAM10 complexes likely still form in PANC-1 cells, ADAM10 may be replaced as the principal interactor. By comparison, ADAM10 is likely the major Tspan15-interacting protein in AsPC-1 cells, as the expression of both proteins revealed a reciprocal relationship. As such, the effect of any novel binding partners on Tspan15's role in pancreatic cancer remains to be determined.

In oesophageal carcinoma cell lines, β-TrCP, a key component of the NF-κB signalling pathway, has been reported to co-immunoprecipitate with Tspan15 (Zhang et al., 2018), providing further evidence that Tspan15 has other interactors. However, this thesis found no evidence to support this interaction (Section 6.2.2) nor the proposed downstream activation of NF-κB (Section 6.2.3). Although the underlying cause for this disparity remains undetermined, several possibilities should be considered. Firstly, the expression levels of β-TrCP may be affected by differences in growth conditions linked to FBS formulation. Secondly, different Tspan15 antibodies were used between the two studies. Whilst a Tspan15 knockout cell validated antibody (Koo et al., 2020) was utilised in this study, the antibody used by Zhang et al. (2018) was not validated in their cells depleted of Tspan15 and has since been withdrawn from production. As such, the possibility of non-specific binding

cannot be excluded for the Tspan15 antibody that was used to show an interaction with β-TrCP. Finally, the lysate proteomes likely differed due to lysis buffer choice; the previous study used a much more stringent detergent, likely solubilising nuclear proteins (Zhang et al., 2018). Thus, it is conceivable that the observed interactions may be due to nuclear proteins binding non-specifically to antibodies in the Co-IP. Furthermore, despite mRNA data suggesting that β-TrCP is widely expressed in cell lines, including HEK-293T (Thul et al., 2017), Tspan15 was shown not to modulate NF-κB signalling in these cells (Section 5.2.8). While this seemingly fails to support Tspan15's proposed role within the NF-κB pathway, it could also imply that the interaction between Tspan15 and β-TrCP is cell type-dependent. This would also explain why β-TrCP has not been identified as a Tspan15-associated protein by mass-spectrometry (Jouannet et al., 2016; Sidahmed-Adrar et al., 2019; Koo et al., 2020). Moving forward, it would be useful to further explore this proposed interaction using cell lines with robust expression of both Tspan15 and β-TrCP.

The proteomic analysis of Tspan15 interactors in U2OS and HepG2 cells also supports the hypothesis that Tspan15 may interact with additional proteins. Although both studies identified ADAM10 as the most abundant Tspan15-interacting protein, they also identified a large number of additional associated proteins (Jouannet et al., 2016; Sidahmed-Adrar et al., 2019). However, the majority are likely interacting with Tspan15 indirectly, as cells were lysed in 1% Brij97, a low-stringency lysis buffer. In addition, none of the putative Tspan15-associated proteins have been confirmed by follow-up experiments. Therefore, although definitive binding partners beyond ADAM10 remain to be determined, the possibility of transient, low-frequency interactions with these proteins and others cannot be excluded.

7.6 Tspan15 may exist outside of a 1:1 heterodimer with ADAM10

The cryo-EM structure of a Tspan15/ADAM10 complex reveals a 1:1 heterodimer (Lipper et al., 2023). However, there were limitations associated with this structural analysis. For example, the

complex was purified in detergent micelles (Lipper et al., 2023), which prevents the identification of structural contributions from membrane lipids of a complete bilayer. Additionally, the transmembrane and cytoplasmic regions of ADAM10 were not visualised (Lipper et al., 2023). As ADAM10 can dimerise via its cytoplasmic domain with structural support from the transmembrane region (Xu et al., 2012; Deng et al., 2014), it is tempting to speculate that Tspan15 and ADAM10 may form a tetrameric complex. Similar to the structure shown previously for CD9 with EWI-F or EWI-2 (Oosterheert et al., 2020; Umeda et al., 2020), a central ADAM10 dimer could be bound on either side by a Tspan15 molecule. Indeed a tail-truncated ADAM10 mutant, which is unable to dimerise, impairs Tspan15 surface expression despite being trafficked to the cell surface (Koo, 2021). This demonstrates that ADAM10 dimers may be preferential for Tspan15 binding.

Interestingly, this study has also shown that Tspan15 can be stably overexpressed in ADAM10 KO HEK-293T cells (Section 5.2.4), indicating that Tspan15 has the potential to exist and function on its own. This is further supported by unpublished data from PANC-1 and AsPC-1 cells (Tomlinson lab). However, it is important to acknowledge that overexpressing Tspan15 may affect its stabilisation by increasing self-association in nanoclusters.

To further explore the stoichiometry of Tspan15/ADAM10 complexes, as well as the possibility of Tspan15 monomers and homodimers, super-resolution microscopy, such as stimulated emission depletion (STED) microscopy, could be used. As a precedent, this technique has previously enabled the visualisation of endogenously expressed tetraspanin proteins (CD37, CD53, CD81, and CD82) within their native membrane environments, and as such resulted in a better understanding of the structural organisation of tetraspanin-enriched nanodomains (Zuidscherwoude et al., 2015). Furthermore, the structure could be visualised by cryo-EM in its native membrane environment using styrene-maleic acid lipid particles (SMALPs) (Knowles et al., 2009; Lee et al., 2016; Pollock et al., 2018) to extract the complex.

7.7 Therapeutic potential of inhibiting Tspan15 to inhibit invasion

Tspan15 is overexpressed and a potential marker of poor prognosis in pancreatic adenocarcinoma (Section 3.2.1) and liver hepatocellular carcinoma (Section 3.2.4), for which effective therapeutics are urgently required; liver cancer is the third-leading cause of cancer death worldwide, whilst the incidence of pancreatic cancer almost equals mortality (Sung et al., 2021). Chapter 5 revealed that Tspan15 has the potential to promote cancer cell invasion in an ADAM10-dependent manner (Section 5.2.13). This was proposed to be via N-cadherin shedding and FGFR signalling. As such, targeting Tspan15 to inhibit Tspan15/ADAM10-mediated cleavage of N-cadherin should be considered as a possible novel anti-cancer strategy. This approach would likely reduce the toxicity associated with targeting ADAM10 directly, as a smaller substrate repertoire would be affected. However, as Tspan15 is not exclusively expressed on tumour cells (Uhlen et al., 2015; Human Protein Atlas 2024), there may be challenges associated with specifically targeting the disease state. Furthermore, the Tspan15/ADAM10 complex does cleave additional substrates (Section 1.5.2.2) and thus targeting Tspan15 may still result in unwanted side effects. Although targeting the interaction between shed N-cadherin and FGFRs may offer additional specificity for inhibiting the Tspan15/ADAM10/N-cadherin/FGFR axis, this is likely associated with the same challenge of selectively targeting cancer cells. As the contact interface with FGFRs is likely conserved between full-length and shed N-cadherin (Williams et al., 2001), restricted targeting of aberrant signalling may be difficult. Consequently, inhibitors against Tspan15 remain the most promising therapeutic option to target the pro-invasive effect of Tspan15/ADAM10-mediated shedding of N-cadherin.

Despite the promising therapeutic potential of targeting Tspan15 over ADAM10, further work is required to design functional antibodies or nanobodies that block tumour cell invasion. This is especially important, as the four anti-Tspan15 antibodies (1C12, 4A4, 5D3, 5F4) generated by the Tomlinson group (Koo et al., 2020) were shown not to impair the invasive capabilities of HEK-293T cells (Section 5.2.20). These antibodies aren't completely non-functional though; two of the four,

1C12 and 4A4, inhibit Tspan15/ADAM10-mediated shedding of transfected VE-cadherin (Koo et al., 2020) and betacellulin (Tomlinson lab, unpublished data) by ~50%. It is tempting to speculate that this relatively subtle effect on shedding is due to the antibody epitope. Whilst 1C12 has been shown to bind Tspan15 away from the ADAM10 interaction site (Lipper et al., 2022), it likely still displaces the ADAM10 catalytic domain to some extent (Lipper et al., 2023). As Tspan15 positions the metalloprotease domain relative to the plasma membrane for optimal shedding (Lipper et al., 2023), this displacement may reduce cleavage efficiency. However, it is intriguing to consider that the remaining proteolytic activity is sufficient to maintain cell invasion. It is also important to note that VE-cadherin (Koo et al., 2020) and betacellulin (Tomlinson lab, unpublished data) were overexpressed in the cell-based shedding assays. Consequently, it is possible that the Tspan15 antibodies do not have a functional effect on the shedding of endogenous substrates, which would explain their insufficiency to block invasion within this study.

Moving forward, novel antibodies or nanobodies, which target the contact interface between Tspan15 and the ADAM10 metalloprotease domain, could have therapeutic benefits. Through sufficiently displacing the catalytic domain of ADAM10, these antibodies or nanobodies may be able to selectively inhibit Tspan15/ADAM10-mediated shedding to impair cancer cell invasion. Nanobodies should be considered as an alternative to traditional antibodies as they are better suited to *in vivo* tumour targeting (Bannas et al., 2017; Yang and Shah, 2020). One of the major benefits is their nanoscale dimensions (Bannas et al., 2017; Yang and Shah, 2020). Given that ADAM10 partially occludes the Tspan15 ectodomain (Lipper et al., 2023), this is particularly beneficial for targeting Tspan15. However, specifically targeting Tspan15 on tumours remains an important avenue for future research.

7.8 Concluding remarks

This project provided further evidence to support Tspan15's role in promoting invasion and characterised one of the potential underlying mechanisms. Strikingly, Tspan15 was shown to promote invasion in an ADAM10-dependent manner, providing evidence for the first time that the Tspan15/ADAM10 scissor exhibits pro-invasive activity. Mechanistically, this was linked to its N-cadherin sheddase activity and likely downstream FGFR signalling. An alternative, previously proposed mechanism in which Tspan15 promotes NF-κB signalling (Zhang et al., 2018) was also explored. However, the data obtained failed to validate Tspan15's involvement in this pathway. As such further investigation is required to fully characterise the underlying mechanisms. Regardless, this study demonstrated the significance of Tspan15 and ADAM10 in cancer, with expression being elevated in a range of tumours and associated with patient survival. Tspan15 is, therefore, a promising therapeutic target for Tspan15- and Tspan15/ADAM10-associated cancers. Future studies should assess whether Tspan15 inhibition can target the pro-invasive effect of Tspan15/ADAM10, as well as identify a cohort of patients that may benefit from such treatment.

APPENDIX

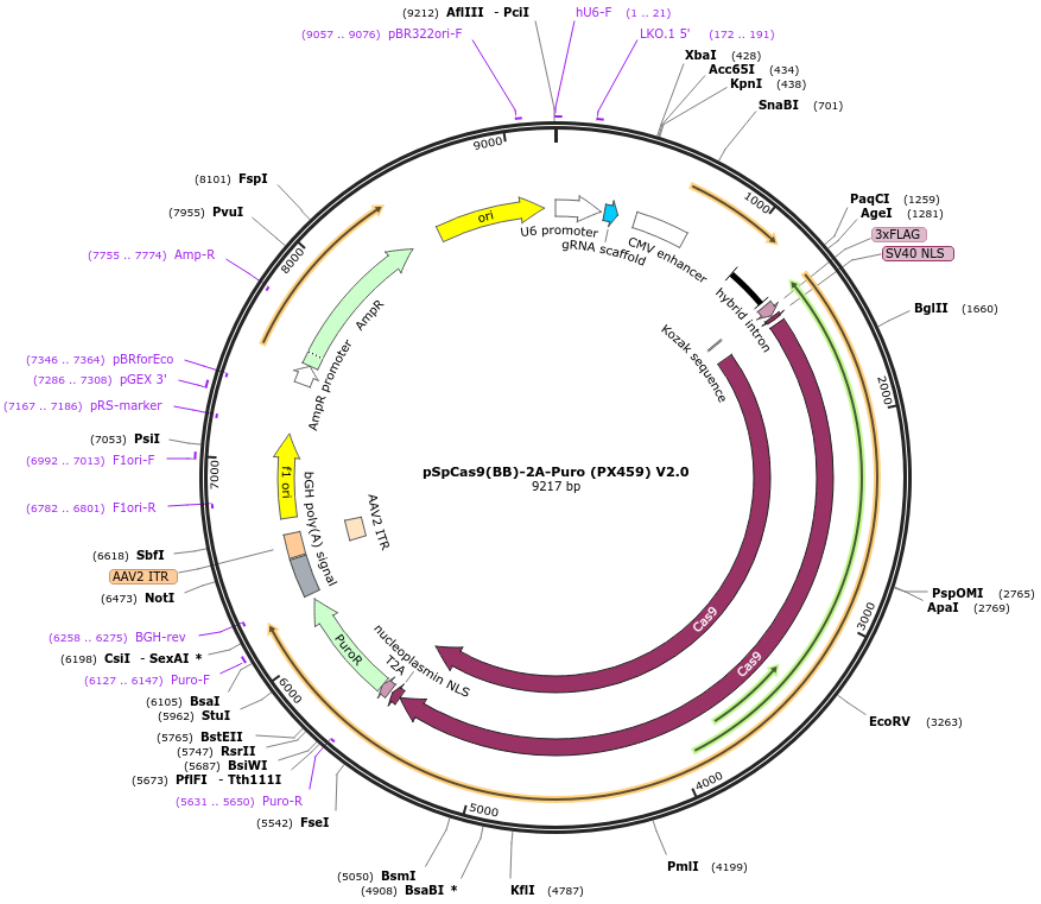


Figure A 2: pSpCas9(BB)-2A-Puro (PX459) V2.0 plasmid map. The ADAM10 and Tspan15 guide oligos were annealed and clones into the pSpCas9(BB)-2A-Puro (PX459) V2.0 plasmid (Addgene plasmid #62988) (Ran et al., 2013).

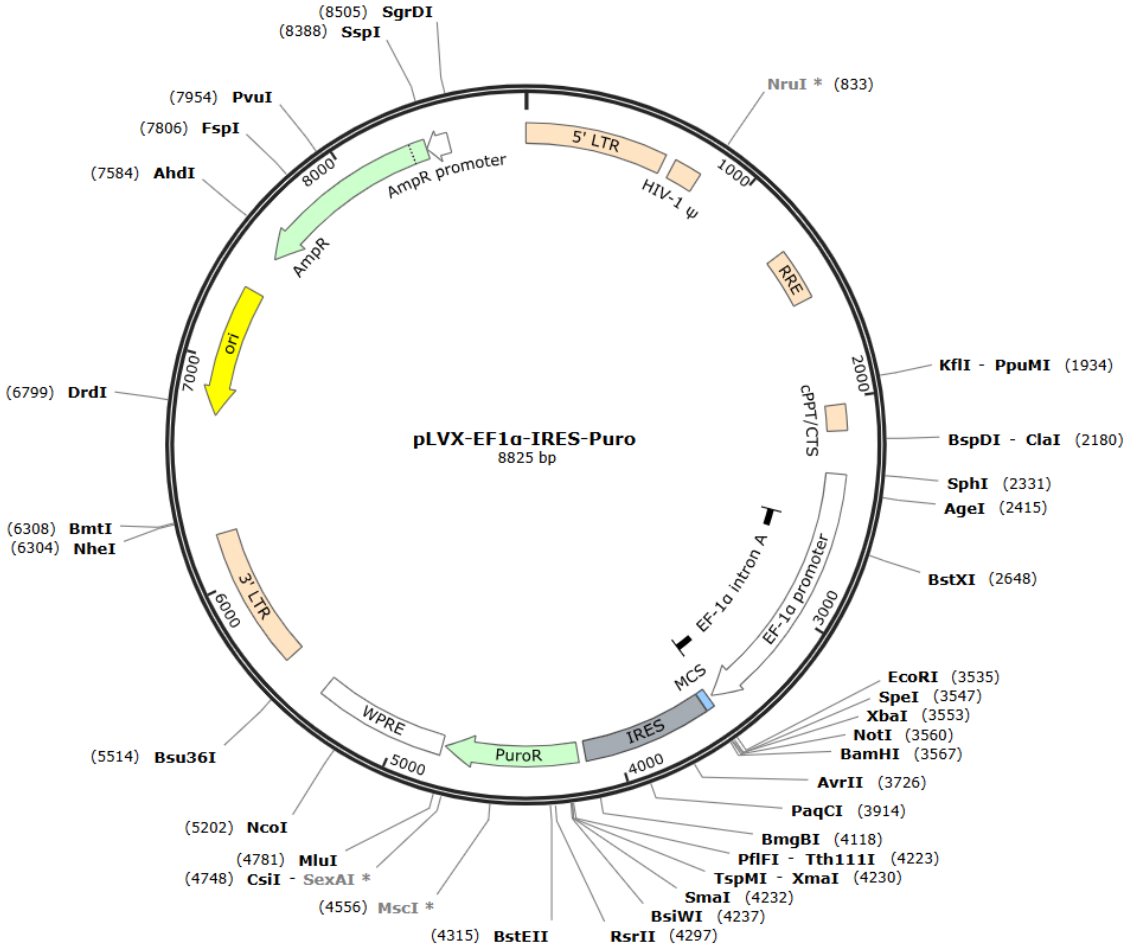


Figure A 3: pLVX-EF1α-IRES-Puro lentiviral transfer plasmid map. The N-terminal FLAG-tagged human Tspan15 sequence was subcloned into the pLVX-EF1α-IRES-Puro lentiviral plasmid (Clontech, USA).

Table A 1: Summary of genes encoding identified proteins from hiSPECS analysis. Most significantly (p≤0.05 using a two-tailed t-test) reduced and increased protein hits from HEK-293T ADAM10 and Tspan15 KO clones compared to WT cells. Data were adjusted for the false discovery rate correction. Transmembrane proteins are highlighted in bold with those that are isoform-dependent marked with a *.

ADAM10 KO vs WT		**Tspan15 KO vs WT**		**ADAM10 KO vs WT + Tspan15 KO vs WT**	
Significantly reduced hits in KO vs WT cells	**Significantly increased hits in KO vs WT cells**	**Significantly reduced hits in KO vs WT cells**	**Significantly increased hits in KO vs WT cells**	**Significantly reduced hits in both KOs vs WT cells**	**Significantly increased hits in both KOs vs WT cells**
CDH11	**TMPO***	COL12A1	**ENPP1**	MAN2B1	FSTL1
TPP1	**CLSTN2**	IGFBP3	PLA2G15	**B4GALT5**	PRSS23
GNPTG	PCSK5	PEBP1	COCH	CD109	CILP2
NPTX1	C1R	**MRC2**	TGM1	NELL1	PRCP
CPVL	SMPD1	CNTN1	**MAN2A1**	**CACHD1**	**ATF6B**
GLB1	COL6A2	**CASC4**	**MGAT2**	CDH13	**ATF6**
HSPB1	SEMA3C	CRTAC1	GGH	**CDH2**	SERPINE2
HEXB	TNC	COL1A1	**LMAN2**	HEXA	**QSOX1***
PLBD2	SEMA3F	ABI3BP	NOV		HYOU1
AOC3	**CANT1**	COL5A2	**MET**		SMOC1
NPTX2	NELL2	CALD1	QPCT		GBA
PTPRU	TFPI	RGMA	SPON1		HS6ST2
NEU1	ACTA1	**PKHD1L1**	**PVR***		NID2
SEMA7A	ACTC1	PCOLCE	CTSV		**B4GALT3**
PLXDC2	ACTG2	TGFB1	**PTPRU**		Sema3c
PSAP	ACTA2	C1QTNF3	ADAM17		HMGB1
CTSC		APOB	CTSC		HMGB1P1
PLOD1		TNXB	NACA		**B4GAT1**
		PRH1			MINPP1
		COL2A1			PPIC
					ADAM9
					COL4A2
					ADAMTS1
					PXDN
					CLSTN1
					IFI30
					FBLN1
					CLN5
					HMGB2
					PLAT
					HLA-C
					HLA-B
					EXT1
					CHST3
					OAF

					GOLM1 NPC2 **CPE*** **B3GNT2** PLTP PPT1 PCOLCE2 STC2 **DAG1** COL6A1 RNASET2 BMP1 **NRP1** TIMP1

REFERENCES

Abel, E. V., Kim, E. J., Wu, J., Hynes, M., Bednar, F., Proctor, E., Wang, L., Dziubinski, M. L. & Simeone, D. M. 2014. The Notch pathway is important in maintaining the cancer stem cell population in pancreatic cancer. *PLoS One,* 9**,** e91983.

Ablinger, C., Eibl, C., Geisler, S. M., Campiglio, M., Stephens, G. J., Missler, M. & Obermair, G. J. 2022. α(2)δ-4 and Cachd1 Proteins Are Regulators of Presynaptic Functions. *Int J Mol Sci,* 23**,** 9885-9908.

Aleskandarany, M. A., Negm, O. H., Green, A. R., Ahmed, M. A., Nolan, C. C., Tighe, P. J., Ellis, I. O. & Rakha, E. A. 2014. Epithelial mesenchymal transition in early invasive breast cancer: an immunohistochemical and reverse phase protein array study. *Breast Cancer Res Treat,* 145**,** 339-348.

Amin, N. & Vincan, E. 2012. The Wnt signaling pathways and cell adhesion. *Front Biosci (Landmark Ed),* 17**,** 784-804.

Anders, A., Gilbert, S., Garten, W., Postina, R. & Fahrenholz, F. 2001. Regulation of the alpha-secretase ADAM10 by its prodomain and proprotein convertases. *Faseb j,* 15**,** 1837-1839.

Araki, K., Shimura, T., Suzuki, H., Tsutsumi, S., Wada, W., Yajima, T., Kobayahi, T., Kubo, N. & Kuwano, H. 2011. E/N-cadherin switch mediates cancer progression via TGF-β-induced epithelial-to-mesenchymal transition in extrahepatic cholangiocarcinoma. *Br J Cancer,* 105**,** 1885-1893.

Arduise, C., Abache, T., Li, L., Billard, M., Chabanon, A., Ludwig, A., Mauduit, P., Boucheix, C., Rubinstein, E. & Le Naour, F. 2008. Tetraspanins regulate ADAM10-mediated cleavage of TNF-alpha and epidermal growth factor. *J Immunol,* 181**,** 7002-7013.

Arima, T., Enokida, H., Kubo, H., Kagara, I., Matsuda, R., Toki, K., Nishimura, H., Chiyomaru, T., Tatarano, S., Idesako, T., Nishiyama, K. & Nakagawa, M. 2007. Nuclear translocation of ADAM-10 contributes to the pathogenesis and progression of human prostate cancer. *Cancer Sci,* 98**,** 1720-1726.

Aster, J. C., Pear, W. S. & Blacklow, S. C. 2008. Notch signaling in leukemia. *Annu Rev Pathol,* 3**,** 587-613.

Baker, B. M. & Chen, C. S. 2012. Deconstructing the third dimension: how 3D culture microenvironments alter cellular cues. *J Cell Sci,* 125**,** 3015-3024.

Bannas, P., Hambach, J. & Koch-Nolte, F. 2017. Nanobodies and Nanobody-Based Human Heavy Chain Antibodies As Antitumor Therapeutics. *Front Immunol,* 8**,** 1603.

Berditchevski, F. & Odintsova, E. 2007. Tetraspanins as regulators of protein trafficking. *Traffic,* 8**,** 89-96.

Berditchevski, F., Odintsova, E., Sawada, S. & Gilbert, E. 2002. Expression of the palmitoylation-deficient CD151 weakens the association of alpha 3 beta 1 integrin with the tetraspanin-enriched microdomains and affects integrin-dependent signaling. *J Biol Chem,* 277**,** 36991-37000.

Berditchevski, F., Zutter, M. M. & Hemler, M. E. 1996. Characterization of novel complexes on the cell surface between integrins and proteins with 4 transmembrane domains (TM4 proteins). *Mol Biol Cell,* 7**,** 193-207.

Berg, S., Kutra, D., Kroeger, T., Straehle, C. N., Kausler, B. X., Haubold, C., Schiegg, M., Ales, J., Beier, T., Rudy, M., Eren, K., Cervantes, J. I., Xu, B., Beuttenmueller, F., Wolny, A., Zhang, C., Koethe, U., Hamprecht, F. A. & Kreshuk, A. 2019. ilastik: interactive machine learning for (bio)image analysis. *Nat Methods,* 16**,** 1226-1232.

Braley, A., Kwak, T., Jules, J., Harja, E., Landgraf, R. & Hudson, B. I. 2016. Regulation of Receptor for Advanced Glycation End Products (RAGE) Ectodomain Shedding and Its Role in Cell Function. *J Biol Chem,* 291**,** 12057-12073.

Brou, C., Logeat, F., Gupta, N., Bessia, C., LeBail, O., Doedens, J. R., Cumano, A., Roux, P., Black, R. A. & Israël, A. 2000. A novel proteolytic cleavage involved in Notch signaling: the role of the disintegrin-metalloprotease TACE. *Mol Cell,* 5**,** 207-216.

Brummer, T., Müller, S. A., Pan-Montojo, F., Yoshida, F., Fellgiebel, A., Tomita, T., Endres, K. & Lichtenthaler, S. F. 2019. NrCAM is a marker for substrate-selective activation of ADAM10 in Alzheimer's disease. *EMBO Mol Med,* 11**,** e9695.

Brummer, T., Pigoni, M., Rossello, A., Wang, H., Noy, P. J., Tomlinson, M. G., Blobel, C. P. & Lichtenthaler, S. F. 2018. The metalloprotease ADAM10 (a disintegrin and metalloprotease 10) undergoes rapid, postlysis autocatalytic degradation. *Faseb j,* 32**,** 3560-3573.

Buchanan, P. C., Boylan, K. L. M., Walcheck, B., Heinze, R., Geller, M. A., Argenta, P. A. & Skubitz, A. P. N. 2017. Ectodomain shedding of the cell adhesion molecule Nectin-4 in ovarian cancer is mediated by ADAM10 and ADAM17. *J Biol Chem,* 292**,** 6339-6351.

Cacciamali, A., Villa, R. & Dotti, S. 2022. 3D Cell Cultures: Evolution of an Ancient Tool for New Applications. *Front Physiol,* 13**,** 836480-836495.

Caescu, C. I., Jeschke, G. R. & Turk, B. E. 2009. Active-site determinants of substrate recognition by the metalloproteinases TACE and ADAM10. *Biochem J,* 424**,** 79-88.

Cai, C., Zhang, M., Liu, L., Zhang, H., Guo, Y., Lan, T., Xu, Y., Ma, P. & Li, S. 2022. ADAM10-cleaved ephrin-A5 contributes to prostate cancer metastasis. *Cell Death Dis,* 13**,** 453-464.

Cavallaro, U. & Christofori, G. 2004. Cell adhesion and signalling by cadherins and Ig-CAMs in cancer. *Nat Rev Cancer,* 4**,** 118-132.

Chaimowitz, N. S., Martin, R. K., Cichy, J., Gibb, D. R., Patil, P., Kang, D. J., Farnsworth, J., Butcher, E. C., McCright, B. & Conrad, D. H. 2011. A disintegrin and metalloproteinase 10 regulates antibody production and maintenance of lymphoid architecture. *J Immunol,* 187**,** 5114-5122.

Chang, W. H., Cerione, R. A. & Antonyak, M. A. 2021. Extracellular Vesicles and Their Roles in Cancer Progression. *Methods Mol Biol,* 2174**,** 143-170.

Charrin, S., Jouannet, S., Boucheix, C. & Rubinstein, E. 2014. Tetraspanins at a glance. *J Cell Sci,* 127**,** 3641-3648.

Charrin, S., le Naour, F., Silvie, O., Milhiet, P. E., Boucheix, C. & Rubinstein, E. 2009. Lateral organization of membrane proteins: tetraspanins spin their web. *Biochem J,* 420**,** 133-154.

Charrin, S., Manié, S., Oualid, M., Billard, M., Boucheix, C. & Rubinstein, E. 2002. Differential stability of tetraspanin/tetraspanin interactions: role of palmitoylation. *FEBS Lett,* 516**,** 139-144.

Chen, K., Yuan, X., Wang, S., Zheng, F., Fu, Z., Shen, Z., Cheng, X., Wang, Y., Tang, S., Ni, H., Wang, F., Lu, G., Wu, Y., Xia, D. & Lu, W. 2023. MAP4K4 promotes ovarian cancer metastasis through diminishing ADAM10-dependent N-cadherin cleavage. *Oncogene,* 42**,** 1438-1452.

Chen, W. H., Horoszewicz, J. S., Leong, S. S., Shimano, T., Penetrante, R., Sanders, W. H., Berjian, R., Douglass, H. O., Martin, E. W. & Chu, T. M. 1982. Human pancreatic adenocarcinoma: in vitro and in vivo morphology of a new tumor line established from ascites. *In Vitro,* 18**,** 24-34.

Choi, Y., Lee, H. J., Jang, M. H., Gwak, J. M., Lee, K. S., Kim, E. J., Kim, H. J., Lee, H. E. & Park, S. Y. 2013. Epithelial-mesenchymal transition increases during the progression of in situ to invasive basal-like breast cancer. *Hum Pathol,* 44**,** 2581-2589.

Ciołczyk-Wierzbicka, D. & Laidler, P. 2018. The inhibition of invasion of human melanoma cells through N-cadherin knock-down. *Medical Oncology,* 35**,** 42-51.

Consortium, T. U. 2022. UniProt: the Universal Protein Knowledgebase in 2023. *Nucleic Acids Research,* 51**,** D523-D531.

Cottrell, G. S., Soubrane, C. H., Hounshell, J. A., Lin, H., Owenson, V., Rigby, M., Cox, P. J., Barker, B. S., Ottolini, M., Ince, S., Bauer, C. C., Perez-Reyes, E., Patel, M. K., Stevens, E. B. & Stephens, G. J. 2018. CACHD1 is an α2δ-Like Protein That Modulates Ca(V)3 Voltage-Gated Calcium Channel Activity. *J Neurosci,* 38**,** 9186-9201.

Croft, A. P., Campos, J., Jansen, K., Turner, J. D., Marshall, J., Attar, M., Savary, L., Wehmeyer, C., Naylor, A. J., Kemble, S., Begum, J., Dürholz, K., Perlman, H., Barone, F., McGettrick, H. M.,

Fearon, D. T., Wei, K., Raychaudhuri, S., Korsunsky, I., Brenner, M. B., Coles, M., Sansom, S. N., Filer, A. & Buckley, C. D. 2019. Distinct fibroblast subsets drive inflammation and damage in arthritis. *Nature,* 570**,** 246-251.

De Craene, B. & Berx, G. 2013. Regulatory networks defining EMT during cancer initiation and progression. *Nat Rev Cancer,* 13**,** 97-110.

Deer, E. L., González-Hernández, J., Coursen, J. D., Shea, J. E., Ngatia, J., Scaife, C. L., Firpo, M. A. & Mulvihill, S. J. 2010. Phenotype and genotype of pancreatic cancer cell lines. *Pancreas,* 39**,** 425-435.

Deng, W., Cho, S., Su, P. C., Berger, B. W. & Li, R. 2014. Membrane-enabled dimerization of the intrinsically disordered cytoplasmic domain of ADAM10. *Proc Natl Acad Sci U S A,* 111**,** 15987-15992.

Dornier, E., Coumailleau, F., Ottavi, J. F., Moretti, J., Boucheix, C., Mauduit, P., Schweisguth, F. & Rubinstein, E. 2012. TspanC8 tetraspanins regulate ADAM10/Kuzbanian trafficking and promote Notch activation in flies and mammals. *J Cell Biol,* 199**,** 481-496.

Düsterhöft, S., Lokau, J. & Garbers, C. 2019. The metalloprotease ADAM17 in inflammation and cancer. *Pathology - Research and Practice,* 215**,** 152410-152416.

Ebsen, H., Lettau, M., Kabelitz, D. & Janssen, O. 2014. Identification of SH3 domain proteins interacting with the cytoplasmic tail of the a disintegrin and metalloprotease 10 (ADAM10). *PLoS One,* 9**,** e102899.

Edwards, A. & Brennan, K. 2021. Notch Signalling in Breast Development and Cancer. *Front Cell Dev Biol,* 9**,** 692173-692197.

Edwards, D. R., Handsley, M. M. & Pennington, C. J. 2008. The ADAM metalloproteinases. *Mol Aspects Med,* 29**,** 258-289.

Ehrhardt, C., Schmolke, M., Matzke, A. T., Knoblauch, A., Will, C., Wixler, V. & Ludwig, S. 2006. Polyethylenimine, a cost-effective transfection reagent. *Signal Transduction,* 6**,** 179-184.

Eschenbrenner, E., Jouannet, S., Clay, D., Chaker, J., Boucheix, C., Brou, C., Tomlinson, M. G., Charrin, S. & Rubinstein, E. 2020. TspanC8 tetraspanins differentially regulate ADAM10 endocytosis and half-life. *Life Sci Alliance,* 3**,** e201900444.

Fassl, A., Tagscherer, K. E., Richter, J., Berriel Diaz, M., Alcantara Llaguno, S. R., Campos, B., Kopitz, J., Herold-Mende, C., Herzig, S., Schmidt, M. H. H., Parada, L. F., Wiestler, O. D. & Roth, W. 2012. Notch1 signaling promotes survival of glioblastoma cells via EGFR-mediated induction of anti-apoptotic Mcl-1. *Oncogene,* 31**,** 4698-4708.

Feldinger, K., Generali, D., Kramer-Marek, G., Gijsen, M., Ng, T. B., Wong, J. H., Strina, C., Cappelletti, M., Andreis, D., Li, J. L., Bridges, E., Turley, H., Leek, R., Roxanis, I., Capala, J., Murphy, G., Harris, A. L. & Kong, A. 2014. ADAM10 mediates trastuzumab resistance and is correlated with survival in HER2 positive breast cancer. *Oncotarget,* 5**,** 6633-6646.

Fu, L., Liu, N., Han, Y., Xie, C., Li, Q. & Wang, E. 2014. ADAM10 regulates proliferation, invasion, and chemoresistance of bladder cancer cells. *Tumour Biol,* 35**,** 9263-9268.

Funahashi, Y., Hernandez, S. L., Das, I., Ahn, A., Huang, J., Vorontchikhina, M., Sharma, A., Kanamaru, E., Borisenko, V., Desilva, D. M., Suzuki, A., Wang, X., Shawber, C. J., Kandel, J. J., Yamashiro, D. J. & Kitajewski, J. 2008. A notch1 ectodomain construct inhibits endothelial notch signaling, tumor growth, and angiogenesis. *Cancer Res,* 68**,** 4727-4735.

Gaida, M. M., Haag, N., Günther, F., Tschaharganeh, D. F., Schirmacher, P., Friess, H., Giese, N. A., Schmidt, J. & Wente, M. N. 2010. Expression of A disintegrin and metalloprotease 10 in pancreatic carcinoma. *Int J Mol Med,* 26**,** 281-288.

Gao, P., Xing, A. Y., Zhou, G. Y., Zhang, T. G., Zhang, J. P., Gao, C., Li, H. & Shi, D. B. 2013. The molecular mechanism of microRNA-145 to suppress invasion–metastasis cascade in gastric cancer. *Oncogene,* 32**,** 491-501.

Garcia Garcia, C. J., Abi Jaoude, J. & Taniguchi, C. M. 2021. ADAM10 Evens Out the Double-Edged Sword of Radiotherapy in Pancreatic Cancer. *Cancer Res,* 81**,** 3158-3159.

Gardiner, E. E., Karunakaran, D., Shen, Y., Arthur, J. F., Andrews, R. K. & Berndt, M. C. 2007. Controlled shedding of platelet glycoprotein (GP)VI and GPIb-IX-V by ADAM family metalloproteinases. *J Thromb Haemost,* 5**,** 1530-1537.

Gavert, N., Sheffer, M., Raveh, S., Spaderna, S., Shtutman, M., Brabletz, T., Barany, F., Paty, P., Notterman, D., Domany, E. & Ben-Ze'ev, A. 2007. Expression of L1-CAM and ADAM10 in human colon cancer cells induces metastasis. *Cancer Res,* 67**,** 7703-7712.

Germain, M., Chasman, D. I., de Haan, H., Tang, W., Lindström, S., Weng, L. C., de Andrade, M., de Visser, M. C., Wiggins, K. L., Suchon, P., Saut, N., Smadja, D. M., Le Gal, G., van Hylckama Vlieg, A., Di Narzo, A., Hao, K., Nelson, C. P., Rocanin-Arjo, A., Folkersen, L., Monajemi, R., Rose, L. M., Brody, J. A., Slagboom, E., Aïssi, D., Gagnon, F., Deleuze, J. F., Deloukas, P., Tzourio, C., Dartigues, J. F., Berr, C., Taylor, K. D., Civelek, M., Eriksson, P., Psaty, B. M., Houwing-Duitermaat, J., Goodall, A. H., Cambien, F., Kraft, P., Amouyel, P., Samani, N. J., Basu, S., Ridker, P. M., Rosendaal, F. R., Kabrhel, C., Folsom, A. R., Heit, J., Reitsma, P. H., Trégouët, D. A., Smith, N. L. & Morange, P. E. 2015. Meta-analysis of 65,734 individuals identifies TSPAN15 and SLC44A2 as two susceptibility loci for venous thromboembolism. *Am J Hum Genet,* 96**,** 532-542.

Giuliano, C. J., Lin, A., Girish, V. & Sheltzer, J. M. 2019. Generating Single Cell-Derived Knockout Clones in Mammalian Cells with CRISPR/Cas9. *Curr Protoc Mol Biol,* 128**,** e100.

Gordón-Alonso, M., Sala-Valdés, M., Rocha-Perugini, V., Pérez-Hernández, D., López-Martín, S., Ursa, A., Alvarez, S., Kolesnikova, T. V., Vázquez, J., Sánchez-Madrid, F. & Yáñez-Mó, M. 2012. EWI-2 association with α-actinin regulates T cell immune synapses and HIV viral infection. *J Immunol,* 189**,** 689-700.

Gravdal, K., Halvorsen, O. J., Haukaas, S. A. & Akslen, L. A. 2007. A switch from E-cadherin to N-cadherin expression indicates epithelial to mesenchymal transition and is of strong and independent importance for the progress of prostate cancer. *Clin Cancer Res,* 13**,** 7003-7011.

Guerreiro, E. M., Vestad, B., Steffensen, L. A., Aass, H. C. D., Saeed, M., Øvstebø, R., Costea, D. E., Galtung, H. K. & Søland, T. M. 2018. Efficient extracellular vesicle isolation by combining cell media modifications, ultrafiltration, and size-exclusion chromatography. *PLoS One,* 13**,** e0204276.

Guo, J., He, L., Yuan, P., Wang, P., Lu, Y., Tong, F., Wang, Y., Yin, Y., Tian, J. & Sun, J. 2012. ADAM10 overexpression in human non-small cell lung cancer correlates with cell migration and invasion through the activation of the Notch1 signaling pathway. *Oncol Rep,* 28**,** 1709-1718.

Haining, E. J., Yang, J., Bailey, R. L., Khan, K., Collier, R., Tsai, S., Watson, S. P., Frampton, J., Garcia, P. & Tomlinson, M. G. 2012. The TspanC8 subgroup of tetraspanins interacts with A disintegrin and metalloprotease 10 (ADAM10) and regulates its maturation and cell surface expression. *J Biol Chem,* 287**,** 39753-39765.

Han, Y., Li, Z., Wu, Q., Liu, H., Sun, Z., Wu, Y. & Luo, J. 2022. B4GALT5 high expression associated with poor prognosis of hepatocellular carcinoma. *BMC Cancer,* 22**,** 392-403.

Hanahan, D. 2022. Hallmarks of Cancer: New Dimensions. *Cancer Discov,* 12**,** 31-46.

Hanahan, D. & Weinberg, R. A. 2000. The hallmarks of cancer. *Cell,* 100**,** 57-70.

Hanahan, D. & Weinberg, R. A. 2011. Hallmarks of cancer: the next generation. *Cell,* 144**,** 646-674.

Harrison, N., Koo, C. Z. & Tomlinson, M. G. 2021. Regulation of ADAM10 by the TspanC8 Family of Tetraspanins and Their Therapeutic Potential. *Int J Mol Sci,* 22**,** 6707-6723.

Hartmann, D., de Strooper, B., Serneels, L., Craessaerts, K., Herreman, A., Annaert, W., Umans, L., Lübke, T., Lena Illert, A., von Figura, K. & Saftig, P. 2002. The disintegrin/metalloprotease ADAM 10 is essential for Notch signalling but not for alpha-secretase activity in fibroblasts. *Hum Mol Genet,* 11**,** 2615-2624.

Hazan, R. B., Phillips, G. R., Qiao, R. F., Norton, L. & Aaronson, S. A. 2000. Exogenous expression of N-cadherin in breast cancer cells induces cell migration, invasion, and metastasis. *J Cell Biol,* 148**,** 779-790.

Herranz, D., Ambesi-Impiombato, A., Sudderth, J., Sánchez-Martín, M., Belver, L., Tosello, V., Xu, L., Wendorff, A. A., Castillo, M., Haydu, J. E., Márquez, J., Matés, J. M., Kung, A. L., Rayport, S., Cordon-Cardo, C., DeBerardinis, R. J. & Ferrando, A. A. 2015. Metabolic reprogramming induces resistance to anti-NOTCH1 therapies in T cell acute lymphoblastic leukemia. *Nat Med,* 21**,** 1182-1189.

Heuberger, J. & Birchmeier, W. 2010. Interplay of cadherin-mediated cell adhesion and canonical Wnt signaling. *Cold Spring Harb Perspect Biol,* 2**,** a002915.

Hiroshima, K., Shiiba, M., Oka, N., Hayashi, F., Ishida, S., Fukushima, R., Koike, K., Iyoda, M., Nakashima, D., Tanzawa, H. & Uzawa, K. 2019. Tspan15 plays a crucial role in metastasis in oral squamous cell carcinoma. *Exp Cell Res,* 384**,** 111622-111631.

Hossen, M. B., Islam, M. A., Reza, M. S., Kibria, M. K., Horaira, M. A., Tuly, K. F., Faruqe, M. O., Kabir, F. & Mollah, M. N. H. 2023. Robust identification of common genomic biomarkers from multiple gene expression profiles for the prognosis, diagnosis, and therapies of pancreatic cancer. *Comput Biol Med,* 152**,** 106411-106427.

Huff, J., Bergter, A., Birkenbeil, J., Kleppe, I., Engelmann, R. & Krzic, U. 2017. The new 2D Superresolution mode for ZEISS Airyscan. *Nature Methods,* 14**,** 1223-1223.

Hulit, J., Suyama, K., Chung, S., Keren, R., Agiostratidou, G., Shan, W., Dong, X., Williams, T. M., Lisanti, M. P., Knudsen, K. & Hazan, R. B. 2007. N-cadherin signaling potentiates mammary tumor metastasis via enhanced extracellular signal-regulated kinase activation. *Cancer Res,* 67**,** 3106-3116.

Human Protein Atlas 2024. *The Human Protein Atlas* [Online]. Human Protein Atlas. Available: https://www.proteinatlas.org/ [Accessed January 15 2024].

Huppert, S. S., Le, A., Schroeter, E. H., Mumm, J. S., Saxena, M. T., Milner, L. A. & Kopan, R. 2000. Embryonic lethality in mice homozygous for a processing-deficient allele of Notch1. *Nature,* 405**,** 966-970.

Jia, Y., Xiao, Z., Gongsun, X., Xin, Z., Shang, B., Chen, G., Wang, Z. & Jiang, W. 2018. CEP55 promotes the proliferation, migration and invasion of esophageal squamous cell carcinoma via the PI3K/Akt pathway. *Onco Targets Ther,* 11**,** 4221-4232.

Jiang, J., Chen, X., Shen, J., Wei, Y., Wu, T., Yang, Y., Wang, H., Zong, H., Yang, J., Zhang, S., Xie, J., Kong, X., Liu, W. & Gu, J. 2006. Beta1,4-galactosyltransferase V functions as a positive growth regulator in glioma. *J Biol Chem,* 281**,** 9482-9489.

Jorissen, E., Prox, J., Bernreuther, C., Weber, S., Schwanbeck, R., Serneels, L., Snellinx, A., Craessaerts, K., Thathiah, A., Tesseur, I., Bartsch, U., Weskamp, G., Blobel, C. P., Glatzel, M., De Strooper, B. & Saftig, P. 2010. The disintegrin/metalloproteinase ADAM10 is essential for the establishment of the brain cortex. *J Neurosci,* 30**,** 4833-4844.

Jouannet, S., Saint-Pol, J., Fernandez, L., Nguyen, V., Charrin, S., Boucheix, C., Brou, C., Milhiet, P. E. & Rubinstein, E. 2016. TspanC8 tetraspanins differentially regulate the cleavage of ADAM10 substrates, Notch activation and ADAM10 membrane compartmentalization. *Cell Mol Life Sci,* 73**,** 1895-1915.

Junge, H. J., Yang, S., Burton, J. B., Paes, K., Shu, X., French, D. M., Costa, M., Rice, D. S. & Ye, W. 2009. TSPAN12 regulates retinal vascular development by promoting Norrin- but not Wnt-induced FZD4/beta-catenin signaling. *Cell,* 139**,** 299-311.

Karamatic Crew, V., Burton, N., Kagan, A., Green, C. A., Levene, C., Flinter, F., Brady, R. L., Daniels, G. & Anstee, D. J. 2004. CD151, the first member of the tetraspanin (TM4) superfamily detected on erythrocytes, is essential for the correct assembly of human basement membranes in kidney and skin. *Blood,* 104**,** 2217-2223.

Kazarov, A. R., Yang, X., Stipp, C. S., Sehgal, B. & Hemler, M. E. 2002. An extracellular site on tetraspanin CD151 determines alpha 3 and alpha 6 integrin-dependent cellular morphology. *J Cell Biol,* 158**,** 1299-1309.

Kim, J. B., Islam, S., Kim, Y. J., Prudoff, R. S., Sass, K. M., Wheelock, M. J. & Johnson, K. R. 2000. N-Cadherin extracellular repeat 4 mediates epithelial to mesenchymal transition and increased motility. *J Cell Biol,* 151**,** 1193-1206.

Kitadokoro, K., Bordo, D., Galli, G., Petracca, R., Falugi, F., Abrignani, S., Grandi, G. & Bolognesi, M. 2001. CD81 extracellular domain 3D structure: insight into the tetraspanin superfamily structural motifs. *Embo j,* 20**,** 12-18.

Knowles, T. J., Finka, R., Smith, C., Lin, Y. P., Dafforn, T. & Overduin, M. 2009. Membrane proteins solubilized intact in lipid containing nanoparticles bounded by styrene maleic acid copolymer. *J Am Chem Soc,* 131**,** 7484-7485.

Kohutek, Z. A., diPierro, C. G., Redpath, G. T. & Hussaini, I. M. 2009. ADAM-10-mediated N-cadherin cleavage is protein kinase C-alpha dependent and promotes glioblastoma cell migration. *J Neurosci,* 29**,** 4605-4615.

Koo, C. Z. 2021. *Characterising the tetraspanin/ADAM10 'molecular scissors' for the platelet collagen and fibrin receptor GPVI.* PhD thesis.

Koo, C. Z., Harrison, N., Noy, P. J., Szyroka, J., Matthews, A. L., Hsia, H. E., Muller, S. A., Tushaus, J., Goulding, J., Willis, K., Apicella, C., Cragoe, B., Davis, E., Keles, M., Malinova, A., McFarlane, T. A., Morrison, P. R., Nguyen, H. T. H., Sykes, M. C., Ahmed, H., Di Maio, A., Seipold, L., Saftig, P., Cull, E., Pliotas, C., Rubinstein, E., Poulter, N. S., Briddon, S. J., Holliday, N. D., Lichtenthaler, S. F. & Tomlinson, M. G. 2020. The tetraspanin Tspan15 is an essential subunit of an ADAM10 scissor complex. *J Biol Chem,* 295**,** 12822–12839.

Koo, C. Z., Matthews, A. L., Harrison, N., Szyroka, J., Nieswandt, B., Gardiner, E. E., Poulter, N. S. & Tomlinson, M. G. 2022. The Platelet Collagen Receptor GPVI Is Cleaved by Tspan15/ADAM10 and Tspan33/ADAM10 Molecular Scissors. *Int J Mol Sci,* 23**,** 2440-2458.

Kovalenko, O. V., Metcalf, D. G., DeGrado, W. F. & Hemler, M. E. 2005. Structural organization and interactions of transmembrane domains in tetraspanin proteins. *BMC Struct Biol,* 5**,** 11.

Krebs, L. T., Xue, Y., Norton, C. R., Shutter, J. R., Maguire, M., Sundberg, J. P., Gallahan, D., Closson, V., Kitajewski, J., Callahan, R., Smith, G. H., Stark, K. L. & Gridley, T. 2000. Notch signaling is essential for vascular morphogenesis in mice. *Genes Dev,* 14**,** 1343-1352.

Labernadie, A., Kato, T., Brugués, A., Serra-Picamal, X., Derzsi, S., Arwert, E., Weston, A., González-Tarragó, V., Elosegui-Artola, A., Albertazzi, L., Alcaraz, J., Roca-Cusachs, P., Sahai, E. & Trepat, X. 2017. A mechanically active heterotypic E-cadherin/N-cadherin adhesion enables fibroblasts to drive cancer cell invasion. *Nat Cell Biol,* 19**,** 224-237.

Lade-Keller, J., Riber-Hansen, R., Guldberg, P., Schmidt, H., Hamilton-Dutoit, S. J. & Steiniche, T. 2013. E- to N-cadherin switch in melanoma is associated with decreased expression of phosphatase and tensin homolog and cancer progression. *Br J Dermatol,* 169**,** 618-628.

Lammerding, J., Kazarov, A. R., Huang, H., Lee, R. T. & Hemler, M. E. 2003. Tetraspanin CD151 regulates alpha6beta1 integrin adhesion strengthening. *Proc Natl Acad Sci U S A,* 100**,** 7616-7621.

Latysheva, N., Muratov, G., Rajesh, S., Padgett, M., Hotchin, N. A., Overduin, M. & Berditchevski, F. 2006. Syntenin-1 is a new component of tetraspanin-enriched microdomains: mechanisms and consequences of the interaction of syntenin-1 with CD63. *Mol Cell Biol,* 26**,** 7707-7718.

Le Naour, F., André, M., Boucheix, C. & Rubinstein, E. 2006. Membrane microdomains and proteomics: lessons from tetraspanin microdomains and comparison with lipid rafts. *Proteomics,* 6**,** 6447-6454.

Lee, S. B., Schramme, A., Doberstein, K., Dummer, R., Abdel-Bakky, M. S., Keller, S., Altevogt, P., Oh, S. T., Reichrath, J., Oxmann, D., Pfeilschifter, J., Mihic-Probst, D. & Gutwein, P. 2010. ADAM10 is upregulated in melanoma metastasis compared with primary melanoma. *J Invest Dermatol,* 130**,** 763-773.

Lee, S. C., Knowles, T. J., Postis, V. L., Jamshad, M., Parslow, R. A., Lin, Y. P., Goldman, A., Sridhar, P., Overduin, M., Muench, S. P. & Dafforn, T. R. 2016. A method for detergent-free isolation of membrane proteins in their local lipid environment. *Nat Protoc,* 11**,** 1149-1162.

Letunic, I. & Bork, P. 2021. Interactive Tree Of Life (iTOL) v5: an online tool for phylogenetic tree display and annotation. *Nucleic Acids Research,* 49**,** W293-W296.

Li, Q., Sun, M., Wang, M., Feng, M., Yang, F., Li, L., Zhao, J., Chang, C., Dong, H., Xie, T. & Chen, J. 2021. Dysregulation of Wnt/β-catenin signaling by protein kinases in hepatocellular carcinoma and its therapeutic application. *Cancer Sci,* 112**,** 1695-1706.

Lichtenthaler, S. F., Lemberg, M. K. & Fluhrer, R. 2018. Proteolytic ectodomain shedding of membrane proteins in mammals-hardware, concepts, and recent developments. *Embo j,* 37**,** e99456.

Lieber, M., Mazzetta, J., Nelson-Rees, W., Kaplan, M. & Todaro, G. 1975. Establishment of a continuous tumor-cell line (panc-1) from a human carcinoma of the exocrine pancreas. *Int J Cancer,* 15**,** 741-747.

Lin, X., Huang, M., Xie, F., Zhou, H., Yang, J. & Huang, Q. 2016. Gemcitabine inhibits immune escape of pancreatic cancer by down regulating the soluble ULBP2 protein. *Oncotarget,* 7**,** 70092-70099.

Lindström, S., Wang, L., Smith, E. N., Gordon, W., van Hylckama Vlieg, A., de Andrade, M., Brody, J. A., Pattee, J. W., Haessler, J., Brumpton, B. M., Chasman, D. I., Suchon, P., Chen, M. H., Turman, C., Germain, M., Wiggins, K. L., MacDonald, J., Braekkan, S. K., Armasu, S. M., Pankratz, N., Jackson, R. D., Nielsen, J. B., Giulianini, F., Puurunen, M. K., Ibrahim, M., Heckbert, S. R., Damrauer, S. M., Natarajan, P., Klarin, D., de Vries, P. S., Sabater-Lleal, M., Huffman, J. E., Bammler, T. K., Frazer, K. A., McCauley, B. M., Taylor, K., Pankow, J. S., Reiner, A. P., Gabrielsen, M. E., Deleuze, J. F., O'Donnell, C. J., Kim, J., McKnight, B., Kraft, P., Hansen, J. B., Rosendaal, F. R., Heit, J. A., Psaty, B. M., Tang, W., Kooperberg, C., Hveem, K., Ridker, P. M., Morange, P. E., Johnson, A. D., Kabrhel, C., Trégouët, D. A. & Smith, N. L. 2019. Genomic and transcriptomic association studies identify 16 novel susceptibility loci for venous thromboembolism. *Blood,* 134**,** 1645-1657.

Lipper, C. H., Egan, E. D., Gabriel, K.-H. & Blacklow, S. C. 2023. Structural basis for membrane-proximal proteolysis of substrates by ADAM10. *Cell,* 186**,** 3632-3641.e3610.

Lipper, C. H., Gabriel, K. H., Seegar, T. C. M., Dürr, K. L., Tomlinson, M. G. & Blacklow, S. C. 2022. Crystal structure of the Tspan15 LEL domain reveals a conserved ADAM10 binding site. *Structure,* 30**,** 206-214.e204.

Liu, H., Zhou, Q., Wei, W., Qi, B., Zeng, F., Bao, N., Li, Q., Guo, F. & Xia, S. 2020. The potential drug for treatment in pancreatic adenocarcinoma: a bioinformatical study based on distinct drug databases. *Chin Med,* 15**,** 26.

Liu, J., Xiao, Q., Xiao, J., Niu, C., Li, Y., Zhang, X., Zhou, Z., Shu, G. & Yin, G. 2022. Wnt/β-catenin signalling: function, biological mechanisms, and therapeutic opportunities. *Signal Transduct Target Ther,* 7**,** 3-26.

Liu, J., Ye, L., Lin, K., Zhong, T., Luo, J., Wang, T., Suo, L., Mo, Q., Li, S., Chen, Q. & Yu, Y. 2023. miR-4299 inhibits tumor progression in pancreatic cancer through targeting ADAM17. *Mol Cell Biochem,* 478**,** 1727-1742.

Liu, L., Meng, T., Zheng, X., Liu, Y., Hao, R., Yan, Y., Chen, S., You, H., Xing, J. & Dong, Y. 2019. Transgelin 2 Promotes Paclitaxel Resistance, Migration, and Invasion of Breast Cancer by Directly Interacting with PTEN and Activating PI3K/Akt/GSK-3β Pathway. *Mol Cancer Ther,* 18**,** 2457-2468.

Liu, R., Qin, X. P., Zhuang, Y., Zhang, Y., Liao, H. B., Tang, J. C., Pan, M. X., Zeng, F. F., Lei, Y., Lei, R. X., Wang, S., Liu, A. C., Chen, J., Zhang, Z. F., Zhao, D., Wu, S. L., Liu, R. Z., Wang, Z. F. & Wan, Q. 2018. Glioblastoma recurrence correlates with NLGN3 levels. *Cancer Med,* 7**,** 2848-2859.

Liu, S., Zhang, W., Liu, K., Ji, B. & Wang, G. 2015. Silencing ADAM10 inhibits the in vitro and in vivo growth of hepatocellular carcinoma cancer cells. *Mol Med Rep,* 11**,** 597-602.

Loh, C. Y., Chai, J. Y., Tang, T. F., Wong, W. F., Sethi, G., Shanmugam, M. K., Chong, P. P. & Looi, C. Y. 2019. The E-Cadherin and N-Cadherin Switch in Epithelial-to-Mesenchymal Transition: Signaling, Therapeutic Implications, and Challenges. *Cells,* 8**,** 1118-1151.

Lyon, C. A., Wadey, K. S. & George, S. J. 2016. Soluble N-cadherin: A novel inhibitor of VSMC proliferation and intimal thickening. *Vascul Pharmacol,* 78**,** 53-62.

Ma, B., Zhang, H. Y., Bai, X., Wang, F., Ren, X. H., Zhang, L. & Zhang, M. Z. 2016. ADAM10 mediates the cell invasion and metastasis of human esophageal squamous cell carcinoma via regulation of E-cadherin activity. *Oncol Rep,* 35**,** 2785-2794.

Madeira, F., Pearce, M., Tivey, A. R. N., Basutkar, P., Lee, J., Edbali, O., Madhusoodanan, N., Kolesnikov, A. & Lopez, R. 2022. Search and sequence analysis tools services from EMBL-EBI in 2022. *Nucleic acids research,* 50**,** W276-W279.

Manders, E. M. M., Verbeek, F. J. & Aten, J. A. 1993. Measurement of co-localization of objects in dual-colour confocal images. *J Microsc,* 169**,** 375-382.

Marcello, E., Gardoni, F., Di Luca, M. & Pérez-Otaño, I. 2010. An arginine stretch limits ADAM10 exit from the endoplasmic reticulum. *J Biol Chem,* 285**,** 10376-10384.

Maretzky, T., Reiss, K., Ludwig, A., Buchholz, J., Scholz, F., Proksch, E., de Strooper, B., Hartmann, D. & Saftig, P. 2005. ADAM10 mediates E-cadherin shedding and regulates epithelial cell-cell adhesion, migration, and beta-catenin translocation. *Proc Natl Acad Sci U S A,* 102**,** 9182-9187.

Marie, P. J. & Haÿ, E. 2013. Cadherins and Wnt signalling: a functional link controlling bone formation. *Bonekey Rep,* 2**,** 330-335.

Matthews, A. L. 2019. *Regulation of the major platelet collagen and fibrin receptor GPVI by ADAM10 and Tspanc8 tetraspanins.* PhD thesis.

Matthews, A. L., Koo, C. Z., Szyroka, J., Harrison, N., Kanhere, A. & Tomlinson, M. G. 2018. Regulation of Leukocytes by TspanC8 Tetraspanins and the "Molecular Scissor" ADAM10. *Front Immunol,* 9**,** 1451-1460.

Matthews, A. L., Noy, P. J., Reyat, J. S. & Tomlinson, M. G. 2017a. Regulation of A disintegrin and metalloproteinase (ADAM) family sheddases ADAM10 and ADAM17: The emerging role of tetraspanins and rhomboids. *Platelets,* 28**,** 333-341.

Matthews, A. L., Szyroka, J., Collier, R., Noy, P. J. & Tomlinson, M. G. 2017b. Scissor sisters: regulation of ADAM10 by the TspanC8 tetraspanins. *Biochem Soc Trans,* 45**,** 719-730.

Mattila, P. K., Feest, C., Depoil, D., Treanor, B., Montaner, B., Otipoby, K. L., Carter, R., Justement, L. B., Bruckbauer, A. & Batista, F. D. 2013. The actin and tetraspanin networks organize receptor nanoclusters to regulate B cell receptor-mediated signaling. *Immunity,* 38**,** 461-474.

Mazur, P. K., Einwächter, H., Lee, M., Sipos, B., Nakhai, H., Rad, R., Zimber-Strobl, U., Strobl, L. J., Radtke, F., Klöppel, G., Schmid, R. M. & Siveke, J. T. 2010. Notch2 is required for progression of pancreatic intraepithelial neoplasia and development of pancreatic ductal adenocarcinoma. *Proc Natl Acad Sci U S A,* 107**,** 13438-13443.

Mizuno, S., Yoda, M., Shimoda, M., Tohmonda, T., Okada, Y., Toyama, Y., Takeda, S., Nakamura, M., Matsumoto, M. & Horiuchi, K. 2015. A Disintegrin and Metalloprotease 10 (ADAM10) Is Indispensable for Maintenance of the Muscle Satellite Cell Pool. *J Biol Chem,* 290**,** 28456-28464.

Moretto, E., Longatti, A., Murru, L., Chamma, I., Sessa, A., Zapata, J., Hosy, E., Sainlos, M., Saint-Pol, J., Rubinstein, E., Choquet, D., Broccoli, V., Schiavo, G., Thoumine, O. & Passafaro, M. 2019. TSPAN5 Enriched Microdomains Provide a Platform for Dendritic Spine Maturation through Neuroligin-1 Clustering. *Cell Rep,* 29**,** 1130-1146.

Moss, M. L., Bomar, M., Liu, Q., Sage, H., Dempsey, P., Lenhart, P. M., Gillispie, P. A., Stoeck, A., Wildeboer, D., Bartsch, J. W., Palmisano, R. & Zhou, P. 2007. The ADAM10 prodomain is a

specific inhibitor of ADAM10 proteolytic activity and inhibits cellular shedding events. *J Biol Chem,* 282**,** 35712-35721.

Mrozik, K. M., Blaschuk, O. W., Cheong, C. M., Zannettino, A. C. W. & Vandyke, K. 2018. N-cadherin in cancer metastasis, its emerging role in haematological malignancies and potential as a therapeutic target in cancer. *BMC Cancer,* 18**,** 939-955.

Mueller, A. C., Piper, M., Goodspeed, A., Bhuvane, S., Williams, J. S., Bhatia, S., Phan, A. V., Van Court, B., Zolman, K. L., Peña, B., Oweida, A. J., Zakem, S., Meguid, C., Knitz, M. W., Darragh, L., Bickett, T. E., Gadwa, J., Mestroni, L., Taylor, M. R. G., Jordan, K. R., Dempsey, P., Lucia, M. S., McCarter, M. D., Del Chiaro, M., Messersmith, W. A., Schulick, R. D., Goodman, K. A., Gough, M. J., Greene, C. S., Costello, J. C., Neto, A. G., Lagares, D., Hansen, K. C., Van Bokhoven, A. & Karam, S. D. 2021. Induction of ADAM10 by Radiation Therapy Drives Fibrosis, Resistance, and Epithelial-to-Mesenchyal Transition in Pancreatic Cancer. *Cancer Res,* 81**,** 3255-3269.

Mullooly, M., McGowan, P. M., Kennedy, S. A., Madden, S. F., Crown, J., N, O. D. & Duffy, M. J. 2015. ADAM10: a new player in breast cancer progression? *Br J Cancer,* 113**,** 945-951.

Mumm, J. S., Schroeter, E. H., Saxena, M. T., Griesemer, A., Tian, X., Pan, D. J., Ray, W. J. & Kopan, R. 2000. A ligand-induced extracellular cleavage regulates gamma-secretase-like proteolytic activation of Notch1. *Mol Cell,* 5**,** 197-206.

Nelson, W. J. & Nusse, R. 2004. Convergence of Wnt, beta-catenin, and cadherin pathways. *Science,* 303**,** 1483-1487.

Nicolas, M., Wolfer, A., Raj, K., Kummer, J. A., Mill, P., van Noort, M., Hui, C. C., Clevers, H., Dotto, G. P. & Radtke, F. 2003. Notch1 functions as a tumor suppressor in mouse skin. *Nat Genet,* 33**,** 416-421.

Nieman, M. T., Prudoff, R. S., Johnson, K. R. & Wheelock, M. J. 1999. N-cadherin promotes motility in human breast cancer cells regardless of their E-cadherin expression. *J Cell Biol,* 147**,** 631-644.

Nikopoulos, K., Gilissen, C., Hoischen, A., van Nouhuys, C. E., Boonstra, F. N., Blokland, E. A. W., Arts, P., Wieskamp, N., Strom, T. M., Ayuso, C., Tilanus, M. A. D., Bouwhuis, S., Mukhopadhyay, A., Scheffer, H., Hoefsloot, L. H., Veltman, J. A., Cremers, F. P. M. & Collin, R. W. J. 2010. Next-generation sequencing of a 40 Mb linkage interval reveals TSPAN12 mutations in patients with familial exudative vitreoretinopathy. *Am J Hum Genet,* 86**,** 240-247.

Noy, P. J., Yang, J., Reyat, J. S., Matthews, A. L., Charlton, A. E., Furmston, J., Rogers, D. A., Rainger, G. E. & Tomlinson, M. G. 2016. TspanC8 Tetraspanins and A Disintegrin and Metalloprotease 10 (ADAM10) Interact via Their Extracellular Regions: EVIDENCE FOR DISTINCT BINDING MECHANISMS FOR DIFFERENT TspanC8 PROTEINS. *J Biol Chem,* 291**,** 3145-3157.

Oosterheert, W., Xenaki, K. T., Neviani, V., Pos, W., Doulkeridou, S., Manshande, J., Pearce, N. M., Kroon-Batenburg, L. M., Lutz, M., van Bergen En Henegouwen, P. M. & Gros, P. 2020. Implications for tetraspanin-enriched microdomain assembly based on structures of CD9 with EWI-F. *Life Sci Alliance,* 3**,** e202000883.

Palomero, T., Lim, W. K., Odom, D. T., Sulis, M. L., Real, P. J., Margolin, A., Barnes, K. C., O'Neil, J., Neuberg, D., Weng, A. P., Aster, J. C., Sigaux, F., Soulier, J., Look, A. T., Young, R. A., Califano, A. & Ferrando, A. A. 2006. NOTCH1 directly regulates c-MYC and activates a feed-forward-loop transcriptional network promoting leukemic cell growth. *Proc Natl Acad Sci U S A,* 103**,** 18261-18266.

Perl, A. K., Wilgenbus, P., Dahl, U., Semb, H. & Christofori, G. 1998. A causal role for E-cadherin in the transition from adenoma to carcinoma. *Nature,* 392**,** 190-193.

Peschon, J. J., Slack, J. L., Reddy, P., Stocking, K. L., Sunnarborg, S. W., Lee, D. C., Russell, W. E., Castner, B. J., Johnson, R. S., Fitzner, J. N., Boyce, R. W., Nelson, N., Kozlosky, C. J., Wolfson, M. F., Rauch, C. T., Cerretti, D. P., Paxton, R. J., March, C. J. & Black, R. A. 1998. An essential role for ectodomain shedding in mammalian development. *Science,* 282**,** 1281-1284.

Pike, J. A., Styles, I. B., Rappoport, J. Z. & Heath, J. K. 2017. Quantifying receptor trafficking and colocalization with confocal microscopy. *Methods,* 115**,** 42-54.

Plentz, R., Park, J. S., Rhim, A. D., Abravanel, D., Hezel, A. F., Sharma, S. V., Gurumurthy, S., Deshpande, V., Kenific, C., Settleman, J., Majumder, P. K., Stanger, B. Z. & Bardeesy, N. 2009. Inhibition of gamma-secretase activity inhibits tumor progression in a mouse model of pancreatic ductal adenocarcinoma. *Gastroenterology,* 136**,** 1741-1749.

Pollock, N. L., Lee, S. C., Patel, J. H., Gulamhussein, A. A. & Rothnie, A. J. 2018. Structure and function of membrane proteins encapsulated in a polymer-bound lipid bilayer. *Biochim Biophys Acta Biomembr,* 1860**,** 809-817.

Polyak, K. & Weinberg, R. A. 2009. Transitions between epithelial and mesenchymal states: acquisition of malignant and stem cell traits. *Nat Rev Cancer,* 9**,** 265-273.

Poulter, J. A., Ali, M., Gilmour, D. F., Rice, A., Kondo, H., Hayashi, K., Mackey, D. A., Kearns, L. S., Ruddle, J. B., Craig, J. E., Pierce, E. A., Downey, L. M., Mohamed, M. D., Markham, A. F., Inglehearn, C. F. & Toomes, C. 2010. Mutations in TSPAN12 cause autosomal-dominant familial exudative vitreoretinopathy. *Am J Hum Genet,* 86**,** 248-253.

Poulter, J. A., Davidson, A. E., Ali, M., Gilmour, D. F., Parry, D. A., Mintz-Hittner, H. A., Carr, I. M., Bottomley, H. M., Long, V. W., Downey, L. M., Sergouniotis, P. I., Wright, G. A., MacLaren, R. E., Moore, A. T., Webster, A. R., Inglehearn, C. F. & Toomes, C. 2012. Recessive mutations in TSPAN12 cause retinal dysplasia and severe familial exudative vitreoretinopathy (FEVR). *Invest Ophthalmol Vis Sci,* 53**,** 2873-2879.

Powell, G. T., Zhao, Y., Faro, A., Stickney, H., Novellasdemunt, L., Henriques, P., Gestri, G., White, E. R., Ren, J., Lu, W., Young, R. M., Hawkins, T. A., Cavodeassi, F., Schwarz, Q., Dreosti, E., Raible, D. W., Li, V. S. W., Wright, G. J., Jones, E. Y. & Wilson, S. W. 2022. Cachd1 is a novel Frizzled- and LRP6-interacting protein required for neurons to acquire left-right asymmetric character. *bioRxiv*.

Proweller, A., Tu, L., Lepore, J. J., Cheng, L., Lu, M. M., Seykora, J., Millar, S. E., Pear, W. S. & Parmacek, M. S. 2006. Impaired notch signaling promotes de novo squamous cell carcinoma formation. *Cancer Res,* 66**,** 7438-7444.

Prox, J., Willenbrock, M., Weber, S., Lehmann, T., Schmidt-Arras, D., Schwanbeck, R., Saftig, P. & Schwake, M. 2012. Tetraspanin15 regulates cellular trafficking and activity of the ectodomain sheddase ADAM10. *Cell Mol Life Sci,* 69**,** 2919-2932.

Qian, X., Anzovino, A., Kim, S., Suyama, K., Yao, J., Hulit, J., Agiostratidou, G., Chandiramani, N., McDaid, H. M., Nagi, C., Cohen, H. W., Phillips, G. R., Norton, L. & Hazan, R. B. 2014. N-cadherin/FGFR promotes metastasis through epithelial-to-mesenchymal transition and stem/progenitor cell-like properties. *Oncogene,* 33**,** 3411-3421.

Quintanal-Villalonga, Á., Ferrer, I., Guruceaga, E., Cirauqui, C., Marrugal, Á., Ojeda, L., García, S., Zugazagoitia, J., Muñoz-Galván, S., Lopez-Rios, F., Montuenga, L., Vicent, S., Molina-Pinelo, S., Carnero, A. & Paz-Ares, L. 2020. FGFR1 and FGFR4 oncogenicity depends on n-cadherin and their co-expression may predict FGFR-targeted therapy efficacy. *EBioMedicine,* 53**,** 102683-102698.

Rachagani, S., Macha, M. A., Ponnusamy, M. P., Haridas, D., Kaur, S., Jain, M. & Batra, S. K. 2012. MUC4 potentiates invasion and metastasis of pancreatic cancer cells through stabilization of fibroblast growth factor receptor 1. *Carcinogenesis,* 33**,** 1953-1964.

Radice, G. L. 2013. N-cadherin-mediated adhesion and signaling from development to disease: lessons from mice. *Prog Mol Biol Transl Sci,* 116**,** 263-289.

Ran, F. A., Hsu, P. D., Wright, J., Agarwala, V., Scott, D. A. & Zhang, F. 2013. Genome engineering using the CRISPR-Cas9 system. *Nature Protocols,* 8**,** 2281-2308.

Rascio, F., Spadaccino, F., Rocchetti, M. T., Castellano, G., Stallone, G., Netti, G. S. & Ranieri, E. 2021. The Pathogenic Role of PI3K/AKT Pathway in Cancer Onset and Drug Resistance: An Updated Review. *Cancers (Basel),* 13**,** 3949-3964.

Reiss, K., Maretzky, T., Ludwig, A., Tousseyn, T., de Strooper, B., Hartmann, D. & Saftig, P. 2005. ADAM10 cleavage of N-cadherin and regulation of cell-cell adhesion and beta-catenin nuclear signalling. *Embo j,* 24**,** 742-752.

Ringel, J., Jesnowski, R., Moniaux, N., Lüttges, J., Ringel, J., Choudhury, A., Batra, S. K., Klöppel, G. & Löhr, M. 2006. Aberrant expression of a disintegrin and metalloproteinase 17/tumor necrosis factor-alpha converting enzyme increases the malignant potential in human pancreatic ductal adenocarcinoma. *Cancer Res,* 66**,** 9045-9053.

Robinson, D. R., Kalyana-Sundaram, S., Wu, Y. M., Shankar, S., Cao, X., Ateeq, B., Asangani, I. A., Iyer, M., Maher, C. A., Grasso, C. S., Lonigro, R. J., Quist, M., Siddiqui, J., Mehra, R., Jing, X., Giordano, T. J., Sabel, M. S., Kleer, C. G., Palanisamy, N., Natrajan, R., Lambros, M. B., Reis-Filho, J. S., Kumar-Sinha, C. & Chinnaiyan, A. M. 2011. Functionally recurrent rearrangements of the MAST kinase and Notch gene families in breast cancer. *Nat Med,* 17**,** 1646-1651.

Rosenbaum, D. & Saftig, P. 2023. New insights into the function and pathophysiology of the ectodomain sheddase A Disintegrin And Metalloproteinase 10 (ADAM10). *Febs j,* 291**,** 2733-2766.

Rudan Njavro, J., Klotz, J., Dislich, B., Wanngren, J., Shmueli, M. D., Herber, J., Kuhn, P. H., Kumar, R., Koeglsperger, T., Conrad, M., Wurst, W., Feederle, R., Vlachos, A., Michalakis, S., Jedlicka, P., Müller, S. A. & Lichtenthaler, S. F. 2020. Mouse brain proteomics establishes MDGA1 and CACHD1 as in vivo substrates of the Alzheimer protease BACE1. *Faseb j,* 34**,** 2465-2482.

Sachs, N., Kreft, M., van den Bergh Weerman, M. A., Beynon, A. J., Peters, T. A., Weening, J. J. & Sonnenberg, A. 2006. Kidney failure in mice lacking the tetraspanin CD151. *J Cell Biol,* 175**,** 33-39.

Sadot, E., Simcha, I., Shtutman, M., Ben-Ze'ev, A. & Geiger, B. 1998. Inhibition of beta-catenin-mediated transactivation by cadherin derivatives. *Proc Natl Acad Sci U S A,* 95**,** 15339-15344.

Sahin, U., Weskamp, G., Kelly, K., Zhou, H. M., Higashiyama, S., Peschon, J., Hartmann, D., Saftig, P. & Blobel, C. P. 2004. Distinct roles for ADAM10 and ADAM17 in ectodomain shedding of six EGFR ligands. *J Cell Biol,* 164**,** 769-779.

Saint-Pol, J., Billard, M., Dornier, E., Eschenbrenner, E., Danglot, L., Boucheix, C., Charrin, S. & Rubinstein, E. 2017a. New insights into the tetraspanin Tspan5 using novel monoclonal antibodies. *J Biol Chem,* 292**,** 9551-9566.

Saint-Pol, J., Eschenbrenner, E., Dornier, E., Boucheix, C., Charrin, S. & Rubinstein, E. 2017b. Regulation of the trafficking and the function of the metalloprotease ADAM10 by tetraspanins. *Biochem Soc Trans,* 45**,** 937-944.

Sanchez-Heras, E., Howell, F. V., Williams, G. & Doherty, P. 2006. The fibroblast growth factor receptor acid box is essential for interactions with N-cadherin and all of the major isoforms of neural cell adhesion molecule. *J Biol Chem,* 281**,** 35208-35216.

Sato, T., Shirane, K., Kido, M. & Furukawa, K. 2000. Correlated gene expression between beta-1,4-galactosyltransferase V and N-acetylglucosaminyltransferase V in human cancer cell lines. *Biochem Biophys Res Commun,* 276**,** 1019-1023.

Scharfenberg, F., Helbig, A., Sammel, M., Benzel, J., Schlomann, U., Peters, F., Wichert, R., Bettendorff, M., Schmidt-Arras, D., Rose-John, S., Moali, C., Lichtenthaler, S. F., Pietrzik, C. U., Bartsch, J. W., Tholey, A. & Becker-Pauly, C. 2020. Degradome of soluble ADAM10 and ADAM17 metalloproteases. *Cell Mol Life Sci,* 77**,** 331-350.

Schindelin, J., Arganda-Carreras, I., Frise, E., Kaynig, V., Longair, M., Pietzsch, T., Preibisch, S., Rueden, C., Saalfeld, S., Schmid, B., Tinevez, J.-Y., White, D. J., Hartenstein, V., Eliceiri, K., Tomancak, P. & Cardona, A. 2012. Fiji: an open-source platform for biological-image analysis. *Nature Methods,* 9**,** 676-682.

Schneider, C. A., Rasband, W. S. & Eliceiri, K. W. 2012. NIH Image to ImageJ: 25 years of image analysis. *Nature Methods,* 9**,** 671-675.

Seegar, T. C. M., Killingsworth, L. B., Saha, N., Meyer, P. A., Patra, D., Zimmerman, B., Janes, P. W., Rubinstein, E., Nikolov, D. B., Skiniotis, G., Kruse, A. C. & Blacklow, S. C. 2017. Structural Basis for Regulated Proteolysis by the alpha-Secretase ADAM10. *Cell,* 171**,** 1638-1648.

Seipold, L., Altmeppen, H., Koudelka, T., Tholey, A., Kasparek, P., Sedlacek, R., Schweizer, M., Bar, J., Mikhaylova, M., Glatzel, M. & Saftig, P. 2018. In vivo regulation of the A disintegrin and metalloproteinase 10 (ADAM10) by the tetraspanin 15. *Cell Mol Life Sci,* 75**,** 3251-3267.

Sépult, C., Bellefroid, M., Rocks, N., Donati, K., Gérard, C., Gilles, C., Ludwig, A., Duysinx, B., Noël, A. & Cataldo, D. 2019. ADAM10 mediates malignant pleural mesothelioma invasiveness. *Oncogene,* 38**,** 3521-3534.

Serdaroglu, A., Müller, S. A., Schepers, U., Bräse, S., Weichert, W., Lichtenthaler, S. F. & Kuhn, P. H. 2017. An optimised version of the secretome protein enrichment with click sugars (SPECS) method leads to enhanced coverage of the secretome. *Proteomics,* 17**,** 1600423-1600429.

Servage, K. A., Stefanius, K., Gray, H. F. & Orth, K. 2020. Proteomic Profiling of Small Extracellular Vesicles Secreted by Human Pancreatic Cancer Cells Implicated in Cellular Transformation. *Sci Rep,* 10**,** 7713-7726.

Shah, J., Rouaud, F., Guerrera, D., Vasileva, E., Popov, L. M., Kelley, W. L., Rubinstein, E., Carette, J. E., Amieva, M. R. & Citi, S. 2018. A Dock-and-Lock Mechanism Clusters ADAM10 at Cell-Cell Junctions to Promote α-Toxin Cytotoxicity. *Cell Rep,* 25**,** 2132-2147.

Shapiro, L. & Weis, W. I. 2009. Structure and biochemistry of cadherins and catenins. *Cold Spring Harb Perspect Biol,* 1**,** a003053.

Shapiro, V. S., Mollenauer, M. N., Greene, W. C. & Weiss, A. 1996. c-rel regulation of IL-2 gene expression may be mediated through activation of AP-1. *J Exp Med,* 184**,** 1663-1669.

Shirane, K., Sato, T., Segawa, K. & Furukawa, K. 1999. Involvement of beta-1,4-galactosyltransferase V in malignant transformation-associated changes in glycosylation. *Biochem Biophys Res Commun,* 265**,** 434-438.

Sidahmed-Adrar, N., Ottavi, J. F., Benzoubir, N., Ait Saadi, T., Bou Saleh, M., Mauduit, P., Guettier, C., Desterke, C. & Le Naour, F. 2019. Tspan15 Is a New Stemness-Related Marker in Hepatocellular Carcinoma. *Proteomics,* 19**,** e1900025.

Smith, T. M., Jr., Tharakan, A. & Martin, R. K. 2020. Targeting ADAM10 in Cancer and Autoimmunity. *Front Immunol,* 11**,** 499-511.

South, A. P., Cho, R. J. & Aster, J. C. 2012. The double-edged sword of Notch signaling in cancer. *Semin Cell Dev Biol,* 23**,** 458-464.

Starska, K., Forma, E., Lewy-Trenda, I., Stasikowska-Kanicka, O., Skóra, M. & Bryś, M. 2018. Fibroblast growth factor receptor 1 and 3 expression is associated with regulatory PI3K/AKT kinase activity, as well as invasion and prognosis, in human laryngeal cancer. *Cell Oncol (Dordr),* 41**,** 253-268.

Sterk, L. M., Geuijen, C. A., van den Berg, J. G., Claessen, N., Weening, J. J. & Sonnenberg, A. 2002. Association of the tetraspanin CD151 with the laminin-binding integrins alpha3beta1, alpha6beta1, alpha6beta4 and alpha7beta1 in cells in culture and in vivo. *J Cell Sci,* 115**,** 1161-1173.

Stipp, C. S., Kolesnikova, T. V. & Hemler, M. E. 2003. Functional domains in tetraspanin proteins. *Trends Biochem Sci,* 28**,** 106-112.

Stoeck, A., Lejnine, S., Truong, A., Pan, L., Wang, H., Zang, C., Yuan, J., Ware, C., MacLean, J., Garrett-Engele, P. W., Kluk, M., Laskey, J., Haines, B. B., Moskaluk, C., Zawel, L., Fawell, S., Gilliland, G., Zhang, T., Kremer, B. E., Knoechel, B., Bernstein, B. E., Pear, W. S., Liu, X. S., Aster, J. C. & Sathyanarayanan, S. 2014. Discovery of biomarkers predictive of GSI response in triple-negative breast cancer and adenoid cystic carcinoma. *Cancer Discov,* 4**,** 1154-1167.

Sung, H., Ferlay, J., Siegel, R. L., Laversanne, M., Soerjomataram, I., Jemal, A. & Bray, F. 2021. Global Cancer Statistics 2020: GLOBOCAN Estimates of Incidence and Mortality Worldwide for 36 Cancers in 185 Countries. *CA Cancer J Clin,* 71**,** 209-249.

Susa, K. J., Bradshaw, G. A., Eisert, R. J., Schilling, C. M., Kalocsay, M., Blacklow, S. C. & Kruse, A. C. 2023. A Spatiotemporal Map of Co-Receptor Signaling Networks Underlying B Cell Activation. *bioRxiv*.

Susa, K. J., Kruse, A. C. & Blacklow, S. C. 2024. Tetraspanins: structure, dynamics, and principles of partner-protein recognition. *Trends Cell Biol,* 34**,** 509-522.

Susa, K. J., Rawson, S., Kruse, A. C. & Blacklow, S. C. 2021. Cryo-EM structure of the B cell co-receptor CD19 bound to the tetraspanin CD81. *Science,* 371**,** 300-305.

Susa, K. J., Seegar, T. C., Blacklow, S. C. & Kruse, A. C. 2020. A dynamic interaction between CD19 and the tetraspanin CD81 controls B cell co-receptor trafficking. *Elife,* 9**,** e52337.

Suyama, K., Shapiro, I., Guttman, M. & Hazan, R. B. 2002. A signaling pathway leading to metastasis is controlled by N-cadherin and the FGF receptor. *Cancer Cell,* 2**,** 301-314.

Szyroka, J. 2019. *Regulation of the 'molecular scissor' ADAM10 by tetraspanin Tspan15.* PhD thesis.

Talmadge, J. E. & Fidler, I. J. 2010. AACR centennial series: the biology of cancer metastasis: historical perspective. *Cancer Res,* 70**,** 5649-5669.

Tanaka, H., Kono, E., Tran, C. P., Miyazaki, H., Yamashiro, J., Shimomura, T., Fazli, L., Wada, R., Huang, J., Vessella, R. L., An, J., Horvath, S., Gleave, M., Rettig, M. B., Wainberg, Z. A. & Reiter, R. E. 2010. Monoclonal antibody targeting of N-cadherin inhibits prostate cancer growth, metastasis and castration resistance. *Nat Med,* 16**,** 1414-1420.

Tang, W., Li, M., Qi, X. & Li, J. 2020. β1,4-Galactosyltransferase V Modulates Breast Cancer Stem Cells through Wnt/β-catenin Signaling Pathway. *Cancer Res Treat,* 52**,** 1084-1102.

Tang, Z., Kang, B., Li, C., Chen, T. & Zhang, Z. 2019. GEPIA2: an enhanced web server for large-scale expression profiling and interactive analysis. *Nucleic Acids Res,* 47**,** W556-w560.

Termini, C. M. & Gillette, J. M. 2017. Tetraspanins Function as Regulators of Cellular Signaling. *Front Cell Dev Biol,* 5**,** 34-48.

Thiery, J. P., Acloque, H., Huang, R. Y. & Nieto, M. A. 2009. Epithelial-mesenchymal transitions in development and disease. *Cell,* 139**,** 871-890.

Thul, P. J., Åkesson, L., Wiking, M., Mahdessian, D., Geladaki, A., Ait Blal, H., Alm, T., Asplund, A., Björk, L., Breckels, L. M., Bäckström, A., Danielsson, F., Fagerberg, L., Fall, J., Gatto, L., Gnann, C., Hober, S., Hjelmare, M., Johansson, F., Lee, S., Lindskog, C., Mulder, J., Mulvey, C. M., Nilsson, P., Oksvold, P., Rockberg, J., Schutten, R., Schwenk, J. M., Sivertsson, Å., Sjöstedt, E., Skogs, M., Stadler, C., Sullivan, D. P., Tegel, H., Winsnes, C., Zhang, C., Zwahlen, M., Mardinoglu, A., Pontén, F., von Feilitzen, K., Lilley, K. S., Uhlén, M. & Lundberg, E. 2017. A subcellular map of the human proteome. *Science,* 356**,** eaal3321.

Tian, C., Johnson, K. R., Lett, J. M., Voss, R., Salt, A. N., Hartsock, J. J., Steyger, P. S. & Ohlemiller, K. K. 2021. CACHD1-deficient mice exhibit hearing and balance deficits associated with a disruption of calcium homeostasis in the inner ear. *Hear Res,* 409**,** 108327-108342.

Tosello, V. & Ferrando, A. A. 2013. The NOTCH signaling pathway: role in the pathogenesis of T-cell acute lymphoblastic leukemia and implication for therapy. *Ther Adv Hematol,* 4**,** 199-210.

Tsai, Y. H., VanDussen, K. L., Sawey, E. T., Wade, A. W., Kasper, C., Rakshit, S., Bhatt, R. G., Stoeck, A., Maillard, I., Crawford, H. C., Samuelson, L. C. & Dempsey, P. J. 2014. ADAM10 regulates Notch function in intestinal stem cells of mice. *Gastroenterology,* 147**,** 822-834.

Tsang, J. Y. S., Lee, M. A., Chan, T. H., Li, J., Ni, Y. B., Shao, Y., Chan, S. K., Cheungc, S. Y., Lau, K. F. & Tse, G. M. K. 2018. Proteolytic cleavage of amyloid precursor protein by ADAM10 mediates proliferation and migration in breast cancer. *EBioMedicine,* 38**,** 89-99.

Tucher, J., Linke, D., Koudelka, T., Cassidy, L., Tredup, C., Wichert, R., Pietrzik, C., Becker-Pauly, C. & Tholey, A. 2014. LC-MS based cleavage site profiling of the proteases ADAM10 and ADAM17 using proteome-derived peptide libraries. *J Proteome Res,* 13**,** 2205-2214.

Uemura, K., Kihara, T., Kuzuya, A., Okawa, K., Nishimoto, T., Ninomiya, H., Sugimoto, H., Kinoshita, A. & Shimohama, S. 2006. Characterization of sequential N-cadherin cleavage by ADAM10 and PS1. *Neurosci Lett,* 402**,** 278-283.

Uhlen, M., Fagerberg, L., Hallstrom, B. M., Lindskog, C., Oksvold, P., Mardinoglu, A., Sivertsson, A., Kampf, C., Sjostedt, E., Asplund, A., Olsson, I., Edlund, K., Lundberg, E., Navani, S., Szigyarto, C. A., Odeberg, J., Djureinovic, D., Takanen, J. O., Hober, S., Alm, T., Edqvist, P. H., Berling, H., Tegel, H., Mulder, J., Rockberg, J., Nilsson, P., Schwenk, J. M., Hamsten, M., von Feilitzen, K., Forsberg, M., Persson, L., Johansson, F., Zwahlen, M., von Heijne, G., Nielsen, J. & Ponten, F. 2015. Proteomics. Tissue-based map of the human proteome. *Science,* 347**,** 1260419-1260429.

Umeda, R., Satouh, Y., Takemoto, M., Nakada-Nakura, Y., Liu, K., Yokoyama, T., Shirouzu, M., Iwata, S., Nomura, N., Sato, K., Ikawa, M., Nishizawa, T. & Nureki, O. 2020. Structural insights into tetraspanin CD9 function. *Nat Commun,* 11**,** 1606-1617.

van der Heijden, M., Essers, P. B. M., Verhagen, C. V. M., Willems, S. M., Sanders, J., de Roest, R. H., Vossen, D. M., Leemans, C. R., Verheij, M., Brakenhoff, R. H., van den Brekel, M. W. M. & Vens, C. 2020. Epithelial-to-mesenchymal transition is a prognostic marker for patient outcome in advanced stage HNSCC patients treated with chemoradiotherapy. *Radiother Oncol,* 147**,** 186-194.

van Deventer, S., Arp, A. B. & van Spriel, A. B. 2021. Dynamic Plasma Membrane Organization: A Complex Symphony. *Trends Cell Biol,* 31**,** 119-129.

van Deventer, S. J., Dunlock, V. E. & van Spriel, A. B. 2017. Molecular interactions shaping the tetraspanin web. *Biochem Soc Trans,* 45**,** 741-750.

van Tetering, G., van Diest, P., Verlaan, I., van der Wall, E., Kopan, R. & Vooijs, M. 2009. Metalloprotease ADAM10 is required for Notch1 site 2 cleavage. *J Biol Chem,* 284**,** 31018-31027.

van Zelm, M. C., Smet, J., Adams, B., Mascart, F., Schandené, L., Janssen, F., Ferster, A., Kuo, C. C., Levy, S., van Dongen, J. J. & van der Burg, M. 2010. CD81 gene defect in humans disrupts CD19 complex formation and leads to antibody deficiency. *J Clin Invest,* 120**,** 1265-1274.

Venkatesh, H. S., Tam, L. T., Woo, P. J., Lennon, J., Nagaraja, S., Gillespie, S. M., Ni, J., Duveau, D. Y., Morris, P. J., Zhao, J. J., Thomas, C. J. & Monje, M. 2017. Targeting neuronal activity-regulated neuroligin-3 dependency in high-grade glioma. *Nature,* 549**,** 533-537.

Vleminckx, K., Vakaet, L., Jr., Mareel, M., Fiers, W. & van Roy, F. 1991. Genetic manipulation of E-cadherin expression by epithelial tumor cells reveals an invasion suppressor role. *Cell,* 66**,** 107-119.

Wang, M., Ren, D., Guo, W., Huang, S., Wang, Z., Li, Q., Du, H., Song, L. & Peng, X. 2016. N-cadherin promotes epithelial-mesenchymal transition and cancer stem cell-like traits via ErbB signaling in prostate cancer cells. *Int J Oncol,* 48**,** 595-606.

Weber, G. L., Parat, M. O., Binder, Z. A., Gallia, G. L. & Riggins, G. J. 2011a. Abrogation of PIK3CA or PIK3R1 reduces proliferation, migration, and invasion in glioblastoma multiforme cells. *Oncotarget,* 2**,** 833-849.

Weber, S., Niessen, M. T., Prox, J., Lüllmann-Rauch, R., Schmitz, A., Schwanbeck, R., Blobel, C. P., Jorissen, E., de Strooper, B., Niessen, C. M. & Saftig, P. 2011b. The disintegrin/metalloproteinase Adam10 is essential for epidermal integrity and Notch-mediated signaling. *Development,* 138**,** 495-505.

Weber, S. & Saftig, P. 2012. Ectodomain shedding and ADAMs in development. *Development,* 139**,** 3693-3709.

Weng, A. P., Ferrando, A. A., Lee, W., Morris, J. P. t., Silverman, L. B., Sanchez-Irizarry, C., Blacklow, S. C., Look, A. T. & Aster, J. C. 2004. Activating mutations of NOTCH1 in human T cell acute lymphoblastic leukemia. *Science,* 306**,** 269-271.

Wetzel, S., Seipold, L. & Saftig, P. 2017. The metalloproteinase ADAM10: A useful therapeutic target? *Biochim Biophys Acta Mol Cell Res,* 1864**,** 2071-2081.

Wheelock, M. J., Shintani, Y., Maeda, M., Fukumoto, Y. & Johnson, K. R. 2008. Cadherin switching. *J Cell Sci,* 121**,** 727-735.

Williams, E. J., Furness, J., Walsh, F. S. & Doherty, P. 1994. Activation of the FGF receptor underlies neurite outgrowth stimulated by L1, N-CAM, and N-cadherin. *Neuron,* 13**,** 583-594.
Williams, E. J., Williams, G., Howell, F. V., Skaper, S. D., Walsh, F. S. & Doherty, P. 2001. Identification of an N-cadherin motif that can interact with the fibroblast growth factor receptor and is required for axonal growth. *J Biol Chem,* 276**,** 43879-43886.
Wolpert, F., Tritschler, I., Steinle, A., Weller, M. & Eisele, G. 2014. A disintegrin and metalloproteinases 10 and 17 modulate the immunogenicity of glioblastoma-initiating cells. *Neuro Oncol,* 16**,** 382-391.
Wong, E., Maretzky, T., Peleg, Y., Blobel, C. P. & Sagi, I. 2015. The Functional Maturation of A Disintegrin and Metalloproteinase (ADAM) 9, 10, and 17 Requires Processing at a Newly Identified Proprotein Convertase (PC) Cleavage Site. *J Biol Chem,* 290**,** 12135-12146.
Woods, N., Trevino, J., Coppola, D., Chellappan, S., Yang, S. & Padmanabhan, J. 2015. Fendiline inhibits proliferation and invasion of pancreatic cancer cells by interfering with ADAM10 activation and β-catenin signaling. *Oncotarget,* 6**,** 35931-35948.
Woods, N. K. & Padmanabhan, J. 2013. Inhibition of amyloid precursor protein processing enhances gemcitabine-mediated cytotoxicity in pancreatic cancer cells. *J Biol Chem,* 288**,** 30114-30124.
Xie, Q., Guo, H., He, P., Deng, H., Gao, Y., Dong, N., Niu, W., Liu, T., Li, M., Wang, S., Wu, Y. & Li, J. L. 2021. Tspan5 promotes epithelial-mesenchymal transition and tumour metastasis of hepatocellular carcinoma by activating Notch signalling. *Mol Oncol,* 15**,** 3184-3202.
Xu, P., Liu, J., Sakaki-Yumoto, M. & Derynck, R. 2012. TACE activation by MAPK-mediated regulation of cell surface dimerization and TIMP3 association. *Sci Signal,* 5**,** ra34.
Xu, S., Zhu, X., Zhang, S., Yin, S., Zhou, L., Chen, C. & Gu, J. 2001. Over-expression of beta-1,4-galactosyltransferase I, II, and V in human astrocytoma. *J Cancer Res Clin Oncol,* 127**,** 502-506.
Yamada, M., Sumida, Y., Fujibayashi, A., Fukaguchi, K., Sanzen, N., Nishiuchi, R. & Sekiguchi, K. 2008. The tetraspanin CD151 regulates cell morphology and intracellular signaling on laminin-511. *Febs j,* 275**,** 3335-3351.
Yang, E. Y. & Shah, K. 2020. Nanobodies: Next Generation of Cancer Diagnostics and Therapeutics. *Front Oncol,* 10**,** 1182-1199.
Yang, X., Claas, C., Kraeft, S. K., Chen, L. B., Wang, Z., Kreidberg, J. A. & Hemler, M. E. 2002. Palmitoylation of tetraspanin proteins: modulation of CD151 lateral interactions, subcellular distribution, and integrin-dependent cell morphology. *Mol Biol Cell,* 13**,** 767-781.
Yang, Y., Liu, X. R., Greenberg, Z. J., Zhou, F., He, P., Fan, L., Liu, S., Shen, G., Egawa, T., Gross, M. L., Schuettpelz, L. G. & Li, W. 2020. Open conformation of tetraspanins shapes interaction partner networks on cell membranes. *Embo j,* 39**,** e105246.
Yauch, R. L., Berditchevski, F., Harler, M. B., Reichner, J. & Hemler, M. E. 1998. Highly stoichiometric, stable, and specific association of integrin alpha3beta1 with CD151 provides a major link to phosphatidylinositol 4-kinase, and may regulate cell migration. *Mol Biol Cell,* 9**,** 2751-2765.
Yauch, R. L. & Hemler, M. E. 2000. Specific interactions among transmembrane 4 superfamily (TM4SF) proteins and phosphoinositide 4-kinase. *Biochem J,* 351 Pt 3**,** 629-637.
Yoshihara, K., Shahmoradgoli, M., Martínez, E., Vegesna, R., Kim, H., Torres-Garcia, W., Treviño, V., Shen, H., Laird, P. W., Levine, D. A., Carter, S. L., Getz, G., Stemke-Hale, K., Mills, G. B. & Verhaak, R. G. W. 2013. Inferring tumour purity and stromal and immune cell admixture from expression data. *Nature Communications,* 4**,** 2612-2623.
Yoshizumi, A., Kuboki, S., Takayashiki, T., Takano, S., Takayanagi, R., Sonoda, I. & Ohtsuka, M. 2023. Tspan15-ADAM10 signalling enhances cancer stem cell-like properties and induces chemoresistance via Notch1 activation in ICC. *Liver Int,* 43**,** 2275-2291.
You, B., Shan, Y., Shi, S., Li, X. & You, Y. 2015. Effects of ADAM10 upregulation on progression, migration, and prognosis of nasopharyngeal carcinoma. *Cancer Sci,* 106**,** 1506-1514.

Yuan, Q., Yu, H., Chen, J., Song, X. & Sun, L. 2020a. ADAM10 promotes cell growth, migration, and invasion in osteosarcoma via regulating E-cadherin/β-catenin signaling pathway and is regulated by miR-122-5p. *Cancer Cell Int,* 20**,** 99.

Yuan, Q., Yu, H., Chen, J., Song, X. & Sun, L. 2020b. ADAM10 promotes cell growth, migration, and invasion in osteosarcoma via regulating E-cadherin/β-catenin signaling pathway and is regulated by miR-122-5p. *Cancer Cell Int,* 20**,** 99-111.

Zhang, B., Zhang, Z., Li, L., Qin, Y. R., Liu, H., Jiang, C., Zeng, T. T., Li, M. Q., Xie, D., Li, Y., Guan, X. Y. & Zhu, Y. H. 2018. TSPAN15 interacts with BTRC to promote oesophageal squamous cell carcinoma metastasis via activating NF-kappaB signaling. *Nat Commun,* 9**,** 1423-1435.

Zhang, L., Abedin, M., Jo, H. N., Levey, J., Dinh, Q. C., Chen, Z., Angers, S. & Junge, H. J. 2023. A Frizzled4-LRP5 agonist promotes blood-retina barrier function by inducing a Norrin-like transcriptional response. *iScience,* 26**,** 107415-107435.

Zhang, X., Liu, G., Kang, Y., Dong, Z., Qian, Q. & Ma, X. 2013. N-cadherin expression is associated with acquisition of EMT phenotype and with enhanced invasion in erlotinib-resistant lung cancer cell lines. *PLoS One,* 8**,** e57692.

Zhang, Y., Li, B., Ji, Z. Z. & Zheng, P. S. 2010. Notch1 regulates the growth of human colon cancers. *Cancer,* 116**,** 5207-5218.

Zhou, H., Ma, H., Wei, W., Ji, D., Song, X., Sun, J., Zhang, J. & Jia, L. 2013. B4GALT family mediates the multidrug resistance of human leukemia cells by regulating the hedgehog pathway and the expression of p-glycoprotein and multidrug resistance-associated protein 1. *Cell Death Dis,* 4**,** e654.

Zhuang, J., Wei, Q., Lin, Z. & Zhou, C. 2015. Effects of ADAM10 deletion on Notch-1 signaling pathway and neuronal maintenance in adult mouse brain. *Gene,* 555**,** 150-158.

Zimmerman, B., Kelly, B., McMillan, B. J., Seegar, T. C. M., Dror, R. O., Kruse, A. C. & Blacklow, S. C. 2016. Crystal Structure of a Full-Length Human Tetraspanin Reveals a Cholesterol-Binding Pocket. *Cell,* 167**,** 1041-1051.

Zuidscherwoude, M., Göttfert, F., Dunlock, V. M., Figdor, C. G., van den Bogaart, G. & van Spriel, A. B. 2015. The tetraspanin web revisited by super-resolution microscopy. *Sci Rep,* 5**,** 12201-12219.

Zunke, F. & Rose-John, S. 2017. The shedding protease ADAM17: Physiology and pathophysiology. *Biochim Biophys Acta Mol Cell Res,* 1864**,** 2059-2070.